# CHARACTERIZATION AND SPECIATION OF THE LOW MOLECULAR MASS IRON POOL IN BLOOD

A Dissertation

by

NATHANIEL MATHEW DZIUBA

Submitted to the Office of Graduate and Professional Studies of
Texas A&M University
in partial fulfillment of the requirements for the degree of

DOCTOR OF PHILOSOPHY

| | |
|---|---|
| Chair of Committee, | Paul A. Lindahl |
| Committee Members, | David Barondeau |
| | Vishal Gohil |
| | Frank Raushel |
| Head of Department, | Josh Wand |

May 2020

Major Subject: Biochemistry

# ABSTRACT

The foci of this work were in characterizing and speciating the low molecular mass (LMM) iron pool in blood. We operationally define this pool as non-proteinaceous iron species with masses $<$10 kDa. In iron overload disorders (e.g., hemochromatosis) some portion of this pool is involved in organ damage and is termed non-transferrin bound iron (NTBI). NTBI has been poorly characterized and is thought to be ferric citrate. The blood's major iron transport protein, transferrin (Tf), is typically 30% saturated; when saturation levels are elevated, NTBI concentrations typically increase due to the unregulated trafficking of iron into the blood.

The first part of this work involves work done on characterizing the LMM pool of iron in blood. Characterization (i.e., mass, concentration, number of species, chemical identity) of the LMM pool of iron was performed using an anaerobic and chilled liquid chromatography system, coupled to an inductively coupled plasma mass spectrometer (LC-ICP-MS). Flow-through solutions (FTS) from filtered plasma were injected onto a size-exclusion column (SEC). In the second part of this work, the intact circulatory and digestive system of an iron-deficient pig was used to detect endogenously formed NTBI by tracing labeled nutrient iron ($^{57}Fe^{II}$-ascorbate). Blood was sampled from before and after the liver to observe NTBI formation and the effect of the liver via LC-ICP-MS.

Two to six conserved LMM species with apparent masses ranging from 400-2500 Da and concentrations ranging from 10-100 nM were detected in blood from various healthy mammals and hemochromatosis (HC) humans. Of these, the species in the 400 -500 Da range were the most reproducible. HC human FTS did not show any difference relative to that of a healthy human, possibly due to the treatment of their disease. Comparison of the observed species in FTSs with ferric citrate standards showed similar, though not identical, elution profiles. Ferric citrate was not the predominate species in healthy blood plasma, though it could be a constituent. $^{57}Fe$ traced nutrient iron was predominately bound to Tf with no detectable intermediates, suggesting that nutrient iron is channeled to Tf with forming stable-intermediate species. Endogenous ($^{56}Fe$) LMM iron species were observed with masses ranging from 400-1600 Da. The liver both absorbed and released LMM iron species to a modest degree, indicative of its role in iron metabolism. The endogenous species detected are thought to be generated from red blood cell recycling.

DEDICATION

*To my father, mother, sister, and friends who have kept me levelheaded during my studies. Thank you.*

# ACKNOWLEDGEMENTS

This dissertation would not have been possible without the support from many individuals. I would like to especially thank my advisor, Dr. Paul A. Lindahl, for his unwavering support and guidance over the course of my Ph.D. studies. Dr. Lindahl has given me every opportunity and chance to succeed in my studies. Under his tutelage, I was able to take part in an exciting and amazing project, which ultimately became the focus of this dissertation. He taught me what it meant to be a researcher and through this I gained a deeper level of understanding of the scientific method. He also imparted the knowledge that no matter how hard you try, sometimes experiments don't work out the first time, and that is okay. Working under him, I was also able to work on, maintain, and upgrade an amazing one-of-a-kind system, gaining priceless experiences in the process. I could not have asked for a more patient and generous advisor. I would especially like to thank Dr. Lindahl for allowing me to write my dissertation remotely, so I could be with my father during his battle with cancer. I would also like to thank my committee members: Dr. Frank Raushel, Dr. Vishal Gohil, and Dr. David Barondeau for taking the time to give me their advice, expertise, and feedback on my projects over the course of my studies.

I would like to thank previous and present members of the Lindahl Lab for their scientific input and morale support over the years. To the following former lab members: Dr. Joshua Wofford and Dr. Michael Moore, Cody Lupardus; and current lab members: Rachel Shepherd, Joshua Kim, Hailey Brawley, Waseem Vali, and Salvador Fernandez;

thank you for your constructive feedback, support, and comradery over the years. I would especially like to thank Dr. Trang Nyugen for the stimulating conversations about science and her much needed support and insight in all things related to life, science, and graduate school.

I would like to thank the administration in the Biochemistry Department, Chemistry Department, and the staff at the Texas A&M Veterinary Medical Park for all of their assistance throughout the years. I want to thank the newly appointed Academic Advisor Justine deGruyter in the Department of Biochemistry for all of the help and advice she has given me in preparation for my dissertation and defense. I especially want to thank my previous Academic Advisor Rafael Almanzar, for the much needed assistance and guidance when navigating graduate school and for always making the students his top priority. I would also like to thank two individuals who are always hidden in the dungeon of the Department of Chemistry: machinist William Seward, for his help in modifying and fabricating instruments, devices, and gear needed for my graduate studies; and Bill Merka in the glass shop, for making and fixing our glass gear in a timely manner whenever they were broken. I would like to thank my collaborator Dr. Joanne Hardy for her work and support in my dissertation projects. Without her work and support over these long years I would not have had such an amazing project to work on.

I would like to thank my father and mother for the unending and unequivocal support throughout all my academic ventures. I would also like to thank my friends who have supported me over the years while in graduate school and tolerated my

shenanigans: Joel Ferrer, Johnathan Thompson, Blaine Babineau, Trever Reininger, Chase Wiley, and Sin-Yu Shana Liu. I would also like to thank Sin-Ning Cindy Liu for her profuse support and words of encouragement during my graduate career.

# CONTRIBUTORS AND FUNDING SOURCES

## Contributors

This work was supervised by a dissertation committee consisting of advisor Professor Paul A. Lindahl and Professors Frank M. Raushel and David P. Barondeau of the Department of Chemistry and Professor Vishal M. Gohil of the Department of Biochemistry and Biophysics.

The LC-ICP-MS system used in the dissertation studies was initially designed and built by a previous lab member: Dr. Sean McCormick. All animal surgeries and post-op care were performed by Dr. Joanne Hardy of the Department of Large Animal Clinical Services (Texas A&M University). Animal husbandry was performed by Texas A&M University Veterinary Medical Park.

All other work conducted for the dissertation was completed by the student independently.

## Funding Sources

This work was made possible in part by the National Institute of Health Grant Number R35 GM127021, the Robert A. Welch foundation under Grant Number A1170, a grant from Texas A&M University College of Veterinary Medicine Grant Number RGS 16-04, and a grant from Texas A&M University Strategic Transformative Research program Its contents are solely the responsibility of the authors and do not necessarily

represent the official view of the National Institute of Health and the Robert A. Welch foundation.

# NOMENCLATURE

| | |
|---|---|
| Apo-Tf | Apo-transferrin |
| BDI | Bleomycin detectable iron |
| CAV | Caudal vena cava |
| CBC | Complete blood count |
| CPN | Ceruloplasmin |
| CRV | Cranial vena cava |
| Da | Daltons |
| DCI | Directly chelatable iron |
| DFO | Desferrioxamine |
| DMT1 | Divalent metal transporter 1 |
| DYCB | Duodenal cytochrome B reductase |
| FPN | Ferroportin |
| EPO | Erythropoietin |
| ERFE | Erythroferrone |
| FTN | Ferritin |
| FTS | Flow-through solution |
| HC | Hemochromatosis |
| HFE | Hemochromatosis protein |
| HILIC | Hydrophilic interaction chromatography |
| HJV | Hemojuvelin |

| | |
|---|---|
| HMM | High-molecular mass |
| Holo-Tf | Holo-transferrin |
| HP | Hepcidin |
| HPN | Haephestin |
| ICP-MS | Inductively coupled plasma mass spectrometry |
| IL-6 | Interleukin-6 |
| LC | Liquid chromatography |
| LF | Lactoferrin |
| LMM | Low-molecular mass |
| LTCCS | L-type calcium channels |
| MCO | Multi-copper oxidase |
| MDA | Malondialdehyde |
| MDCI | Mobilizer-dependent chelatable iron |
| MP-2 | Maltriptase-2 |
| MPS | Mononuclear phagocyte system |
| NTBI | Non-transferrin bound iron |
| NTA | Nitrolotriacetic acid |
| P1 | Pig 1 |
| P2 | Pig 2 |
| P3 | Pig 3 |
| P4 | Pig 4 |
| PCBP1 | Poly C binding protein 1 |

| | |
|---|---|
| PCBP2 | Poly C binding protein 2 |
| PV | Portal vein |
| RBCs | Red blood cells |
| ROS | Reactive oxygen species |
| SEC | Size-exclusion chromatography |
| TAMU | Texas A&M University |
| TIBC | Total iron binding capacity |
| Tf | Transferrin |
| TBI | Transferrin-bound-iron |
| TfR1 | Transferrin receptor 1 |
| TfR2 | Transferrin receptor 2 |
| Tf-sat | Transferrin saturation |
| TTCCs | T-type calcium channels |
| VAP | Venous access port |

TABLE OF CONTENTS

Page

LIST OF FIGURES

Page

LIST OF TABLES

Page

# 1. INTRODUCTION AND LITERATURE REVIEW

## 1.1. Introduction

Iron is an incredibly important metal for humans. As a civilization, our usage of this metal is what ushered in the iron age from the bronze age.[1] Ultimately, our mastery of the element has helped shape modern civilization as we know it today. In addition to being vital to human civilization, iron is also an essential nutrient in the bodies of healthy humans. Iron is required for the proper function of many proteins—the functions of which vary widely, ranging from DNA replication and DNA repair, to cellular respiration.[2–4]

Iron is classified as a transition metal which is defined by IUPAC as "an element whose atom has an incomplete d-sub shell, or which can give rise to cations with an incomplete d-sub shell." [5] Under a 0 oxidation state, it has the electron arrangement of [Ar] $3d^6$ $4s^2$ and can exist in a number of different oxidation states in nature, from 0 to +5, but is typically found in the ferrous (+2) or ferric (+3) oxidation states.[6]

Iron is the most widely present transition metal in biological systems.[7,8] Transition metals can form coordinate covalent bonds with a variety of ligands to create metal complexes. The type of ligand that is bound to a metal depends on the metal's oxidation state and can greatly alter the characteristic of a metal in aqueous solution (e.g., increasing its solubility).

Consider an acidified solution of solubilized ferric chloride. Hydrolysis of the ferric ions occurs when the solution's pH is raised to 7, forming a hydroxide coordinated iron complex called ferric hydroxide that is water insoluble.[9] However, if a soluble

ligand like citrate is added prior to the adjustment of pH, an iron citrate complex is formed that is water soluble.[9] Organisms can utilize either small ligands or proteins to increase the solubility and bioavailability of ferric ions, such that these ions can be transported without being hydrolyzed and be taken up by the organism.[9]

Although iron is essential to the human body, it can generate reactive oxygen species (ROS) in a catalytic cycle through the Fenton and Haber-Weiss reactions, if it is over-abundant and unprotected (i.e, not bound in a protein "cage").[10] The iron-dependent generation of ROS mainly concerns patients who have an iron-overload disorder/condition (i.e., the body has an over-abundance of iron).[11,12] If left untreated, this Fe-generated ROS can damage proteins, lipids, and DNA, which can lead to tissue/organ damage and other life-threatening complications.[13]

Iron overload in the blood occurs from blood transfusions and/or genetic conditions like hemochromatosis (an illness where the body has improper regulation of iron homeostasis causing increased iron absorption). These iron overloading events generate a pool of iron called non-transferrin bound iron (NTBI).[14,15] NTBI can be absorbed into the cells to form an intracellular labile iron pool—or cytosolic iron pool—which is responsible for generating ROS.[16] The studies presented in this dissertation were centered on isolating NTBI chromatographically, probing possible identities and elucidating a probable iron trafficking pathway that would allow for NTBI formation. The conclusions presented herein give insight into iron metabolism in regards to NTBI.

### 1.1.1. Iron Trafficking in Mammalian System

The process of how iron is absorbed from food by the digestive system, transported throughout the body in the blood, and processed intracellularly is well-studied but still not completely understood. There is currently no known pathway for the human body that is dedicated to excreting iron. There are two ways in which the body can lose iron: 1) through blood loss or 2) through the shedding of the epithelial layer of the digestive system and skin.[17] Iron in the blood comes from three main sources: (a) red blood cell recycling by the mononuclear phagocytes, (b) mobilization of iron stores from ferritin, and (c) diet.[18] The body needs approximately 20 mg of iron daily.[17] 1-2 mg of iron are lost to epithelial shedding and around 1-2 mg of iron come from the diet, while the remaining iron is gained through recycling the iron from the heme in red blood cells or from ferritin stores.[17] Healthy adults are able to acquire enough iron through a balanced diet, and iron supplements (oral or intravenous) are only administered in situations of iron deficiency.[19]

Herein, I will discuss the trafficking pathway of iron to the bloodstream and to the cells from (a) a food source, (b) iron stores, and (c) red blood cell recycling. Iron can pass from food sources to the bloodstream and cells. Food is digested in the stomach and the digested products, including iron, enter the small intestines. Here, iron from the food is absorbed in the intestine epithelial cells.[18] These cells are polarized, with an apical side facing the inside of the intestines, and a basolateral side facing the blood stream. Iron is absorbed on the apical side.[18] Iron from food is present as either heme and/or non-heme. Non-heme iron is typically in the ferric or ferrous oxidation state and must be

in the ferrous state to be absorbed directly. If it is not, ferric ions are reduced into the ferrous state by apical membrane-bound duodenal cytochrome B reductase (DCYB).[20] The reduced iron is then taken up by the proton-coupled transporter protein: divalent metal transport 1 (DMT1), which is present on the apical membrane and enters into the cytosolic iron pool.[21] Heme is taken up on the apical side of the enterocyte by the heme carrier protein 1 (HCP1) and is subsequently degraded by heme oxygenase 1 (HO-1) to produce biliverdin, carbon monoxide, and iron. [22,23] The released iron from heme will presumably follow a similar trafficking pathway as the absorbed iron from the non-heme iron sources.

Additionally, iron may be mobilized from intracellular stores of iron in ferritin, which is an iron storage protein composed of 24 subunits.[17] These subunits can be heavy or light chain; the subunit ratios of these chains varies depending on the tissue that is expressing ferritin.[24] For example, the heart has a higher ratio of heavy chains, while the liver has a higher ratio of light chains. [24] Iron is chaperoned by poly C binding protein 2 (PCBP2), where it then binds to the ferroxidase domain of ferritin located in the H-chain.[25] The oxidized iron then enters into the central canal of the protein to make up the iron core. The core of ferritin may hold up to 4500 iron atoms, and is similar in composition to the mineral ferrihydrite ($5Fe_2O_3 \bullet 9H_2O$).[26,27] Iron from ferritin can be mobilized by cells on an as-needed basis. In this process, holo-ferritin is degraded in lysosomes. The protein shell of ferritin is degraded in the lysosome, which causes the solubilization of the iron core.[17] Then, the solubilized iron is reduced by intracellular agents (e.g., glutathione or ascorbic acid).[28] Once the iron is solubilized, DMT1 is

localized to the lysosomal membrane, and the iron is exported into the cytosol—adding to the cytosolic/labile iron pool.[28] PCBP1/2 can bind to iron, from the cytosolic iron pool, and shuttle it for storage to ferritin (FTN). PCPB2 can also shuttle the iron towards the basolateral membrane to the membrane-bound iron transport protein ferroportin (FPN).[29,30]

Lastly, iron can also be recycled in the body via the reticuloendothelial system/mononuclear phagocyte system (MPS). This system is composed of macrophages, monocytes, and precursor cells by recycling senescent red blood cells.[31] These cell types reside in many locations, including the kidney, liver, and spleen.[32] Research on RBC clearance suggests that during an illness, the liver is the primary organ to clear and recycle RBCs from circulation.[33] The recycling process represents the largest supply of iron utilized by the body to produce nascent red blood cells. Recycled blood cells release approximately 20 mg of iron to supply erythropoiesis daily, compared to the 1-2 mg of iron coming in from nutrient sources.[34] These red pulp macrophages in the spleen are considered the primary macrophages which can recycle senescent red blood cells that have aged approximately 120 days.[35] These senescent cells have lost their flexibility/plasticity and are consequently recycled when they can no longer pass through the inter-endothelial slits in the red pulp of the spleen.[36] Other mechanisms can signal to the macrophages to target and recycle RBCs. These targeting signals include the clustering of Band 3 transmembrane membrane protein, the presence of phosphatidyl serine on the plasma membrane, and an oxidative stress induced alteration in the CD47 membrane protein.[36] MPS can also absorb and process free-hemoglobin and free-heme

present in the blood. Free hemoglobin in the blood is bound to the soluble protein haptoglobin, and the haptoglobin-hemoglobin complex is bound to the CD163 receptor for internalization.[37] Free-heme is bound by the soluble scavenging protein hemopexin and is bound by the CD91 receptor for internalization.[38] When the iron in the red blood cells, scavenged heme or hemoglobin is freed, it can be stored within FTN or be exported out of the cell by FPN to be oxidized by a multicopper oxidase (MCO).

Ferroportin (FPN) operates via a calcium cofactor that stimulates transporter activity.[39] Iron is bound to the intracellular side of FPN in a proposed inward-open conformation. A conformational change occurs, which closes the intracellular side of FPN and exposes the extracellular side. This causes an outward-open conformation, such that the iron is presented towards the blood at the basolateral side of the enterocyte.[40]

Iron exported by FPN is subsequently bound by transferrin (Tf), which is the major iron transport protein in the body. For Tf to bind to the exported iron, it first needs to be oxidized from the ferrous state to the ferric state.[41] This oxidation is performed by multicopper oxidases (MCOs), which oxidize iron by performing a four-electron reduction of oxygen to produce two molecules of water, with the reduced iron as the source of the electrons.[42] There are three known MCOs: ceruloplasmin (CPN), haephestin (HPN), and zyklopen. Each of these MCOs are expressed in different regions and are thought to serve in different pathways of iron trafficking. CPN is a soluble MCO present in the blood, and is thought to primarily oxidize iron that is exported from macrophages or hepatocytes.[41,43] HPN is a membrane bound MCO, heavily expressed in

enterocytes, representing the main MCO involved in enterocyte iron trafficking.[43,44] Zyklopen is present in placental tissues.[45]

Tf is an 80 kDa glycoprotein found in the blood that is primarily synthesized by the liver and is capable of binding of two ferric ions.[46,47] This protein acts as an iron buffer in the blood and is responsible for transporting iron to cells in need. The two ferric ions are bound in two separate lobes located at the N-terminal and C-terminal domains of the protein, with the C-terminal being the larger lobe.[48] The reported thermodynamic equilibrium binding constants for these sites are $K_1 = 4.7 \times 10^{20}$ $M^{-1}$ and $K_2 = 2.4 \times 10^{19}$ $M^{-1}$.[49] A synergistic anion—typically bicarbonate—is coordinated to the iron in the Tf-Fe complex. [50,51] In healthy individuals, the Tf concentration is approximately 30 µM and 30% saturated with iron.[52]

When apo-transferrin (apo-Tf) is fully loaded, the resulting holo-transferrin (holo-Tf) can be taken in by various cells via either of two transferrin receptors (TfR1 and TfR2), which are ubiquitously expressed in all vertebrates.[53] TfR1 is primarily responsible for holo-Tf cellular uptake, whereas TfR2 has a role in the regulation of iron homeostasis.[54,55] TfR1 is a disulfide-linked dimeric membrane protein that can bind two holo-TFNs. Cells in need of iron can internalize holo-Tf and recycle apo-Tf back into the blood. When holo-Tf binds to TfR1, the internalization of holo-Tf – TfR1 complex is initiated via clathrin-mediated endocytosis.[56] After internalization, the endosome is acidified. While Tf preferentially binds ferric ions at pH 7.4, Tf releases ferric ions under acidic conditions.[57] Additionally, at acidic pHs, the transferrin receptor releases holo-Tf and preferentially binds to apo-Tf.[58] A metalloreductase—STEAP3—is required

for the reduction of ferric ions in the endosome.[59] Reduction must occur before these ions can be exported by DMT1. Both STEAP3 and DMT1 are present on the endosome membrane.[59,60] The iron exported by DMT1 from the endosome enters into the cytosolic iron pool, after which the endosome is trafficked to the plasma membrane where apo-Tf and TfR1 can be recycled for another cycle of iron-binding and delivery.[58]

The exact process by which Tf binds to the exported and oxidized iron remains murky. There are two potential pathways for Tf to bind to iron. Iron can be released into the bloodstream as a small metal complex, whereby Tf then sequesters this form of iron. Alternatively, Tf could interact with a FPN-HPN complex when the complex presents iron to Tf.

If iron enters into the bloodstream first, it will enter either as a ferrous ion or ferric ion post-oxidation. When ferric ions enter an aqueous solution at a pH of 7.4 and are unligated, they are extremely unstable and will precipitate out of solution to form ferric hydroxide particles.[9] If this route is correct, then some small component in the blood may exist as a form of NTBI. The alternative is that Tf forms a stable protein-protein complex with either CPN or HPN, and forms NTBI only if Tf saturation reaches a certain threshold. NTBI has been detected when transferrin saturation (Tf-sat) reaches approximately 45% or more.[61,62] This is typically observed in iron overload disorders—which are discussed in further detail later—which indicates a pathway where iron is exported without Tf binding to it.

The first pathway of iron release (i.e., iron entering initially into the bloodstream) has many uncertainties regarding the redox chemistry of iron. On the other hand, the

alternative pathway (i.e., via a protein-protein complex) also has some uncertainties: e.g. whether a protein-protein interaction exists between Tf and FPN and/or CPN/HPN. There is a controversy regarding a potential interaction between Tf and CPN/HPN. This controversy involves whether a protein-protein interaction exists between these proteins and if an interaction does exist if it is physiologically relevant. A study using surface plasmon resonance suggests that there is no interaction between Tf with either CPN or HPN. [63] A study from another group using fluorescence emission spectroscopy, showed possible interactions between CPN and Tf; and CPN and lactoferrin (LF), a homolog of Tf present in milk.[64] However, the evidence presenting an interaction was later called into question by yet another research group, which reported that a Tf-CPN complex would not form under physiological concentrations.[65]

When the iron buffering capacity reaches the threshold for the formation of NTBI, organs like the liver, heart, and pancreas can absorb this iron.[66] The liver is the primary organ for absorbing NTBI, as it filters all of the blood of any metabolites produced from the other organs. Using NTBI analogs (e.g., ferrous sulfate + ascorbate, ferric citrate) the liver can absorb these NTBI analogues with approximately one pass through the liver, with a half-life of approximately 30 seconds.[67–69] Zip14—part of the zinc transporter family of proteins—is a membrane protein that is present on hepatocytes and is involved in the NTBI import pathway.[70,71] In order to be transported, NTBI must be in the reduced form, which can be achieved through ferrireductases that are present on the plasma membrane, or through ascorbate reduction.[66] When the liver is unable to absorb the circulating NTBI, the heart will absorb the NTBI pool through the proposed

L-type calcium channels (LTCCs) and/or the T-type calcium channels (TTCCs).[72] The formation of NTBI is dependent on the correct functioning of iron metabolism regulation.

### 1.1.2. Iron Homeostasis: Regulation and Disorders

The ability to control the amount of iron entering into the blood helps to prevent the body from becoming overburdened with iron, which if left unchecked, could lead to ROS formation and cellular damage. The human body has evolved a straightforward means of systemic iron regulation through a small peptide hormone called hepcidin (HP) that is encoded by the HAMP gene.[73,74] HP is mainly expressed and secreted from the liver in a 25-amino acid bioactive form.[75] A minor level of mRNA expression has been detected in the heart and spinal cord.[76] HP has a half-life of several minutes.[77] It is rapidly produced by the liver and cleared from the bloodstream by the kidneys. [78,79] A small amount of HP is excreted out of the body in the urine.[78] The rapid production and clearance of the hormone allows the body to quickly adapt to the iron concentration in the blood and alter the rate of iron efflux into the blood.[75]

HP alters the blood iron concentration through its ability to negatively regulate the post-translational expression of FPN on cell membranes.[80] When there is high iron concentrations in the blood, HP is expressed and it interacts with FPN. The interaction of FPN and HP initiates the targeted ubiquination of FPN, causing it to be internalized and degraded, and thus preventing the efflux of iron out of the cell and into the blood.[80] An alternative mechanism of how HP acts on FPN has been recently reported. This mechanism focusses on HP's ability to block the function of FPN without stimulating

endocytosis. This mechanism involves the entry of HP into the extracellular cleft of FPN which acts as a cork to occlude iron transport.[81] HP can also induce ubiquitnation-dependent proteasomal degradation of DMT1 in Caco cell strain and in ex vivo experiments using mouse duodenal segments, with no change in FPN protein levels in the latter experiments.[82] Taken together, these experiments suggest a tissue-specific difference in the means by which HP regulates iron (e.g., intestinal vs macrophage). Changes in DMT1 levels would prevent iron absorption via enterocytes, thereby limiting the amount of iron that can be absorbed from nutrient sources. On the other hand, changes in FPN levels in macrophages would prevent the transport of iron either from red blood cell recycling or from the mobilization of iron stores.

The regulation of HP occurs at the transcriptional level by different signals; two well-known pathways that upregulate HP are the BMP6/SMAD and IL-6 pathways. BMP6/SMAD involves iron sensing in the blood to initiate regulation. The sensing of iron involves different proteins involved in hemochromatosis, including TFR2, hemochromatosis protein (HFE), and hemojuvulin (HJV). During conditions of high serum iron, there is an increase in Tf-sat. TFR1 can bind to holo-Tf for iron absorption, but it also interacts with HFE. This latter interaction is negatively inhibited by holo-Tf, which causes the displacement of HFE from TFR1. This subsequently triggers an interaction of TFR2 and HFE to form a potential final complex of TFR2/HFE/HJV.[83,84] This final complex induces the BMP6 pathway, as HFE has been shown to stabilize the membrane protein ALK3, a BMP receptor, and HJV, a BMP coreceptor.[85–87] Signaling through the BMP6 pathway causes activation of *sons of mothers against*

*decapentaplegic homologue* (SMAD) transcription factors (1/5/8 and 4) to modify the expression of HAMP.[88–90]

The IL-6 pathway involves interleukin-6 (IL-6) cytokine, which is released during inflammation. Inflammation will typically occur during pathogenic invasion, during which the body will increase expression of HP. This reaction is a bodily defense against invading pathogens to limit the amount of iron in the blood that can be consumed by these organisms.[91] HP is an acute-phase protein that is upregulated during inflammation.[92] The upregulation of HP is induced by the cytokine IL-6.[92] IL-6 binds to cytokine receptors on the plasma membrane, where a complex forms with the tyrosine kinase JAK, which then causes signal transduction via *signal transducer and activator of transcription 3* (STAT3).[93,94] Additionally, there may be some level of interaction between the two well-known hepcidin regulatory pathways, as shown through previous research.[89]

Down regulation of HP also occurs, especially during conditions of anemia and iron deficiency. During anemia, the body requires iron to generate more RBCs through erythropoiesis.[95] Erythropoietin (EPO) is a hormone generated by the kidneys that is responsible for stimulating erythropoiesis. However, it is not responsible for down-regulating HP.[95] Down-regulation of HP during erythropoietic stimulation occurs by the hormone erythroferrone (ERFE), which is stimulated by EPO.[96,97] Other pathways and signals are also responsible for the down-regulation of HP. These include the TMPRSS6 pathway, growth factors, and sex hormones.

The TMPRSS6 pathway involves the serine protease matriptase-2 (MP-2), which is encoded by the TMPRSS6 gene, and is a negative regulator of the BMP-SMAD pathway. Low iron concentrations stabilize MP-2, which causes the cleavage of HJV, which prevents signal transduction to express HP.[98,99] Various growth factors and sex hormones also suppress HAMP expression (e.g., hepatocyte growth factor, epidermal growth factor, testosterone, estrogen).[100,101] Though these alternative signaling molecules reduce HP levels, the exact role of these signals in pathogenic responses have yet to be fully determined.

The dysregulation of iron homeostasis occurs through the misregulation of HP. These conditions are the basis for many iron-related disorders, and the primary example is genetic or hereditary hemochromatosis (HC). HC has 5 different forms, each due to a mutation in a different iron regulatory protein. The most prevalent form of HC is Type 1—which is due to a mutation in HFE—with 90% having a cysteine to tyrosine mutation at amino acid 282 (C282Y).[102,103] The other types are rarer, and include: Type 2 (mutation in HJV or HAMP), Type 3(TFR2 mutation), Type 4 (FPN mutation, also called ferroportin disease which has two different sub-types), and Type 5 (mutation in the ferritin heavy chain protein)].[103]

There are also other iron-related disorders that are not within the family of HC disorders, such as thalassemia (THL). THL is a form of inherited anemia, which appears in the major, intermedia, and minor forms. In this disease, hemoglobin is mutated in either it's alpha or beta globulin chain, with mutations in the beta chain being more prevalent.[104] These mutations prevent the proper formation of the globulin chains and

cause RBCs to be nonfunctional and misshapen, which increases their clearance rate from the body.[104] This disorder causes the stimulation of erythropoiesis, resulting in increased production of ERFE, and consequently a decrease in HP production.[97] The resulting increase in intestinal iron absorption can lead to iron overload in non-transfusion dependent cases.[105]

Iron related disorders are usually diagnosed using either standard clinical assays or genetic studies.[106,107] One assay is a complete blood count (CBC) which measures different parts of blood. The measurements from a CBC most commonly used for diagnostic purposes in iron overload disorders include: RBC count, mean corpuscula volume (RBC volume), hemoglobin concentration, and hematocrit (% of packed RBC to total blood volume).[108] There are other components of the CBC that can give further diagnostic information for clinicians on iron disorders.

Another set of assays make up an iron panel, which can include serum iron levels (iron bound to Tf), serum ferritin level (serum ferritin protein concentration), total iron-binding capacity (total amount of iron that Tf can bind), unsaturated iron-binding capacity (amount of apo-transferrin), and Tf-sat (% of holo-transferrin).[108] These assays are very important in providing information for diagnosing iron disorders. An individual with HC will typically have elevated Tf-sat levels, elevated serum iron levels, and elevated serum ferritin levels if the individual is left untreated.[107] Here we include a note of caution regarding the use of these assays: they are not capable of strictly diagnosing HC, but they can give indicators that a genetic test should be performed to confirm the

presence of a disorder.[103] There are some individuals who have Type 1 HC, but do not exhibit elevated Tf-sat at all, or not until later in life.[103]

When iron overload disorders are present, it is imperative that action is taken immediately to treat the disorder. If left untreated, iron can deposit into various tissues, generate ROS, and cause tissue damage. A large concern is iron loading in the liver, which can cause liver cirrhosis, and loading in the heart, which can cause hypertrophy and later cardiac arrest in severe cases.[109,110] The cause for the iron loading and tissue damage is thought to be due to the NTBI pool that is present in iron overload disorders.[111,112] Treatments for these disorders revolve around either utilizing the excess iron or converting iron into a chemically inert form (which prevents ROS). The treatment of HC involves either phlebotomy or chelator therapy.[107] Phlebotomy helps reduce the RBC count, which can generate more RCB using the surplus iron that is absorbed. In rare cases where phlebotomy treatments fail, a chelator is used to remove the iron from the blood. The typical treatment of thalassemia is the reverse of these iron overload treatments, A RBC transfusion is given to address the anemia, but these transfusions can cause elevated serum iron levels, which then requires chelation therapy to remove generated NTBI from RBC degradation.[106,110,113]

### 1.1.3. NTBI Pool

Under non-pathogenic conditions, the body tightly regulates iron metabolism to prevent excess iron from causing cellular damage. When this regulation system fails (e.g., in HC or in transfusional iron overload), a pool of iron is present in the blood that is not bound to Tf, which is termed non-transferrin bound iron (NTBI). The major

concern for iron overload disorders is the toxicity of the NTBI pool. Thus, patients are treated to maintain serum iron levels within a tolerable range and prevent the formation of an NTBI pool. The nomenclature for this pool of iron is confusing, as ferritin, hemoglobin, and other metal-containing proteins present in the blood can fall into this catchall category, but they don't refer to NTBI. In the context of the extant literature, references to the NTBI pool are specific to the forms of iron that are present as metal complexes coordinated with small nonproteinaceous ligands, that can cause damage to cells. The NTBI pool has been further divided into components that can be chelatable and/or redox active. The NTBI pool has been further divided into components based on the various assays used to detect this pool. These assays detect the pool through either the use of chelators or by ROS byproducts formed from the redox active component of the pool. Though, these are just operational definitions of NTBI, as its true identity is unknown.

NTBI was first discovered in the blood of beta-thalassemic patients, most of whom had undergone transfusional therapy to treat their disorder.[114] Sera from these individuals were shown to have iron that was not bound to Tf. The presence of this iron was detected in two ways: a) using DEAE-Sephadex-CDS chromatography, and b) quantifying the iron in LMM (< 30 kDa) sera flow-through-solution (FTS). The FTS was generated using size-exclusion-ultracentrifugation-filtration. Both methods utilized colorimetric iron chelators for the detection of iron. The presence of a non-transferrin form of iron garnered attention in the field as a possible reason for the tissue damage observed in severe forms of thalassemia. The same form of iron was later implicated in

other iron overload disorders. The discovery of NTBI led researchers to characterize and quantify this form of iron as a measurable biomarker of iron overload diseases.

NTBI is suspected of damaging tissues, specifically through its redox-active component(s).[115,116] Researchers and medical professionals have characterized and quantified this pool of iron, by examining either the low molecular mass (LMM) pool in the blood or the specific components that are redox active. Despite these efforts, the biochemical nature/identity of the NTBI pool remains undetermined.[117]

One method of quantifying the NTBI pool is by using chelators. Typically, a chelator is added to a serum sample, and then the sample is filtered through a size-exclusion membrane to remove proteins. This yields an LMM eluent, which is analyzed spectroscopically or by high performance liquid chromatography.[117] The pool of iron has been categorized into two different groups based on the chelators used for detection, which are: (a) mobilizer-dependent chelatable iron (MDCI), species in the pool that can be chelated by a mobilizing agent like nitrilotriacetic acid (NTA); and (b) directly cheatable iron (DCI), which are chelated by deferrioxamine (DFO). [62,118,119] Mobilizing agents tend to be small molecules that can bind to iron and are capable of shuttling or mobilizing the iron to other ligands with higher affinities to iron. Another way to quantify and characterize the NTBI pool is through the detection of ROS byproducts. To this end, a bleomycin detectable iron (BDI) assay is commonly used. In this assay, bleomycin and DNA are mixed together to generate a ROS byproduct, which is detected with a chromogenic compound.[120]

The observation that these categories exist would suggest that the NTBI pool is not a single uniform species, but rather composed of different components. When HC plasma/sera samples were incubated with DFO for 24 hours, there was a slight increase in the ligand signals detected by NMR. Suggesting DFO can chelate a portion of the NTBI rather slowly.[121] A different study that assessed the presence of DCI in HC patients observed some patients with no DCI, though these patients tested positive for MDCI when using a MDCI assay.[122] More importantly though, this categorization and distinction could merely be due to the different methods used to define NTBI, as there are still issues reported with these assays. These distinctions should be taken as an operational definition for quantified NTBI as the true nature/identity of NTBI is unknown.

The range of NTBI concentration varies depending on the specific iron overload disorder, the severity of the disorder, and among other factors like how it is detected. This range can be determined via the plethora of assays that are available to determine the concentration of NTBI (the entire LMM pool or the redox active components). In healthy individuals, less than 1 μM of NTBI is present in the blood, with Tf being around 30% saturated, which allows for any NTBI formed to be sequestered.[115] Though the range of NTBI present in pathogenic states can vary greatly depending on the severity, currently there is no schema in place to grade the severity of an individual's iron overload disorder. However, an individual's Tf-sat and serum ferritin level have been used as markers of severity, as they are typically used to assess treatment options.[103] There is a positive correlation between Tf-sat and NTBI concentration, as

well as between serum ferritin and iron stores.[123,124] Results from two international round-robin studies gave a concentration range of NTBI from below zero to 14 μM.[123,124] These studies assessed various quantification methodologies (chelator, fluorescent, ROS based) amongst 5-6 laboratories by analyzing the same set of samples between the labs for each study (the exact samples differed for each study).[123,124] Regardless of the severity of a disorder, different assays gave different NTBI concentrations, although similar results were obtained for assays operating on similar principles.[123,124] Not every assay measured the same component of the NTBI pool, thus giving different concentrations between these different assays and further indicating the potential complexity of species present in the NTBI pool.

Although there have been great strides in simplifying, validating, and standardizing NTBI assays over the past decade, there are still downfalls with the current methodologies. For instance, NTA is used in many assays. Though it is a good chelator, there are concerns regarding the high concentrations it is commonly used at and its possible side reaction with transferrin-bound-iron (TBI). Assays that use NTA at a concentration of 80 mM have been suspected of giving potentially erroneous results. A systematic study testing for optimal NTA concentrations reported that NTA can chelate iron from Tf at high concentrations, thus giving erroneous results.[125] Another study has shown that the use of NTA can give rise to false negatives if Tf is not adequately saturated, either endogenously or exogenously.[126] Aside from chelator based assays, the BDI assay has also been shown to have some interference from hemoglobin, with a positive correlation observed between NTBI and hemoglobin concentration.[120]

Hemolysis of RBCs can increase hemolysis concentration in sera or plasma samples. Hemolysis can occur from improper blood drawing and/or sample processing.[127] Whatever assay is used, the current assays require steps to prevent false testing results from obscuring valuable information. This is likely to remain the case until a more accurate and less problematic assay is developed.

The assays used to quantify NTBI could be drastically improved if the chemical identity of this pool was clearly defined, especially in the type of iron complexes that comprise the NTBI pool. It is possible for any metabolite in the blood that can coordinate with iron to form a part of the NTBI pool. Such potential ligands include amino acids, acetate, citrate, and phosphate.[128] Computer simulations on the equilibria of iron complexes in blood plasma with 40 different ligands suggested that citrate is the primary ligand for ferric ions in blood plasma.[128] Additionally, citrate and possibly acetate were also suggested to be the primary ligands for ferric ions from NMR and HPLC experiments performed on thalassemic sera, although the exact identity of the metal complex has yet to be proven.[121] The identity of a ligand of the NTBI pool has led to studies that use ferric citrate as an analog of NTBI. To date, studies on the aqueous solution chemistry of ferric citrate have been performed by mimicking physiological conditions. These studies have determined that the most probable ferric citrate species are monoferric complexes at healthy iron concentrations, and oligomeric ferric complexes under high iron concentrations (i.e., iron overload disorders).[129,130] More speciation studies are needed to examine the quantity and composition of the species in the NTBI pool, specifically in pathologically presenting iron overloaded individuals or

iron overload models. Since blood plasma is a heterogeneous solution, it is likely that NTBI contains more than just purely ferric-citrate complexes.

### 1.1.4. Approach to Understanding NTBI

To fully understand NTBI, it is necessary to identify the complex(es) and the coordinating ligand environment. It is also crucial to understand how NTBI is generated, specifically at a mechanistic/molecular level. Both of these conditions require an appropriate technique that is capable of: a) preserving the nature of NTBI (i.e., preserving the coordinated ligand environment), and b) are sensitive enough to detect small concentrations when sample volume is limited. In addition to an adequate technique, a model system is required that allows for large sample blood volumes and has a similar metabolism to that of humans.

Few studies have truly attempted to characterize the NTBI pool. Of the study cited most frequently, the researchers used biophysical techniques.[121] The techniques utilized either disrupted the ligand environment of the NTBI or they used inadequate separation techniques to speciate the NTBI pool. In order to characterize NTBI, we first developed a technique that would allow the separation of the NTBI pool based on its molecular weight and detect the intrinsically present iron. This technique would also allow us to probe potential identities of NTBI. The results from these experiments are presented in Section 2 of this dissertation.

Many studies on NTBI focus on how the body reacts to its presence, how it is absorbed or cleared by the body, and how the body/organs/tissues are damaged. There are no studies that probe the generation of NTBI in a live animal. There are speculations

regarding NTBI generation from iron exported from the digestive route into the blood, though none of these claims have been proven. We decided to test how NTBI can be generated from nutrient sources and to what extent it can be absorbed by the liver. This was done through a novel experiment that utilized a pig's intact digestive and circulatory system as the experimental system. The results from these experiments are presented in Section 3 of this dissertation.

### 1.2. References


1 E. Prehistory, European prehistory: a survey, *Choice Rev. Online*, 2003, **40**, 40-3486-40–3486.

2 J. Rudolf, V. Makrantoni, W. J. Ingledew, M. J. R. Stark and M. F. White, The DNA Repair Helicases XPD and FancJ Have Essential Iron-Sulfur Domains, *Mol. Cell*, 2006, **23**, 801–808.

3 I. Miyabe, T. A. Kunkel and A. M. Carr, The Major Roles of DNA Polymerases Epsilon and Delta at the Eukaryotic Replication Fork Are Evolutionarily Conserved, *PLoS Genet.*, 2011, **7**, e1002407.

4 E. Gnandt, K. Dörner, M. F. J. Strampraad, S. de Vries and T. Friedrich, The multitude of iron–sulfur clusters in respiratory complex I, *Biochim. Biophys. Acta - Bioenerg.*, 2016, **1857**, 1068–1072.

5 R. M. Hartshorn, K. H. Hellwich, A. Yerin, T. Damhus and A. T. Hutton, Brief guide to the nomenclature of inorganic chemistry, *Pure Appl. Chem.*, 2015, **87**, 1039–1049.

6 J. Silver, in *Chemistry of Iron*, ed. J. Silver, Springer Netherlands, Dordrecht,

1993, pp. 1–29.

7 W. Maret, The Metals in the Biological Periodic System of the Elements: Concepts and Conjectures, *Int. J. Mol. Sci.*, 2016, **17**, 66.

8 R. R. Crichton and J. L. Pierre, Old iron, young copper: From Mars to Venus, *BioMetals*, 2001, **14**, 99–112.

9 D. J. Kosman, Iron metabolism in aerobes: Managing ferric iron hydrolysis and ferrous iron autoxidation, *Coord. Chem. Rev.*, 2013, **257**, 210–217.

10 J. P. Kehrer, The Haber–Weiss reaction and mechanisms of toxicity, *Toxicology*, 2000, **149**, 43–50.

11 B. Murillo-Ortiz, J. Ramírez Emiliano, W. I. Hernández Vázquez, S. Martínez-Garza, S. Solorio-Meza, F. Albarrán-Tamayo, E. Ramos-Rodríguez and L. Benítez- Bribiesca, Impact of Oxidative Stress in Premature Aging and Iron Overload in Hemodialysis Patients, *Oxid. Med. Cell. Longev.*, 2016, **2016**, 1–8.

12 X. Chai, D. Li, X. Cao, Y. Zhang, J. Mu, W. Lu, X. Xiao, C. Li, J. Meng, J. Chen, Q. Li, J. Wang, A. Meng and M. Zhao, ROS-mediated iron overload injures the hematopoiesis of bone marrow by damaging hematopoietic stem/progenitor cells in mice, *Sci. Rep.*, 2015, **5**, 10181.

13 H. Sies, C. Berndt and D. P. Jones, Oxidative Stress, *Annu. Rev. Biochem.*, 2017, **86**, 715–748.

14 O. Loréal, I. Gosriwatana, D. Guyader, J. Porter, P. Brissot and R. C. Hider, Determination of non-transferrin-bound iron in genetic hemochromatosis using a new HPLC-based method, *J. Hepatol.*, 2000, **32**, 727–733.

15 E. A. Hod, N. Zhang, S. A. Sokol, B. S. Wojczyk, R. O. Francis, D. Ansaldi, K. P. Francis, P. Della-Latta, S. Whittier, S. Sheth, J. E. Hendrickson, J. C. Zimring, G. M. Brittenham and S. L. Spitalnik, Transfusion of red blood cells after prolonged storage produces harmful effects that are mediated by iron and inflammation, *Blood*, 2010, **115**, 4284–4292.

16 H. Glickstein, Intracellular labile iron pools as direct targets of iron chelators: a fluorescence study of chelator action in living cells, *Blood*, 2005, **106**, 3242–3250.

17 M. C. Linder, Mobilization of stored iron in mammals: A review, *Nutrients*, 2013, **5**, 4022–4050.

18 M. U. Muckenthaler, S. Rivella, M. W. Hentze and B. Galy, A Red Carpet for Iron Metabolism, *Cell*, 2017, **168**, 344–361.

19 T. D. Johnson Wimbley and D. Y. Graham, Diagnosis and management of iron deficiency anemia in the 21st century, *Therap. Adv. Gastroenterol.*, 2011, **4**, 177–184.

20 A. T. McKie, D. Barrow, G. O. Latunde-Dada, A. Rolfs, G. Sager, E. Mudaly, M. Mudaly, C. Richardson, D. Barlow, A. Bomford, T. J. Peters, K. B. Raja, S. Shirali, M. A. Hediger, F. Farzaneh and R. J. Simpson, An iron-regulated ferric reductase associated with the absorption of dietary iron, *Science (80-. ).*, 2001, **291**, 1755–1759.

21 H. Gunshin, B. Mackenzie, U. V Berger, Y. Gunshin, M. F. Romero, W. F. Boron, S. Nussberger, J. L. Gollan and M. A. Hediger, Cloning and

characterization of a mammalian proton-coupled metal-ion transporter, *Nature*, 1997, **388**, 482–488.

22 S. Le Blanc, M. D. Garrick and M. Arredondo, Heme carrier protein 1 transports heme and is involved in heme-Fe metabolism, *AJP Cell Physiol.*, 2012, **302**, C1780–C1785.

23 S. F. Medical and X. Francisco, Microsomal Heme Oxygenase, *J. Biol. Chem.*, 1969, **244**, 6388–6394.

24 P. Arosio, T. Adelman and J. Drysdale, On ferritin heterogeneity, *J. Biol. Chem.*, 1978, **253**, 4451–4458.

25 D. M. Lawson, A. Treffry, P. J. Artymiuk, P. M. Harrison, S. J. Yewdall, A. Luzzago, G. Cesareni, S. Levi and P. Arosio, Identification of the ferroxidase centre in ferritin, *FEBS Lett.*, 1989, **254**, 207–210.

26 K. M. Towe, Structural Distinction between Ferritin and Iron-Dextran (Imferon), *J. Biol. Chem.*, 1981, **256**, 9377–9378.

27 J. M. Bradley, N. E. Le Brun and G. R. Moore, Ferritins: Furnishing proteins with iron Topical Issue in Honor of R.J.P. Williams, *J. Biol. Inorg. Chem.*, 2016, **21**, 13–28.

28 A. La, T. Nguyen, K. Tran, E. Sauble, D. Tu, A. Gonzalez, T. Z. Kidane, C. Soriano, J. Morgan, M. Doan, K. Tran, C. Y. Wang, M. D. Knutson and M. C. Linder, Mobilization of iron from ferritin: New steps and details, *Metallomics*, 2018, **10**, 154–168.

29 I. Yanatori, D. R. Richardson, K. Imada and F. Kishi, Iron export through the

transporter ferroportin 1 is modulated by the iron chaperone PCBP2, *J. Biol. Chem.*, 2016, **291**, 17303–17318.

30 S. Leidgens, K. Z. Bullough, H. Shi, F. Li, M. Shakoury-Elizeh, T. Yabe, P. Subramanian, E. Hsu, N. Natarajan, A. Nandal, T. L. Stemmler and C. C. Philpott, Each member of the poly-r(C)-binding protein 1 (PCBP) family exhibits iron chaperone activity toward ferritin, *J. Biol. Chem.*, 2013, **288**, 17791–17802.

31 R. van Furth, Z. A. Cohn, J. G. Hirsch, J. H. Humphrey, W. G. Spector and H. L. Langevoort, The mononuclear phagocyte system: a new classification of macrophages, monocytes, and their precursor cells., *Bull. World Health Organ.*, 1972, **46**, 845–852.

32 S. H. Lee, Quantitative analysis of total macrophage content in adult mouse tissues. Immunochemical studies with monoclonal antibody F4/80, *J. Exp. Med.*, 1985, **161**, 475–489.

33 I. Theurl, I. Hilgendorf, M. Nairz, P. Tymoszuk, D. Haschka, M. Asshoff, S. He, L. M. S. Gerhardt, T. A. W. Holderried, M. Seifert, S. Sopper, A. M. Fenn, A. Anzai, S. Rattik, C. McAlpine, M. Theurl, P. Wieghofer, Y. Iwamoto, G. F. Weber, N. K. Harder, B. G. Chousterman, T. L. Arvedson, M. McKee, F. Wang, O. M. D. Lutz, E. Rezoagli, J. L. Babitt, L. Berra, M. Prinz, M. Nahrendorf, G. Weiss, R. Weissleder, H. Y. Lin and F. K. Swirski, On-demand erythrocyte disposal and iron recycling requires transient macrophages in the liver, *Nat. Med.*, 2016, **22**, 945–951.

34 P. Ponka, M. Tenenbein and J. W. Eaton, in *Handbook on the Toxicology of*

*Metals*, eds. S. Nordberg, Gunnar (Department of Public Health and CLinical Medicine, Umea University, U. Fowler, Bruce (Rollins School of Public Health, Emory University, Atlanta, GA, and Center for Alaska Native Health Research, University of Alaska, Fairbanks, Fairbanks, AK and S. S. Nordberg, Monica (Institute of Enviormental Medicin, Karolinska Institute, Acedemic Press, 4th edn., 2015, vol. 50, pp. 879–902.

35 R. E. Mebius and G. Kraal, Structure and function of the spleen, *Nat. Rev. Immunol.*, 2005, **5**, 606–616.

36 T. R. L. Klei, S. M. Meinderts, T. K. van den Berg and R. van Bruggen, From the cradle to the grave: The role of macrophages in erythropoiesis and erythrophagocytosis, *Front. Immunol.*, , DOI:10.3389/fimmu.2017.00073.

37 M. Kristiansen, J. H. Graversen, C. Jacobsen, O. Sonne, H. J. Hoffman, S. K. A. Law and S. K. Moestrup, Identification of the haemoglobin scavenger receptor, *Nature*, 2001, **409**, 198–201.

38 V. Hvidberg, M. B. Maniecki, C. Jacobsen, P. Højrup, H. J. Møller and S. K. Moestrup, Identification of the receptor scavenging hemopexin-heme complexes, *Blood*, 2005, **106**, 2572–2579.

39 C. N. Deshpande, T. A. Ruwe, A. Shawki, V. Xin, K. R. Vieth, E. V Valore, B. Qiao, T. Ganz, E. Nemeth, B. Mackenzie and M. Jormakka, Calcium is an essential cofactor for metal efflux by the ferroportin transporter family, *Nat. Commun.*, 2018, **9**, 3075.

40 M. C. Bonaccorsi di Patti, F. Polticelli, G. Cece, A. Cutone, F. Felici, T.

Persichini and G. Musci, A structural model of human ferroportin and of its iron binding site, *FEBS J.*, 2014, **281**, 2851–2860.

41 Z. L. Harris, A. P. Durley, T. K. Man and J. D. Gitlin, Targeted gene disruption reveals an essential role for ceruloplasmin in cellular iron efflux, *Proc. Natl. Acad. Sci. U. S. A.*, 1999, **96**, 10812–10817.

42 H. Komori and Y. Higuchi, Structural insights into the O 2 reduction mechanism of multicopper oxidase, *J. Biochem.*, 2015, **158**, 293–298.

43 E. Xu, M. Chen, J. Zheng, Z. Maimaitiming, T. Zhong and H. Chen, Deletion of hephaestin and ceruloplasmin induces a serious systemic iron deficiency and disrupts iron homeostasis, *Biochem. Biophys. Res. Commun.*, 2018, **503**, 1905–1910.

44 J. Gitschier, C. D. Vulpe, Y.-M. Kuo, T. L. Murphy, L. Cowley, C. Askwith, N. Libina and G. J. Anderson, Hephaestin, a ceruloplasmin homologue implicated in intestinal iron transport, is defective in the sla mouse., *Nat. Genet.*, 1999, **21**, 195–199.

45 H. Chen, Z. K. Attieh, B. A. Syed, Y. Kuo, V. Stevens, B. K. Fuqua, H. S. Andersen, C. E. Naylor, R. W. Evans, L. Gambling, R. Danzeisen, M. Bacouri-Haidar, J. Usta, C. D. Vulpe and H. J. McArdle, Identification of Zyklopen, a New Member of the Vertebrate Multicopper Ferroxidase Family, and Characterization in Rodents and Human Cells, *J. Nutr.*, 2010, **140**, 1728–1735.

46 R. L. Idzerda, H. Huebers, C. A. Finch and G. S. McKnight, Rat transferrin gene expression: Tissue-specific regulation by iron deficiency, *Proc. Natl. Acad. Sci.*

*U. S. A.*, 1986, **83**, 3723–3727.

47 R. Aasa, B. G. Malmström, P. Saltman and T. Vänngård, The specific binding of iron(III) and copper(II) to transferrin and conalbumin, *Biochim. Biophys. Acta*, 1963, **75**, 203–222.

48 J. Wally, P. J. Halbrooks, C. Vonrhein, M. A. Rould, S. J. Everse, A. B. Mason and S. K. Buchanan, The crystal structure of iron-free human serum transferrin provides insight into inter-lobe communication and receptor binding, *J. Biol. Chem.*, 2006, **281**, 24934–24944.

49 P. Aisen, A. Leibman and J. Zweier, Stoichiometric and site characteristics of the binding of iron to human transferrin, *J. Biol. Chem.*, 1978, **253**, 1930–1937.

50 G. W. Bates and M. R. Schlabach, The nonspecific binding of Fe3+to transferrin in the absence of synergistic anions, *J. Biol. Chem.*, 1975, **250**, 2177–2181.

51 G. W. Bates, The Synergistic of Anions Fe3 + by Transferrin, 1975, **250**, 2182–2189.

52 R. Fulwood, C. L. Johnson, J. D. Bryner, E. W. Gunter and C. R. McGrath, *Hematological Nutritional Biochemistry Reference and Data for 74 Years of Age : United States, 1976-80*, National Center for Health Statistics, 1982, vol. 11.

53 L. A. Lambert and S. L. Mitchell, Molecular evolution of the transferrin receptor/glutamate carboxypeptidase II family, *J. Mol. Evol.*, 2007, **64**, 113–128.

54 C. E. Herbison, K. Thorstensen, A. C. G. Chua, R. M. Graham, P. Leedman, J. K. Olynyk and D. Trinder, The role of transferrin receptor 1 and 2 in transferrin-bound iron uptake in human hepatoma cells, *Am. J. Physiol. Physiol.*, 2009, **297**,

C1567–C1575.

55 E. Corradini, M. Rozier, D. Meynard, A. Odhiambo, H. Y. Lin, Q. Feng, M. C. Migas, R. S. Britton, J. L. Babitt and R. E. Fleming, Iron Regulation of Hepcidin Despite Attenuated Smad1,5,8 Signaling in Mice Without Transferrin Receptor 2 or Hfe, *Gastroenterology*, 2011, **141**, 1907–1914.

56 M. Ehrlich, W. Boll, A. Van Oijen, R. Hariharan, K. Chandran, M. L. Nibert and T. Kirchhausen, Endocytosis by random initiation and stabilization of clathrin-coated pits, *Cell*, 2004, **118**, 591–605.

57 J. Princiotto, Functional heterogeneity and pH-dependent dissociation properties of human transferrin, *Biochim. Biophys. Acta - Gen. Subj.*, 1976, **428**, 766–771.

58 A. Dautry-Varsat, A. Ciechanover and H. F. Lodish, pH and the recycling of transferrin during receptor-mediated endocytosis., *Proc. Natl. Acad. Sci.*, 1983, **80**, 2258–2262.

59 R. S. Ohgami, D. R. Campagna, E. L. Greer, B. Antiochos, A. McDonald, J. Chen, J. J. Sharp, Y. Fujiwara, J. E. Barker and M. D. Fleming, Identification of a ferrireductase required for efficient transferrin-dependent iron uptake in erythroid cells, *Nat. Genet.*, 2005, **37**, 1264–1269.

60 M. Tabuchi, T. Yoshimori, K. Yamaguchi, T. Yoshida and F. Kishi, Human NRAMP2/DMT1, which mediates iron transport across endosomal membranes, is localized to late endosomes and lysosomes in HEp-2 cells, *J. Biol. Chem.*, 2000, **275**, 22220–22228.

61 W. Breuer, C. Hershko and Z. I. Cabantchik, The importance of non-transferrin

bound iron in disorders of iron metabolism, *Transfus. Sci.*, 2000, **23**, 185–192.

62 B. P. Esposito, W. Breuer, P. Sirankapracha, P. Pootrakul, C. Hershko and Z. I. Cabantchik, Labile plasma iron in iron overload: Redox activity and susceptibility to chelation, *Blood*, 2003, **102**, 2670–2677.

63 D. M. Hudson, M. J. Krisinger, T. A. M. Griffiths and R. T. A. MacGillivray, Neither human hephaestin nor ceruloplasmin forms a stable complex with transferrin, *J. Cell. Biochem.*, 2008, **103**, 1849–1855.

64 N. T. Ha-Duong, C. Eid, M. Hémadi and J. M. El Hage Chahine, In vitro interaction between ceruloplasmin and human serum transferrin, *Biochemistry*, 2010, **49**, 10261–10263.

65 V. B. Vasilyev, A. Y. Vlasenko, E. T. Zakharova, A. V. Sokolov, I. V. Voynova and V. A. Kostevich, Comparison of interaction between ceruloplasmin and lactoferrin/transferrin: to bind or not to bind, *Biochem.*, 2017, **82**, 1073–1078.

66 M. D. Knutson, Non-transferrin-bound iron transporters, *Free Radic. Biol. Med.*, 2019, **133**, 101–111.

67 P. Brissot, T. L. Wright, W. L. Ma and R. A. Weisiger, Efficient clearance of non-transferrin-bound iron by rat liver. Implications for hepatic iron loading in iron overload states, *J. Clin. Invest.*, 1985, **76**, 1463–1470.

68 C. M. Craven, J. Alexander, M. Eldridge, J. P. Kushner, S. Bernstein and J. Kaplan, Tissue distribution and clearance kinetics of non-transferrin-bound iron in the hypotransferrinemic mouse: a rodent model for hemochromatosis., *Proc. Natl. Acad. Sci. U. S. A.*, 1987, **84**, 3457–3461.

69 T. L. Wright, P. Brissot, Wei-Lan Ma and R. A. Weisiger, Characterization of non-transferrin-bound iron clearance by rat liver, *J. Biol. Chem.*, 1986, **261**, 10909–10914.

70 J. P. Liuzzi, F. Aydemir, H. Nam, M. D. Knutson and R. J. Cousins, Zip14 (Slc39a14) mediates non-transferrin-bound iron uptake into cells., *Proc. Natl. Acad. Sci. U. S. A.*, 2006, **103**, 13612–7.

71 H. Nam, C. Y. Wang, L. Zhang, W. Zhang, S. Hojyo, T. Fukada and M. D. Knutson, ZIP14 and DMT1 in the liver, pancreas, and heart are differentially regulated by iron deficiency and overload: Implications for tissue ironuptake in iron-related disorders, *Haematologica*, 2013, **98**, 1049–1057.

72 S. Kumfu, S. C. Chattipakorn, S. Fucharoen and N. Chattipakorn, Dual T-type and L-type calcium channel blocker exerts beneficial effects in attenuating cardiovascular dysfunction in iron-overloaded thalassaemic mice, *Exp. Physiol.*, 2016, **101**, 521–539.

73 C. Pigeon, G. Ilyin, B. Courselaud, P. Leroyer, B. Turlin, P. Brissot and O. Loréal, A New Mouse Liver-specific Gene, Encoding a Protein Homologous to Human Antimicrobial Peptide Hepcidin, Is Overexpressed during Iron Overload, *J. Biol. Chem.*, 2001, **276**, 7811–7819.

74 A. Roettol, G. Papanikolaou, M. Politou, F. Alberti, D. Girelli, J. Christakis, D. Loukopoulos and C. Camaschella, Mutant antimicrobial peptide hepcidin is associated with severe juvenile hemochromatosis, *Nat. Genet.*, 2003, **33**, 21–22.

75 V. Sangkhae and E. Nemeth, Regulation of the Iron Homeostatic Hormone

Hepcidin, *Adv. Nutr. An Int. Rev. J.*, 2017, **8**, 126–136.

76 C. H. Park, E. V. Valore, A. J. Waring and T. Ganz, Hepcidin, a Urinary Antimicrobial Peptide Synthesized in the Liver, *J. Biol. Chem.*, 2001, **276**, 7806–7810.

77 J. J. Xiao, W. Krzyzanski, Y. M. Wang, H. Li, M. J. Rose, M. Ma, Y. Wu, B. Hinkle and J. J. Perez-Ruixo, Pharmacokinetics of anti-hepcidin monoclonal antibody Ab 12B9m and hepcidin in cynomolgus monkeys, *AAPS J.*, 2010, **12**, 646–657.

78 T. Ganz and E. Nemeth, Iron Balance and the Role of Hepcidin in Chronic Kidney Disease, *Semin. Nephrol.*, 2016, **36**, 87–93.

79 E. Fung and E. Nemeth, Manipulation of the hepcidin pathway for therapeutic purposes, *Haematologica*, 2013, **98**, 1667–1676.

80 E. Nemeth, Hepcidin Regulates Cellular Iron Efflux by Binding to Ferroportin and Inducing Its Internalization, *Science (80-. ).*, 2004, **306**, 2090–2093.

81 K. R. Vieth, B. Qiao, E. Nemeth, G. Jung, E. V. Valore, B. Mackenzie, A. C. Sek, S. Aschemeyer, S. Rivella, D. Stefanova, M. Jormakka, T. A. Ruwe, T. Ganz and C. Casu, Structure-function analysis of ferroportin defines the binding site and an alternative mechanism of action of hepcidin, *Blood*, 2017, **131**, 899–910.

82 C. Brasselagnel, Z. Karim, P. Letteron, S. Bekri, A. Bado and C. Beaumont, Intestinal DMT1 cotransporter is down-regulated by hepcidin via proteasome internalization and degradation, *Gastroenterology*, 2011, **140**, 1261-1271.e1.

83 F. D'Alessio, M. W. Hentze and M. U. Muckenthaler, The hemochromatosis

proteins HFE, TfR2, and HJV form a membrane-associated protein complex for hepcidin regulation, *J. Hepatol.*, 2012, **57**, 1052–1060.

84 J. Gao, J. Chen, M. Kramer, H. Tsukamoto, A. S. Zhang and C. A. Enns, Interaction of the Hereditary Hemochromatosis Protein HFE with Transferrin Receptor 2 Is Required for Transferrin-Induced Hepcidin Expression, *Cell Metab.*, 2009, **9**, 217–227.

85 X. G. Wu, Y. Wang, Q. Wu, W. H. Cheng, W. Liu, Y. Zhao, C. Mayeur, P. J. Schmidt, P. B. Yu, F. Wang and Y. Xia, HFE interacts with the BMP type I receptor ALK3 to regulate hepcidin expression, *Blood*, 2014, **124**, 1335–1343.

86 J. L. Babitt, F. W. Huang, D. M. Wrighting, Y. Xia, Y. Sidis, T. A. Samad, J. A. Campagna, R. T. Chung, A. L. Schneyer, C. J. Woolf, N. C. Andrews and H. Y. Lin, Bone morphogenetic protein signaling by hemojuvelin regulates hepcidin expression, *Nat. Genet.*, 2006, **38**, 531–539.

87 E. Corradini, M. Rozier, D. Meynard, A. Odhiambo, H. Y. Lin, Q. Feng, M. C. Migas, R. S. Britton, J. L. Babitt and R. E. Fleming, Iron regulation of hepcidin despite attenuated Smad1,5,8 signaling in mice without transferrin receptor 2 or Hfe, *Gastroenterology*, 2011, **141**, 1907–1914.

88 L. Kautz, D. Meynard, A. Monnier, V. Darnaud, R. Bouvet, R.-H. Wang, C. Deng, S. Vaulont, J. Mosser, H. Coppin and M.-P. Roth, Iron regulates phosphorylation of Smad1/5/8 and gene expression of Bmp6, Smad7, Id1, and Atoh8 in the mouse liver, *Blood*, 2008, **112**, 1503–1509.

89 R. H. Wang, C. Li, X. Xu, Y. Zheng, C. Xiao, P. Zerfas, S. Cooperman, M.

Eckhaus, T. Rouault, L. Mishra and C. X. Deng, A role of SMAD4 in iron metabolism through the positive regulation of hepcidin expression, *Cell Metab.*, 2005, **2**, 399–409.

90 B. Andriopoulos Jr, E. Corradini, Y. Xia, S. A. Faasse, S. Chen, L. Grgurevic, M. D. Knutson, A. Pietrangelo, S. Vukicevic, H. Y. Lin and J. L. Babitt, BMP6 is a key endogenous regulator of hepcidin expression and iron metabolism, *Nat. Genet.*, 2009, **41**, 482–487.

91 K. Michels, E. Nemeth, T. Ganz and B. Mehrad, Hepcidin and Host Defense against Infectious Diseases, *PLoS Pathog.*, 2015, **11**, 1–14.

92 E. Nemeth, S. Rivera, V. Gabayan, C. Keller, S. Taudorf, B. K. Pedersen and T. Ganz, IL-6 mediates hypoferremia of inflammation by inducing the synthesis of the iron regulatory hormone hepcidin, *J. Clin. Invest.*, 2004, **113**, 1271–1276.

93 M. Vittoria, V. Falzacappa, M. V. Spasic, R. Kessler, J. Stolte, M. W. Hentze and M. U. Muckenthaler, STAT3 mediates hepatic hepcidin expression and its inflammatory stimulation, *Blood*, 2015, **109**, 353–359.

94 B. D. Maliken, J. E. Nelson and K. V. Kowdley, The hepcidin circuits act: Balancing iron and inflammation, *Hepatology*, 2011, **53**, 1764–1766.

95 Zivot A, Lipton JM, Narla A and Blanc L, Erythropoiesis : insights into pathophysiology and treatments in 2017, *Mol. Med.*, 2018, **24**, 1–15.

96 L. Kautz, G. Jung, E. V Valore, S. Rivella, E. Nemeth and T. Ganz, Identification of erythroferrone as an erythroid regulator of iron metabolism., *Nat. Genet.*, 2014, **46**, 678–84.

97 L. Kautz, G. Jung, X. Du, V. Gabayan, J. Chapman, M. Nasoff, E. Nemeth and T. Ganz, Erythroferrone contributes to hepcidin suppression and iron overload in a mouse model of β-thalassemia, *Blood*, 2015, **126**, 2031–2037.

98 L. Silvestri, A. Pagani, A. Nai, I. De Domenico, J. Kaplan and C. Camaschella, The Serine Protease Matriptase-2 (TMPRSS6) Inhibits Hepcidin Activation by Cleaving Membrane Hemojuvelin, *Cell Metab.*, 2008, **8**, 502–511.

99 N. Zhao, C. P. Nizzi, S. A. Anderson, J. Wang, A. Ueno, H. Tsukamoto, R. S. Eisenstein, C. A. Enns and A.-S. Zhang, Low Intracellular Iron Increases the Stability of Matriptase-2, *J. Biol. Chem.*, 2015, **290**, 4432–4446.

100 A. Katsarou and K. Pantopoulos, Hepcidin Therapeutics, *Pharmaceuticals*, 2018, **11**, 127.

101 J. B. Goodnough, E. Ramos, E. Nemeth and T. Ganz, Inhibition of hepcidin transcription by growth factors, *Hepatology*, 2012, **56**, 291–299.

102 J. N. Feder, A. Gnirke, W. Thomas, Z. Tsuchihashi, D. A. Ruddy, A. Basava, F. Dormishian, R. Domingo, M. C. Ellis, A. Fullan, L. M. Hinton, N. L. Jones, B. E. Kimmel, G. S. Kronmal, P. Lauer, V. K. Lee, D. B. Loeb, F. A. Mapa, E. McClelland, N. C. Meyer, G. A. Mintier, N. Moeller, T. Moore, E. Morikang, C. E. Prass, L. Quintana, S. M. Starnes, R. C. Schatzman, K. J. Brunke, D. T. Drayna, N. J. Risch, B. R. Bacon and R. K. Wolff, A novel MHC class I-like gene is mutated in patients with hereditary haemochromatosis, *Nat. Genet.*, 1996, **13**, 399–408.

103 E. J. Fitzsimons, J. O. Cullis, D. W. Thomas, E. Tsochatzis and W. J. H. Griffiths,

Diagnosis and therapy of genetic haemochromatosis (review and 2017 update), *Br. J. Haematol.*, 2018, **181**, 293–303.

104 H. Shirzadfar and N. Mokhtari, Critical Review on Thalassemia : Types , Symptoms and Treatment, *Crimson Publ.*, 2018, **1**, 2–5.

105 A. T. Taher, J. Porter, V. Viprakasit, A. Kattamis, S. Chuncharunee, P. Sutcharitchan, N. Siritanaratkul, R. Galanello, Z. Karakas, T. Lawniczek, J. Ros, Y. Zhang, D. Habr and M. D. Cappellini, Deferasirox reduces iron overload significantly in nontransfusion-dependent thalassemia: 1-Year results from a prospective, randomized, double-blind, placebo-controlled study, *Blood*, 2012, **120**, 970–977.

106 H. L. Muncie and J. S. Campbell, Alpha and beta thalassemia, *Am. Fam. Physician*, 2009, **80**, 339-344.

107 B. K. Crownover and C. J. Covey, Hereditary hemochromatosis., *Am. Fam. Physician*, 2013, **87**, 183–90.

108 M. Worwood, A. M. May and B. J. Bain, in *Dacie and Lewis Practical Haematology*, Elsevier, 12th edn., 2017, pp. 165–186.

109 B. R. Bacon, P. C. Adams, K. V. Kowdley, L. W. Powell and A. S. Tavill, Diagnosis and management of hemochromatosis: 2011 Practice Guideline by the American Association for the Study of Liver Diseases, *Hepatology*, 2011, **54**, 328–343.

110 D. J. Pennell, J. E. Udelson, A. E. Arai, B. Bozkurt, A. R. Cohen, R. Galanello, T. M. Hoffman, M. S. Kiernan, S. Lerakis, A. Piga, J. B. Porter, J. M. Walker and J.

Wood, Cardiovascular function and treatment in β-thalassemia major: A consensus statement from the american heart association, *Circulation*, 2013, **128**, 281–308.

111 A. Piga, F. Longo, L. Duca, S. Roggero, T. Vinciguerra, R. Calabrese, C. Hershko and M. D. Cappellini, High nontransferrin bound iron levels and heart disease in thalassemia major, *Am. J. Hematol.*, 2009, **84**, 29–33.

112 C. Le Lan, O. Loréal, T. Cohen, M. Ropert, H. Glickstein, F. Lainé, M. Pouchard, Y. Deugnier, A. Le Treut, W. Breuer, Z. I. Cabantchik and P. Brissot, Redox active plasma iron in C282Y/C282Y hemochromatosis, *Blood*, 2005, **105**, 4527–4531.

113 A. L. Peters, R. K. Kunanayagam, R. van Bruggen, D. de Korte, N. P. Juffermans and A. P. J. Vlaar, Transfusion of 35-day stored red blood cells does not result in increase of plasma non-transferrin bound iron in human endotoxemia, *Transfusion*, 2016, **57**, 53–59.

114 C. Hershko, G. Graham, G. W. Bates and E. a Rachmilewitz, Non-specific serum iron in thalassaemia: an abnormal serum iron fraction of potential toxicity., *Br. J. Haematol.*, 1978, **40**, 255–263.

115 G. J. Anderson, Non-transferrin-bound iron and cellular toxicity., *J. Gastroenterol. Hepatol.*, 1999, **14**, 105–8.

116 M. Patel and D. V. S. S. Ramavataram, Non transferrin bound iron: Nature, manifestations and analytical approaches for estimation, *Indian J. Clin. Biochem.*, 2012, **27**, 322–332.

117 Z. I. Cabantchik, Labile iron in cells and body fluids: Physiology, pathology, and pharmacology, *Front. Pharmacol.*, , DOI:10.3389/fphar.2014.00045.

118 W. Breuer, H. Ghoti, A. Shattat, A. Goldfarb, A. Koren, C. Levin, E. Rachmilewitz and Z. I. Cabantchik, Non-transferrin bound iron in Thalassemia: Differential detection of redox active forms in children and older patients, *Am. J. Hematol.*, 2012, **87**, 55–61.

119 P. Pootrakul, Labile plasma iron (LPI) as an indicator of chelatable plasma redox activity in iron-overloaded -thalassemia/HbE patients treated with an oral chelator, *Blood*, 2004, **104**, 1504–1510.

120 L. Von Bonsdorff, E. Lindeberg, L. Sahlstedt, J. Lehto and J. Parkkinen, Bleomycin-detectable iron assay for non-transferrin-bound iron in hematologic malignancies, *Clin. Chem.*, 2002, **48**, 307–314.

121 M. Grootveldl, J. D. Bell, B. Halliwellni, O. Aruomaq, A. Bornford and P. J. Sadlere, Non-transferrin-bound Iron in Plasma or Serum from Patients with Idiopathic Hemochromatosis. Characterization by high-performance liquid chromatography and nuclear magnetic resonance Chem spectroscopy, *J. Biol. Chem.*, 1989, **264**, 4417–4422.

122 W. Breuer, M. J. J. Ermers, P. Pootrakul, A. Abramov, C. Hershko and Z. I. Cabantchik, Desferrioxamine-chelatable iron, a component of serum non-transferrin-bound iron, used for assessing chelation therapy, *Blood*, 2001, **97**, 792–798.

123 E. M. G. Jacobs, J. C. M. Hendriks, B. L. J. H. Van Tits, P. J. Evans, W. Breuer,

Y. L. Ding, E. H. J. M. Jansen, K. Jauhiainen, B. Sturm, J. B. Porter, B. Scheiber-Mojdehkar, L. Von Bonsdorff, Z. I. Cabantchik, R. C. Hider and D. W. Swinkels, Results of an international round robin for the quantification of serum non-transferrin-bound iron: Need for defining standardization and a clinically relevant isoform, *Anal. Biochem.*, 2005, **341**, 241–250.

124 L. de Swart, J. C. M. Hendriks, L. N. van der Vorm, Z. I. Cabantchik, P. J. Evans, E. A. Hod, G. M. Brittenham, Y. Furman, B. Wojczyk, M. C. H. Janssen, J. B. Porter, V. E. J. M. Mattijssen, B. J. Biemond, M. A. Mackenzie, R. Origa, R. Galanello, R. C. Hider and D. W. Swinkels, Second international round robin for the quantification of serum non-transferrin-bound iron and labile plasma iron in patients with iron-overload disorders, *Haematologica*, 2016, **101**, 38–45.

125 A. M. Kolb, N. P. M. Smit, R. Lentz-Ljuboje, S. Osanto and J. van Pelt, Non-transferrin bound iron measurement is influenced by chelator concentration, *Anal. Biochem.*, 2009, **385**, 13–19.

126 I. Gosriwatana, O. Loreal, S. Lu, P. Brissot, J. Porter and R. C. Hider, Quantification of non-transferrin-bound iron in the presence of unsaturated transferrin., *Anal. Biochem.*, 1999, **273**, 212–20.

127 L. Heireman, P. Van Geel, L. Musger, E. Heylen, W. Uyttenbroeck and B. Mahieu, Causes, consequences and management of sample hemolysis in the clinical laboratory, *Clin. Biochem.*, 2017, **50**, 1317–1322.

128 P. M. May, P. W. Linder and D. R. Williams, Computer simulation of metal-ion equilibria in biofluids: models for the low-molecular-weight complex distribution

of calcium(II), magnesium(II), manganese(II), iron(III), copper(II), zinc(II), and lead(II) ions in human blood plasma, *J. Chem. Soc. Dalt. Trans.*, 1977, **2**, 588.

129 A. M. N. Silva, X. Kong, M. C. Parkin, R. Cammack and R. C. Hider, Iron(iii) citrate speciation in aqueous solution, *Dalt. Trans.*, 2009, 8616.

130 P. Vukosav, M. Mlakar and V. Tomišić, Revision of iron(III)–citrate speciation in aqueous solution. Voltammetric and spectrophotometric studies, *Anal. Chim. Acta*, 2012, **745**, 85–91.

# 2. LOW-MOLECULAR-MASS IRON IN HEALTHY BLOOD PLASMA IS NOT PREDOMINATELY FERRIC CITRATE*

## 2.1. Introduction

Ferrous ions enter the body via enterocytes lining the duodenum,[1–4] and they pass into the blood through the membrane-bound protein ferroportin.[5,6] Multicopper oxidases hephaestin and/or ceruloplasmin oxidize $Fe^{II}$ ions in the blood,[7] and the resulting $Fe^{III}$ species bind metal-free transferrin (abbreviated apo-Tf). Transferrin is an 80 kDa glycoprotein present in the blood at concentrations of 25–50 μM.[8] Iron-bound transferrin (called holo-Tf) distributes iron to other cells in the body by binding receptors on cellular surfaces followed by import into the cell by endocytosis.

Blood plasma contains other iron-containing proteins besides transferrin; these include ferritin, haptoglobin, albumin, and hemopexin. Ferritin is a 450 kDa complex with a hollow core that binds ferric oxyhydroxide nanoparticles. Most ferritins are located within cells and function to store iron. The physiological role of extracellular blood-borne ferritins is less well defined but expression and loading levels are correlated to disease.[9,10]

* Reproduced and adapted by permission from The Royal Society of Chemistry. " Low-molecular-mass iron in healthy blood plasma is not predominately ferric citrate" by Nathaniel Dziuba, Joanne Hardy, and Paul A. Lindahl, 2018. *Metallomics*, 10, 802-817, Copyright 2018 by Royal Society of Chemistry.
https://doi.org/10.1039/C8MT00055G

Haptoglobin and hemopexin diminish stress caused by hemolysis.[11] Haptoglobin coordinates free hemoglobin to generate a 150 kDa haptoglobin:hemoglobin complex that is absorbed by the liver.[12–15] Hemopexin (63 kDa) binds free heme in the blood as a detoxification mechanism.[16] With a concentration of ca. 600 μM, albumin (67 kDa) is the most prevalent protein in the blood; it coordinates iron weakly.[17–20]

Plasma iron is highly dynamic and turns-over every few hours.[1] The generation and utilization of plasma iron during erythrocyte recycling dominates plasma iron dynamics. In healthy individuals, nutrient iron import represents a minor perturbation of this process.[1] Nutrient iron import is regulated by hepcidin.[21] This peptide hormone is produced by the liver under high-iron conditions. Hepcidin binds ferroportin which promotes degradation of this membrane-bound iron exporter. This blocks nutrient iron import into the blood. Individuals with the iron-overload disease hereditary hemochromatosis generate insufficient hepcidin such that excessive nutrient iron flows into the blood.[22]

Tf also serves as an iron buffer in the blood. In healthy individuals, only ca. 30% is holo-Tf. The remaining apo-Tf provides a receptacle for nutrient iron as the iron enters the blood after a meal. Once all apo-Tf is saturated, further iron enters the blood as a poorly characterized toxic complex (or group of complexes) called non-transferrin-bound iron, abbreviated NTBI.[22–26] The name NTBI is confusing because the iron bound to ferritin, albumin, haptoglobin, and hemopexin is, in one sense, NTBI. However, in this paper, we will use the term more restrictively as particular LMM (defined as ≤10 kDa) iron complexes found in plasma and sera.

NTBI is not composed of all LMM iron complexes in the blood but only those that are absorbed by the liver rapidly and quantitatively.[27,28] NTBI is imported by Zip14 zinc receptors on the plasma membrane of hepatocytes.[29] The livers of untreated hemochromatosis patients accumulate massive amounts of NTBI-derived iron which can lead to cirrhosis. NTBI is absorbed by the heart and other organs.[27,30,31] Iron loading into the heart is less extreme than into the liver but more damaging. This is why heart disease is the leading cause of death in hemochromatosis.[32] These are the particular LMM iron complexes in the blood that we define as NTBI. Sadly, the chemical identity of this damaging material is unknown.

The concentration of NTBI is reportedly low or even undetectable in healthy individuals. This is probably because NTBI binds apo-Tf tightly and/or because NTBI is absorbed near-quantitatively by the liver. The concentration of NTBI in the plasma of healthy mammals ranges from 0.1–1.5 μM. In contrast, the NTBI concentration in the plasma of HFE(–/–) mice and hemochromatosis humans ranges from 3.7 to 10 μM.[18,23,25,31,33,34] (Mutations in the HFE gene are the most common cause of hereditary hemochromatosis.)

NTBI is commonly defined operationally as the iron in blood plasma that can be chelated under established assay conditions. One problem with such assays is that they destroy NTBI during detection, making it impossible to identify NTBI. Also, different assays using different chelators or reaction conditions generate different results.[33] Stronger chelators may remove iron from sites that are not truly NTBI such as those on proteins. For example, ultrafiltrates in which all proteins have been removed from the

sera of β-thalassemia (another iron-overload disease) patients contain 0.5 μM iron.[19] However, when NTA, a common chelator for NTBI assays, is added before ultrafiltration (i.e. to solutions containing holo-Tf and other iron-containing proteins) the resulting ultrafiltrates contain 5 μM iron. NTA probably removes iron bound to proteins in sera. The additional 4.5 μM iron that coordinates to NTA in sera is probably not NTBI according to our definition but it generally is counted as such by these assays. Due to the ambiguities caused by defining NTBI operationally, little is known regarding the number of NTBI species, their concentrations, or other chemical properties.

Although the chemical composition of NTBI is unknown, ferric citrate leads the list of NTBI candidates, so much so that the two names are used synonymously. Citrate is present in blood plasma at concentrations of *ca.* 100 μM,[19,35,36] and equilibrium calculations indicate that ferric citrate complexes are quite stable under these conditions.[36–38] Complicating the analysis is the formation of different complexes of citrate and ferric ions depending on the iron:citrate ratio and pH. A 1:100 ratio (the approximate physiological ratio found in plasma) favors dimers (though not exclusively), a 1:10 ratio favors oligomers, and a 1:10,000 ratio favors monomers.[19,38] Hepatocytes and T lymphocytes import oligomeric ferric citrate species faster than other iron-citrate species[39] suggesting that they possess a specific carrier for importing oligomeric ferric citrate. Other cell types also import ferric citrate, in these cases using DMT1 and ZIP14 carriers.[26,40–42]

The objective of this study was to detect and speciate LMM iron-containing species in flow-through solutions (FTSs) from mammalian plasma, and then evaluate

whether any detected species might be the long-sought-after NTBI. To do this, we employed a liquid chromatography system located in a refrigerated anaerobic glove box interfaced with an online inductively coupled plasma mass spectrometer. We have used this LC-ICP-MS system previously to detect LMM iron complexes in mitochondria[43] and the brain.[44]

LC-based studies aimed at detecting NTBI have been carried out previously. Simpson *et al*. passed mouse serum through a Sephadex G200 column and detected iron in a chromatography peak associated with masses <10 kDa.[45] However, they did not resolve the peak into individual molecular species. Hider *et al*. employed LC-ICP-MS to evaluate iron in sera.[20] In the high molecular mass (HMM) region, they detected iron-bound ferritin and Tf. Iron-bound albumin was also detected when standards were run. The LMM region exhibited a weak iron peak but they were also unable to resolve it into its molecular components. Grootveld *et al*.[46] used HPLC to detect LMM peaks in plasma from hemochromatosis patients and controls, but again they did not resolve the observed peak into molecular components. Our group has also used LC-ICP-MS to investigate iron in mouse plasma,[47] but in that study we focused on proteins in the HMM region, not on the LMM region where low-intensity unresolved features were observed.

Here we resolve LMM iron-containing species in plasma and sera by employing a size-exclusion LC column designed for LMM peptides. We also employed other strategies (like performing the LC in a refrigerated anaerobic glove box and rigorously cleaning the columns) to improve reproducibility and minimize artifacts. That being said, LMM iron complexes are notoriously difficult to isolate, characterize, and identify

because ligand dissociation/re-association rates can be very rapid (this is why such complexes are labile and susceptible to chelation). Iron complexes are particularly difficult to study because they are also redox active, and $Fe^{III}$ vs. $Fe^{II}$ ions coordinate ligands with different affinities. Moreover, aqueous $Fe^{III}$ ions are highly insoluble and tend to aggregate, albeit at kinetically slow rates. Finally, the concentration of LMM iron in the blood is very low, and these species would be undetectable without the extreme sensitivity of ICP-MS. Fortunately, we were able to negotiate through these difficulties and obtain new insights into the nature of NTBI in blood plasma and sera.

## 2.2. Experimental procedures

### 2.2.1. Standards

Ferric citrate standards were prepared by method C as described,[19] except that the iron standard was not purchased commercially. Rather, an $FeCl_3$ stock was generated by dissolving $FeCl_3$ hexahydrate (Sigma Aldrich) in high purity water (HPW; defined as water that has been deionized, filtered (>18 MΩ cm), and distilled). To this solution was added trace-metal-grade concentrated nitric acid (Fisher-Sci, abb. TMGNA), achieving a final concentration of 1.14 mM iron and 2% (v/v) acid.

A 100 mM stock citric acid solution was prepared from citric acid (Sigma Aldrich) in HPW, with the pH unadjusted. The citrate stock and HPW contained insignificant concentrations (*ca.* 30 nM) of contaminating iron.

Ferric citrate standards were prepared by mixing different volumes of the iron and citrate stock solutions in 100 mM MOPS pH 7.4 and HPW to achieve final iron concentrations of either 1 μM (for standards) or 50 μM (for spiking experiments). The

iron:citrate molar ratios ranged from 1:10 to 1:10,000. The final MOPS concentration was 20 mM. Solutions were prepared fresh and then typically aged in the dark for 24 h (though some were aged for 30 min) in the glovebox before use.

Standards used for the LMM calibration curve included: Blue Dextran (Sigma, 2 MDa, 0.1 mg $mL^{-1}$); Ni-BPS (1531 Da, 200 μM) made from nickel sulfate hexahydrate (Sigma) and bathophenanthrolinedisulfonic acid (Acros Organic); AMP (Acros Organic, 347 Da, 200 μM), ATP (Sigma, 507 Da, 200 μM); cyanocobalamin (Fisher, 1355 Da, 50 μM); bovine insulin (Fisher, 5777 Da, 50 μM); and cytochrome c (equine heart, Sigma, 12 384 Da, 20 μM). Standards used for the high molecular mass calibration curve included: carbonic anhydrase (bovine erythrocyte, Sigma, 29 kDa, 100 μM); human haptoglobin (Millipore, 200 kDa, 12.5 μM); ferritin (equine spleen, Sigma, 400 kDa, 50 μM); apo-transferrin (human, Athens Research & Technology, 80 kDa, 12.5 μM); and cytochrome c (Acros Organic, 200 μM). Solutions of all LMM standards were prepared in HPW. All HMM standards were prepared in 20 mM MOPS pH 7.4, 100 mM NaCl using HPW. All concentrations indicated are final.

### 2.2.2. Blood acquisition and fractionation

Experiments involving human blood were approved by the IRB administration committee at Texas A&M University (IRB-2017- 0020). Experiments involving nonhuman mammals were similarly approved by the Animal Use Protocol committee (IACUC 2015- 0034). Blood for plasma was collected using a 6 mL lithium heparin BD Vacutainer blood collection tube. Blood for sera was collected using either a 10 mL glass BD Vacutainer tube or a 1 L polyethylene centrifuge bottle. Plasma blood samples

were kept on ice for 15 min–2 h until processing and serum blood was set on ice for 30 min and then left to coagulate for 35 min at room temperature until processing. Plasma/sera samples were then fractionated by centrifugation (Sorvall Evolution RC centrifuge). The samples were spun using a GSA or SLC-6000 rotor with custom-built plastic inserts, each of which held 2 vacutainer tubes, at 2000 RCF and 4°C for 10 min. The spun vacutainers were carefully transferred to a chilled (8°C) anaerobic (<5 ppm $O_2$) glove box (Mbraun Labmaster 120). The samples were transferred to 2.5 mL Eppendorf tubes, removed from the glove box, and either used immediately (fresh) or frozen with liquid $N_2$ and stored at −80°C.

Pig blood was collected from healthy female Yorkshire pigs. Horse blood was collected from healthy horses. Mouse blood was pooled from 3–5 mice. Human blood was collected by staff at the Gulf Coast Regional Blood Centers in College Station TX and Conroe TX. Human blood was processed without freezing within 1–2 h post collection.

### 2.2.3. Plasma and serum processing

Some fresh or frozen-and-thawed plasma or serum samples were filtered through new 0.45 mm cellulose acetate syringe tip filters (VWR) to generate HMM samples. Other samples were filtered using a pressurized (75 psi Ar) Amicon stir-cell concentrator (Model 8003) fitted with a 10 kDa regenerated cellulose membrane (YM-10, Millipore). The solution that flowed through the membrane will be referred to as the flow-through solution (FTS). Membranes were conditioned by soaking them overnight in HPW. Two mL of HPW was passed through the membrane in the assembled filtration system prior

to applying the sample. The Amicon filtration step took *ca.* 2 h. The initial flow-through liquid (about half of the total volume collected) was discarded. The retained half was collected in a 2.5 mL Eppendorf tube. The Amicon system was cleaned by soaking all components except the base, the head, and the membrane in 10% bleach for 10 min followed by analytical rinsing with tap water and HPW after each use. The Amicon sample output tube was rinsed with 10% TMGNA for 20 min and rinsed with HPW after each use.

### 2.2.4. Experimental protocols for each figure

Figure 2-1 and 2-2: plasma or sera FTSs (300 μL) were injected onto the Superdex peptide column using 20 mM ammonium bicarbonate pH 8.5 mobile phase.

Figure 2-3: ferric citrate solutions (300 μL) with 1 μM iron were injected and run under different mobile phases. Citrate was present at iron:citrate molar ratios of 1:10, 1:1,000, or 1:10,000. Mobile phases: 20 mM ammonium bicarbonate pH 8.5, 20 mM ammonium acetate pH 6.5, and 20 mM sodium acetate pH 4.5.

Figure 2-4: ferric citrate solution and controls (300 μL) were injected and run under different mobile phases. The ferric citrate solution contained 1 μM iron with an iron:citrate molar ratio of 1:100. Controls of 100 μM citric acid in 20 mM MOPS pH 7.4 and 1 μM $FeCl_3$ in 20 mM MOPS pH 7.4 were also run. Similar mobile phases were used as in Figure 2-3.

Figure 2-5: the ferric citrate standard used for the spike contained 50 μM iron, 5 mM citrate, and 1.25 M MOPS at pH 7.4. Seven μL of this solution was added to 343 mL of FTS. The spiked solution was incubated in the dark for either 30 min or 24 h

before injection onto the column (same column conditions as for Figure 2-1). The $FeCl_3$ solution used for the spike contained 50 μM $FeCl_3$ and was prepared in 2% (v/v) TMGNA. A solution of 100 mM MOPS pH 7.4 was also prepared. To 350 μL of FTS was added 40 μL (or 10 μL) of the $FeCl_3$ stock solution and 120 μL (or 30 μL) of the MOPS solution. The final solution of 510 μL (or 390 μL) contained 3.9 μM (or 1.3 μM) $FeCl_3$ and 23.5 mM (or 7.7 mM) MOPS. The spiked FTS was incubated in the dark for 24 h and then injected into the column as in Figure 2-1.

Figure 2-6: a 50 μM apo-Tf solution was prepared in 20 mM MOPS pH 7.4, and 100 mM NaCl. To 460 μL of FTS was added 40 μL of the apo-Tf solution, and the resulting solution (containing 4 μM Tf) was incubated for 30 min in the glove box and injected into the column as described for Figure 2-1.

Figure 2-7: FTS spikes were prepared as for Figure 2-6. 150 μL of spiked FTS was injected onto the Superdex 200 column in which the mobile phase was 20 mM ammonium bicarbonate pH 8.5.

Figure 2-8: plasma solutions were treated as in Figure 2-7.

Figure 2-9: serum and some plasma samples were injected directly onto the Superdex 200 column (as for Figure 2-7). Other plasma samples were spiked with either 4 μM (final concentration) $^{57}Fe^{III}Cl_3$ or $^{57}Fe^{III}$ citrate. $^{57}Fe$ oxide powder (Isoflex USA) was treated with a minimal volume of aqua regia to dissolve the powder. Once dissolved, the solution was diluted with HPW to a final concentration of 80 mM making a $^{57}FeCl_3$ acid stock. To this acid stock, a 3 molar excess of sodium citrate (Sigma-Aldrich) was added until a pH of 5 was reached and then diluted to volume with HPW.

For the $^{57}Fe^{III}Cl_3$ spike, a 40 μM $^{57}FeCl_3$ solution was prepared by serial dilution of a 40 mM $^{57}FeCl_3$ acidified stock (diluted from an 80 mM acid stock with HPW) using 50 mM MOPS pH 7.4. To a 315 μL plasma solution was added 35 μL of the $^{57}FeCl_3$ stock (affording a 4 mM ferric chloride spike). The resulting 350 μL sample was injected onto the column after 30 min incubation. For the $^{57}Fe^{III}$ citrate spike, a 40 μM $^{57}Fe^{III}$ citrate (iron:citrate 1:3 molar ratio) solution was prepared by diluting a 40 mM $^{57}Fe$ citrate pH 4.5 solution using 50 mM MOPS pH 7.4. To 315 μL of plasma solution was added 35 mL of the resulting $^{57}Fe$ citrate solution, affording a 4 mM ferric citrate spike. The resulting 350 μL sample was injected onto the column after 30 min incubation. Plasma solutions were injected as in Figure 2-7.

Figure 2-10: FTSs were treated as in Figure 2-1, but with a mobile phase of 20 mM ammonium acetate pH 6.5.

Figure 2-11: $FeCl_3$ spikes were performed similar to that of Figure 2-5, namely by adding 40 mL of a 40 μM $FeCl_3$ solution to the FTS. Ferric citrate spikes were performed as in Figure 2-5, except that 28 μL of a 50 μM ferric citrate standard was added to 322 μL of FTS. The resulting 350 μL solution was incubated for 24 h and then injected onto the column prepared as for Figure 2-4.

Figure 2-12: FTSs were treated as in Figure 2-1, but with a mobile phase of 20 mM sodium acetate pH 4.5.

Figure 2-14: human hemochromatosis FTS and a 1 μM ferric citrate solution (iron:citrate 1:100; prepared fresh, incubated 24 h) were separately transferred into a 4 mm pathlength quartz cuvette. Spectra were collected on a Hitachi U-3310

spectrophotometer with a Headon PMT using UV Solutions 2.2 Software. Spectra were collected with a wavelength range of 191–800 nm using a 2 mm slit width, 300 nm $min^{-1}$ scan speed, and a 0.5 nm sampling interval. The lamp change mode was 340 nm.

### 2.2.5. Size-exclusion chromatography analysis

An Agilent 1260 Bioinert quaternary pump (G5611A) HPLC system with a manual injector (G5628A), fraction collector (G5664A), and UV-vis diode array (G4212B) was kept in an 8 °C chilled, $N_2$-atmosphere glove box. The liquid chromatography parameters were as follows: either 20 mM ammonium bicarbonate (Sigma- Aldrich) pH 8.5, 20 mM ammonium acetate (Sigma-Aldrich) pH 6.5, or 20 mM sodium acetate pH 4.5 (Sigma-Aldrich) was used as the mobile phase. All solutions were degassed using a Schlenk-line in which ultra-high purity argon inert gas had been passed through a deoxygenation catalyst. A flow rate of 0.350 mL $min^{-1}$ was used for all column types. Chemstation for LC 3D System (vB.04.03) Software was used for data analysis.

The LC was interfaced with an on-line inductively coupled plasma mass spectrometer (ICP-MS; Agilent 7700x, Tokyo Japan) as described.[43] The ICP-MS parameters used were: RF power, 1550 W; Ar flow rate, 15 L $min^{-1}$; carrier gas flow rate, 1.05 L $min^{-1}$; collision cell He flow rate, 4.1 mL $min^{-1}$; sample skimmer cones, Ni, Ni. The elements detected were: $^{31}P$, $^{34}S$, $^{45}Sc$, $^{48}Ti$, $^{55}Mn$, $^{56}Fe$, $^{57}Fe$, $^{59}Co$, $^{60}Ni$, $^{63}Cu$, $^{65}Cu$, $^{66}Zn$, $^{68}Zn$, $^{89}Y$, and $^{95}Mo$. The ICP-MS was tuned daily and a second time per day if the instrument was used continuously for longer than 12 h. A stock tuning solution (Agilent, 5188-6564) containing 10 ppm of Ce, Co, Li, Tl, and Y with 2% nitric acid (v/v) was used to prepare a 1 ppb tuning solution that was diluted with HPW and

acidified with 2% (v/v) TMGNA. The tuning counts were adjusted to the manufacturer's recommendations in both no-gas and helium collision mode. ICP-MS Masshunter Workstation Software for ICP-MS (v.B.01.01) was used for data analysis.

PEEK sample loops were incubated with 3 loop-volumes of 10% TMGNA in high purity water for 3 h on the bench top and then rinsed with 3 loop-volumes of high purity water. The sample loop was installed into the injector and rinsed with 3 loop-volumes of the mobile phase prior to injecting the sample. LMM analysis was performed by injecting 300 μL of solution onto two Superdex Peptide 10/300 GL (GE Healthcare) columns connected in series. The sample analysis time was 2 h and 38 min. HMM analysis was performed by injecting 150 μL of solution onto a Superdex 200 10/300 GL (GE Healthcare) column; the sample analysis time was 80 min.

The columns were cleaned at the end of each working day as described.[43] The chelator cocktail used for cleaning was made up with HPW and contained 10 mM ascorbic acid (Acros Organics), 1 mM citric acid (Sigma-Aldrich), and the following chelators at 5 μM final concentration: EDTA (Sigma-Aldrich), EGTA (Sigma-Aldrich), 1,10-phenanthroline (Acros Organics), 2,20-bipyridine (Alfa Aesar), bathocuprosulfonate (Sigma-Aldrich), and deferoxamine mesylat (Calbiochem). The chelator cocktail was degassed before use on the Schlenk line. The chelator cocktail was passed through the column at a flow rate of 0.150 mL $min^{-1}$. A gradient was performed for the cleaning cycle with the columns being flushed with HPW for 10 min, then a 20 min gradient from the current mobile phase to the chelator cocktail. 60 mL of the chelator cocktail was passed through the column, after which a 30 min gradient to the

desired mobile phase was performed. The desired mobile phase flowed through the column until a sample was injected.

During analysis, the column was equilibrated at a flow rate of 0.350 mL $min^{-1}$ for 1 h. Then, the baseline of the ICP-MS detection response was monitored for 30 min, and the sample was injected. In the event of spurious peaks or column contamination, the column was allowed to equilibrate until the baseline became flat; then the sample was reinjected.

A ghost column was used to determine the relative abundance of material that was retained or absorbed from the SEC columns. The ghost column consisted of a piece of PEEK tubing connecting the injection port to the diode array. This tubing replaced the originally installed column. Sample or standards were injected onto the ghost column and the elemental detection response of the injected material was recorded by ICP-MS. This method gave single peaks of all detected isotopes of interest, affording a quantitative representation of the detection response for the sample of interest. Peak areas were determined using peak fitting software supplied by Agilent. The ghost column analyte areas were compared to the total area of the sample which had been run on the SEC column to determine the extent of iron adsorption to or desorption from the column. HMM peaks were deconvoluted with FitYK software.[48]

**2.2.6. Molecular mass assignment**

The apparent molecular mass associated with each chromatographic peak was calculated using a standard curve. Nine known species were used to generate the LMM calibration curve and five known species were used to generate the HMM calibration

curve. The concentrations and masses used are described above. The elution volume (*Ve*) of each species was determined using either the ICP-MS or the UV-vis diode array. The void volume (*Vo*) of the size-exclusion columns was determined to be 15.4 mL for the Superdex Peptide columns and 8.48 mL for the Superdex 200 column using blue dextran. The calibration curve was generated by plotting the logarithm of the molecular weight *vs. Ve/Vo*. A best-fit linear regression analysis was generated from the data points.[43] The best-fit linear regression for the LMM calibration curve was calculated to be: logarithm of Mass (in Da) = $-1.1233 \cdot (V_e/V_o) + 5.5239$, with $R^2$ of 0.8524. The HMM calibration curve was calculated to be: logarithm of mass (in Da) = $-1.1002 \cdot (V_e/V_o) + 6.6186$, with $R^2$ of 0.9889. Mass determinations for the LMM and HMM standards used for the calibration curves gave errors of 3–30% and 1–20%, respectively. All metal-containing species used in calibration were detected by ICP-MS while those lacking metals were detected by UV-vis.

**2.2.7. Elemental concentrations**

50 mL of plasma or 100 mL of LMM FTS were aliquoted into a 15 mL plastic screw-top polypropylene tube (BD Falcon) along with sufficient TMGNA to afford a final concentration of 2% (v/v) of acid and sufficient HPW to afford a total volume of 5 mL. Samples were generated in triplicate. Fresh reagent blank and control samples were prepared in duplicate for every 25 unknown samples run. The reagent blank was prepared using HPW and 2% (v/v) TMGNA. The control sample was prepared similarly except that the atomic-absorption standard was used instead of HPW. The tubes were sealed by wrapping electrical tape around the cap. The samples were incubated in an

oven for 14–16 h at 75 °C and then chilled for 1 h at 4 °C. The samples were diluted to a final volume of 5 mL for plasma and 3 mL for LMM FTS post-chilling using HPW. Calibration curves were generated from an atomic absorption standard (Inorganic Venture, Christiansburg Virginia, USA) containing P, S, Cu, Mn, Zn, Fe, $^{57}$Fe, Co, Mo, and Ti and prepared to a final TMGNA concentration of 2% (v/v) of acid and diluted using HPW. Elemental analysis was performed by ICP-MS using He collision mode. The elements detected were: $^{31}$P, $^{45}$Sc, $^{48}$Ti, $^{55}$Mn, $^{56}$Fe, $^{57}$Fe, $^{59}$Co, $^{60}$Ni, $^{63}$Cu, $^{66}$Zn, $^{89}$Y, and $^{95}$Mo. An internal standard of Sc and Y (Inorganic Venture, IV-IPMS-71D) was added to the flow entering the nebulizer via a T junction. The detection response for each element was normalized to the Sc counts to adjust for instrument drift, sample introduction variability, and matrix effects. The Y detection response was used to diagnose unusual instrument behaviour and help in troubleshooting.

## 2.3. Results

### 2.3.1. LMM iron-containing species in healthy blood plasma

The average iron concentrations of plasma samples ($n$ = 10) and the corresponding FTSs ($n$ = 11) were 21 ± 7 μM, and 1.1 ± 0.2 μM, respectively. Thus, *ca.* 5% of the iron in healthy plasma was due to LMM iron complexes. The LC-ICP-MS chromatograms of 15 FTSs from the plasma of pigs, horses, mice, and humans exhibited iron-detected peaks in the LMM region (Figure 2-1). In these runs, the mobile phase of the LMM column was buffered at pH 8.5.

We distinguished two regions in these chromatograms, called variable and anchor. The variable region spanned apparent masses between 600 and 2500 Da whereas

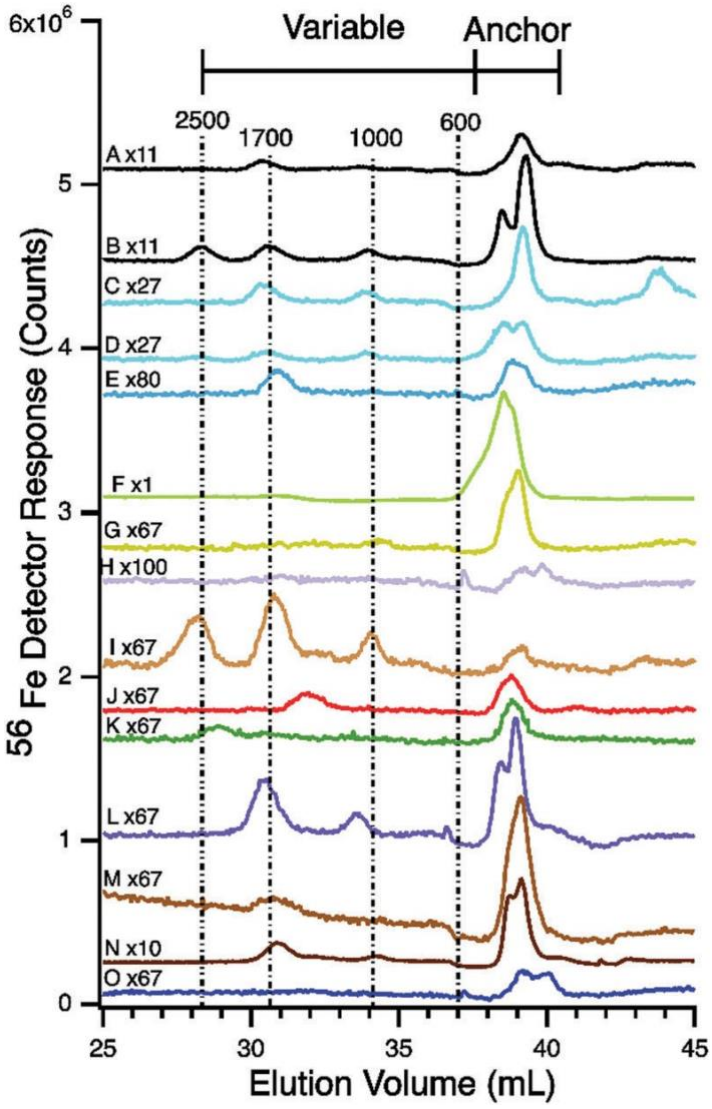


**Figure 2-1: $^{56}$Fe-Detected chromatograms of mammalian plasma flow-through solutions.**
(A) Pig 1, before feeding; (B) Pig 1, after feeding; (C) Pig 2 before feeding; (D) Pig 2 after feeding; (E) Horse 1; (F) Horse 2; (G) Mouse 1; (H) Horse 3; (I) Mouse 2; (J) Human hemochromatosis patient 1; (K) Human hemochromatosis patient 2; (L) Human hemochromatosis patient 3; (M) Human hemochromatosis patient 4; (N) human control 1 after eating a steak; (O) human control 1 after fasting 24 h. The mobile phase of the column was 20 mM ammonium bicarbonate pH 8.5. Human samples were run fresh; others were frozen and rethawed. Intensities were multiplied by various factors relative to trace F, as indicated. The same color indicates the same sample. Reprinted with permission.[49]

the anchor region included apparent masses between 350 and 550 Da. These and other mass estimates based on elution volumes are apparent because they were determined by calibration against the elution time of various standards (see Experimental procedures). We estimate ±30% uncertainties for these masses.

As the name implies, the peaks in the anchor region were more reproducible than those in the variable region. Two partially resolved iron-containing species were routinely observed in the anchor region, to be called $Fe_{400}$ and $Fe_{500}$ where the numbers refer to approximate masses in Da. These two species are best represented in traces B, D, L, N, and O of Figure 2-1. Four iron-containing peaks were observed (collectively) in the variable region – including $Fe_{2500}$, $Fe_{1700}$, $Fe_{1000}$, and $Fe_{600}$. Of these, $Fe_{2500}$, $Fe_{1700}$, and $Fe_{1000}$ were most reproducible; $Fe_{600}$ was not present in Figure 2-1 traces but was observed in the traces of other figures (*e.g.* Figure 2-2).

We examined fresh *vs.* frozen-and-thawed FTSs from the plasma of two horses to evaluate the stability of the detected LMM iron-containing species. No significant differences were observed (Figure 2-2, traces A *vs.* B, and traces D *vs.* E). There were greater differences between the chromatograms of the two horses ($Fe_{1700}$ was reproducibly intense in the traces from Horse 1 but absent in the traces from Horse 2). Anchor peaks were observed in the traces from both animals. Traces of sera were indistinguishable from those of plasma (Figure 2-2, B *vs.* C). We also re-ran the samples after incubating them in the glove box for 1 (Figure 2-2F) and 9 (Figure 2-2G) days. Minor differences were evident, relative to the original trace (Figure 2-2E).

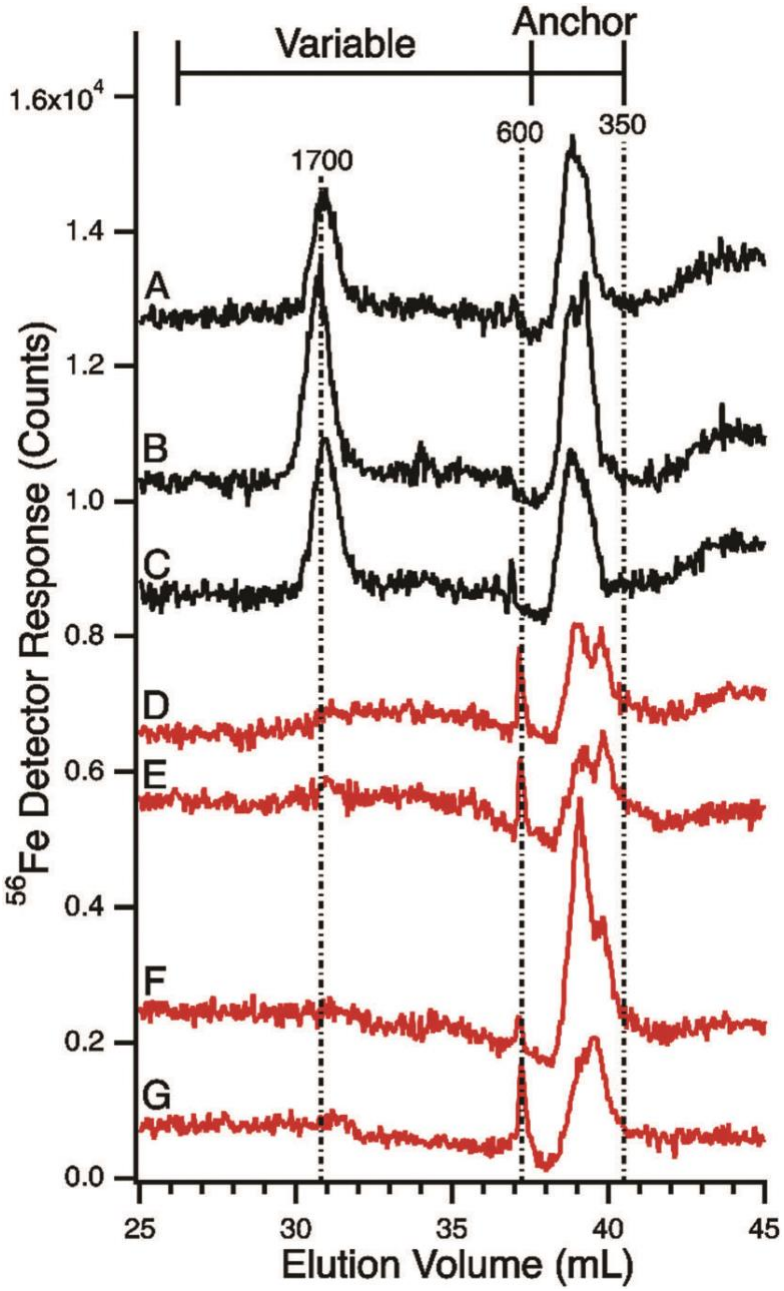


**Figure 2-2: Stability of LMM iron species in plasma and serum.**
$^{56}$Fe-Detected LC-ICP-MS chromatograms of flow-through solutions from horse plasma and serum were run using conditions of Figure 2-2-1. Black lines are Horse 1, red lines are Horse 2. (A) Fresh plasma; (B) frozen plasma; (C) frozen serum; (D) fresh plasma; (E) frozen plasma; (F) same as E but after incubating in a refrigerated glove box for 1 day and then refiltering through the 10 kDa cutoff membrane; (G) same as (F) but after incubating for 9 days. Column conditions as in Figure 2-2-1. Reprinted with permission. [49]

### 2.3.2. LC-ICP-MS traces of ferric citrate at pH 8.5

Given the likelihood that NTBI was ferric citrate, we wondered whether solutions of this complex would afford the same suite of signals as observed for FTSs from plasma/sera. We prepared various solutions of ferric citrate and applied them to our LC column after 24 h of "aging". We used the same conditions as had been used to run the plasma FTSs. Allowing the ferric citrate solutions to ''age'' is important because the kinetics of ferric ions coordinating to citrate is slow.[19,50] Larger oligomers of ferric citrate reportedly develop with aging.[19] Consistent with this, the intensity of a peak at 2500 Da increased after a ferric citrate solution was incubated for 24 h rather than for 30 min (Figure 2-4, traces A *vs.* B).

The molar ratio of iron to citrate also affects which ferric citrate complex(es) is/are generated.[19] Consistent with this, we observed different peaks (at pH 8.5), ranging from 1200–4100 Da, depending on the ratio used (the 4100 Da peak was observed with the 1:10 ratio). Peaks associated with ferric citrate shifted toward lower masses as the iron:citrate molar ratio changed from 1:10 → 1:100 → 1:1000 → 1:10 000 (see Fig. S1 for ratios other than 1:100). Silva *et al.* reported a similar phenomenon.[38] A control trace of 100 mM citric acid alone was devoid of iron intensity (Figure 2-4C). No ferric citrate-associated peaks were observed at 400 or 500 Da regardless of ratio. This suggests that these anchor peaks do not correspond to ferric citrate. On the other hand, at the physiological ratio of 1:100, a 2500 Da peak is observed in both ferric citrate and. occasionally in plasma FLSs. Thus, our results are mixed, providing a modicum of

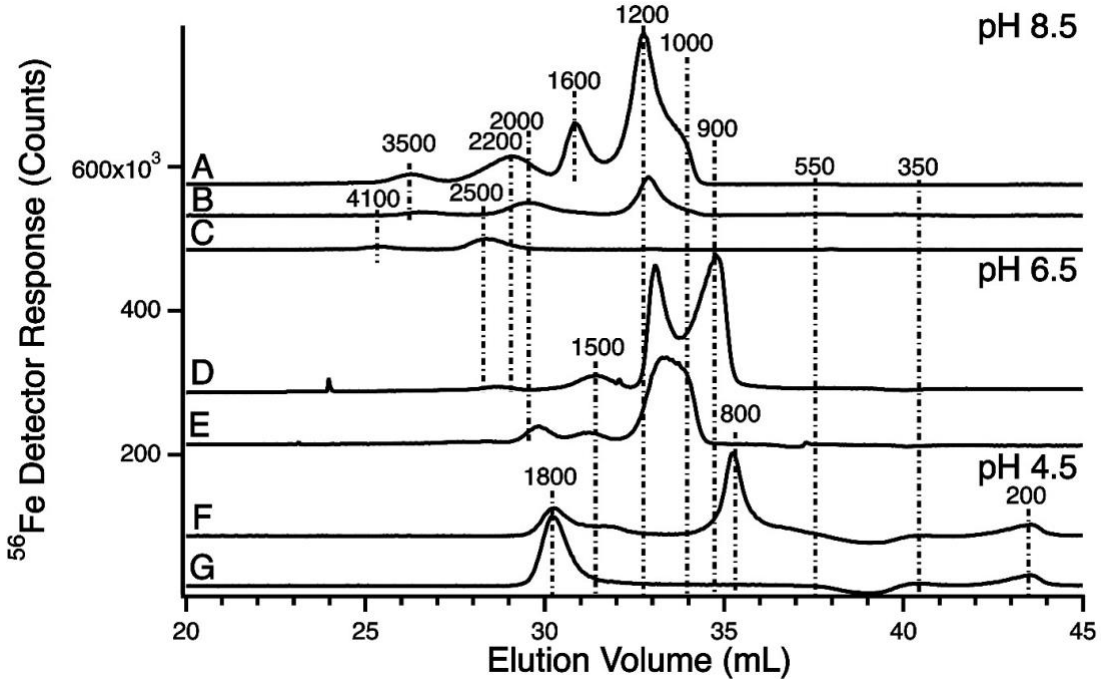


**Figure 2-3: LC-ICP-MS traces of Fe$^{III}$ citrate run at different iron:citrate ratios and different mobile phase pH.**

All traces are of ferric citrate standard solutions which contained 1μM Fe and various concentrations of citrate. A and D, 10 mM citrate; B, E, and F, 1 mM citrate; C and G, 10 μM citrate. Mobile phase pH is indicated. Reprinted with permission.[49]

evidence that the LMM iron in plasma is ferric citrate, but also providing strong evidence that blood plasma contains LMM iron species other than ferric citrate.

### 2.3.3. Iron adsorption onto the column

The combined peak intensities of the ferric citrate traces also varied with iron:citrate molar ratio. The 1:100 solution exhibited strong combined intensity (Figure 2-4A), whereas the 1:10 solution exhibited less intense features (Figure 2-3). When 1 μM $FeCl_3$ was analyzed without any citrate, the chromatograms were devoid of iron intensity, similar to Figure 2-4C. These results imply that some iron adsorbed onto the column. A greater percentage of ferric ions was adsorbed using solutions containing less citrate. Consistent with this, Evans *et al.*[19] reported that at iron:citrate ratios of 1:1 and 1:10, the predominant species in solution is ferric hydroxide which is highly insoluble and liable to adhere to chromatography columns. To some extent, citrate coordination protects ferric ions from being adsorbed.

The concentration of iron-containing complexes that we detected in plasma FTSs corresponded to as little as ~30 nM. This prompted us to evaluate the extent of recovery of ferric citrate standards on the column. Recovery was low, indicating that iron adsorbed onto the column. However, the observed peak elution volumes for the various iron:citrate ratios were reproducible. Others have reported similar iron adsorption on Superdex peptide columns.[51] The adsorption of iron by the column was noticeable because the total amount of iron in our samples was low. A similar extent of adsorption was insignificant for studies involving iron complexes at higher concentrations.[43,44]

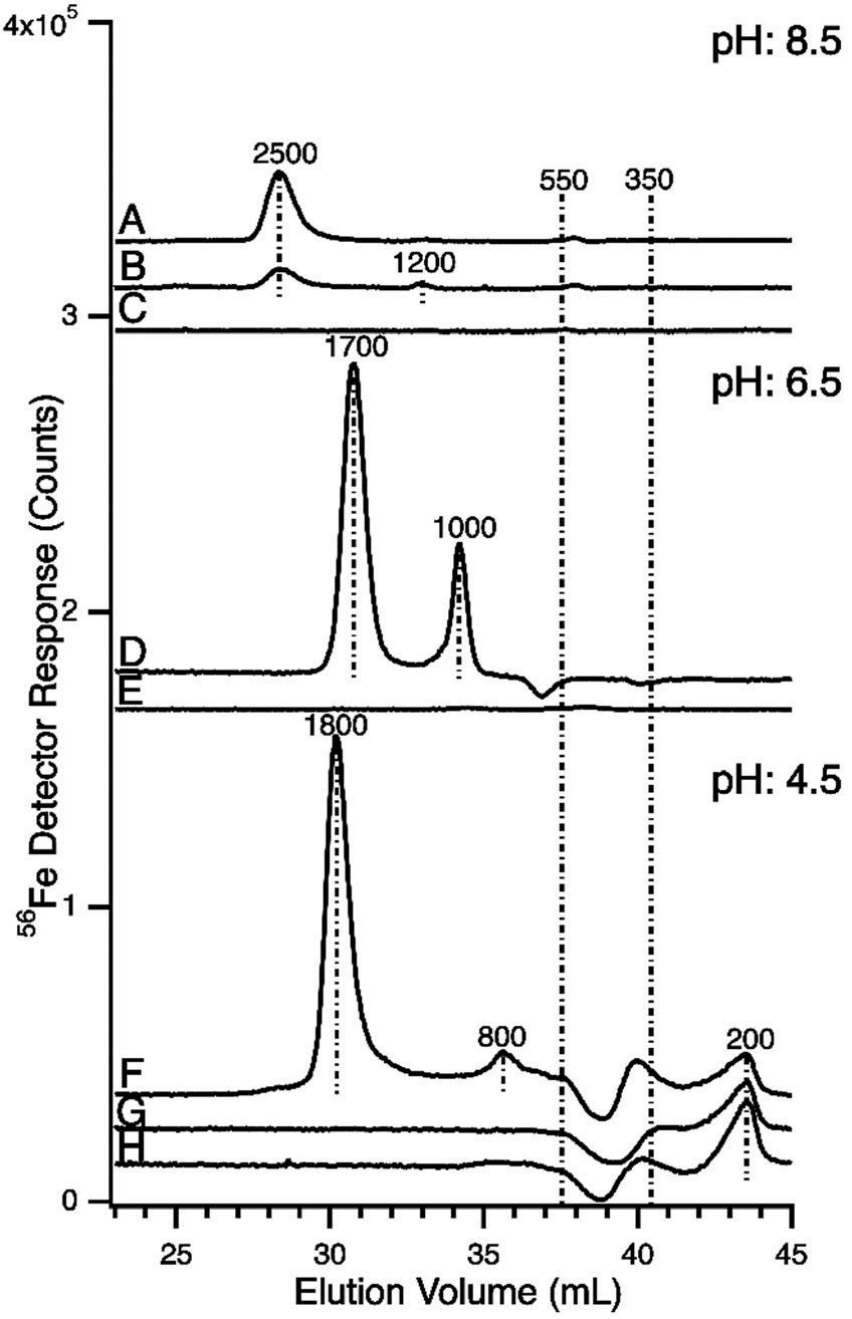


**Figure 2-4: LC-ICP-MS traces of ferric citrate standards.**
Chromatographed at pH 8.5 (A–C), 6.5 (D and E), and 4.5 (F and G). (A, D, and F) were prepared using 1 μM $FeCl_3$, 1:100 iron:citrate ratio, and aged for 24 h; (B) same as A except aged 30 min; (C, E, and H) 100 μM citric acid in 20 mM MOPS pH 7.4 with no iron added; (G) 1 μM $FeCl_3$ with no citrate added. Each injection was 300 μL incubated them for different times. Reprinted with permission.[49]

### 2.3.4. Spiking FTSs with ferric citrate

If the peaks in the anchor region of FTSs were due to ferric citrate, then adding additional ferric citrate (at the 1:100 ratio expected for plasma) should increase the intensities of the same peaks. On the other hand, if the anchor peaks were not due to ferric citrate, then spiking FTSs with ferric citrate would yield peaks of the same apparent masses as observed for ferric citrate solutions (*e.g.* at 2500 and 1200 Da). To examine this, we added 1 μM ferric citrate standard (1:100) to horse and pig FTSs and FTS samples which were incubated at room temp or 8 °C showed no significant chromatographic differences. Regardless of incubation time, the intensities of the anchor peaks were unaffected and new peaks developed at 2400 and 1200 Da (Figure 2-5C and G) relative to the pre-spiked FTS (Figure 2-5D and H). These peaks may have arisen from ferric citrate, but the intensities are very low, precluding any such assignment. This experiment also suggests that the anchor peaks are not due to ferric citrate.

The developed peaks in the spiking experiment were far less intense than expected for spiking FTSs with 1 μM ferric citrate (the same concentration used to generate Figure 2-4A). We speculate that the exposure of ferric citrate to the FTS prompted the partial dissociation of the complex followed by adsorption of some ferric ions onto the column. Our calculations suggest that much of the added ferric citrate adsorbed onto the column; only a modest portion generated the newly developed peaks. This implies that ferric citrate is not particularly stable in plasma FTSs.

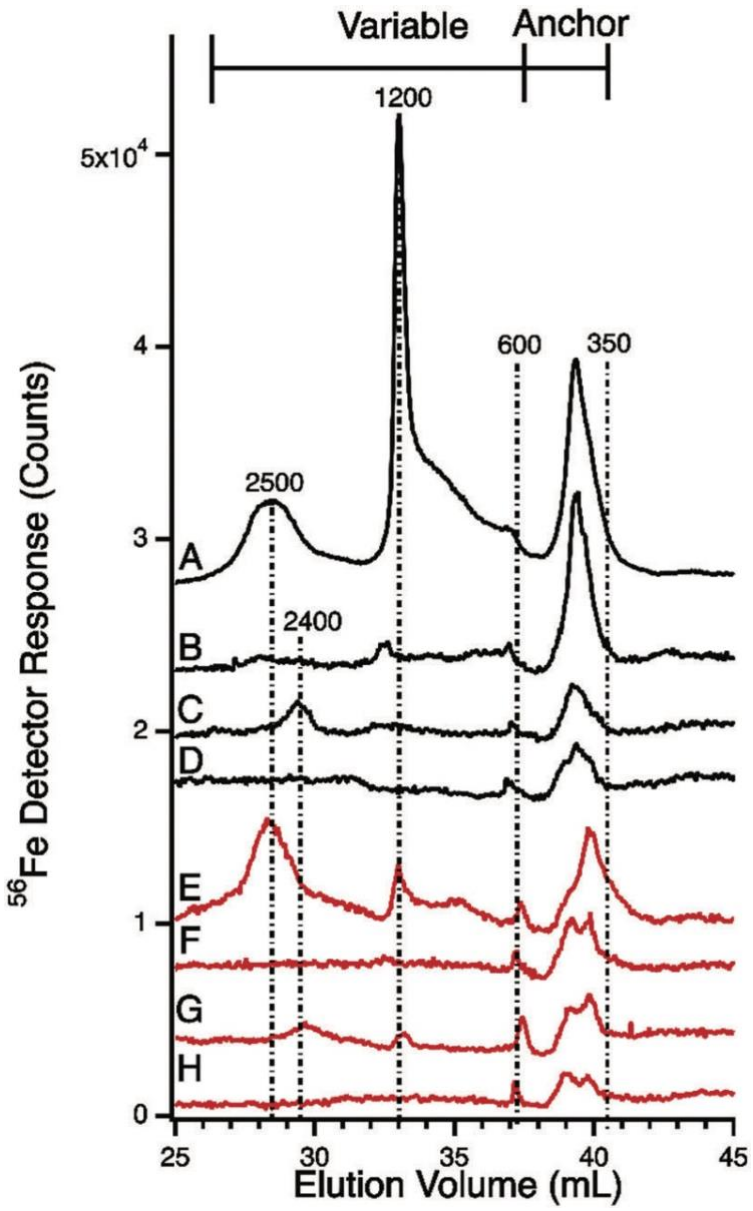


**Figure 2-5: $^{56}$Fe-Detected chromatograms of flow-through solutions of pig serum (black) and horse plasma (red) before and after spiking.**
(A) After spiking with 4 μM $FeCl_3$ (24 h incubation); (B) after spiking with 1 μM $FeCl_3$ (7 h incubation); (C) after spiking with 1 μM $Fe^{III}$ citrate (1:100, 30 min incubation); (D) before spiking; (E) after spiking with 4 μM $FeCl_3$ (24 h incubation); (F) after spiking with 1 μM $FeCl_3$ (7 h incubation); (G) after spiking with 1 μM $Fe^{III}$ citrate (1:100, 24 h incubation); (H) before spiking. Column conditions as in Figure 2-2-1. Reprinted with permission.[49]

### 2.3.5. Spiking FTSs with $FeCl_3$

We next probed the coordinating ability of FTSs by spiking them with 1 or 4 μM $FeCl_3$. The 1 μM spike incubated for 7 h (Figure 2-5B and F) showed little change in the variable region relative to the controls (Figure 2-5D and H). There was an increase in the anchor region peaks for trace B but not for trace F. The 4 μM spike (Figure 2-5A and E) generated variable-region peaks at 2500 and 1200 Da relative to the controls. These traces also exhibited unresolved iron absorption between 1200 and 600 Da. The peak intensities in the anchor region increased in the 4 μM $FeCl_3$ spikes relative to the 1 μM spikes. However, the intensities were still significantly less than expected given the concentration of added iron. Again, we conclude that much of the added ferric ions bound to the column. The low-intensity 1200 and 2500 peaks that developed in the $FeCl_3$ spike may have arisen from the formation of a slight amount of ferric citrate (using the endogenous citrate ions in FTSs), but the observed peak intensity ratio was not as expected if this were the case. Peaks in the anchor region probably arose from other iron complexes.

### 2.3.6. Spiking FTSs with apo-Tf

We next wondered whether the LMM iron complexes in the anchor region would bind apo-Tf or whether these complexes coexist with apo-Tf. To examine this, we spiked plasma FTSs with 4 μM apo-Tf, passed the solution through the LMM column, and collected chromatograms in the LMM and void regions (Figure 2-6, upper and lower panels, respectively). As expected, apo-Tf alone did not exhibit significant peaks in the LMM region (Figure 2-6E), but it did exhibit a holo-Tf peak in the void due to residual

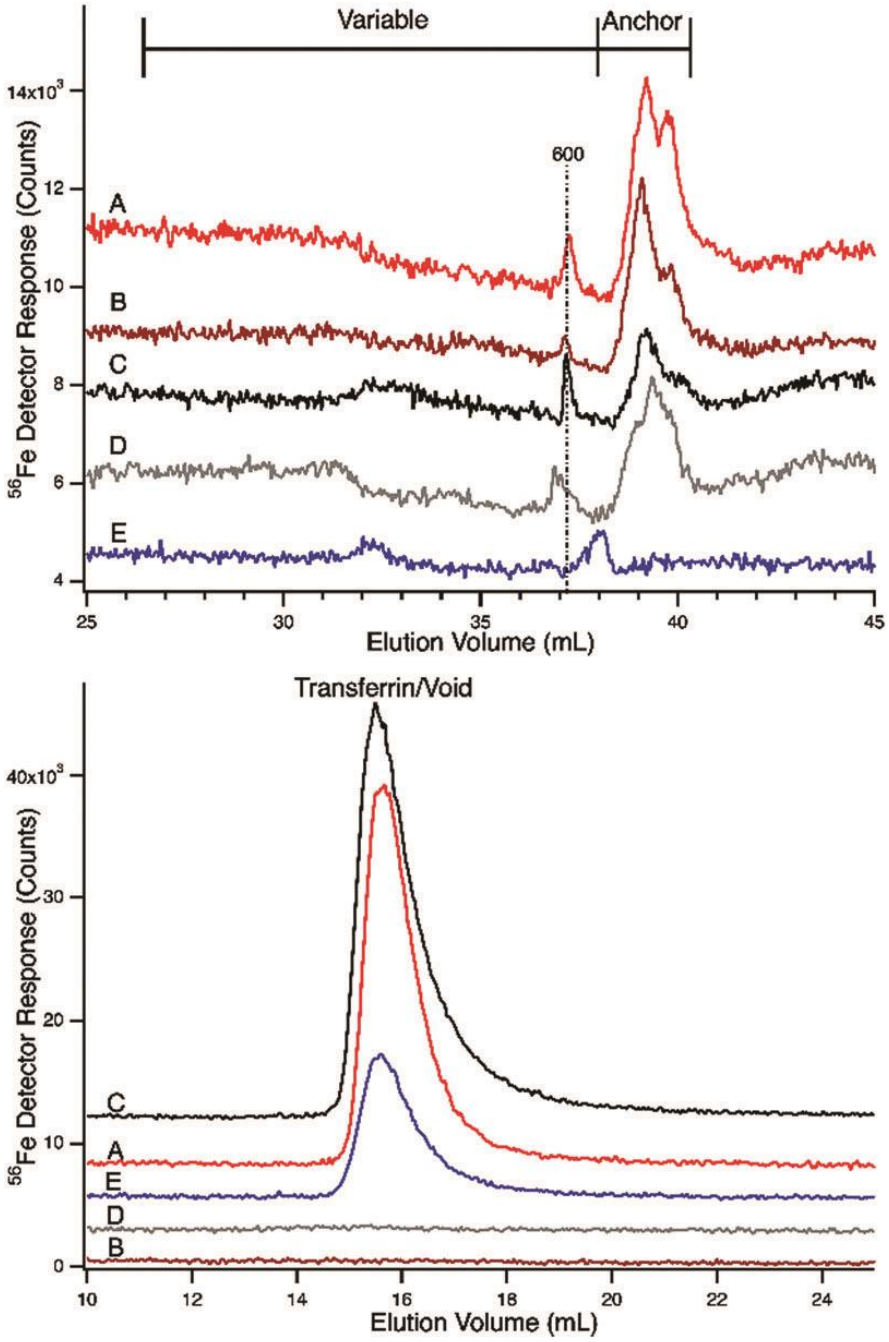


**Figure 2-6: $^{56}$Fe-Detected chromatograms of flow-through solutions from horse plasma (A and B) or pig serum (C and D) before and after spiking with 4 µM apo-Tf.**

Upper panel, the LMM region; lower panel, HMM region (the void volume was at ca. 14 mL). (A) FTS spiked with apo-Tf; (B) FTS before spike; (C) FTS spiked with apo-Tf; (D) FTS before spike; (E) apo-Tf alone. Column conditions were as in Figure. 2-1. Color coding on the top panel matches that on the bottom panel. Reprinted with permission.[49]

binding of endogenous iron. The plasma FTSs without apo-Tf exhibited LMM features in the anchor region but not in the void (Figure 2-6B and D). The anchor peak intensities were essentially unchanged in the traces of the spiked FTSs (Figure 2-6A and C) whereas intense holo-Tf peaks were observed in the HMM region. Our results indicate that apo-Tf coordinates iron in the FTSs but not the iron species associated with the anchor region. The LMM iron complexes associated with the anchor region coexist with the transferrin system. Since LMM peaks in the variable region were not observed in this particular experiment, it remains possible that apo-Tf binds iron associated with variable region peaks.

A similar experiment was performed using the HMM column in which proteins are resolved. Again, there was an increase in the intensity of the holo-Tf peak when apo-Tf was added to FTS (Figure 2-7C). This indicates that the added apo-Tf coordinated some iron in the FTS. The experiment of Figure 2-6 indicates that this is not the iron associated with the observed LMM iron-containing anchor species. Apo-Tf probably bound iron that would have otherwise been adsorbed on the column.

### 2.3.7. LC-ICP-MS traces of HMM species in plasma

The HMM column resolves holo-Tf and other iron-containing proteins in plasma, including ferritin, haptoglobin (complexed with hemoglobin), albumin, and hemopexin (bound with heme). The HMM region of plasma was dominated by holo-Tf and a neighboring partially-resolved species assigned to iron-bound albumin (Figure 2-8C–L). Minor variable-intensity peaks eluting between 9 and 11 mL may have arisen from the haptoglobin: hemoglobin complex and/or from ferritin (Figure 2-8B). The species

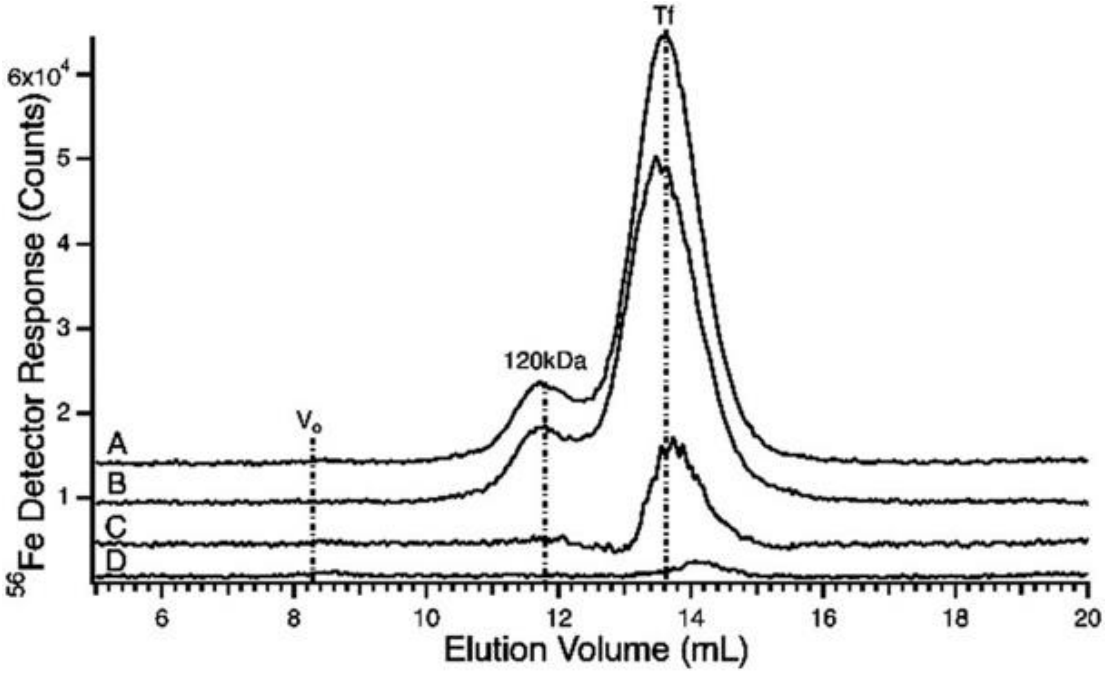


**Figure 2-7: $^{56}$Fe-Detected chromatograms of pig serum flow-through solutions spiked with 4 μM apo-Tf using the HMM column using 20 mM ammonium bicarbonate pH 8.5 mobile phase.**

(A) Pig serum FTS spiked with apo-Tf; (B) 4 μM apo-Tf alone; (C) difference between traces A and B; (D) pig serum FTS alone. Reprinted with permission.[49]

around 12 mL elution volume, evident in some traces, probably arose from a high-mass form of transferrin (Figure 2-8A, peak at 120 kDa).

### 2.3.8. Plasma traces after spiking with $^{57}$ferric citrate and $^{57}FeCl_3$

We performed two spiking experiments to evaluate whether $^{57}$Fe citrate and/or $^{57}FeCl_3$ could bind these iron-related proteins. In one experiment, we added 4 μM $^{57}Fe^{III}$ citrate (1:100 molar ratio) to fresh horse plasma and incubated for 30 min. The sample exhibited a far more intense $^{57}$Fe-bound transferrin/ albumin peak than the control (Figure 2-9, top panel, A *vs.* C). It also exhibited more intense $^{57}$Fe peaks in the LMM region and a peak corresponding to a mass of *ca.* 20 kDa (Figure 2-9, top panel, A *vs.* C). We have not assigned the 20 kDa species but assume that it is proteinaceous. The corresponding $^{56}$Fe-detection traces were essentially unchanged by the spike (Figure 2-9, lower panel). This confirms that most of the added $^{57}Fe^{III}$ citrate bound to apo-Tf and albumin. Some of that iron became associated with the unknown 20 kDa protein, and a small portion remained as LMM species. These results show that there is no specific or dedicated ferric citrate binding site on apo-Tf. The iron from ferric citrate can bind to many proteins.

The other $^{57}$Fe spiking experiment was performed by incubating fresh plasma with 4 μM $^{57}FeCl_3$ for 30 min, followed by passage down the column. The resulting $^{57}$Fe trace (Figure 2-9, upper panel, B) was intermediate in intensity between the control and the $^{57}Fe^{III}$ citrate spike. This demonstrates that $^{57}FeCl_3$ can also bind apo-Tf and albumin (but curiously not the 20 kDa protein). The kinetics of binding to these proteins may be

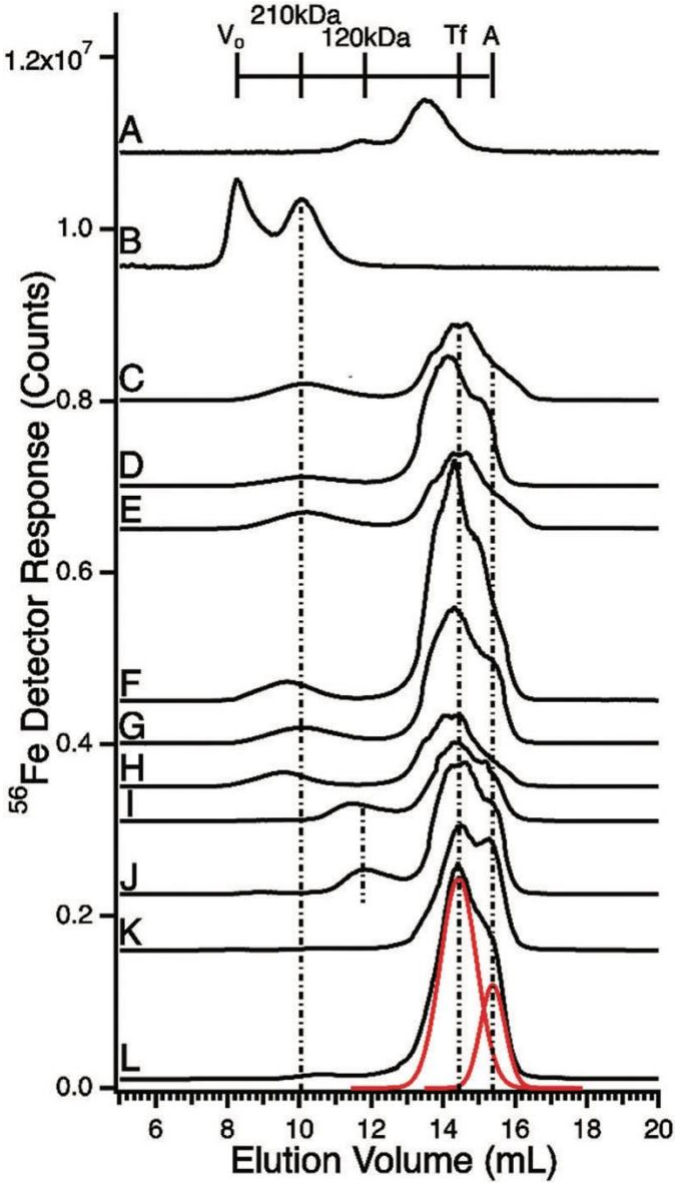


**Figure 2-8: LC-ICP-MS($^{56}$Fe) chromatograms of plasma from humans, horses, and mice.**

(A) Transferrin standard; (B) ferritin standard; (C) human control (steak); (D) human control (fasting); (E) hemochromatosis patient 1; (F) hemochromatosis patient 2; (G) hemochromatosis patient 3; (H) hemochromatosis patient 4; (I) Horse 1; (J) Horse 2; (K) Mouse 1; (L) Mouse 2. An offset artifact near the top of some peaks, due to switching detector sensitivity, was electronically removed. The transferrin standard in A eluted slightly earlier than transferrin in other samples due to matrix effects of the plasma. Red lines in L are simulations of Tf and albumin peaks. Column conditions were as in Figure. 2-6. Reprinted with permission.[49]

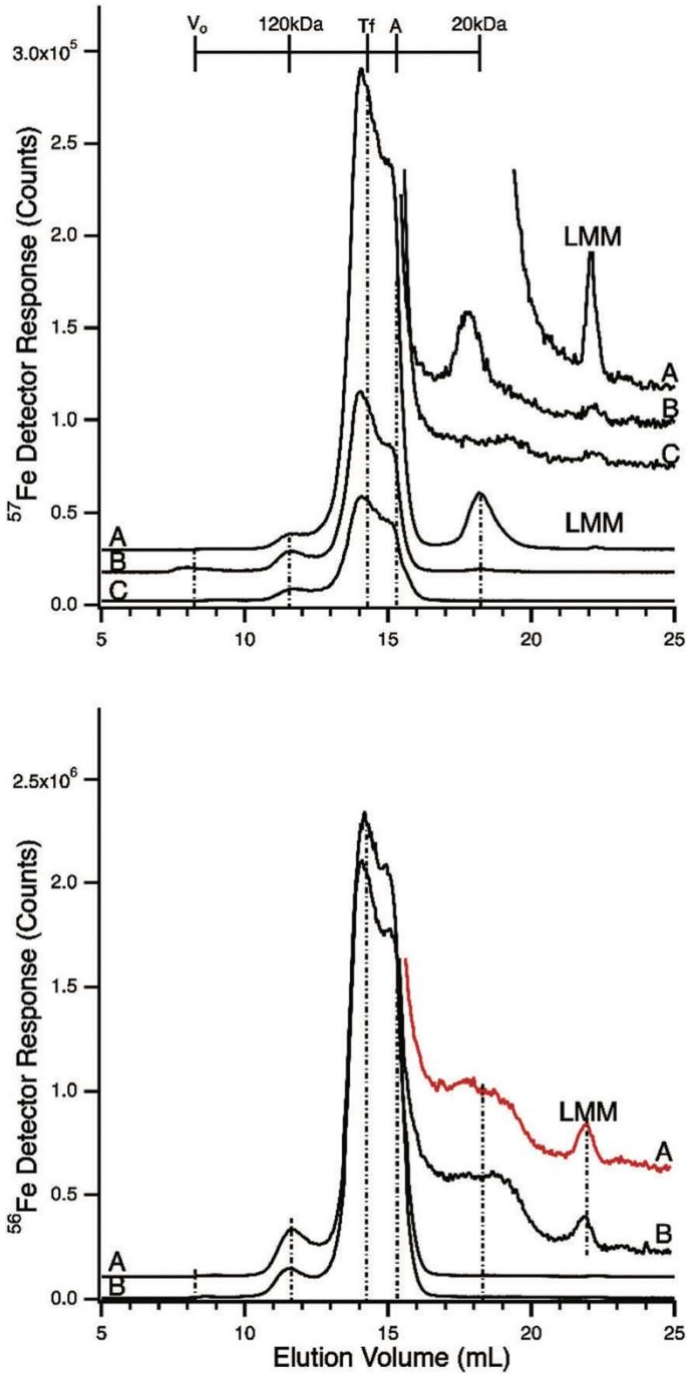


**Figure 2-9: LC-ICP-MS($^{56}$Fe,$^{57}$Fe) chromatograms of horse plasma (and serum) before and after spiking with $^{57}Fe^{III}$ citrate and $^{57}FeCl_3$.**

Top panel, $^{57}$Fe detection: (A) plasma spiked with 4 μM $^{57}Fe^{III}$ citrate (1:100 ratio); (B) plasma spiked with 4 μM $^{57}FeCl_3$; (C) plasma before spike. Dilution factors due to spiking were applied to traces A (1.1) and B (1.7) such that the intensities of all traces can be compared. Samples were incubated in the glovebox for 30 min after spiking. Expected elution volumes for ferritin (*Vo*), the haptoglobin:hemoglobin complex, transferrin, albumin, an unassigned 20 kDa iron-containing protein and LMM complexes are indicated. Inset show details of the LMM region. Bottom panel, $^{56}$Fe detection: (A) plasma before spike; (B) serum before spike. Column conditions were as in Figure 2-7. Reprinted with permission.[49]

slower than that involving ferric citrate.[19] Some $^{57}Fe^{III}$ ions from $^{57}FeCl_3$ may have precipitated from solution and adsorbed onto the column whereas less $^{57}Fe^{III}$ citrate did this (consistent with the stronger LMM peak in the ferric citrate spike *vs.* in the ferric chloride spike; see Figure 2-9, upper panel, inset).

### 2.3.9. LC-ICP-MS traces of the FTSs buffered at pH 6.5

We lowered the pH of the LMM column mobile phase to 6.5 to reduce the amount of iron that adsorbed onto the column.[52] FTSs that were run down the pH 6.5 column did not exhibit peaks at 2500 Da or 1700 Da (Figure 2-10), in contrast to those obtained at pH 8.5. The peak intensities in the anchor regions were similar to those of samples run at pH 8.5. Some traces exhibited a feature at 1100 Da as well as broad incompletely resolved peaks at <300 Da. We refer to these latter iron species as "post-anchor". We conjecture that post-anchor species are related to hexaaqua coordinated iron. Post-anchor iron may adsorb onto the column when buffered to pH 8.5. This form of iron may also bind apo-Tf. We also examined fresh *vs.* frozen-and-thawed FTSs from plasma to evaluate the stability of the detected LMM iron-containing species at pH 6.5. No significant differences were observed (Figure 2-10, traces A *vs.* B).

### 2.3.10. LC-ICP-MS traces of ferric citrate when the column mobile phase was buffered at pH 6.5

To determine whether ferric citrate would run differently at pH 6.5 than at 8.5, we passed 1 μM ferric citrate solutions (using different iron:citrate ratios) through the column buffered at pH 6.5. At the physiological 1:100 ratio, dominant peaks were evident at 1700 and 1000 Da (Figure 2-4D) – somewhat different than those observed at

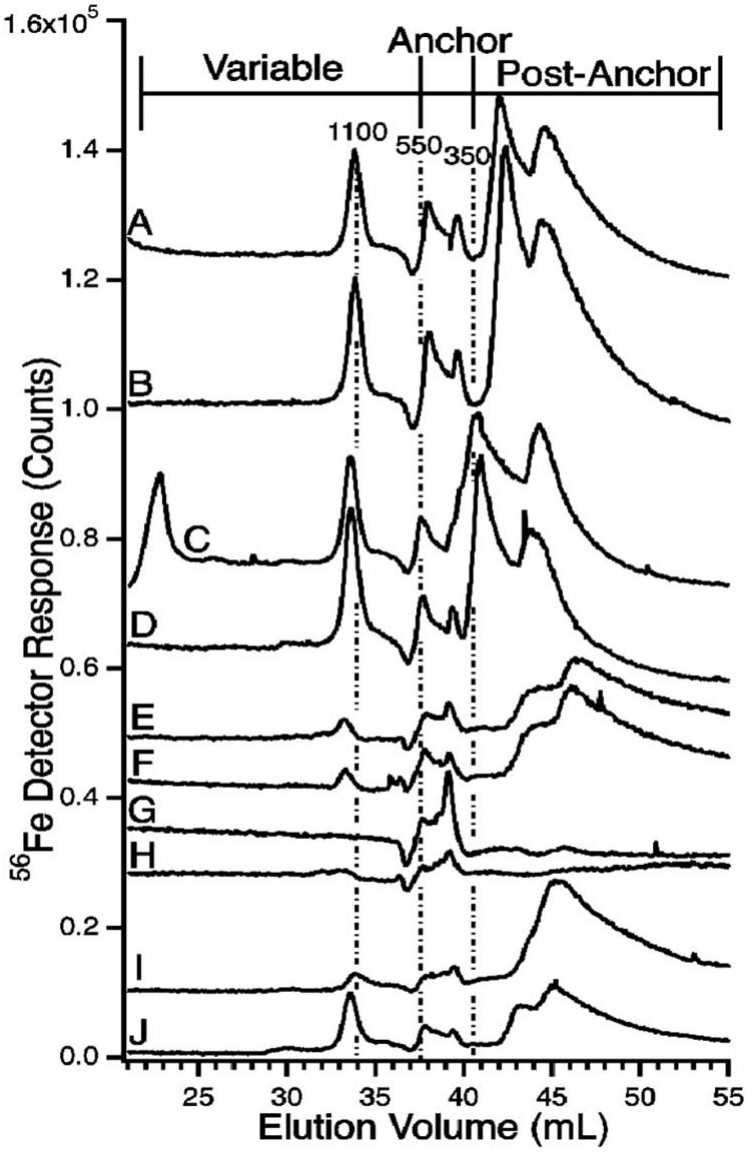


**Figure 2-10: LC-ICP-MS($^{56}$Fe) chromatograms of flow-through solutions using the LMM column and 20 mM ammonium acetate pH 6.5 mobile phase.**
The same samples were used to generate traces in Figure 2-1. All samples were frozen and thawed unless indicated otherwise. Trace labels are as follows: (A) Horse 1 (fresh); (B) Horse 1; (C) Horse 2; (D) Horse 3; (E) human control 1 (fasting); (F) human control 1 (steak); (G) human hemochromatosis patient 1; (H) human hemochromatosis patient 2; (I) human hemochromatosis patient 3; (J) human hemochromatosis patient 4. The minor negative detector response at 37 mL is an artifact associated with low pH mobile phase. Reprinted with permission.[49]

pH 8.5. Similar to the situation at pH 8.5, more iron from the ferric citrate solution bound to the column at iron:citrate ratios of 1:10 than at ratios of 1:100, 1:1000 or 1:10,000. A control of 100 μM citric acid alone was also devoid of iron intensity (Figure 2-4E), indicating that the free ligand was not generating artifact species in the standards. A similar trace was observed for an $FeCl_3$ control.

Ferric citrate at 1:100 ratio was also run through a "ghost" column (*i.e.* peek tubing) to assess sample recovery. There was some iron absorption on the column from ferric citrate at pH 6.5, but much less than at pH 8.5. At pH 6.5 we were able to achieve near full recovery of the ferric citrate standard off the column, but only at physiologically relevant concentrations. More ferric ions must dissociate from citrate at lower citrate concentrations, promoting iron adsorption onto the column. This suggests that the post-anchor iron in FTSs (which represents a significant fraction of total LMM iron in plasma) is not ferric citrate.

We again investigated whether the FTS peak intensities are enhanced when solutions are spiked with ferric citrate or $FeCl_3$. Plasma FTSs were spiked with 4 μM ferric citrate (1:100 ratio) and run down the column equilibrated at pH 6.5. The LMM trace was dominated by peaks at 3500, 1500, and 1000 Da (Figure 2-11A). The 1000 Da peak was similar to that seen in traces of ferric citrate solutions (Figure 2-4D), while the broad 1500 Da peak migrated differently than the 1700 Da peak in ferric citrate solutions. Neither peak was observed in the control FTSs (Figure 2-11C). These results again suggest that ferric citrate is not the dominant LMM iron complex in plasma.

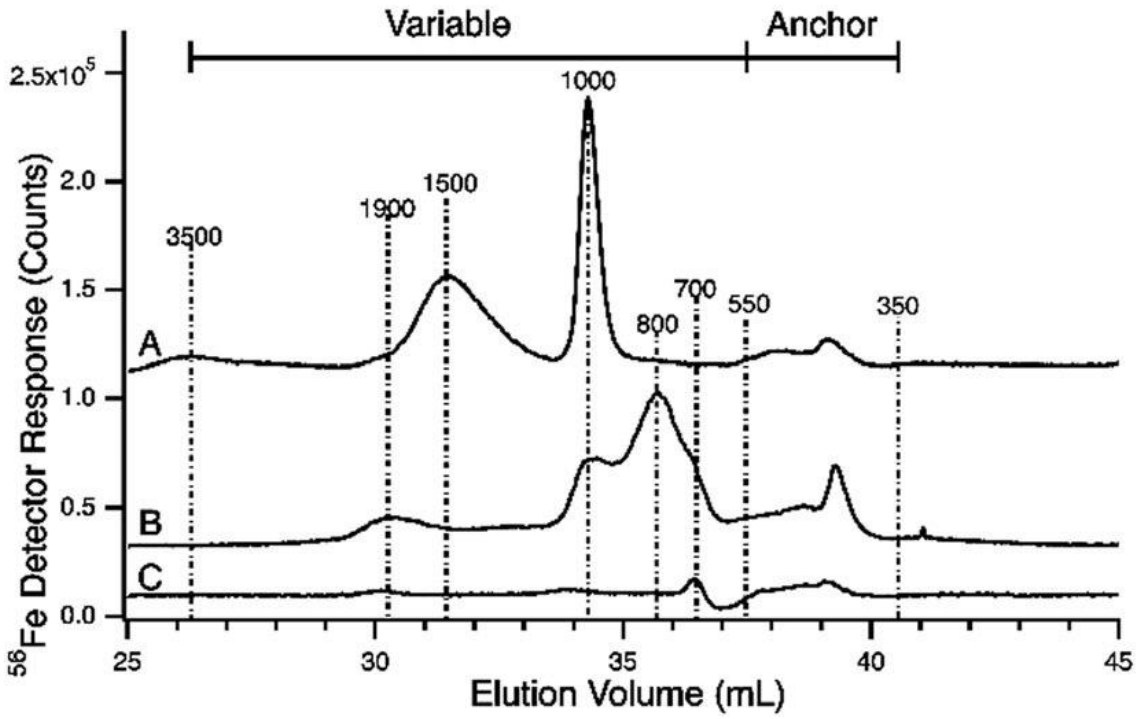


**Figure 2-11: LC-ICP-MS($^{56}$Fe) chromatograms of pig serum flow-through solutions in which the mobile phase was 20 mM ammonium acetate pH 6.5.**
(A) After ferric citrate spike (4 μM, 1:100 ratio); (B) after $FeCl_3$ spike (4 μM); (C) before spikes. The minor negative detector response at 37 mL is an artifact associated with low pH mobile phase. Reprinted with permission.[49]

We also spiked FTSs with 4 μM $FeCl_3$ and ran the resulting solution down the column buffered at pH 6.5. The resulting trace exhibited peaks at 1900, 1000, 800, and 400 Da (Figure 2-11B). The species at 1000 Da was similar to the major peak observed in the previous spike. The species at 400 Da comigrated with anchor region species.

### 2.3.11. LC-ICP-MS traces of FTSs and ferric citrate solutions when the column was buffered at pH 4.5

We ran plasma FTSs down the LMM column buffered at pH 4.5 to more completely explore the effect of pH on the observed peaks. Peaks were observed at 1000, 800, 700, 550, 400, and 350 Da, albeit with some sample variation (Figure 2-12). There was also a broad but reproducible absorption in the post-anchor region. The decline in detector response at *ca.* 38 mL elution volume (causing a depression in the baseline) was associated with the low pH of the mobile phase. The effect was particular to iron, as similar depressions were not observed in traces of other metals (from the same runs). A similar depression was observed in traces of ferric citrate solutions (Figure 2-4F). In these traces, intense peaks were observed at 1800 and 800 Da, with the 1800 Da peak dominating at 1:100 ratios. The 800 Da peak comigrated with a peak of the same approximate mass in the plasma FTSs, but the dominating 1800 Da peak in the ferric citrate traces was absent in FTSs. A control of 100 μM citric acid alone was devoid of iron intensity (Figure 2-4H), indicating that the free ligand was not generating artifact species in the standards. A similar trace was observed for the $FeCl_3$ control (Figure 2-4G). For the ferric citrate standard traces, there was no iron absorption in the post-anchor

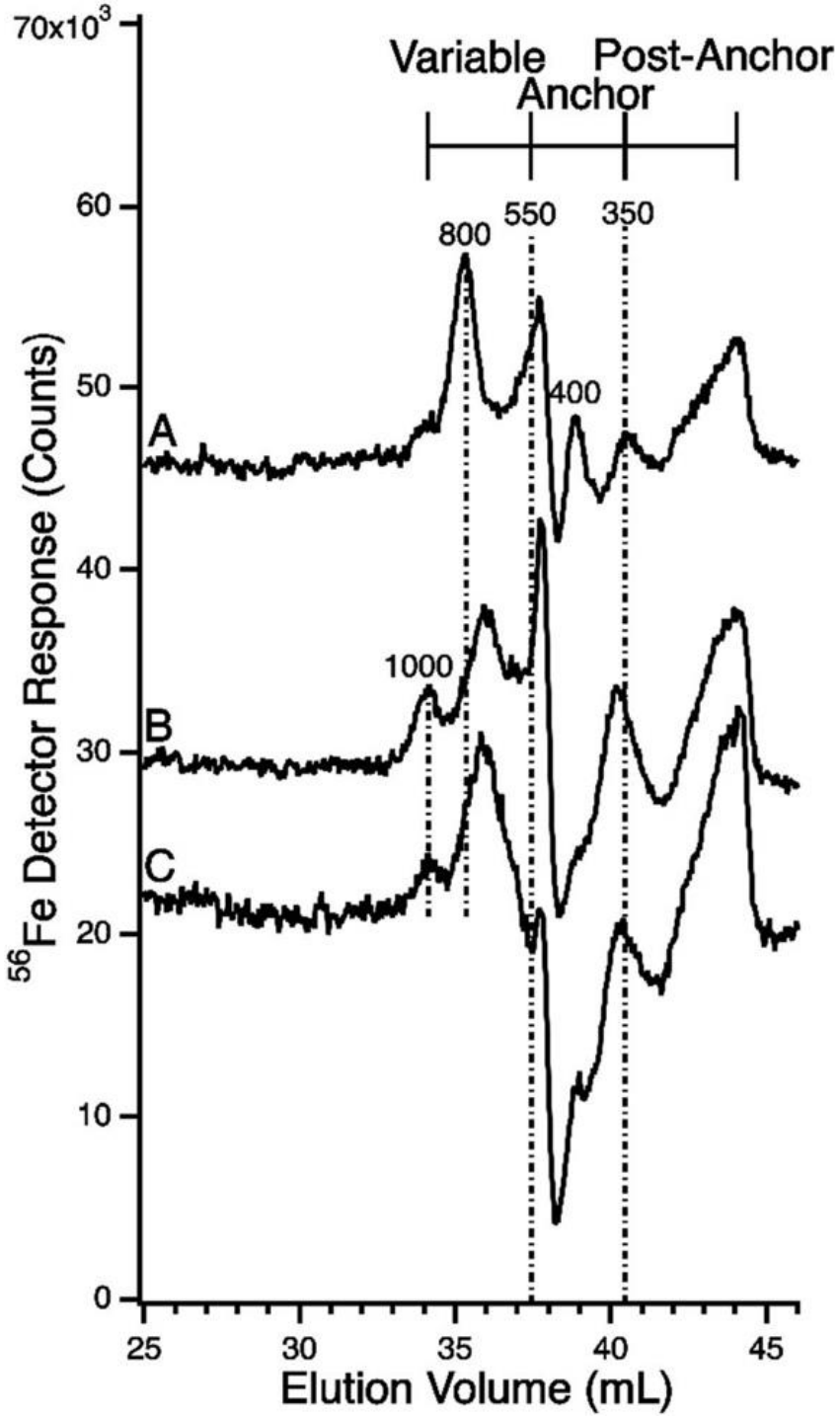


**Figure 2-12: LC-ICP-MS($^{56}$Fe) chromatograms of horse flow-through solutions using the LMM column with 25 mM MOPS pH 4.5 mobile phase.**
All samples were frozen and thawed. (A) Horse 1; (B) Horse 2; (C) Horse 3. Reprinted with permission.[49]

region. This again suggests that the post-anchor iron evident in the FTS traces is not ferric citrate. The absence of $Fe_{1800}$ in the FTSs also suggests the lack of ferric citrate.

**2.4. Discussion**

In this study, we have resolved, for the first time, a half-dozen LMM iron-containing species obtained from blood plasma and sera. The apparent masses of the species ranged from <300 Da to *ca.* 2500 Da. Two species with masses of *ca.* 400 and 500 Da were reliably present in the samples, regardless of column pH, and are referred to as anchors. The presence of the other species, with masses ranging from 600 to 2500 Da, was more variable.

We have not studied the cause of the individual variation of peak intensities systematically, but factors such as the health of the animal may contribute. There were no noticeable differences in samples that were run fresh *vs.* after freezing-and-thawing, or with changes in temperature or incubation time.

We attempted to minimize variations caused by instrumentation. We operated the column in a refrigerated anaerobic glove box to avoid oxidizing soluble $Fe^{II}$ to $Fe^{III}$ and to slow-down ligand exchange processes. Aqueous $Fe^{III}$ ions are far less soluble than aqueous $Fe^{II}$ ions at neutral pH and easily adsorb onto the column. We cleaned the column daily after use with a chelator cocktail, and occasionally ran blank buffer samples to make sure that species of interest for this study were not observed. If significant peaks or rolling baselines were observed, the column was cleaned again until the baselines were flat.

The variability of the peaks did not seem to be strongly affected by nutrient status, though a more systematic study is needed to establish this. The pH 6.5 trace from a healthy human volunteer who ate a 10 oz. steak within an hour of giving blood (Figure 2-10F) was nearly identical to that from the same person after fasting 24 h (Figure 2-10E). At pH 8.5, intensity differences were apparent (Figure 2-1N *vs.* 1O), but further studies are required to evaluate significance.

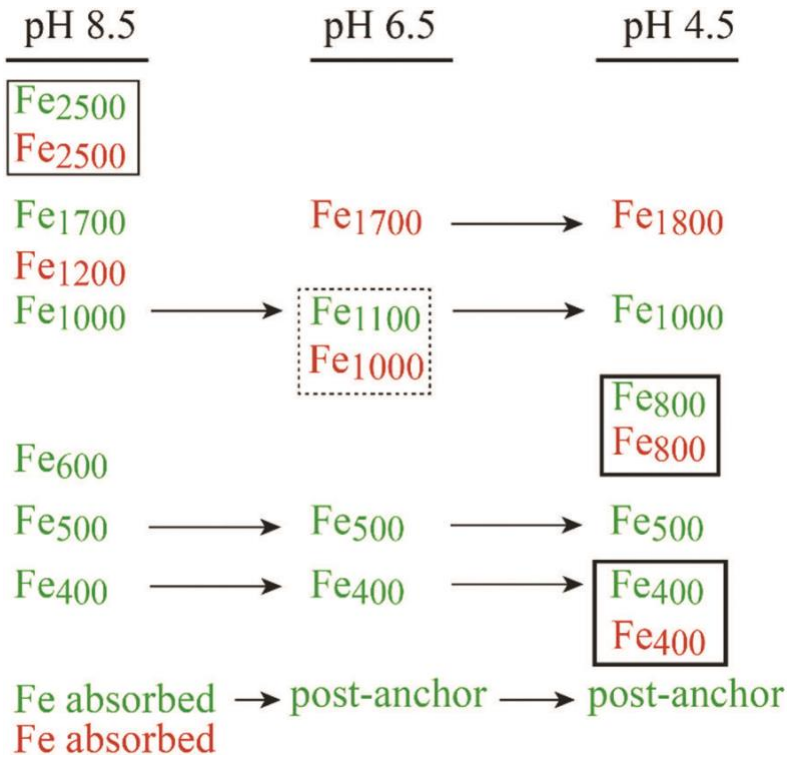


**Figure 2-13: Summary of LMM iron species observed in plasma flow-through solutions (green) and ferric citrate solutions (red) obtaining with different column mobile phase pH.**
Species that comigrate are placed in boxes. The dashed box indicates uncertainty. Species that are observed at more than one pH are designated with arrows. Reprinted with permission.[49]

No differences were evident in humans with hemochromatosis relative to healthy controls. We had expected that traces from such patients would have exhibited either more intense LMM iron peaks or additional peaks that would have either been absent in controls or present at lower intensities. The four patients whose plasma was examined routinely donated blood as a means of controlling their condition, and we suspect that doing so was effective in maintaining low NTBI levels. Perhaps the blood of individuals who have not been treated for the disease would contain additional species or higher concentrations of the observed LMM iron species. However, we were unable to identify such individuals within the timeframe of the study.

The iron concentration in FTSs was *ca.* 1 μM but the collective iron concentration associated with the LMM iron complexes was in the hundreds of nM; a significant portion, also in the hundreds of nM, adsorbed on the column, especially at higher pH. These low-concentration iron-containing species would not have been detectable if not for the high sensitivity of our LC-ICP-MS system. The proportion of iron in the FLS the adsorbed on the column depended on the pH of the mobile phase buffer of the column, with less adsorption at pH's 6.5 and 4.5 than at pH 8.5.

Ferric citrate leads the list of NTBI candidates but the peaks observed in the FTS traces were not obviously the same as in the traces of ferric citrate (run under identical conditions and at the physiologically relevant 1:100 molar ratio). The observed iron species in plasma FTSs and ferric citrate solutions are summarized in Figure 2-13.

Within the variable region, the peaks corresponding to masses of 2500, 1700, 1000, and 600 Da were observed when the column was buffered at pH 8.5. Of these,

$Fe_{1700}$ was the most commonly observed. Under the same conditions, ferric citrate was present as $Fe_{2500}$ (major) and $Fe_{1200}$ (minor). A significant portion of FTS iron and ferric citrate adsorbed onto the column under these conditions.

When the column was buffered at pH 6.5, the most common peak (besides the anchors) in the FTS was $Fe_{1100}$. Also observed were broad peaks in the very low mass "post-anchor" region. Much of this iron adsorbed onto the column at pH 8.5. In contrast, the dominant ferric citrate species under these conditions were $Fe_{1700}$ (major) and $Fe_{1000}$ (minor); no post-anchor iron was observed.

When the column was buffered at pH 4.5, $Fe_{1800}$ was the dominant peak in ferric citrate traces, with minor peaks similar to $Fe_{800}$ and perhaps $Fe_{400}$. FTSs at pH 4.5 did not exhibit the $Fe_{1800}$ peak and had a balanced intensity distribution of *ca.* 4 peaks that included $Fe_{800}$ and $Fe_{400}$ among others. Significant levels of post-anchor iron were also observed. Less ferric citrate iron adsorbed onto the column at the lower pHs, and we conclude that this column-adsorbing/post-anchor form of iron in FTS is probably not ferric citrate. We estimate that this form of iron represents at least half of the iron in the FTS.

Considered collectively, our results do not support the view that ferric citrate is the dominant or even a major LMM iron species in healthy blood plasma or sera. We cannot exclude the possibility that a small proportion of FTS consists of ferric citrate or the possibility that citrate ions are one of many ligands of other LMM iron complexes in FTS. In any event, our results paint a very different picture of the LMM iron in healthy blood plasma – one in which ferric citrate plays a minor role if any.

The conclusion that NTBI is ferric citrate is largely due to a heavily cited study by Grootveld *et al.*[46] Similar to our study, those authors used HPLC to study speciation of NTBI from FTSs of plasma and sera, and they investigated plasma from hemochromatosis patients. Unlike our study, they also examined plasma and FTSs using NMR spectroscopy.

By NMR, Grootveld *et al.* found that the plasma of such patients contained more citrate than that of the healthy controls (*ca.* 400 *vs.* 100 μM). They discovered that the free citrate concentrations increased ~2-fold when a chelator was added to blood plasma. The authors concluded that the iron in the FTS must be bound to citrate and that the free citrate concentration increased because the chelator removed iron from the ferric citrate in plasma. However, even if the chelator removed all of the iron in plasma (measured to be 1–10 mM), the free citrate level would have only increased by a few percent. Thus, their conclusion does not follow from their results. The observed 2-fold increase in the NMR citrate signal intensity upon chelator treatment must have been due to other causes.

Grootveld *et al.* also observed a gradual decline in the free citrate NMR signals when 100–500 μM $FeCl_3$ was added to plasma samples. They reasonably concluded that the added ferric ions coordinated to free citrate, causing paramagnetic broadening. However, the concentration of iron added was 100 to 500 times higher than that present in plasma (and about 100 times higher than that used in our study). Their observation, although real, is not physiologically relevant.

The same authors also determined the HPLC elution volume of ferric citrate and discovered a co-migrating peak in plasma and sera FTSs that increased in intensity when samples were spiked with $FeCl_3$. They concluded that this comigrating peak arose from ferric citrate. Our first concern is that they monitored the absorbance at 340 nm, not by measuring iron directly as we did in our ICP-MS-detected traces. Thus, the peak may or may not have originated from an iron-containing species. Also, they used a reversed-phase LC column in which ferric citrate eluted in the void volume. Other LMM metal complexes might have also eluted in the void and contributed to the same peak. Changing pH, solvent composition, and ionic strength altered the retention times of other detected peaks but not the elution time of the peak attributed to ferric citrate. Grootweld *et al.* regarded this as confirming evidence that the peak arose from ferric citrate. However, if ferric citrate eluted in the void volume, changing properties that affected retention times on the column would probably not affect void peaks.

Grootveld *et al.* reported that ferric citrate and plasma FTSs had overlapping UV-vis spectra, and they used this result to conclude that ferric citrate was the dominant chromophore in FTS. However, the presented spectra were featureless and lacked distinction. Prompted by this, we collected spectra of FTS and ferric citrate (at physiological concentrations and at a 1:100 molar ratio). Spectra of FTSs exhibited more structure than that of ferric citrate (Figure 2-14A–C). From these spectra, we cannot exclude the possibility that FTS contains some ferric citrate but neither do they provide any positive evidence that it does. If FTS contains ferric citrate, it is clearly not the dominant chromophore.

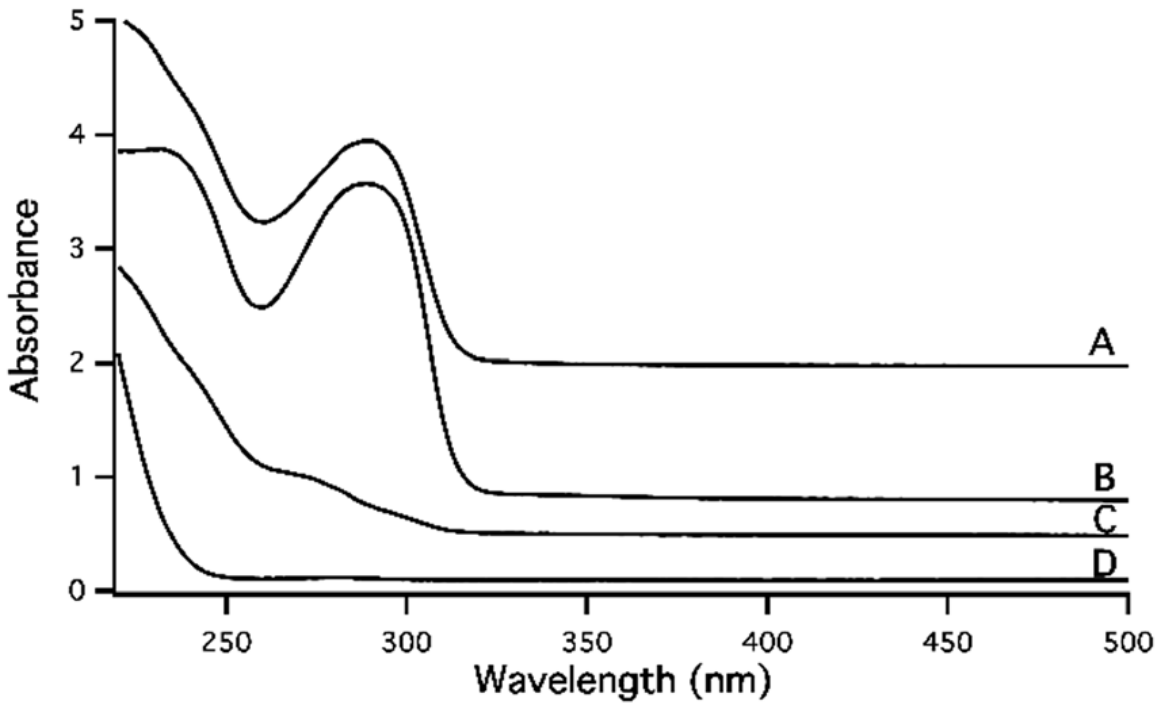


**Figure 2-14: Electronic absorption spectra of plasma flow-through solution and ferric citrate standard at 1:100 iron to citrate ratio.**
(A) Human hemochromatosis patient 4; (B) human control (fasting); (C) Horse 6; (D) ferric citrate solution, prepared using 1 μM $FeCl_3$ and 100 μM citric acid in 20 mM MOPS pH 7.4 samples were aged 24 h prior to collecting the spectrum. Pathlength of the quartz cuvette was 4 mm; plotted absorbance values have been normalized to that which would have been observed using a 1 cm pathlength. Spectra were offset for visualization. Reprinted with permission.[49]

We were also concerned that the HPLC chromatograms of the plasma and ultrafiltrate (what we call FTS) presented by Grootveld *et al.* were nearly identical (in ref. 47, see Figure 2-5 B1 and B2 for the plasma traces and Figure 2-6 for the ultrafiltrate trace). This seems unlikely given the far greater compositional complexity of plasma *vs.* FTSs. Finally, the authors didn't explain (or even comment) why their HPLC traces extended so dramatically below the baseline. We had a similar qualitative problem (for iron at pH 4.5 only) but in their case, the extent to which the traces extended below the baseline was >5-times the ferric citrate peak intensity. In our worst trace, the negative "peak" intensity was equal to that of the above-baseline signals.

We conclude that the Grootveld *et al.*[46] study provides no compelling evidence for the presence of ferric citrate in blood plasma or sera under normal physiological conditions, or in blood from patients with hemochromatosis. Their major conclusion – that plasma NTBI is ferric citrate – simply does not follow from the data presented. Given the problems associated with their experiments, we are surprised that the paper has been cited hundreds of times over the past 30 years without any previous mention of any of these problems.

Other support for the notion that NTBI = ferric citrate comes from thermodynamic calculations which indicate that multiple ferric citrate species should be extremely stable under the conditions in the plasma.[36,37] We have no reason to doubt the veracity of these results, but we reiterate the cautionary comment of Evans *et al.*[19] that thermodynamics is not the only factor that dictates what reaction chemistry is observed. Reaction kinetics can be important, and the kinetics of forming ferric citrate is

surprisingly slow.[19] Given that the iron in the plasma turns-over every few hours,[1] the slow kinetics of ferric citrate formation rather than the thermodynamic stability of the resulting complex may prevent this complex from dominating the LMM iron species in the blood.

The coexistence of the LMM anchor species with apo-Tf contrasts with the view that NTBI in plasma binds extraordinarily tightly to apo-Tf. Assuming the dissociation reaction {holo-Tf ⇄ apo-Tf + NTBI}, the ratio [apo-Tf]/[holo-Tf] = 0.6/0.4, and [NTBI]=0.1 μM, $K_d$ would be ~0.15 mM, which is much weaker than reported.[36,53–56] (Quantitative comparisons may be difficult because different equilibrium expressions were assumed in the cited papers.) In any event, our results show that there are LMM iron complexes in the plasma that can coexist with apo-Tf. Watt and co-workers have found that the binding of phosphate to ferric citrate prevents binding to apo-Tf,[57] and further studies are underway to evaluate whether this could be related to coexistence.

We initially assumed that the LMM iron species detected here originated directly from nutrient iron absorption, but the possibility that they originate from erythrocyte recycling also seems reasonable. Circulating erythrocytes have a 120-day lifespan after which they are degraded by macrophages in the liver (Kuppfer cells) and in the spleen (red pulp macrophages). Heme oxygenase in these macrophages breaks down heme and releases iron (in an unknown form) into the blood where it migrates to the bone marrow for erythropoiesis. Relative to nutrient iron import, erythrocyte recycling involves far more iron with far higher flux rates,[5] and it (rather than nutrient iron import) may control the LMM iron-containing species that we have observed. Conceivably, these

macrophages may release the detected LMM iron species, which are then delivered to the bone marrow to generate new erythrocytes. In this case, the LMM iron species detected here may not be NTBI as we define it in the Introduction, but rather LMM species involved in erythrocyte recycling. Further studies are underway to understand the origin of the detected LMM iron species and to detect the "real" NTBI that is generated exclusively under iron overload conditions.

## 2.5. References


1 T. Ganz, Systemic iron homeostasis, *Physiol. Rev.*, 2013, **93**, 1721–1741.

*2* S. Gulec, G. J. Anderson and J. F. Collins, Mechanistic and regulatory aspects of intestinal iron absorption, *Am. J. Physiol.: Gastrointest. Liver Physiol.*, 2014, **307**, G397–G409.

3 M. D. Knutson, Iron transport proteins: gateways of cellular and systemic iron homeostasis, *J. Biol. Chem.*, 2017, **292**, 12735–12743.

4 M. U. Muckenthaler, S. Rivella, M. W. Hentze and B. Galy, A red carpet for iron metabolism, *Cell*, 2017, **168**, 344–361.

5 H. Drakesmith, E. Nemeth and T. Ganz, Ironing out Ferroportin, *Cell Metab.*, 2015, **22**, 777–787.

6 C. J. Mitchell, A. Shawki, T. Ganz, E. Nemeth and B. Mackenzie, Functional properties of human ferroportin, a cellular iron exporter reactive also with cobalt and zinc, *Am. J. Physiol.: Cell Physiol.*, 2014, **306**, C450–C459.

7 B. K. Fuqua, Y. Lu, D. Darshan, D. M. Frazer, S. J. Wilkins, N. Wolkow, A. G. Bell, J. Hsu, C. C. Yu, H. Chen, J. L. Dunaief, G. J. Anderson and C. D. Vulpe, The multicopper ferroxidase hephaestin enhances intestinal iron absorption in mice, *PLoS One*, 2014, 9, e98792, DOI: 10.1371/journal.pone.0098792.

8 E. Gimenez, F. Benavente, J. Barbosa and V. Sanz-Nebot, Towards a reliable molecular mass determination of intact glycoproteins by matrix-assisted laser desorption/ionization time-of-flight mass spectrometry, *Rapid Commun. Mass Spectrom.*, 2007, **21**, 2555–2563.

9 E. G. Meyron-Holtz, S. Moshe-Belizowski and L. A. Cohen, A possible role for secreted ferritin in tissue iron distribution, *J. Neural Transm.*, 2011, **118**, 337–347.

10 W. Wang, M. A. Knovich, L. G. Coffman, F. M. Torti and S. V. Torti, Serum ferritin: past, present, and future, *Biochim. Biophys. Acta*, 2010, **1800**, 760–769.

11 E. Tolosano, S. Fagoonee, E. Hirsch, F. G. Berger, H. Baumann, L. Silengo and F. Altruda, Enhanced splenomegaly and severe liver inflammation in haptoglobin/hemopexin double-null mice after acute hemolysis, *Blood*, 2002, **100**, 4201–4208.

12 K. Kino, H. Tsunoo, Y. Higa, M. Takami, H. Hamaguchi and H. Nakajima, Hemoglobin-haptoglobin receptor in rat-liver plasma membrane, *J. Biol. Chem.*, 1980, **255**, 9616–9620.

13 M. Kristiansen, J. H. Graversen, C. Jacobsen, O. Sonne, H. J. Hoffman, S. K. A. Law and S. K. Moestrup, Identification of the haemoglobin scavenger receptor, *Nature*, 2001, **409**, 196–201.

14 J. C. Wejman, D. Hovsepian, J. S. Wall, J. F. Hainfeld and J. Greer, Structure of haptoglobin and the haptoglobin-hemoglobin complex by electron microscopy, *J. Mol. Biol.*, 1984, **174**, 319–341.

15 M. R. Langlois and J. R. Delanghe, Biological and clinical significance of haptoglobin polymorphism in humans, *Clin. Chem.*, 1996, **42**, 1589–1600.

16 N. Takahashi, Y. Takahashi and F. W. Putnam, Structure of human hemopexin O-glycosyl and N-glycosyl sites and unusual clustering of tryptophan residues, *Proc. Natl. Acad. Sci. U. S. A.*, 1984, **81**, 2021–2025.

17 D. C. Carter and J. X. Ho, Structure of serum albumin, *Adv. Protein Chem.*, 1994, **45**, 153–203.

18 X. M. He and D. C. Carter, Atomic structure and chemistry of human serum albumin, *Nature*, 1992, **358**, 209–215.

19 R. W. Evans, R. Rafique, A. Zarea, C. Rapisarda, R. Cammack, P. J. Evans, J. B. Porter and R. C. Hider, Nature of non- transferrin-bound iron: studies on iron citrate complexes and thalassemic sera, *J. Biol. Inorg. Chem.*, 2008, **13**, 57–74.

20 R. C. Hider, A. M. N. Silva, M. Podinovskaia and Y. M. Ma, Monitoring the efficiency of iron chelation therapy: the potential of nontransferrin-bound iron, *Ann. N. Y. Acad. Sci.*, 2010, **1202**, 94–99.

21 G. Nicolas, L. Viatte, M. Bennoun, C. Beaumont, A. Kahn and S. Vaulont, Hepcidin, a new iron regulatory peptide, *Blood Cells, Mol., Dis.*, 2002, **29**, 327–335.

22 A. Pietrangelo, Hereditary hemochromatosis: pathogenesis, diagnosis, and treatment, *Gastroenterology*, 2010, **139**, 393–408.

23 A. C. G. Chua, J. K. Olynyk, P. J. Leedman and D. Trinder, Nontransferrin-bound iron uptake by hepatocytes is increased in the Hfe knockout mouse model of hereditary hemochromatosis, *Blood*, 2004, **104**, 1519–1525.

24 C. Hershko and T. E. A. Peto, Non-transferrin plasma iron, *Br. J. Haematol.*, 1987, **66**, 149–151.

25 I. Gosriwatana, O. Loreal, S. Lu, P. Brissot, J. Porter and R. C. Hider, Quantification of non-transferrin-bound iron in the presence of unsaturated transferrin, *Anal. Biochem.*, 1999, **273**, 212–220.

26 P. Brissot, M. Ropert, C. Le Lan and O. Loreal, Non- transferrin bound iron: a key role in iron overload and iron toxicity, *Biochim. Biophys. Acta*, 2012, **1820**, 403–410.

27 P. Brissot, T. L. Wright, W. L. Ma and R. A. Weisiger, Efficient clearance of non-transferrin-bound iron by rat liver: implications for hepatic iron loading in iron overload states, *J. Clin. Invest.*, 1985, **76**, 1463–1470.

28 I. Yanatori, D. R. Richardson, K. Imada and F. Kishi, Iron export through the transporter ferroportin 1 is modulated by the iron chaperone PCBP2, *J. Biol. Chem.*, 2016, **291**, 17303–17318.

29 J. J. Pinilla-Tenas, B. K. Sparkman, A. Shawki, A. C. Illing, C. J. Mitchell, N. N. Zhao, J. P. Liuzzi, R. J. Cousins., M. D. Knutson and B. Mackenzie, Zip14 is a complex broad-scope metal-ion transporter whose functional properties support roles in the cellular uptake of zinc and nontransferrin- bound iron, *Am. J. Physiol.*, 2011, **301**, C862–C871.

30 C. J. Brewer, R. I. Wood and J. C. Wood, mRNA regulation of cardiac iron transporters and ferritin subunits, *Exp. Hematol.*, 2014, **42**, 1059–1067.

31 J. M. C. Gutteridge, D. A. Rowley, E. Griffiths and B. Halliwell, Low-molecular-weight iron complexes and oxygen radical reactions in idiopathic hemochromatosis, *Clin. Sci.*, 1985, **68**, 463–467.

32 F. W. Huang, J. L. Pinkus, G. S. Pinkus, M. D. Fleming and N. C. Andrews, A mouse model of juvenile hemochromato- sis, *J. Clin. Invest.*, 2005, **115**, 2187–2191.

33 L. de Swart, J. C. M. Hendriks, L. N. van der Vorm, Z. I. Cabantchik, P. J. Evans, E. A. Hod, G. M. Brittenham, Y. Furman, B. Wojczyk, M. C. H. Janssen, J. B. Porter, V. E. J. Mattijssen, B. J. Biemond, M. A. MacKenzie, R. Origa, R. Galanello, R. C. Hider and D. W. Swinkels, Second international round robin for the quantification of serum non-transferrin bound iron and labile plasma iron in patients with iron-overload dis- orders, *Haematologica*, 2016, **10**, 38–45.

34 J. B. Porter, R. D. Abeysinghe, L. Marshall, R. C. Hider and R. Singh, Kinetics of removal and reappearance of non- transferrin-bound plasma iron with deferoxamine, *Blood*, 1996, **88**, 705–713.

35 L. C. Konigsberger, E. Konigsberger, P. M. May and G. T. Hefter, Complexation of iron(III) and iron(II) by citrate. Implications for iron speciation in blood plasma, *J. Inorg. Biochem.*, 2000, **78**, 175–184.

36 P. M. May, P. W. Linder and D. R. Williams, Computer simulation of metal ion equilibria in biofluids: models for the low-molecular-weight complex distribution of

calcium(II), magnesium(II), manganese(II), iron(III), copper(II), zinc(II) and lead(II) ions in human blood plasma, *J. Chem. Soc., Dalton Trans.*, 1977, **6**, 588–595.

37 A. Lawen and D. J. R. Lane, Mammalian iron homeostasis in health and disease: uptake, storage, transport, and molecular mechanisms of action, *Antioxid. Redox Signaling*, 2013, **18**, 2473–2507.

38 A. M. N. Silva, X. L. Kong, M. C. Parkin, R. Cammack and R. C. Hider, Iron(III) citrate speciation in aqueous solution, *Dalton Trans.*, 2009, 8616–8625.

39 J. Arezes, M. Costa, I. Vieira, V. Dias, X. L. Kong, R. Fernandes, M. Vos, A. Carlsson, Y. Rikers, G. Porto, M. Ragnel, R. C. Hider and J. P. Pinto, Non-transferrin-bound iron (NTBI) uptake by T lymphocytes: evidence for the selective acquisition of oligomeric ferric citrate species, *PLoS One*, 2013, 8, e79870, DOI: 10.1371/ journal.pone.0079870.

40 E. Cruz, G. Melo, R. Lacerda, S. Almeida and G. Porto, The CD8+ tlymphocyte profile as a modifier of iron overload in HFE hemochromatosis: an update of clinical and immunological data from 70 C282Y homozygous subjects, *Blood Cells, Mol., Dis.*, 2006, **37**, 33–39.

41 E. M. Cardoso, K. Hagen, M. de Sousa and R. Hultcrantz, Hepatic damage in C282Y homozygotes relates to low numbers of CD8+ cells in the liver lobuli, *Eur. J. Clin. Invest.*, 2001, **31**, 45–53.

42 R. M. Graham, A. C. Chua, C. E. Herbison, J. K. Olynyk and D. Trinder, Liver iron transport, *World J. Gastroenterol.*, 2007, **13**, 4725–4736.

43 S. P. McCormick, M. J. Moore and P. A. Lindahl, Detection of labile low-molecular-mass transition metal complexes in mitochondria, *Biochemistry*, 2015, **54**, 3442–3453.

44 S. P. McCormick, M. Chakrabarti, A. L. Cockrell, J. Park, L. S. Lindahl and P. A. Lindahl, Low-molecular-mass metal complexes in the mouse brain, *Metallomics*, 2013, **5**, 232–241.

45 R. J. Simpson, C. E. Cooper, K. B. Raja, B. Halliwell, P. J. Evans, O. I. Aruoma, S. Singh and A. M. Konijn, Non-transferrin-bound iron species in the serum of hypo-transferrinaemic mice, *Biochim. Biophys. Acta*, 1992, **1156**, 19–26.

46 M. Grootveld, J. D. Bell, B. Halliwell, O. I. Aruoma, A. Bomford and P. J. Sadler, Non-transferrin-bound iron in plasma or serum from patients with idiopathic hemochromatosis. Characterization by high-performance liquid chromatography and nuclear magnetic resonance Chem spectroscopy, *J. Biol. Chem.*, 1989, **15**, 4417–4422.

47 M. Chakrabarti, M. N. Barlas, S. P. McCormick, L. S. Lindahl and P. A. Lindahl, Kinetics of iron import into developing mouse organs determined by a pup-swapping method, *J. Biol. Chem.*, 2015, **290**, 520–528.

48 M. Wojdyr, *Fityk*: a general-purpose peak fitting program, *J. Appl. Crytallogr.*, 2010, **43**, 1126–1128.

49 N. Dziuba, J. Hardy and P. A. Lindahl, Low-molecular-mass iron in healthy blood plasma is not predominately ferric citrate, *Metallomics*, 2018, **10**, 802–817.

50 G. W. Bates, C. Billups and P. Saltman, The kinetics and mechanism of iron(III) exchange between chelates and transferrin, *J. Biol. Chem.*, 1967, **242**, 2810–2815.

51 P. Flis, L. Ouerdane, L. Grillet, C. Curie, S. Mari and R. Lobinski, Inventory of metal complexes circulating in plant fluids: a reliable method based on HPLC coupled with dual element and high-resolution molecular mass spectrometric detection, *New Phytol.*, 2016, **211**, 1129–1141.

52 T. Imamura and H. Kawamoto, Preparation of iron(III) sugar complexes, *J. Fac. Fish. Anim. Husb., Hiroshima Univ.*, 1974, **13**, 181–188.

53 F. Bou-Abdallah and T. R. Terpstra, The thermodynamics and binding properties of the transferrins as studied by isothermal calorimetry, *Biochim. Biophys. Acta*, 2012, **1820**, 318–325.

54 R. B. Martin, J. Savory, S. Brown, R. L. Bertholf and M. R. Wills, Transferrin binding to $Al^{3+}$ and $Fe^{3+}$, *Clin. Chem.*, 1987, **33**, 405–407.

55 P. Aisen, A. Leibman and J. Zweier, Stoichiometric and site characteristics of binding of iron to human transferrin, *J. Biol. Chem.*, 1978, **253**, 1930–1937.

56 W. R. Harris, in *Iron chemistry in molecular and cellular iron transport*, ed. D. M. Templeton, Marcel Dekker Inc., New York, 2002, pp. 1–40.

57 S. Matias, D. W. Belnap, M. T. Smith, M. G. Stewart, I. F. Torres, A. J. Gross and R. K. Watt, Citrate and albumin facilitate transferrin iron loading in the presence of phosphate, *J. Inorg. Biochem.*, 2017, **168**, 107–113.

# 3. LOW-MOLECULAR MASS IRON COMPLEXES IN BLOOD PLASMA OF IRON-DEFICIENT PIGS DO NOT ORIGINATE DIRECTLY FROM NUTRIENT IRON†

## 3.1. Introduction

The majority of iron in humans is found in erythrocytes as iron-containing heme centers, but this transition metal is also essential for many metalloenzymes and processes as diverse as mitochondrial energetics and DNA replication. Approximately 1 mg of iron enters the body daily through the diet, whereas ~25 mg of iron is recycled.[1] Circulating erythrocytes have a 120 day lifespan after which they are degraded by Kuppfer macrophages in the liver and red pulp macrophages in the spleen. Heme oxygenase then degrades heme groups and releases iron into the blood where it migrates to the bone marrow for erythropoiesis.

Nutrient-derived $Fe^{II}$ ions are imported into the blood through ferroportin (FPN), a membrane-bound protein on the basolateral surface of enterocytes that line the intestinal duodenum.[1-3] Also on that surface is hephaestin (HPN), a membrane-bound multicopper oxidase that catalyzes the $O_2$-dependent oxidation of $Fe^{II}$ to $Fe^{III}$.[4] Ceruloplasmin (CPN) is a soluble multicopper oxidase in the blood that catalyzes the same reaction. The resulting nutrient-derived $Fe^{III}$ species are released into the PV and ultimately bind apo-transferrin

†Reproduced and adapted by permission from The Royal Society of Chemistry. "Low-molecular-mass iron complexes in blood plasma of iron-deficient pigs do not originate directly from nutrient iron" by Nathaniel Dziuba, Joanne Hardy, and Paul A. Lindahl, 2019. *Metallomics,* Copyright 2019 by Royal Society of Chemistry. https://doi.org/10.1039/c9mt00152b

(apo-TFN), an 80 kDa glycoprotein in blood that serves as an iron buffer. The chemical nature of the iron species that are exported into the blood prior to coordination by apo-TFN is unestablished but it is presumed to be nonproteinaceous and LMM.

Nutrient iron import is regulated by hepcidin.[1–3] The binding of hepcidin to FPN promotes the degradation of FPN which prevents excessive influx of iron. Individuals with the iron-overload disorder hereditary hemochromatosis generate insufficient hepcidin such that excessive iron enters the blood. In this case, TFN approaches saturation (100% holo-TFN).[5] The spillover hypothesis maintains that once TFN is saturated, further iron enters the blood as one or more toxic complexes called nontransferrin-bound-iron or NTBI.[5–8] $Fe^{III}$ citrate leads the list of NTBI candidates as the concentration of citrate in blood is high and $Fe^{III}$ citrate is stable.[9–11] NTBI is often defined operationally as the labile iron pool in blood plasma that is chelated by a particular chelator under specified conditions. This is not ideal because different assays afford different estimates of NTBI.[12]Moreover, such assays preclude the possibility of speciating NTBI or identifying its ligands since labile iron complexes are destroyed during their detection.

Blood contains numerous iron-bound proteins besides TFN, none of which is NTBI. Haptoglobin and hemopexin bind free hemoglobin and heme in the blood, respectively.[13,14] The resulting complexes are internalized by macrophages and catabolized by the liver.[15,16] Albumin is the most abundant blood-plasma protein.[17] It reversibly binds iron but not tightly.[18–20] Serum ferritin is produced and secreted by spleen and liver macrophages, and perhaps by kidney proximal tubule cells.[21–23] Unlike intracellular ferritin, serum ferritin is

not heavily loaded with $Fe^{III}$ oxyhydroxide aggregates in its central core.[23,24] Some cells have receptors for serum ferritin, which may be involved in inflammation.[25,26]

NTBI analogs are rapidly and quantitatively absorbed by *Zip14* receptors on the plasma membrane of hepatocytes in the liver.[27–29] This organ also releases iron as needed and serves as an iron buffer. Livers of untreated hemochromatosis patients accumulate massive amounts of iron. Once the liver is iron-loaded, NTBI is absorbed by the heart and other organs, which is damaging.[30,31]

NTBI actually develops more gradually than the spillover hypothesis implies. High concentrations of NTBI have been reported in plasma in which TFN was <45% saturated.[8,32] HFE(−/−) mice, which suffer from hemochromatosis, accumulate hepatic iron even when circulating TFN is partially saturated.[4,33] TFN in 4 week old HFE(−/−) mice was only 68% saturated but the Fe concentration in their livers was 3-times normal.[34] These results imply that NTBI levels increase gradually when TFN exceeds ~40% saturation. The concentration of NTBI in healthy plasma is low – only *ca.* 100 nM.[35,36] NTBI concentrations in the plasma of WT and HFE(−/−) mice were 1.5 and 3.7 μM, respectively.[6] In iron-overload diseases, the concentration of NTBI in plasma is 5–10 μM.[19,30,37]

We recently detected a half-dozen low-intensity iron-associated peaks in chromatograms of flow-through solutions (FTSs) of plasma from pigs, horses, mice, and humans with and without hemochromatosis. The masses of these species ranged from 400–2500 Da.[38] We initially assumed that they were NTBI, but their chromatography properties differed from that of $Fe^{III}$ citrate. Also, there were no significant differences between the plasma of healthy individuals and those with hemochromatosis. Plasma iron concentrations

were ~1 μM, with each iron-containing species representing a few hundred nM. As a result of that study, we hypothesized that the concentrations of the LMM iron-containing species would have been higher, or additional peaks would have been observed, if the animals from which blood was drawn had eaten an iron-rich meal just prior to blood sampling AND if blood had been sampled from the PV rather than from the general circulation. We considered that the liver may have absorbed most NTBI generated after a meal and so we may not have detected this species in general circulation blood.

We designed an experiment to test these hypotheses in which catheters were surgically implanted into the PV, caudal vena cava (CAV), and/or cranial vena cava (CRV) of healthy iron-deficient pigs. Blood from these catheters was removed at various times after $^{57}$Fe, a stable isotope that constitutes just 2% of natural-abundance iron, was injected into the stomach. Isotope tracing with $^{57}$Fe allowed us to identify peaks associated directly with nutrient $^{57}$Fe absorption. Blood containing nutrient iron from the intestines and removed from the PV did not pass through the liver. According to our hypothesis, such blood should contain high levels of $^{57}$Fe-labeled NTBI. Our objective was to detect NTBI directly using liquid chromatography and ultimately determine its chemical composition. Although this objective was not met, our results afford new insights into the iron composition of blood.

### 3.2. Experimental Procedures

#### 3.2.1. Pig Acquisition and Maintenance

All experiments involving pigs were approved by Texas A&M University (IACUC 2015-0034 and 2018-0204). Four female Yorkshire pigs (*Sus scrofa domesticus*) weighing ca. 18 - 23 kg were purchased locally, one at a time. Upon arrival

at TAMU, pigs 1, 2, 3 and 4 (named P1, P2, P3, and P4) were placed on an iron-deficient swine diet (Envigo Inc. Rx 2096077; TD.150728) and quarantined 3 wk in a relatively iron-deficient pen with a cement floor and aluminum bars. P2 arrived with a minor abscess on its right rear leg which was treated with topical ointment and allowed to heal completely, as determined by veterinary staff at TAMU, prior to use in this study. P2 was fed the iron-deficient diet for 3 weeks, identical to the other animals. P1, P2, and P3 were conditioned to be comfortable with humans through daily interactions. P4 was additionally trained to be suspended in a custom-built neoprene-coated nylon (McMaster-Carr) sling for extended periods.

### 3.2.2. Surgery and Recovery Procedures

Pigs were placed under general anesthesia, and a feeding tube was installed into the stomach, a polyethylene catheter was installed into the PV, and an identical catheter was installed into either the CAV (P2 and P3) or the CRV (P1), using a procedure similar to that described.[39,59,60] For P4, a venous-access port (VAP, ClearPort Max, Access Technologies, Skokie, IL) was installed in the PV and CAV.

The PV catheter was placed caudal to the bifurcation of the two branches leading into the liver.[61] The distal end of the catheter exited the abdomen and was secured to the neck of the animal for sampling. The CAV catheter was inserted in the femoral vein and advanced into the caudal vena cava.[39] The distal end of the catheter was secured to the animal's back for sampling.

### 3.2.3. Additional Surgical Details

Prior to surgery, the animals are induced with 2.2-6.66 mg/kg tiletamine/zolazepam (Telazol, Zoetis, Florham Park, NJ) intramuscularly. The animals are then intubated and placed on an isoflurane anesthesia. When the animal was under a surgical plane of anesthesia the surgeries were performed.

*Caudal Vein:* The right external jugular vein was exposed and isolated and a ligature was placed cranial to the proposed catheter insertion site using a 3-0 polydioxanone suture (PDS). A 2 mm incision was made in the right external jugular vein. A 1.57 mm OD polyethylene catheter (catheter-only) or a silicone catheter (VAP) was inserted into the vein and advanced 9-10 cm distally. The catheter was secured in place using a Chinese finger trap suture. The catheter was tunneled subcutaneously leaving several loose bends (to allow for growth of the pig). The catheter was flushed with heparinized saline (100IU/mL). If a catheter-only or a VAP was used, then the following procedure was performed.

For the animals with only a catheter, the tubing was made to exit the skin through a separate 1 cm incision inside the 2 cm-lateral to the original incision. The jugular incision was closed in two layers using 2-0 Vicryl in a continuous pattern and 0.4 mm Vetafil. The small tubing exit incision was closed with 0.4 mm Vetafil in a continuous pattern and an adhesive bandage was placed over the incisions. A blunt 18-gauge needle was inserted into the end of the tubing and attached to an injection cap for flushing and blood draws and flushed with saline.

To insert the VAP, a 5-6 cm curvilinear incision was made just in the mid-cervical region. Subcutaneous tissue was undermined to create a pocket for the port. The catheter and the port were connected, and the port was secured to the underlying musculature using a 3-0 **PDS.** The VAP was tested via a blood draw before closure. The port and catheter were flushed with heparinized saline and locked with locking solution. Subcutaneous tissues were closed with 3-0 PDS. The skin was closed in an intradermal pattern using a 2-0 polyglyecapore. Tissue glue was applied to the skin incision to create a seal.

For catheter installation into the portal vein, the animal was placed in dorsal recumbency. The ventral midline and right femoral triangle were aseptically prepared using chloroheximide and alcohol and draped with sterile surgical drapes. A 15 cm ventral midline incision was made starting 2 cm behind the xyphoid and extended through the skin, subcutaneous tissues, linea alba and peritoneum. The spleen was localized, exteriorized and a splenic vein was isolated. A 1.57 mm OD polyethylene catheter (for catheter-only) or a silicone catheter (VAP) was inserted into the splenic vein using the Seldinger technique. The catheter was advanced until the tip was located in the portal vein and was verified by palpation; once correct placement was ensured the catheter was secured using a Chinese finger-trap using 2-0 polyglactin 910. If a catheter-only or a VAP was used, then the following procedure was performed.

For the animals with only a catheter, a blunt 18 gauge needle was inserted into the end of the tubing and attached to an injection cap for flushing and blood draws. The catheter was flushed with heparinized saline (100 IU/mL). A stab incision was made in

the left flank, and the catheter port was made to exit the abdominal cavity through the stab incision and placed in a pouch that was glued to the pigs back. The abdominal incision was closed in 3 layers: the linea alba, using a simple continuous patter with 0-polyglactin 910; the subcutaneous tissues, using a simple continuous patter with 3-0 polyglactin 910; and the sin, using the Ford interlocking pattern with 0-polyamine. For the animal with the VAP, the VAP port was inserted subcutaneously in the paralumbar fossa and tested, in the same manner as the cervical port. The VAP was tested via a blood draw before closure. The port and catheter were flushed with heparinized saline and locked with locking solution. The abdominal incision was closed in 3 layers: the linea alba, using a simple continuous patter with 0-polyglactin 910; the subcutaneous tissues, using a simple continuous patter with 3-0 polyglactin 910; and the sin, using the Ford interlocking pattern with 0-polyamine.

*Gastrostromy Tube:* A gastrostomy tube was installed after installing the PV catheter using the same ventral midline surgical approach as the PV catheter installation. Once the animal is opened the stomach was identified and exteriorized through the ventral midline incision. The location of the gastrostomy tube was identified between the lesser and greater curvature of the stomach. A 1 cm stab incision was made, and the end of the gastrostomy tube was inserted and secured in place using a string suture with 2-0 Vicryl. The stomach was then secured to the body wall using 2 small rows of a continuous suture with 2-0 Vicryl. A small stab incision was made through the left body wall and the tube was exteriorized. The right-angle fixation device was inserted to secure the tube to the body wall and the Y-angle adapter was placed on the tube to facilitate

deeding. The body was closed as previously described in the portal vein installation procedure.

*Post-OP:* The pigs are administered one dose of tulathromycin (Draxxin) and one dose of flunixin meglumine (Banamine). VAPs and/or catheters were maintained by daily flushing with heparinized saline solution for 5 days; the VAPs were locked with a locking solution (taurolidine citrate) post-flushing for 5 days. Afterwards, the VAPs and catheters are maintained weekly. Animals with VAPs are left to heal for two weeks before experiments are conducted; animals with only catheters were allowed to heal for between 3-6 days before experiments are conducted. To draw blood from the VAP, lidocaine solution is subcutaneously injected to the skin overlying the VAP to desensitize the skin, a Huber needle is inserted into the VAP for blood collection. Post blood-collection the VAP was flushed with heparinized saline and locked with locking solution.

*Euthanasia:* Every 12 hours for 1 day prior to euthanasia, 250 IU/kg of heparin was administered subcutaneously. Euthanasia was performed via exsanguination.

### 3.2.4. The $^{57}$Fe import experiment

After P1, P2, and P3 recovered for 3 days, and P4 recovered for 14 days (due to the VAPs), each pig was fasted for 24 h. During the fasting day, 10 mL of an 80 mM $^{57}$Fe solution (prepared by dissolving 95.5% enriched $^{57}$Fe metal (Isoflex USA) in trace metal grade aqua-regia) was mixed in an anaerobic glove box (Mbraun Labmaster 120) with 10 mL of 800 mM sodium ascorbate, generating a 40 mM $^{57}$Fe and 400 mM ascorbate stock solution that was stored in the glove box overnight. The iron in other

samples prepared in the same way was in the ferrous state as demonstrated by Mössbauer spectroscopy. The difference in recovery times was due to use of either a catheter or a VAP.

On the morning after the fast, P1, P2, and P3 were immobilized in an aluminum restraint cage and P4 was placed in the sling. Blood samples were removed from each catheter using either 6 or 10 mL plastic disposable syringes. Samples were transferred to 1–2 lithium-heparinized 6 mL vacutainer tubes (BD Vacutainer, #36788) and placed on ice. These "pre-injection" samples were centrifuged at 2000 × *g* for 12 min immediately after blood was collected. Plasma was collected using a plastic Pasteur pipette, transferred to labeled Eppendorf tubes, and frozen immediately in liquid $N_2$.

At the beginning of the iron-import kinetic experiment ($t = 0$), 20 mL of the stock $^{57}Fe$ solution was injected into the stomach *via* the feeding tube. Aliquots of blood were removed from each catheter at $t = 2$, 5, 10, 15, 25, 60, and 100 min post-injection, transferred to vacutainer tubes, and placed on ice. At the end of the experiment, pigs were exsanguinated using Ringer's buffer to remove residual blood.

Individual animals were treated slightly differently. P1 was given the anaesthetic Telazol shortly after injection of $^{57}Fe$ to calm it enough for reliable sample collection. Also during surgery, the caudal vein was inaccessible in that animal so the cranial vein was used instead. P3 was given anaesthetic early in the experiment to allow the surgical repair of the PV catheter which had unintentionally kinked. For P4, VAPs were used instead of catheters to minimize the kinking problem. However, prior to injection of $^{57}Fe$ into the stomach the PV VAP unintentionally clogged. P4 was sedated for installation of an ear catheter which was

used to infuse 125 mg of ferric gluconate (Santofi-Aventis, Ferrlecit) in 50 mL of saline. This was done intentionally in an effort to saturate transferrin and generate higher levels of NTBI after $^{57}$Fe injection. The solution flowed into P4 at a rate of 0.52 mg Fe per min using a syringe infusion pump (B. Braun). The infusion began 2 h prior to injecting $^{57}$Fe and ended *ca.* 40 min thereafter. P4 was lightly sedated during the infusion and subsequent experiment. The animal was suspended in the sling for infusion and sample collection.

### 3.2.5. Plasma Processing

The blood samples that had been placed on ice during the experiment were centrifuged as above as soon as possible. The plasma layer was removed, transferred to a 2 mL Eppendorf tube, and frozen immediately in liquid $N_2$. At different times after the experiment, individual plasma samples were thawed and brought into a chilled anaerobic glove box (MBraun Labmaster 120, 1-10 ppm $O_2$, 4-8 °C). Measured volumes of plasma (1 – 2 mL) were concentrated using a stirred-cell (Amicon Model 8003) with a regenerated cellulose 10 kDa cut-off membrane (Millipore Sigma, PLGC02510). Approximately 3/4ths of the initial volume was collected as flow-through solution (FTS) which was immediately injected onto a chromatography column. Low-molecular mass analysis was performed on two Superdex Peptide 10/300 GL (GE Healthcare, 17517601) columns connected in series. For high-molecular mass analysis, frozen plasma samples were treated identically except that they were filtered outside of the glovebox using either a 0.2 µm cellulose acetate membrane or a 0.45 µm PES membrane (VWR). The filtrate was returned to the glovebox and immediately injected onto a single Superdex 200 10/300 GL column (GE Healthcare, 17517501). The mobile phase for both columns

was 20 mM ammonium bicarbonate (Fisher Scientific) pH 8.5 that had been degassed using a Schlenk line prior to import into the box. Flow through the column was driven by a Bioinert LC (Agilent 1260 Bio-Inert Quaternary pump with diode array, fraction collector, and manual injection valve) located inside the glove box. Eluate flowed to an ICP-MS (Agilent 7700x) outside of the box and detected for $^{56}Fe$, $^{57}Fe$, and other metals as described.[62] Superdex peptide size exclusion columns were calibrated as described.[62] The Superdex 200 size exclusion column was calibrated by running bovine thyroglobulin (660 kDa, Sigma-Aldrich), equine splenic apo-ferritin (470 kDa), soybean beta-amylase (200 kDa, TCI America), recombinant-equine alcohol dehydrogenase (150 kDa, Sigma-Aldrich), human transferrin (80 kDa, Athens Research and Technology), carbonic anhydrase (29 kDa, Sigma), and cyanocobolamin (1.3 kDa, Fisher BioReagents). These standards were brought up in 20 mM Tris-base (Fisher) and 10 mM NaCl (EMD) and were filtered with either a 0.2 or 0.45 µm syringe filter (VWR) prior to injection. The Superdex 200 column had a void-volume $V_0$ of 8.1 mL. The column was calibrated by plotting the logarithm of the standard molecular weight vs. elution volume $V_e/V_0$. The best-fit linear regression line was $\log(\text{mol. wt}) = -1.7612(V_e/V_0) + 7.7225$ with an $R^2$ of 0.992. All columns were cleaned at the end of the day as described. [62]

### 3.2.6. Quantitative Elemental Analysis

Frozen plasma was thawed and 3 aliquots of 50 – 100 µL each were placed in new 15 mL plastic screw-top Falcon tubes. Concentrated trace-metal-grade nitric acid (120 µL) was added to each tube. The tubes were capped and sealed using electrical tape. Samples were placed in an oven at 70 – 80 °C for 12-14 hr. After digestion,

samples were cooled for > 1 hr, diluted with high-purity water to 6.00 mL, and then analyzed by ICP-MS.

### 3.2.7. Transferrin Saturation Assay

The total iron-binding capacity (TIBC) assay was performed by the Texas Veterinary Diagnostic Laboratory using a Beckman Coulter AU analyzer. The TIBC assay used both the total iron concentration assay and the unsaturated iron-binding capacity assay.

### 3.2.8. Iron Binding Proteins

Standard buffer consisted of 25 mM sodium bicarbonate (Fisher), 20 mM Tris-base (Fisher), and 10 mM NaCl (EMD), prepared in high purity water and adjusted to pH 7.4 using trace-metal-grade HCl (Fisher). Stock solutions of transferrin (Athens Research and Technology) (76 μM) and bovine serum albumin (Sigma) (1.2 mM) were prepared in the standard buffer with or without ferric citrate (70 μM). A 40 mM stock solution of $Fe_{III}$ citrate was prepared by mixing ferrous ammonium sulfate (Fisher) and three molar equivalents of sodium citrate (Fisher) in deionized water. The resulting pH was adjusted to 5 using citric acid (Acros Organics); final concentrations were obtained using deionized water. Transferrin and iron were mixed at a molar ratio of 1:1, and albumin and iron were mixed at a molar ratio of 1:0.058. Resulting solutions were mixed, incubated for 1 h, then passed through a 0.2 μm filter (VWR). Solutions of transferrin, with or without iron added, were mixed 1:1 (volume ratio) with solutions of albumin with or without iron added. Control solutions were mixed 1:1 with buffer. A solution of alcohol dehydrogenase (Sigma) was prepared (10 $mg/mL^{-1}$) in standard

**Table 3-1: Average metal and phosphorus concentrations in blood plasma from the portal vein and either the caudal or cranial vein.**
Values reported for each pig are the average of time points before and after $^{57}Fe$ injection. Values are the average of n = 4-10 independent samples collected at different times during the experiment. Concentrations of Mn and Co were below detection. Corresponding $^{57}Fe$ values are in Figure 3-1. Reprinted with permission. [63]

| **Element** | **Portal Vein** | | | **Caudal (CAV) or Cranial (CRV) Vein** | | | |
|---|---|---|---|---|---|---|---|
| | P1 | P2 | P3 | P1 | P2 | P3 | P4 (CR) |
| **Replicates** | 9 | 9 | 9 | 9 | 4 | 9 | 9 |
| **$^{56}Fe$ (µM)** | 8 ± 3 | 8 ± 4 | 7 ± 1 | 8 ± 5 | 11 ± 7 | 9 ± 2 | 160 ± 40* |
| **Cu (µM)** | 32 ± 4 | 26 ± 2 | 19 ± 2 | 32 ± 2 | 21 ± 1 | 18 ± 1 | 32 ± 2 |
| **Zn (µM)** | 5 ± 2 | 13 ± 1 | 11 ± 2 | 7 ± 7 | 12 ± 1 | 11 ± 1 | 14 ± 1 |
| **Mo (nM)** | 30 ± 30 | 20 ±10 | 40 ± 5 | 10 ±10 | 10 ± 4 | 40 ± 7 | 20 ± 2 |
| **P (mM)** | 6 ± 1 | 4 ± 0.1 | 4 ± 0.3 | 6 ± 1 | 3 ± 0.1 | 4 ± 0.3 | 5 ± 0.2 |

*In P4, the high concentration of $^{56}Fe$ is due to ferric gluconate infusion. The significant uncertainty in iron concentrations may be due to variable levels of hemolysis.

buffer, and mixed in a 1:1:1 volume ratio with stock solutions of $Fe^{III}$ transferrin (prepared using $Fe^{III}$ citrate) and albumin. Ferritin (Sigma; 2 $mg/mL^{-1}$) was prepared in standard buffer except lacking bicarbonate. These solutions were then passed through the Superdex 200 GL column as described above.

### 3.3. Results

#### 3.3.1. Metal Content of Plasma vs. FTSs

Metal concentrations in filtered plasma from the PV and from the CAV/CRV were similar (Table 3-1); $^{56}Fe$ + $^{57}Fe$ concentrations ranged from 10 – 30 μM. FTSs from plasma contain ≤1 μM iron[38], indicating that only 3% - 10% of the iron species in the filtered plasma of iron-deficient pigs have masses < 10 kDa. The $^{57}Fe/^{56}Fe$ ratio in filtered PV plasma from P1, P2, and P3 (and in the CAV plasma of P4) increased significantly over the 100 min experiment (Figure 3-1, top). The P1 $^{57}Fe/^{56}Fe$ concentration ratio increased immediately after injection whereas the P2 – P4 ratios increased after a 5 – 15 min lag. Enrichment was observed for all animals, but the enrichment in P1 was highest. The $^{56}Fe$ concentration in P1 plasma increased slightly after $^{57}Fe$ injection, perhaps as a secondary response to injection. The $^{57}Fe$ enrichment of P4 plasma may have been low due to the $^{56}Fe^{III}$ gluconate infusion prior to the $^{57}Fe$ injection. This infusion may have elicited a secondary response that attenuated $^{57}Fe$ intestinal absorption.

#### 3.3.2. Kinetics of Iron Import

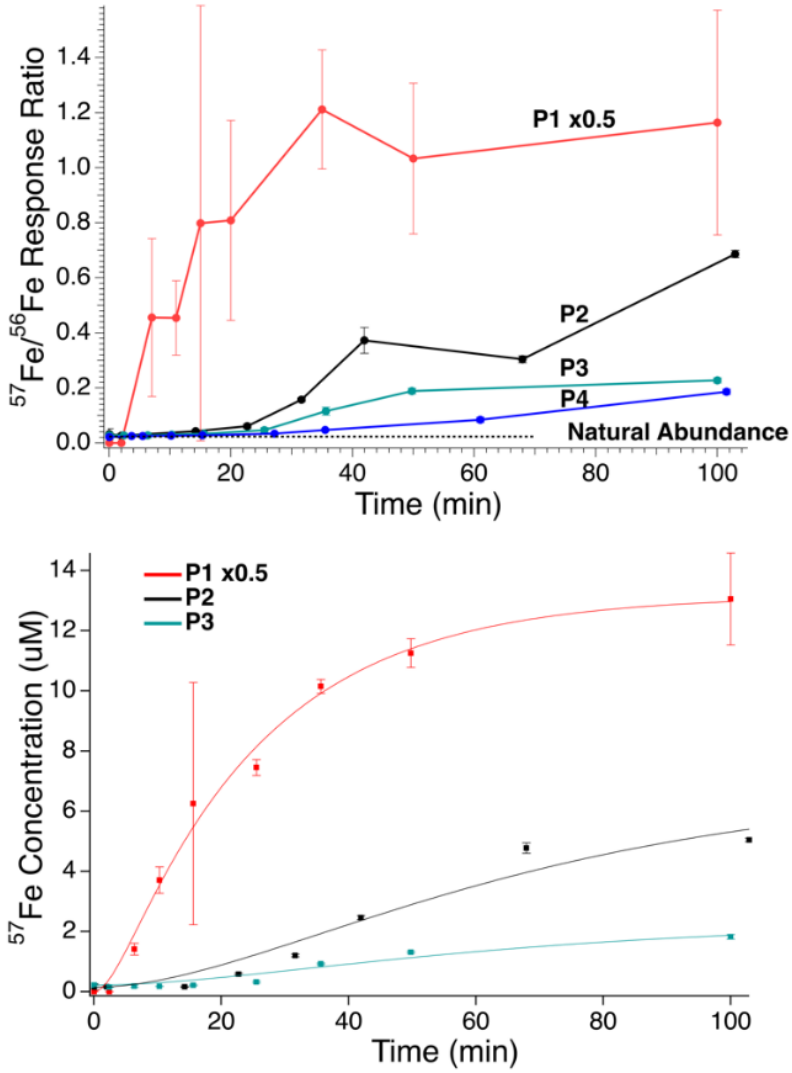


**Figure 3-1: Top Panel: Ratio of $^{57}Fe/^{56}Fe$ concentrations in plasma samples obtained from the PV of P1, P2, and P3, and the CAV of P4 at different times after $^{57}Fe$ injection into the stomach.**
Traces: red, P1; purple, P2; green P3; blue P4. Dashed black line is the ratio of natural abundance of $^{57}Fe/^{56}Fe$. Error bars are standard deviations. Bottom Panel: Plot of $^{57}Fe$ concentration of PV plasma vs. time after injecting $^{57}Fe_{II}$ into the stomachs of P1 (red), P2 (black), and P3 (green). Solid lines are simulations obtained using equation [1] and the parameters in Table 2. The intensity of the P1 plot was reduced 2-fold (×0.5). Reprinted with permission. [63]

**Table 3-2: Best-fit parameters used to fit equation [1] to plots of $^{57}Fe$ in plasma vs. time after injecting $^{57}Fe^{II}$ ascorbate into the stomach of pigs P1, P2 and P3.**
Reprinted with permission. [63]

| Animal | $k_1$ ($min^{-1}$) | $k_2$ ($min^{-1}$) | $a$ ($\mu M$) | $c$ ($\mu M$) |
|---|---|---|---|---|
| P1 | 0.043 | 0.340 | 26 | 0 |
| P2 | 0.029 | 0.027 | 6.7 | 0.15 |
| P3 | 0.027 | 0.034 | 2.1 | 0.22 |

We quantified the kinetics of iron import from the stomach, through the intestines, and into the blood, assuming the sequential reactions $^{57}Fe_{stomach} \xrightarrow{k_1} {}^{57}Fe_{emterocytes} \xrightarrow{k_2} {}^{57}Fe_{plasma}$. $k_1$ and $k_2$ are apparent first-order rate-constants for the transfer of iron from the stomach to the intestines, and from the intestines to the blood, respectively. Simulations were generated (in IgorPro) using equation [1]

$$[^{57}Fe]_{plasma} = a\left(1 + \frac{k_1 e^{-k_2 t} - k_2 e^{-k_1 t}}{k_2 - k_1}\right) + c \qquad [1]$$

where $a$ is an empirical fitting parameter that scales the time-dependent response and $c$ is an empirical off-set parameter that shifts simulations vertically. Simulations were fitted to plots of [$^{57}$Fe] in the PV plasma vs. time after injecting $^{57}$Fe into the stomachs of P1, P2 and P3 (Figure 3-1, bottom solid lines). Optimal $k_1$ values (Table 3-2) were similar for all datasets whereas $k_2$ values were more variable. This implies that the rate of iron absorption from the stomach to the intestines is similar from one animal to the next whereas the rate of iron import from the intestines to the blood is more variable.

### 3.3.3. Chromatography of Standards

Before investigating the $^{57}$Fe-containing species in the plasma, we passed authentic candidate proteins down the same columns and used the same chromatography conditions. Horse spleen ferritin (470 kDa) migrated as two peaks (Figure 3-2A). The first peak corresponded to the void volume ($V_0$) while the second peak corresponded to a mass of 460 kDa. The $V_0$ peak may reflect aggregated ferritin species. Bovine serum albumin (66.5 kDa) binds iron weakly, but its concentration in blood is high (ca. 700 μM) such that it might be a significant iron-binding protein.[39] Albumin incubated with

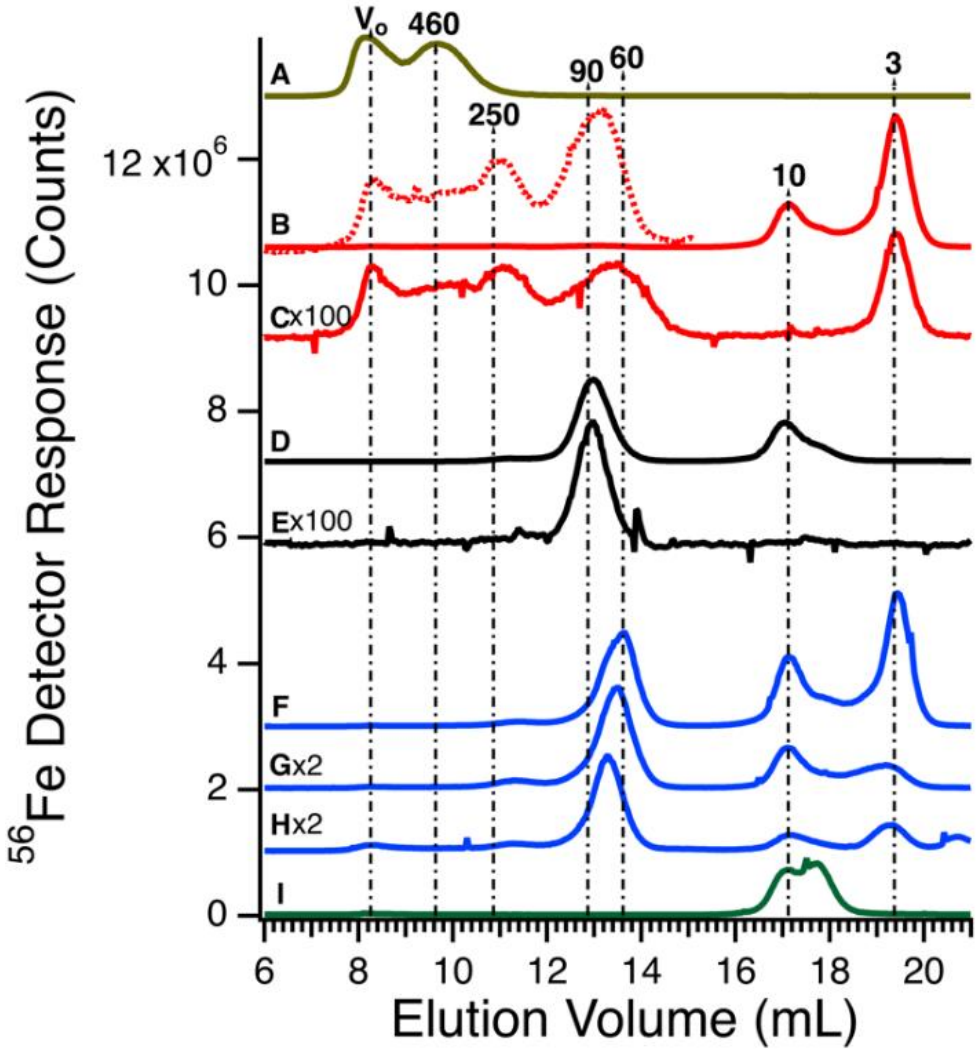


**Figure 3-2: Iron-detected chromatograms of high-molecular mass protein standards.**
(A) Ferritin (4.4 µM, 450 kDa); (B) albumin (600 µM, 60 kDa) plus 0.06 molar equivalents of $Fe^{III}$ citrate. The dotted line is a 100-fold expanded view; (C) albumin (600 µM); (D) transferrin (36 µM, 80 kDa) after incubating with $Fe^{III}$ citrate (36 µM); (E) transferrin (36 µM); (F) transferrin (36 µM), albumin (600 µM), and $Fe^{III}$ citrate (72 µM); (G) same as F except 36 µM $Fe^{III}$ citrate; (H) transferrin (25 µM), albumin (400 µM), alcohol dehydrogenase (22 µM), and $Fe^{III}$ citrate (25 µM); (I) $Fe^{III}$ citrate (72 µM). All concentrations listed are final. The intensity of the indicated traces were multiplied by 100 and 2 (×100 and ×2), respectively. Reprinted with permission. [63]

ca. 0.06 molar equivalents of $Fe^{III}$ citrate exhibited low-intensity iron-detected peaks at $V_0$, 250, 90, 10, and 3 kDa (Figures 3-2B and AB-3). Peaks at 10 and 3 kDa reflect excess iron not bound to albumin; the 10 kDa peak was also observed when $Fe^{III}$ citrate was run alone (Figure 3-2I). Peaks at $V_0$ and 250 kDa may reflect albumin aggregates. An albumin sample that was not incubated with iron exhibited iron-detected peaks at $V_0$, 250, 90, and 3 kDa (the 10 kDa peak due to $Fe^{III}$ citrate was absent) (Figure 3-2C). However, intensities were diminished relative to those incubated with iron. Human Tf (80 kDa) incubated for 1 h with 1 molar equivalent of $Fe^{III}$ citrate migrated according to a mass of 90 kDa (Figure 3-2D); the peak at 10 kDa was likely due to excess $Fe^{III}$ citrate. Tf without added iron exhibited the 90 kDa peak (Figure 3-2E) at a lower intensity.

We were concerned that the similar migration rates of iron-bound albumin and Tf would complicate our analysis. However, the intensity of the albumin peak was much less than that of Tf (even at the 700:1 albumin:Tf molar protein concentration ratio), indicating that any plasma peaks in this mass region are essentially due to Tf. To examine whether the two proteins could be distinguished chromatographically, Tf and albumin were mixed (with added $Fe^{III}$ citrate) to a final concentration similar to those of the individual standards in Figure 3-2, B and D. Interestingly, the Tf peak shifted to an apparent mass of ca. 60 kDa (Figure 3-2F). Repeating the experiment with iron added only to the Tf (half as much iron, overall) yielded similar results (Figure 3-2G). The shift may be due to secondary interactions of albumin acting at high concentrations as a pseudo-salt. The mobile phase contained minimal salt and so an albumin-dependent salting-effect may have caused a significant perturbation. We examined the effect of albumin on the elution of Tf by

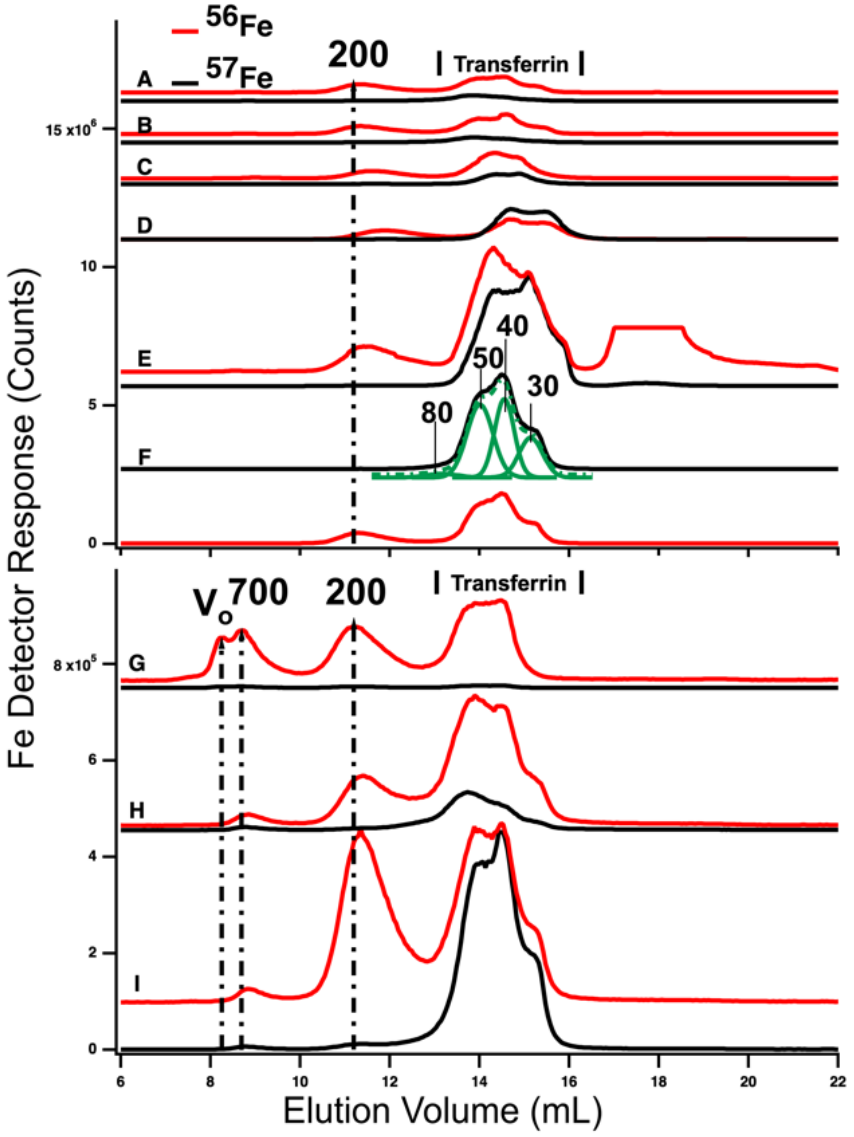


**Figure 3-3: High-molecular mass LC-ICP-MS chromatograms of PV plasma.** Plasma from P1 and P2 were passed through a 0.2 µm filter and then chromatographed. Top panel, P1: (A) pre-injection; (following times all post-injection) (B) 2 min; (C) 10 min; (D) 16 min; (E) 36 min; and (F) 100 min. Bottom panel, P2: (G) pre-injection; (H) 14 min; (I) 100 min post-injection. Red and black lines are $^{56}$Fe and $^{57}$Fe, respectively. In the red trace E, an unidentified peak at ca. 18 mL was truncated. The $^{57}$Fe trace F was fitted for four Gaussian (solid green) peaks which produced a resultant green-dashed trace. FitYK was used in fitting.[64] Assigned peaks are in kDa. Reprinted with permission.[63]

reducing the final concentration of albumin in trace H of Figure 3-2. This shifted the elution volume of Tf towards that in the absence of albumin, supporting our explanation.

### 3.3.4. Chromatograms of High-molecular mass (HMM) Plasma

HMM traces of filtered plasma from P1 and P2 are shown in Figure 3-3 (A→F for P1 and G→I for P2). In both experiments, 2 - 4 dominant $^{56}Fe$ peaks (red lines) were observed before (A and G) and after (B – F and H) injecting $^{57}Fe^{II}$. For the P1 experiment, dominating peaks corresponded to masses of 200 kDa and 50 - 20 kDa. A low-intensity peak in the 700 kDa region was also present (Figure 3-4). The 50 – 20 kDa region consisted of three partially resolved peaks. This was likely due to different forms of Tf. Apparent masses are lower than in traces of purified Tf (85 kDa) and in traces of Tf mixed with albumin (60 kDa). Albumin and other proteins and salts in filtered plasma probably shifted the Tf peaks.

P2 traces exhibited similar peaks except that the 700 kDa peak was more intense. The 50 - 20 kDa region was similarly composed of three unresolved peaks. The 700 kDa peak was probably due to serum ferritin as we are unaware of other iron-containing proteins in the plasma with such a high mass; recall that authentic ferritin exhibited a peak at $V_0$. The peak at 200 kDa is probably due to haptoglobin since we previously determined that authentic haptoglobin migrated in accordance with this mass.[38] The variable intensity of this peak probably reflects a variable extent of hemolysis during sample collection.

Ideally, the $^{56}Fe$ traces associated with P1 and P2 (Figure 3-5, red lines) would have been invariant in terms of species and intensities, since we did not inject $^{56}Fe$ into

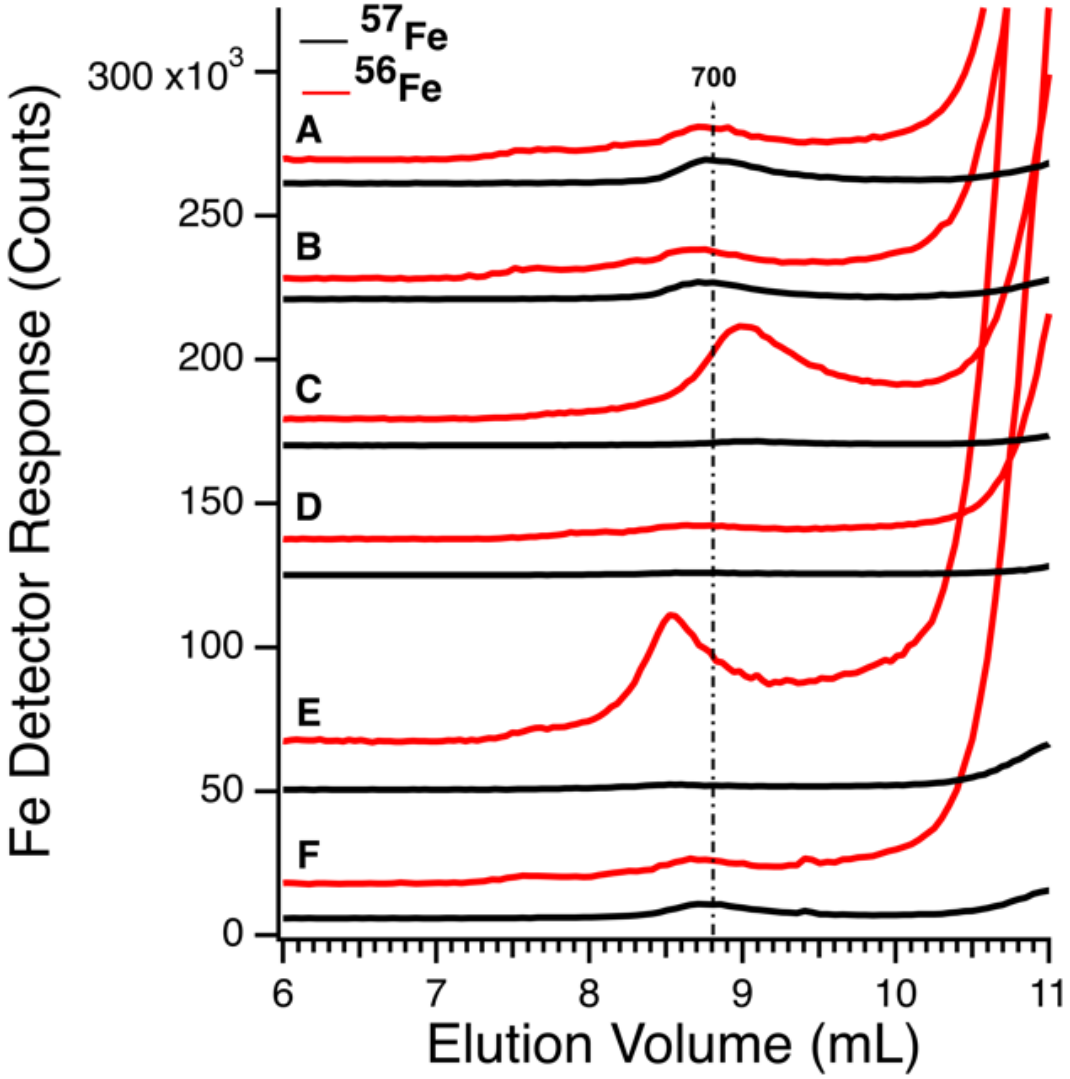


**Figure 3-4: Expanded view of P1 HMM in the 700 kDa region.**
These are the same traces as in Figure 3-3, top panel. The peaks in 700 kDa region were not enriched with $^{57}$Fe during the experiment. Reprinted with permission.[63]

the animals. That expectation was generally realized, but not entirely so. The first four LMM $^{56}$Fe traces of the P1 FTS (Figure 3-3, A - D) were essentially invariant but at longer times, the $^{56}$Fe peak intensities increased (data not shown). A similar phenomenon was observed for P2 (compare Figure 3-3, G vs. H). Perhaps $^{56}$Fe was released (after ~ 30 min delay) from internal bodily stores (e.g. macrophages in the liver and spleen) in response to injecting $^{57}$Fe into the stomach.

Prior to injecting $^{57}$Fe into P1 and P2, the $^{57}$Fe/$^{56}$Fe concentration ratio associated with each of the 2-3 major LC peaks was defined to be natural abundance (2%/94%). For the same peaks obtained from a sample collected 35 min after injecting $^{57}$Fe into P1's stomach, the ratio associated with the Tf peaks in the 50 kDa region was significantly higher than natural abundance (Figure 3E). The same was observed in filtered plasma collected 100 min after $^{57}$Fe injection into P2. (Figure 3-3I). Neither the putative ferritin nor haptoglobin peaks had elevated $^{57}$Fe/$^{56}$Fe ratios. This demonstrates that the $^{57}$Fe injected into the stomach bound apo-Tf as it entered the PV, but did not bind other iron-containing proteins. The iron bound to these other iron-containing proteins obviously originated from nutrient iron, but the import and binding must have occurred well before the current experiment. The ability of apo-Tf to bind nutrient-derived $^{57}$Fe also indicates that the Tf buffer system was not saturating in P1 – P4 experiments. P4 had the lowest extent of $^{57}$Fe enrichment probably because the $^{56}$Fe$^{III}$ gluconate infusion increased Tf saturation to 60%.

The serum ferritin peaks in Figure 3G represented ~30% of the iron in the sample (ignoring the 200 kDa peak) whereas the same peak in Figure 3-3H (sampled from the

**Figure 3-5:Low-molecular mass LC-ICP-MS chromatograms of FTS of PV (Upper panel) and CRV (Lower panel) plasma from experiment P1.**
Upper panel: (A) prior to injection of $^{57}$Fe into the stomach; (following times all post-injection) (B) 6 min; (C) 10 min; (D) 26 min. Red and black traces indicate $^{56}$Fe and $^{57}$Fe, respectively. $^{57}$Fe traces were magnified 10-fold. Lower panel: (A) prior to injecting $^{57}$Fe into the stomach; (following times all post-injection) (B) 2 min; (C) 6 min; (D) 10 min; (E) 15 min; (F) 26 min; (G) 36 min; (H) 50 min; and (I) 100 min. Red and black traces indicate $^{56}$Fe and $^{57}$Fe, respectively. Indicated traces were magnified by factors of 10, 0.5, or 0.05. Reprinted with permission. [63]

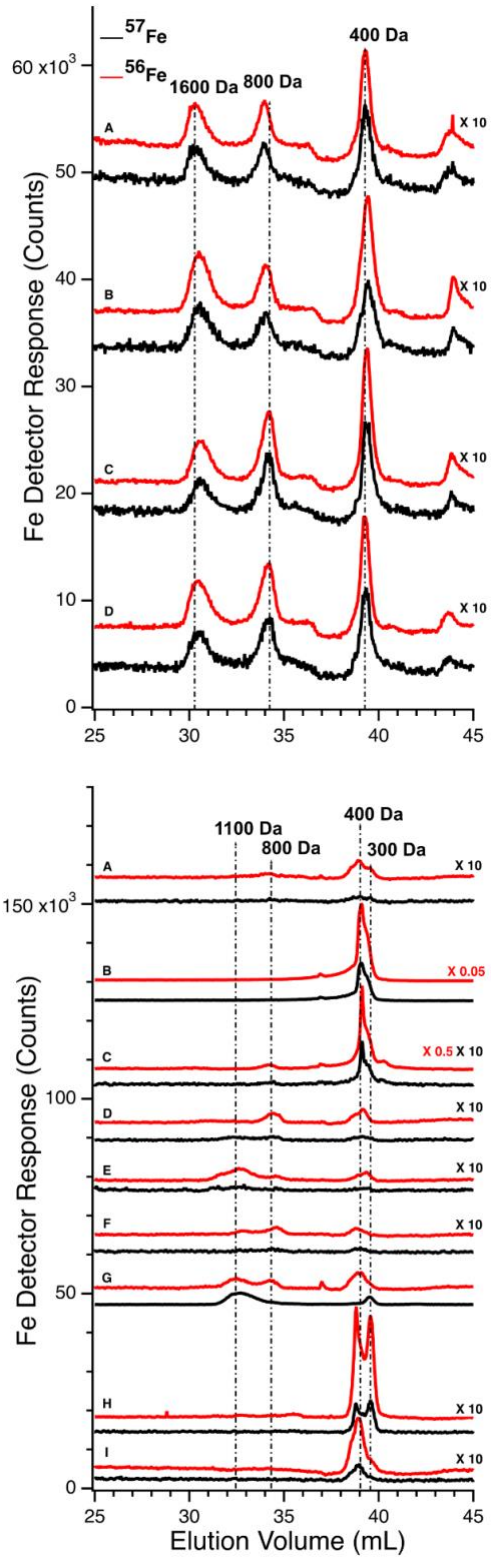
57Fe
56Fe
400 Da
1600 Da
800 Da
60 x10^3
Fe Detector Response (Counts)
A
B
C
D
X 10
0
10
20
30
40
50
25
30
35
40
45
1100 Da
800 Da
400 Da
300 Da
150 x10^3
100
50
X 0.05
X 0.5 X 10
E
F
G
H
I
Elution Volume (mL)

same catheter ~14 min later) was half as intense. The trace of Figure 3-3G matches Figure 3-9D except that blood was removed from the PV rather than CAV. The serum ferritin peak in Figure 3-3G is significantly stronger, implying that the liver absorbed some serum ferritin iron.

### 3.3.5. Chromatograms of FTSs

We also examined FTSs from the same plasma samples using an LC column that resolved LMM species. For P1, chromatograms of the FTSs from the PV and the CRV were obtained (Figure 3-5, top and bottom panels, respectively). The collective intensity of the observed iron-associated peaks was far less than for the HMM iron species in filtered plasma, reflecting the lower concentration of LMM iron in plasma. In the PV FTS, major iron-associated peaks were present at masses 1600, 800, and 400 Da (Figure 3-5). Their intensities were invariant between the time at which the control PV FTS sample was collected and at 35 min post-injection. At later times, the higher-mass LMM species were not always present whereas the 400 Da peaks were routinely present. Similar results were obtained for PV FTSs in the P2 and P3 experiments, where the predominate species observed was at 400 Da (Figure 3-6). For P2 and P3, peaks in the 400 Da region dominated, followed by peaks at 1500 and 1200 Da (Figure 3-6). The same species were present before and after $^{57}$Fe injection. The intensities of the P2 peaks were more scattered than those for P1, and no time-dependent trends were evident. For P3, the major peak was also in the 400 Da region but it was broadened and less resolved. A minor-intensity peak in the 1700 – 1500 Da region was evident in the pre-injection

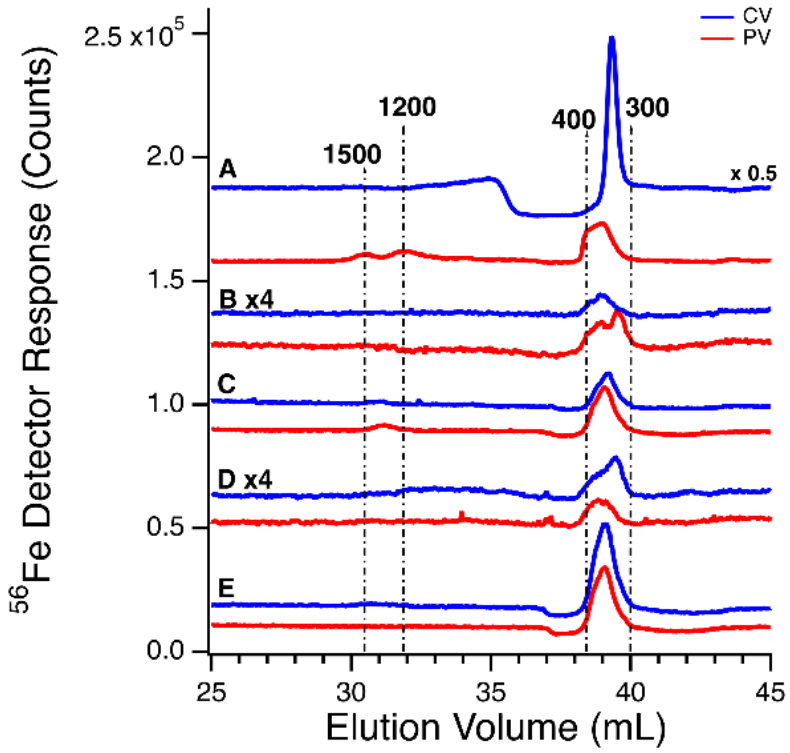


**Figure 3-6: Selected chromatograms showing the effect of passing blood through the liver of iron-deficient pigs on LMM iron species.**
Traces A – C refer to the P3 experiment whereas traces D and E refer to P2; PV plasma is in red, CAV plasma is in blue. A, pre-injection; B, ~ 17 min post-injection; C, ~ 102 min post-injection; D, pre-injection; E, ~ 104 min post-injection. Reprinted with permission. [63]

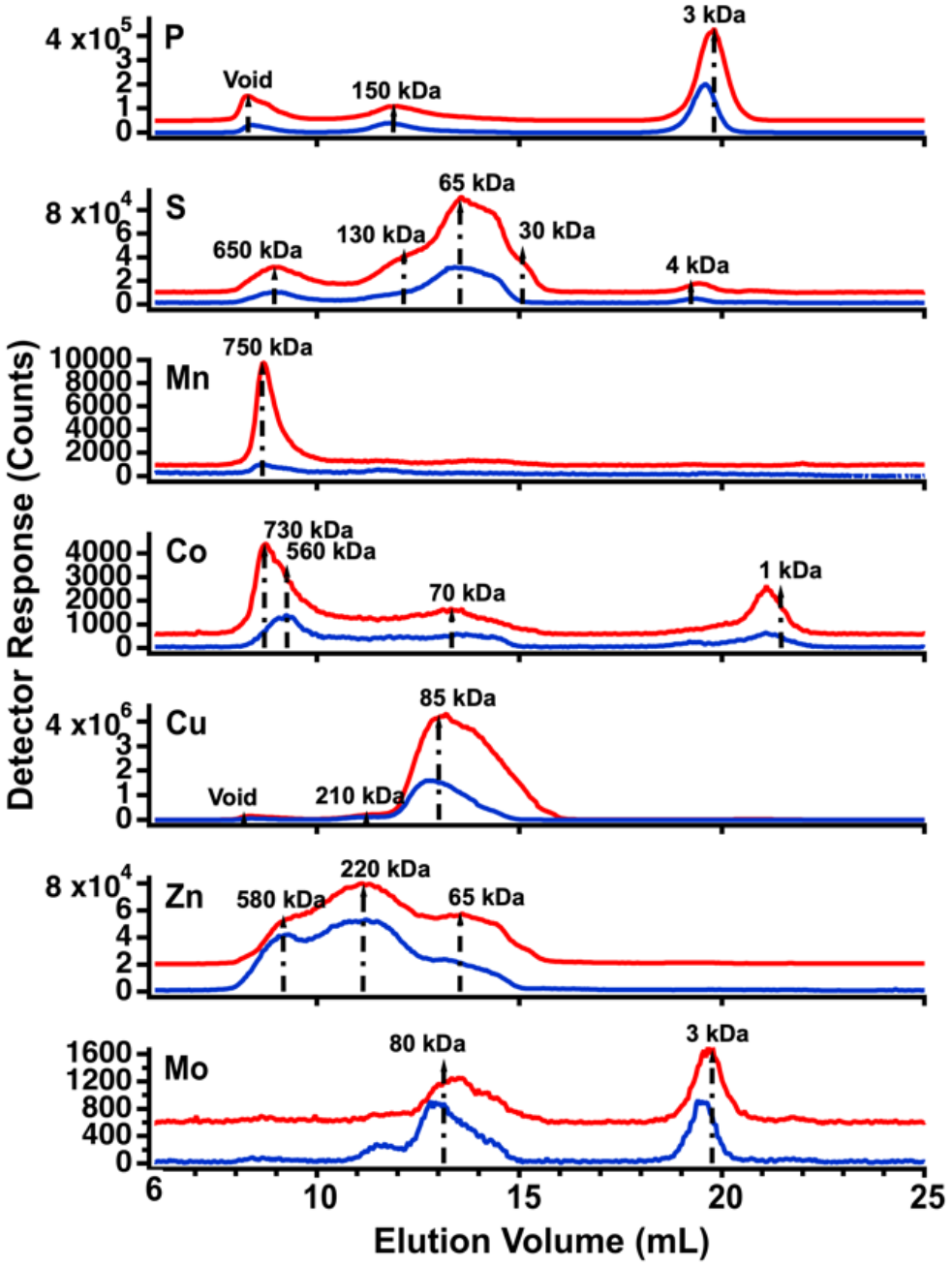


**Figure 3-7: Representative high-molecular weight LC-ICP-MS chromatograms of select isotopes of PV (red) and CAV/CRV (blue) plasma FTS.**
Traces of these elements were essentially invariant with time after $^{57}$Fe injection. Reprinted with permission. [63]

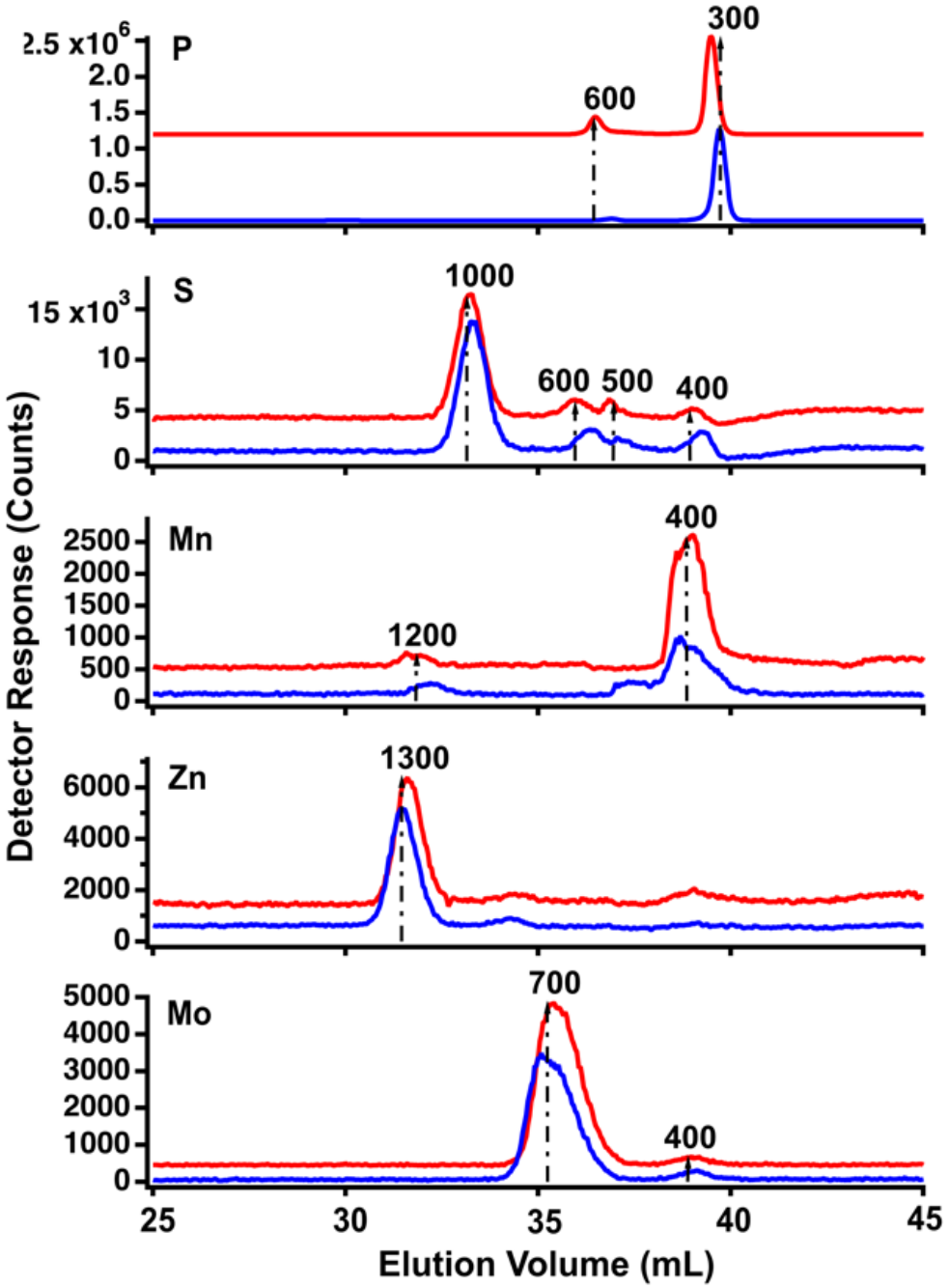


**Figure 3-8: Representative LMM LC-ICP-MS chromatograms of select isotopes in PV (red) vs. CAV/CRV (blue) plasma FTS.**
Copper-detected LMM traces exhibited minor peaks but they were not reproducible from sample-to-sample. Representative LMM traces of phosphorus, sulfur, manganese, zinc, and molybdenum are presented here. Reprinted with permission. [63]

trace, but not in subsequent traces. The peak intensity in the 400 Da region was variable but with no obvious time-dependence. We also monitored other metals in our plasma samples and observed reproducible peaks for P, S, Mn, Co, Cu, and Zn (Figures 3-7 and 3-8).

### 3.3.6. Effect of Liver

We expected that the liver would absorb one or more of the detected LMM iron species as blood from the PV passed through it. That expectation was not fully realized. $^{56}$Fe traces of FTS from the PV and CRV of P1 are shown in Figure 3-5, upper and lower panels, respectively. Similar results were observed for the CAV for P2 and P3. For the pre-injection trace of CRV plasma, the 400 Da region was significantly more intense than in the PV trace, but it lacked the 1600 Da species. The 800 Da species in the PV was present in some CRV traces (Figure 3-5, lower panel, traces C, D, and F) but not in others (trace A). Peaks were reproducibly present in the 400 Da region, similar to in our previous study in which we referred to this region as the "anchor".[38] Differences for the P2 and P3 experiments were also variable (Figure 3-6) in that the intensities of the 400 Da peaks in some samples were greater in the CAV trace than in the corresponding PV trace, whereas in other samples the opposite was observed.

The liver had a stronger effect on Tf. Using the HMM column, chromatograms of filtered plasma from the PV and from the CAV/CRV differed in the shape of the Tf peaks (Figures 3-3 vs. 3-5). For PV traces, the Tf region exhibited three semi-resolved peaks (Figure 3-3), with apparent masses between 50 – 30 kDa. Simulations indicate a 3:2:1 ratio (in terms of iron detection). Tf has different glycosylated isoforms which are

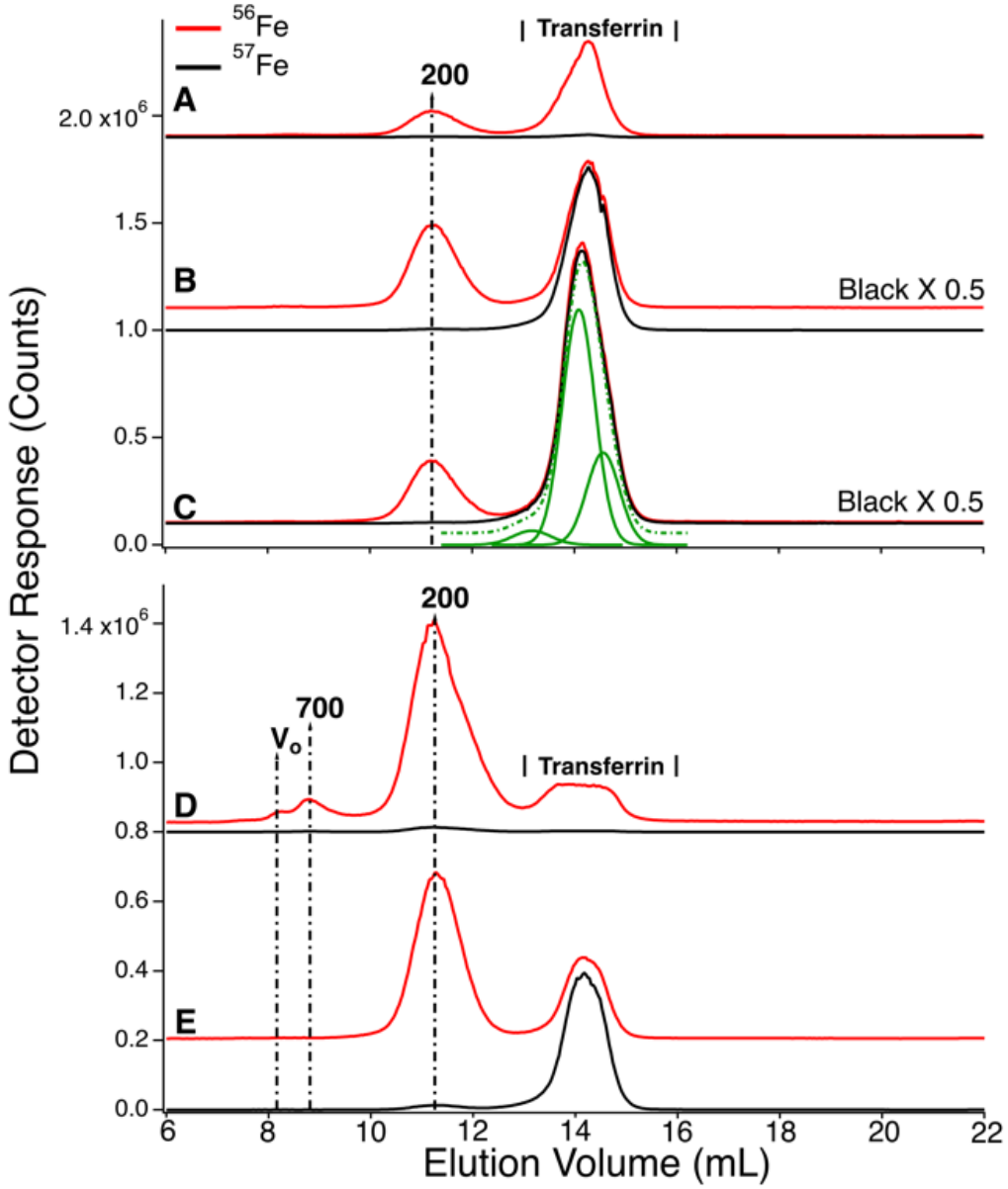


**Figure 3-9: High-molecular mass chromatography traces of filtered plasma from the CAV and CRV.**

Traces A-C are from P1. A, pre-injection (before injecting $^{57}Fe$ into the stomach); B, 28 min post-injection; C, 101 min post-injection. Traces D and E are from P2; D, pre-injection, E, 63 min post-injection. Assigned peak masses are in kDa. A detector switch artifact was removed electronically from the 200 kDa peak in trace D. Trace C was fitted with three (solid green) Gaussian lines which summed to give the dashed line. Simulations used FitYK software. Reprinted with permission. [63]

altered by the liver.[40-44] We suggest that the different peaks reflect different levels of glycosylation; this caused distinct elution profiles in other chromatography studies.[45,46] The Tf peaks in P1, P2, and P3 CAV/CRV plasma samples were more homogeneous (Figure 3-9), with the 50 kDa species dominating. The extent of $^{57}Fe$ enrichment and the overall concentration of $^{57}Fe$ in the CAV/CRV were not significantly different relative to the PV. Thus, it appears that the liver processes different forms of Tf in a manner that renders them more homogeneous. The results of the P4 experiment were more difficult to assess because PV blood was not obtained. Here, the Tf peaks in traces of CAV filtered plasma (Figure 3-10, top panel) exhibited two isoforms. However, P4 was infused with ferric gluconate, and the effect of the liver might have changed.

### 3.3.7. Partial saturation of transferrin did not generate new nutrient-derived LMM Fe species

We attempted to saturate Tf in P4 blood by infusing the animal with $^{56}Fe^{III}$ gluconate for 2 h prior to injecting $^{57}Fe^{II}$ into its stomach. The infusion continued for 40 min after injection. Excess ferric gluconate nanoparticles (250 - 440 kDa) were observed at $V_0$ in traces of filtered P4 plasma from the CAV (Figure 3-10, upper panel, 8.2 mL). The peak was observed before (trace A) and after (traces B – E) injection. Soon after the infusion ceased, the intensity of that peak declined sharply (traces F and G) indicating rapid absorption by the body - probably by the liver. We estimate $t_{1/2}$ to be ~ 30 min for this process.

In the same $^{56}Fe$ traces of Figure 3-10, the intensities and shapes of the Tf region at 50 kDa were largely invariant. The intensity of the same peaks in the $^{57}Fe$ traces

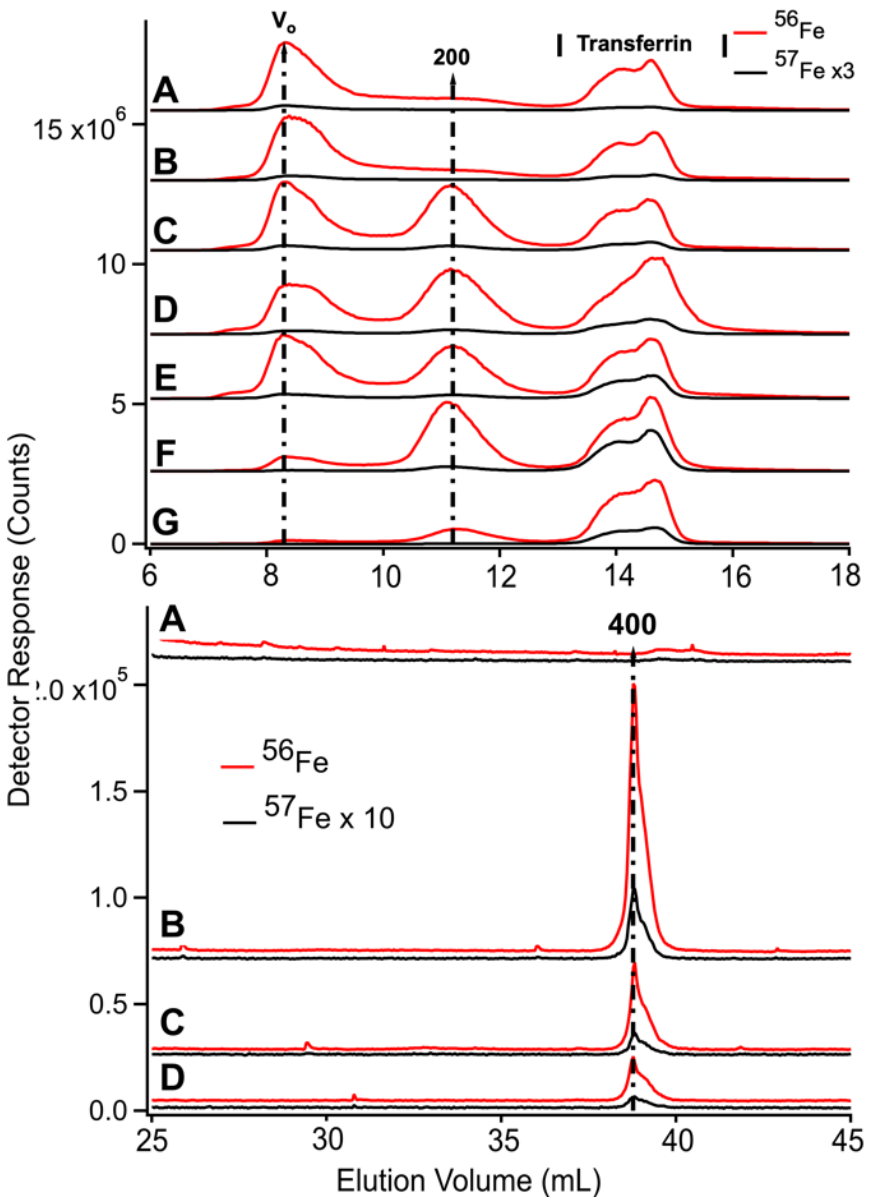


**Figure 3-10: Low-molecular mass (upper) and high-molecular mass (lower) of LC-ICP-MS chromatograms of filtered CAV plasma from P4.**
Upper panel; analysis of filtered plasma. (A) prior to injection of $^{57}$Fe into the stomach; (B) 4 min; (C) 15 min; (D) 25 min; (E) 35 min; (F) 60 min; (G) 100 min post-injection. Red and black lines are $^{56}$Fe and $^{57}$Fe, respectively. Lower panel; analysis of FTS. (A) prior to injection of $^{57}$Fe into the stomach; (B) 10 min; (C) 36 min; (D) 102 min post-injection. The intensities of indicated traces were reduced two-fold (×0.5). Reprinted with permission. [63]

increased as expected at increasing times after injecting $^{57}$Fe into the stomach. Similar to that observed in P1 and P2 experiments, the other peaks in the chromatograms did not become enriched in $^{57}$Fe.

Due to the effects of ferric gluconate, Tf saturation levels were higher than normal; saturation levels were 50%, 71%, 80% and 59% at 0, 25, 60, and 100 min. The 25 and 60 min samples exhibited hemolysis which might have artificially increased saturation measurements. More accurate values are probably 50-60%, similar to the other time-points in the series.

LMM analysis of these samples showed no $^{57}$Fe enrichment beyond natural abundance (Figure 3-10, bottom graph, A-D). However, PV samples could not be collected for the P4 animal and enriched species could have been generated in the PV but quantitatively absorbed by the liver so as to be absent in the CAV. We consider this unlikely because the LMM species in the FTS of PV plasma from P1 (which showed the highest $^{57}$Fe enrichment after injection) were not enriched, even though saturation levels were reasonably high. Saturation levels were 8% at pre-injection, 34% at 25 min post-injection, and 64% at 100 min post-injection (all in the CAV). Although these levels were quite high towards the end of the experiment, the LMM iron-detected peaks in corresponding samples were not $^{57}$Fe-enriched nor were they more intense than in samples from earlier timepoints. Since the liver absorbs Tf, saturation levels could have been even higher in the PV of P1 after injection (and still there was no enrichment of LMM iron species in the PV).

### 3.4. Discussion

Our objective was to detect NTBI in blood plasma using liquid chromatography rather than the more common method of chelator binding and iron-sensitive colorimetric assays. We expected that NTBI would consist of one or more LMM iron complexes derived from nutrient iron and that these complexes would enter the blood prior to binding apo-Tf. We expected that the concentration of NTBI would vary with the saturation of Tf, and that NTBI would be absorbed by the liver such that there would be major differences between PV and CAV/CRV plasma. We tried to increase the intensity of previously detected LMM species (and/or discover new LMM iron species that might be NTBI) by injecting $^{57}Fe$ into the stomachs of iron-deficient pigs and then removing blood before and after passage through the liver. Despite these efforts, none of our expectations were realized. Our conclusions are outlined in the model of Figure 3-11 and in the following paragraphs (with the major conclusion highlighted).

Most iron in healthy nonhemolyzed blood plasma is bound to Tf; a variable percentage is bound to serum ferritin and a small percentage (3-10%) is present as 2-4 LMM iron species. Iron-peaks at ~ 200 kDa were assigned to the haptoglobin:hemoglobin complex but its intensity varied as expected if different samples experienced different levels of hemolysis. Thus, we view the 200 kDa peaks as sampling artifacts.

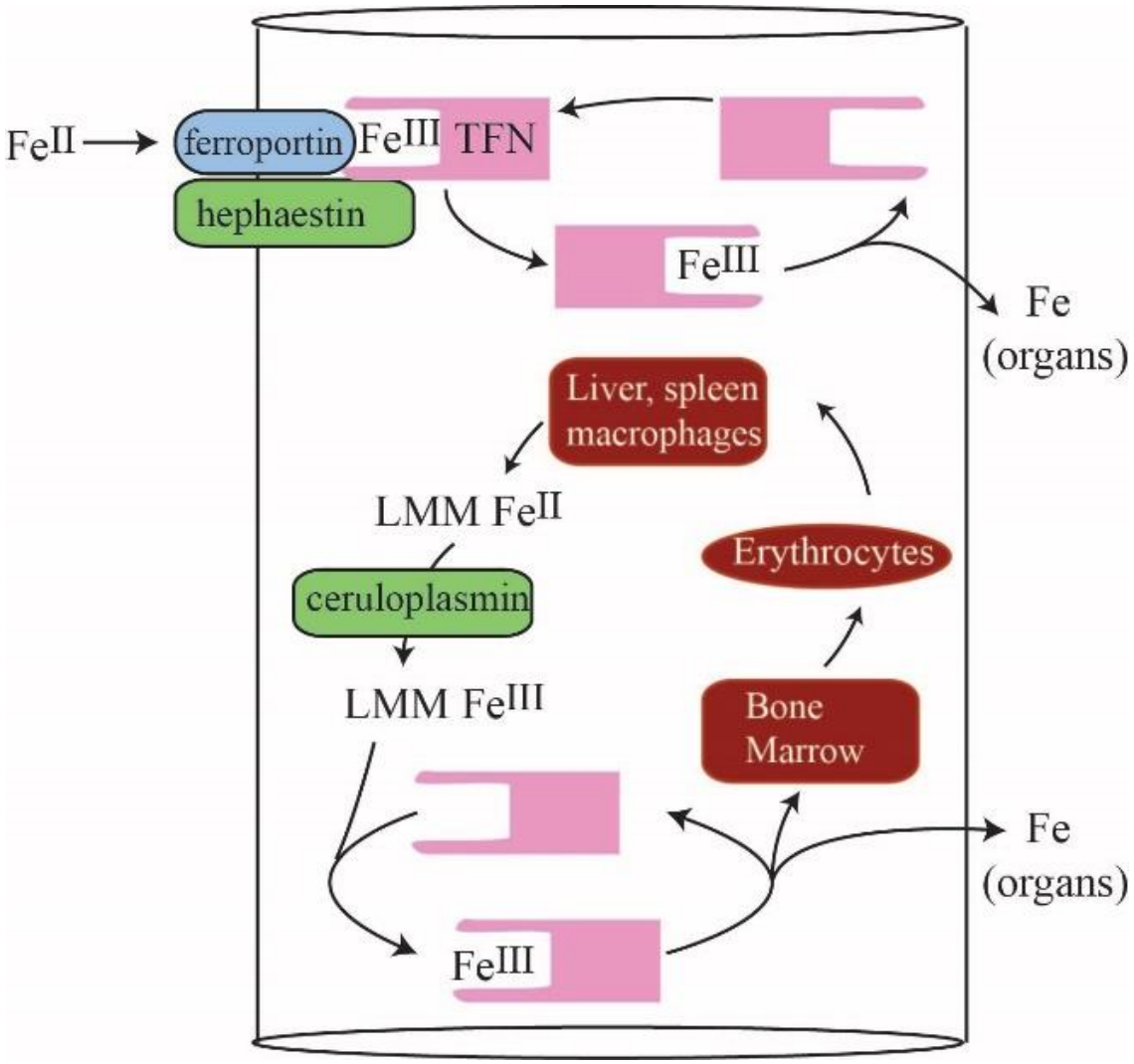


**Figure 3-11: Model for LMM Iron Trafficking in Healthy Blood.**
Nutrient iron is imported through FPN, oxidized by HFN, and transferred to apo-Tf in a channeled step in which no $Fe^{III}$ intermediate forms. During red-cell recycling, low-mass $Fe^{II}$ species from liver and kidney macrophages are proposed to be released into the blood. They become oxidized by CPN to the $Fe^{III}$ state, coordinated to apo-Tf, and then trafficked to the bone marrow for erythropoiesis as well as to organs as needed. The proposed LMM $Fe^{II/III}$ intermediates may be those detected in this study. Reprinted with permission. [63]

The only other HMM iron-containing peak in plasma (eluting at or near $V_0$) was assigned to iron-loaded serum ferritin monomers or aggregates. The intensity of this peak varied from 0% to 40% of plasma iron. This high level of variability was observed in the same animal, sometimes in samples obtained within ca. 10 min of each other. These results support a turnover rate of serum ferritin on the order of minutes as reported previously.[47,48] Our results are consistent with the use of serum ferritin as a signal involved in acute phase response.[49]

The detected LMM Fe species in plasma coexist with apo-Tf, a strong chelator of $Fe^{III}$ ions. The iron species either do not bind apo-Tf or they bind it weakly and reversibly.[38] Assuming the simplistic reaction {Fe + apo-Tf ⇄ Tf} where [Fe] ≈ 0.2 μM and [apo-Tf]/[Tf] ≈ 0.7/0.3, suggests that $K_d$ ≈ 0.5 μM which is not as tight as assumed for iron-binding to Tf.

Nutrient-derived iron that enters the blood binds apo-Tf directly (i.e., channeled from FTN to apo-Tf) without passing through a long-lived LMM Fe intermediate. Otherwise, we would have detected $^{57}$Fe enriched LMM iron species in plasma (unless such species were absorbed onto the chromatography column – a possibility that we cannot rigorously exclude). There is some support in the literature for complex formation of the relevant proteins and perhaps channelling. FPN physically interacts with HPN and CPN.[51,52] FPN and HPN both migrate from the apical to basolaterial surface of enterocytes. The rate of $^{55}$Fe efflux from Xenopus oocytes increases in the presence of apo-Tf and CPN[53-56] consistent with an interaction with FPN. $Fe^{II}$ binding to FPN may stimulate a conformational change that releases cytosolic $Fe^{II}$ into the blood.[54]

CPN helps remove $Fe^{II}$ from FPN; otherwise the $Fe^{II}$ remains on FPN.[57] FPN may act "in concert" with HFN and/or CPN to release Fe.[58] An advantage to channelling is that aqueous $Fe^{II}$ ions would not be present in the blood of healthy individuals, preventing ROS-based reactions. Channels are probably tightly regulated. The LMM iron complexes observed here may not cause excess ROS damage because they are tightly coordinated, in the ferric state, or present at low concentrations.

The LMM Fe species detected in mammalian blood plasma are NOT derived directly from nutrient absorption but rather from internal iron stores. Such stores might include Kupffer macrophages in the liver and/or red pulp macrophages in the spleen. Both degrade red blood cells as a part of red-cell recycling, a process that involves far more iron and higher flux rates than nutrient iron import.[50] These macrophages could have released the observed LMM iron species. Another possibility is that the detected iron species were exported by FPN in erythrocytes or ethryoblasts.[42]

The iron-deficient liver has a modest effect on LMM and HMM iron species; it seems to release iron species with masses in the 400 Da region and absorb iron species in the 500 – 1500 Da region. It also alters the observed isoforms of Tf. The liver probably rapidly removed the ferric gluconate in the blood, as was observed after infusion was halted. The liver acts as an iron buffer to store and mobilize iron as needed.[50]

The intensity of the detected LMM iron species is not correlated to the level of transferrin saturation in the range between 8% and 60%. In all cases, the intensity of the LMM species was low and uncorrelated. This surprising result is difficult to reconcile

with a gradual spill-over mechanism. We cannot exclude the possibility that the intensity of these LMM plasma irons species would increase dramatically at higher saturation. More likely is that they are not directly associated with nutrient iron absorption.

The overall conclusion of our study is that the LMM iron species detected in blood plasma are not the sought-after NTBI species. So what are these LMM species and where is NTBI? HPN is absent in macrophages[65] so $Fe^{II}$ from these cells may be released into the blood and oxidized to $Fe^{III}$ by CPN. We suggest that the LMM iron species that we observe are these $Fe^{II}/Fe^{III}$ species. This explains why the detected LMM iron species are not associated directly with nutrient absorption; rather they may be more closely related to red blood cell recycling processes involving the macrophage release of iron and subsequent oxidation by CPN. These species may also arise from the iron exported by erythroid cells.[42] As far as the elusive NTBI, two possibilities seem reasonable. The first is that the NTBI in our plasma samples was/were adsorbed by our chromatography columns, and thus was/were not observed in our chromatograms. The second is that NTBI only appears in the plasma when Tf saturation is > 60%. We are investigating both possibilities.

### 3.5. References


1 T. Ganz, Systemic iron homeostasis, *Physiol. Rev.*, 2013, **93**, 1721–1741.

2 S. Gulec, G. J. Anderson and J. F. Collins, Mechanistic and regulatory aspects of intestinal iron absorption, *Am. J. Physiol.: Gastrointest. Liver Physiol.*, 2014, **307**, G397–G409.

3 H. Drakesmith, E. Nemeth and T. Ganz, Ironing out Ferro- portin, *Cell Metab.*, 2015, **22**, 777–787.

4 B. K. Fuqua, Y. Lu, D. Darshan, D. M. Frazer, S. J. Wilkins, N. Wolkow, A. G. Bell, J. Hsu, C. C. Yu, H. Chen, J. L. Dunaief, G. J. Anderson and C. D. Vulpe, The multicopper ferroxidase Hephaestin enhances intestinal iron absorption in mice, *PLoS One*, 2014, **9**, e98792.

5 A. Pietrangelo, Hereditary Hemochromatosis: pathogenesis, diagnosis, and treatment, *Gastroenterology*, 2010, **139**, 393–408.

6 A. C. G. Chua, J. K. Olynyk, P. J. Leedman and D. Trinder, Nontransferrin-bound iron uptake by hepatocytes is increased in the Hfe knockout mouse model of hereditary hemochromatosis, *Blood*, 2004, **104**, 1519–1525.

7 P. Brissot, M. Ropert, C. Le Lan and O. Loreal, Non- transferrin bound iron: a key role in iron overload and iron toxicity, *Biochim. Biophys. Acta*, 2012, **1820**, 403–410.

8 W. Breuer, C. Hershko and Z. I. Cabantchik, The importance of non-transferrin bound iron in disorders of iron metabolism, *Transfus. Sci*., 2000, **23**, 185–192.

9 M. Grootveld, J. D. Bell, B. Halliwell, O. I. Aruoma, A. Bomford and P. J. Sadler, Non-transferrin-bound iron in plasma or serum from patients with idiopathic hemochromatosis –characterization by high-performance liquid chromatography and nuclear magnetic resonance, *Chem* spectroscopy. *J. Biol. Chem*, 1989, **264**, 4417-4422.

10 L.-C. Konigsberger, E. Konigsberger, P. M. May and G. T. Hefter, Complexation of iron(III) and iron(II) by citrate. Implications for iron speciation in blood plasma, *J Inorg Biochem*, 2000, **78**, 175–184.

11 P. M. May, P. W. Linder and D. R. Williams, Computer simulation of metal ion equilibria in biofluids: models for the low-molecular-weight complex distribution of calcium(II), magnesium(II), manganese(II), iron(III), copper(II), zinc(II) and lead(II) ions in human blood plasma, *J. Chem. Soc. – Dalton trans.* 1977, **6**, 588-595.

12 L. de Swart, J. C. Hendriks, L. N. van der Vorm, Z. I. Cabantchik, P. J. Evans, E. A. Hod, G. M. Brittenham, Y. Furman, B. Wojczyk, M. C. Janssen, J. B. Porter, V. E. Mattijssen, B. J. Biemond, M. A. MacKenzie, R. Origa, R. Galanello, R. C. Hider and D. W. Swinkels, Second international round robin for the quantification of serum non-transferrin bound iron and liable plasma iron in patients with iron-overload disorders, *Haematologica,* 2016, **10**, 38-45.

13 E. Tolosano, S. Fagoonee, N. Morello, F. Vinchi and V. Fiorito, Heme scavenging and the other facets of hemopexin, *Antioxidants and Redox Signaling*, 2010, **12**, 305-320.

14 D. Chiabrando, F. Vinchi, V. Fiorito, S. Mercurio and E. Tolosano, Heme in pathophysiology: a matter of scavenging, metabolism and trafficking across cell membranes, *Frontiers in Pharmacology*, 2014, **5**, 61.

15 I. Yanatori, M. Tabuchi, Y. Kawai, Y. Yasui, R. Akaji and F. Kishi, Heme and non-heme iron transporters in non-polarized and polarized cells, *BMC Cell Biol*, 2010, **11**, 39-50.

16 D. J. Schaer, F. Vinchi, G. Ingoglia, E. Tolosano and P. W. Buehler, Haptoglobin, hemopexin, and related defense pathways—basic science, clinical perspectives, and drug development, *Frontiers in Physiology*, 2014, **5**, article 415; 13 pages.

17 T. Peters, All about albumin biochemistry, genetics and medical applications, Academic press, 1996.

18 R. A. Lovstad, Interaction of serum albumin with the Fe(III)-citrate complex, *Int. J. Biochem*, 1993, **25**, 1015–1017.

19 R. W. Evans, R. Rafique, A. Zarea, C. Rapisarda, R. Cammack, P. J. Evans, J. B. Porter and R. C. Hider, Nature of non-transferrin-bound iron: studies on iron citrate complexes and thalassemic sera, *J. Biol. Inorg. Chem*, 2008, **13**, 57-74.

20 M. Fasano, S. Curry, E. Terreno, M. Galliano, G. Fanali, P. Narciso, S. Notari and P. Ascenzi, The extraordinary ligand binding properties of human serum albumin, *IUBMB Life*, 2005, **57**, 787-796.

21 S. Recalcati, P. Invernizzi, P. Arosio and G. Cairo, New functions for an iron storage protein: the role of ferritin in immunity and autoimmunity, *J. Autoimmunity*, 2008, **30**, 84-89.

22 S. G. Gehrke, H. Kulaksiz, T. Herrmann, H. D. Riedel, K. Bents, C. Veltkamp and W. Stremmel, Expression of hepcidin in hereditary hemochromatosis: evidence for a

regulation in response to the serum transferrin saturation and to non–transferrin-bound iron, *Blood*, 2010, **116**, 1574-1584.

23 L. A. Cohen, L. Gutierrez, A. Weiss, Y. Leichtmann-Bardoogo, D. L. Zhang, D. R. Crooks, R. Sougrat, A. Morgenstern, B. Galy, M. W. Hentze, F. J. Lazaro, T. A. Rouault and E. G. Meyron-Holtz, Serum ferritin is derived primarily from macrophages through a nonclassical secretory pathway, *Blood*, 2010, **116**, 1574-1584.

24 Arosio, M. Yokota and J. W. Drysdale, Characterization of serum ferritin in iron overload: possible identity to natural apoferritin, *Br. J. Haematol*, 1977, **36**, 199–207.

25 S. Recalcati, P. Invernizzi, P. Arosio and G. Cairo, New functions for an iron storage protein: the role of ferritin in immunity and autoimmunity, *J Autoimmun*, 2008, **30**, 84–89.

26 W. Wang, M. A. Knovich, L. G. Coffman, F. M. Torti and S. V. Torti, Serum ferritin: past, present and future, *Biochim Biophys Acta*, 2010, **1800**, 760–769.

27 P. Brissot, T. L. Wright, W. L. Ma and R. A. Weisiger, Efficient clearance of non-transferrin-bound iron by rat liver: implications for hepatic iron loading in iron overload states, *J Clin Invest*, 1985, **76**, 1463-1470.

28 J. J. Pinilla-Tenas, B. K. Sparkman, A. Shawki, A. C. Illing, C. J. Mitchell, N. N. Zhao, J. P. Liuzzi, R. J. Cousins, M. D. Knutson and B. Mackenzie, Zip14 is a complex broad-scope metal-ion transporter whose functional properties support

roles in the cellular uptake of zinc and nontransferrin-bound iron, *Am J. Cell Physiology*, 2011, **301**, C862-C871.

29 J. P. Liuzzi, F. Aydemir, H. Ham, M. D. Knutson and R. J. Cousins, Zip14 (Slc39a14) mediates non-transferrin-bound iron uptake into cells, *Proc. Natl. Acad. Sci U. S. A.*, 2006, **103**, 13612-13617.

30 J. M. C. Gutteridge, D. A. Rowley, E. Griffiths and B. Halliwell, Low-molecular-weight iron complexes and oxygen radical reactions in idiopathic haemochromatosis, *Clin. Sci.*, 1985, **68**, 463–467.

31 F. W. Huang, J. L. Pinkus, G. S. Pinkus, M. D. Fleming and N. C. Andrews, A mouse model of juvenile hemochromatosis. *J. Clin Invest.*, 2005, 115, 2187-2191.

32 B. P. Esposito, W. Breuer, P. Sirankapracha, P. Pootrakul, C. Hershko and Z. I. Cabantchik, Labile plasma iron in iron overload: redox activity and susceptibility to chelation, *Blood*, 2003; **102**, 2670-2677.

33 B. Sarkar, State of iron(III) in normal human serum – low molecular weight and protein ligands besides transferrin, *Canadian J. Biochem,*. 1970, **48**, 1339-1350.

34 R. E. Fleming, M. C. Migas, X. Y. Zhou, R. S. Britton, E. M. Brunt, S. Tomatsu, A. Waheed, B. R. Bacon and W. S. Sly, Mechanism of increased iron absorption in murine model of hereditary hemochromatosis: increased duodenal expression of the iron transporter DMT1, *Proc Natl Acad Sci U. S. A.*, 1999, **96**, 3143-3148.

35 O. Loreal, I. Gosriwatana, D. Guyader, J. Porter, P. Brissot and R. C. Hider, Determination of non-transferrin-bound iron in genetic hemochromatosis using a new HPLC-based method, *J Hepatol*., 2000, **32**, 727-733.

36 I. Gosriwatana, O. Loreal, S. Lu, P. Brissot, J. Porter and R. C. Hider, Quantification of non-transferrin-bound iron in the presence of unsaturated transferrin, *Anal Biochem*., 1999, **273**, 212-220.

37 J. B. Porter, R. D. Abeysinghe, L. Marshall, R. C. Hider and S. Singh, Kinetics of Removal and Reappearance of Non - Transferrin-Bound Plasma Iron with Deferoxamine Therapy, *Blood,* 1996, **88**, 705–713.

38 N. Dziuba, J. Hardy, P. A. Lindahl, Low-molecular-mass iron in healthy blood plasma is not predominately ferric citrate, *Metallomics,* 2018, **10**, 802-817.

39 M. M. Swindle, Cardiothoracic and Vascular Surgery/Chronic Intravascular Catheterization, Swine in the laboratory. Surgery, anesthesia, imaging and experimental techniques, CRC Press, Taylor & Francis Group, Boca Raton, FL, 2nd edn, 2007, vol 9, 195-259.

40 E. Landberg, E. Astro¨m, B. Kagedal and P. Pahlsson, Disialo-trisialo bridging of transferrin is due to increased branching and fucosylation of the carbohydrate moiety, *Clin. Chim. Acta,* 2012, **414**, 58-64.

41 M. Gudowska, E. Gruszewska, A. Panasiuk, B. Cylwik, M. Swiderska, R. Filisiak, M. Szmitkowski and L. Chrostek, Changed profile of serum transferrin isoforms in liver diseases, *Clin. Lab.*, 2017, **63**, 349-354.

42 N. D. Sharma, R. W. Evans and K. J. Patel, et al., Evidence for the glycosylation of porcine serum transferrin at a single site located within the C-terminal lobe, *Biochim. Biophys. Acta, Protein Struct. Mol. Enzymol.,* 1994, **1206**, 286–288.

43 I. Graham and J. Williams, A comparison of glycopeptides from the transferrins of several species. *Biochem. J.*, 1975, **145**, 263–279.

44 M. Nagae, K. Morita-Matsumoto and S. Arai, et al., Structural change of N-glycan exposes hydrophobic surface of human transferrin, *Glycobiology*, 2014, **24**, 693–702.

45 A. Helander, N. K. Modén, Effect of transferrin glycation on the use of carbohydrate-deficient transferrin as an alcohol biomarker. *Alcohol Alcohol.* 2013, **48**, 478–482.

46 A. Van Campenhout, C. Van Campenhout, A. R. Lagrou and B. Manuel-Y-Keenoy, Effects of in vitro glycation on $Fe^{3+}$ binding and $Fe^{3+}$ isoforms of transferrin, *Clin. Chem.*, 2004, **50**, 1640–1649.

47 M. A. Siimes and P. R. Dallman, New Kinetic Role for Serum Ferritin in Iron Metabolism, *Br. J. Haematol.*, 1974, **28**, 7–18.

48 J. W. Halliday, U. Mack and L. W. Powell, The Kinetics of Serum and Tissue Ferritins: Relation to Carbohydrate Content, *Br. J. Haematol.*, 1979, **42**, 535–546.

49 M. N. Garcia-Casal, S.-R. Pasricha, R. X. Martinez, L. Lopez- Perez and J. P. Peña-Rosas, Serum or plasma ferritin concentration as an index of iron deficiency and overload, *Cochrane Database Syst. Rev.*, 2015, **7**, article CD011817.

50 H. Drakesmith, E. Nemeth and T. Ganz, Ironing out ferroportin, *Cell Metab.*, 2015, **22**, 777-787.

51 S. Y. Jeong and S. David, Glycosylphosphatidylinositol-anchored ceruloplasmin is required for iron efflux from cells in the central nervous system, *J. Biol. Chem.*, 2003, **278**, 27144 - 27148.

52 K. Y. Yeh, M. Yeh, L. Mims and J.Glass, Iron feeding induces ferroportin I and hephaestin migration and interaction in rat duodenal epithelium, *Am. J. Phyisol. Gastrointest. Liver Physiol.*, 2009, **296**, G55-G65.

53 C. J. Mitchell, A. Shawki, T. Ganz, E. Nemeth and B. Mackenzie, Functional properties of human ferroportin, a cellular iron exporter reactive also with cobalt and zinc, *Am J. Physiol. Cell Physiol.*, 2014, **306**, C450-C459.

54 R. Taniguchi, H. E. Kato, J. Font, C. N. Deshpande, M. Wada, K. Ito, R. Ishitani, M. Jormakka and O. Nureki, Outward- and inward-facing structures of a putative bacterial transition-metal transporter with homology to ferroportin, *Nature Comm.*, 2015, article 8545 DOI: 10.1038/ncomms9545.

55 C. J. Mitchell, A. Shawki, T. Ganz, E. Nemeth and B. Mackenzie, Functional properties of human ferroportin, a cellular iron exporter reactive also with cobalt and zinc, *Am. J. Phys. Cell Phys*., 2014, **306**, C450-C459.

56 A. Donovan, Y. Brownlie, J. Zhou, S. J. Shepard, J. Pratt, B. H. Moynihan, A. Paw, B. Drejer, A. Barut, L. T. C. Zapata, C. Brugnara, S. E. Lux, G. S. Pinkus, J. L. Pinkus, P. D. Kingsley, J. Palls, M. D. Fleming, N. C. Andrews and I. Z. Leonard, Positional cloning of zebrafish ferroportin1 identifies a conserved vertebrate iron exporter, *Nature*, 2000, **403**, 776-781.

57 I. DeDomenico, D. M. Ward, M. C. B. di Patti, S. Y. Jeong, S. David, G. Musci and J. Kaplan, Ferroxidase activity is required for the stability of cell surface ferroportin in cells expressing GPI-ceruloplasmin, *EMBO J.*, 2007, **26**, 2823–2831.

58 A. T. McKie, P. Marciani, A. Rolfs, K. Brennan, K. Wehr, D. Barrow, S. Miret, A. Bomford, T. J. Peters, F. Farzaneh, M. A. Hediger, M. W. Hentze and R. J. Simpson, A novel duodenal iron-regulated transporter, IREG1, implicated in the basolateral transfer of iron to the circulation, *Mol. Cell* 2000, **5**, 299-309.

59 R. T. Zijlstra, R. Jha, A. D. Woodward, J. Fouhse and T. A. T. G. van Kempen, Starch and fiber properties affect their kinetics of digestion and thereby digestive physiology in pigs, *J. Anim. Sci.*, 2012, **90**, 49–58.

60 S. Hooda, J. J. Matte, C. W. Wilkinson and R. T. Zijlstra,Technical note: An improved surgical model for the long-term studies of kinetics and quantification of nutrient absorption in swine, *J. of Animal Sci*, 2009, **87**, 2013-2019.

61 B. U. Metzler-Zebeli, M. G. Ganzie, R. Mosenthin and R. T. Zijlstra, Oat beta-glucan and dietary calcium and phosphorus differentially modify intestinal expression of proinflammatory cytokines and monocarboxylate transporter 1 and Cecal morphology in weaned pigs, *J. of Nutr.*, 2012, **142**, 668-674.

62 S. P. McCormick, M. J. Moore and P. A. Lindahl, Detection of labile low-molecular-mass transition metal complexes in mitochondria, *Biochemistry* 2015, 54, 3442-3453.

63 N. Dziuba, J. Hardy and P. A. Lindahl, Low-molecular-mass iron complexes in blood plasma of iron-deficient pigs do not originate directly from nutrient iron, *Metallomics*, 2019, **11**, 1900-1911

64 M. Wojdyr, Fityk: a general purpose peak fitting program, *J. Appl. Crystallogr*., 2010, **43**, 1126-1128.

65 J. Gitschier , C. D. Vulpe, Y.-M Kuo, *et al*. Hephaestin, a ceruloplasmin homologue implicated in intestinal iron transport, is defective in the sla mouse, *Nat. Genet.*, 1999, **21**, 195–199.

# 4. FUTURE WORKS

The work done in this dissertation offers another snapshot of the complexity of the NTBI pool. We successfully speciated the LMM pool of iron inside of healthy blood plasma and sera, using SEC. We were also able to successfully utilize the circulatory and digestive systems of a living animal as a model system. However, the results we hoped for, including the observation of nutrient derived LMM iron species (which might contain NTBI), did not occur. This finding has led to many questions that need to be answered with future research. Notably, research has yet to definitively answer how NTBI species can be generated via endogenous means, and methods have not been developed to speciate these species without the use of chelators. Another issue that has yet to be settled is whether all iron overload diseases generate the same set of LMM iron species that could possibly be NTBI. Here are some programs of study that can build on the knowledge we acquired during these projects.

## 4.1. Various iron overload models: Do they all contain the same LMM pool of iron and when is it present in the blood?

We initially believed that the best way to detect NTBI was to use HC humans and speciate the LMM iron complex in their blood. However, we did not find distinguishable differences between HC and healthy human individuals. We believe that the lack of a difference may result because these individuals with HC take great care of themselves (e.g., iron restrictive diets, regular phlebotomies, etc.). The next best way to detect NTBI would be to use individuals who were recently diagnosed with HC. However, this is not an easy or feasible option. The third best way would be examining

the NTBI in HC models, of which the best available one is mice. There is one notable difficulty regarding mice models: the small amount of blood that can be acquired. Thus, larger models (e.g., pigs) may be preferable since there is much more blood (i.e., orders of magnitude more) accessible for sampling. Since the utilization of a larger animal yields more available blood, a large range of experiments could be performed, such as kinetic experiments. However, the downside of using a large animal model is that there are not genetic models available for iron overload.

The foundational paper which brought attention to the existence of NTBI had discovered NTBI in beta-thalassemic individuals.[1] The discovery of NTBI was then translated into other iron overload disorders like HC. It may be of some benefit to the field to sample murine models of beta-thalassemia and type 1 and 2 HC and determine if the diseases present the same species of LMM iron complexes which may be NTBI. At the same time, it would be beneficial to show if the LMM iron species in the murine models would match those of diseased humans. These experiments would need to be performed on patients who had recently been discovered to have type 1 or 2 HC and had not been treated. These murine model studies could also help answer the question of when NTBI or the LMM pool of iron increases to a detectable level. Many variables (i.e., age, iron concentration in diet, clinical treatments) can be tested to determine their effect on NTBI levels.

We are currently performing experiments on a mouse model of HC to look at the distribution of iron loading in the organs, as a function of age and iron in the diet. At the same time, we are drawing as much blood from these age and feed groups to probe for

the existence of NTBI or an elevated LMM pool of iron during events of iron loading. We are expecting correlations between the mice's age, the amount of iron in the diet, and the loading of iron in the organs (e.g., liver, spleen, kidney, heart, and possibly the brain). See Appendix B for further details.

### 4.2. Impact of the MPS on the LMM pool of iron in the blood

In the second publication, we proposed that the observed endogenous LMM pool of ironing the blood originates from erythrocyte recycling by the MPS. There are a number of different ways to examine this system's ability to generate LMM iron species. From an in vitro perspective, macrophages or monocytes can be isolated from whole blood or from harvested organs.[2,3] Additionally, human-derived macrophage cultures can be purchased online and grown. Then the harvested/grown macrophages can be incubated in various solutions and their response (i.e., the release of LMM iron species) can be monitored chromatographically. These solutions can contain a variety of different components from just basic saline to red blood cells. Since these macrophages process RBCs, the RBCs can be aged to allow for uptake and the macrophage response can be monitored.[4,5] Additionally, the response of the macrophages in the presence or absence of different iron trafficking proteins (CPN and Tf) and regulatory peptide (HP) could also be monitored. As previously observed in Xenopus oocytes, the presence of Tf and CPN increases the rate of iron efflux.[6] This in vitro model could give us insight into the possible LMM iron species the macrophages – and by extension the MPS – are capable of generating. However, in vitro experiments always need to be followed up by in vivo experiments.

An in vivo experiment to examine the effect of the MPS on the generation of LMM iron species in the blood could be performed with simple blood transfusion experiments. It has already been shown that RBC transfusions can increase the amount of detectable NTBI – via chelator assays – and that the age of the RBCs can increase the rate of their clearance and consequently increase the amount of NTBI in the blood.[4,5] A group of pigs could be used for this experiment, where a few are sacrificed to harvest RBCs that will be used for transfusion. Blood matching may need to be performed before the RBCs are transfused into the remaining animals.[7] The effect of recycling RBCs could be monitored chromatographically in the LMM and HMM iron-containing components of the blood plasma/sera. Basic hematological parameters and hepcidin levels could also be monitored during these experiments. If sufficient LMM iron species are present, then the response of elevated HP could be tested by injecting synthesized HP and monitoring the LMM species.

The above experiments could be considered preliminary studies to determine whether the LMM iron pool would be elevated in RBC transfusions when detected chromatographically. If sufficient evidence is collected from these experiments, a single pig could be raised on a diet enriched with $^{57}Fe$. The enrichment could be enough to elevate the abundance of $^{57}Fe$ above natural abundance in the pig's RBCs so the released iron from the MPS can be differentiated chromatographically. When the level of enrichment is high enough, the animal could be sacrificed, and all of its blood harvested and stored as packed RBCs to be used in transfusions. After the RBCs have been transfused into a non-enriched animal and a proper number of samples have been taken,

the transfused animal could be sacrificed and their organs harvested. The isotopic abundance of the organs could be used to examine where the enriched LMM iron species could be originating from. Additionally, the macrophages from the organs or blood could be isolated here, and a similar isotopic abundance could be performed. If the yield of the macrophages and the $^{57}Fe$ concentration is high enough, other spectroscopic techniques could be performed (e.g., Mössbauer). These experiments could provide insight into the species of LMM iron that is released from MPS due to recycled RBCs.

### 4.3. Impact of RBC on the LMM pool of iron in the blood

Recently, there was evidence that mature RBCs express FPN on their plasma membrane.[8] The expression of the FPN was thought to be beneficial when RBCs are attacked by pathogens, specifically malaria. The iron in the RBC could be "dumped" out of the cell in a protective measure against malaria and to protect it against oxidative stress. This suggests that the RBCs might play some role in forming the LMM iron pool in the blood. A simple experiment to examine this phenomenon would be to take red blood cells and incubate them in different solutions ranging from normal saline to different iron trafficking proteins (i.e., CPN, Tf). The response of the RBCs – via the supernatant of the RBC containing solutions – could be monitored chromatographically and through the concentration of iron present in the samples via ICP-MS. If there is a favorable response under the examined conditions, hepcidin could be added to the solutions to examine if the efflux of iron is controlled via FPN (i.e., not due to the leaching of iron off the RBC membrane). These experiments could further develop an alternative pathway of generating LMM iron species.

### 4.4. Expanding separation techniques for the speciation of LMM metal complexes

The Lindahl lab has mainly focused on using size-exclusion chromatography to separate LMM metal complexes. It would be beneficial to expand the types of separations the lab can perform on metal complexes by including hydrophilic interaction liquid chromatography (HILIC) into its repertoire. This is a chromatographic separation technique which has shown some promise in separating metal complexes.[9] A set of potential experiments could be to perform speciation/characterization on known standards with the column. These standards could include strong metal chelates using chelators like EDTA or small ligands like citrate. Then we could perform a few duplicate experiments of past work (e.g., with mitochondrial extracts, vacuolar extracts, whole cell extracts of S. cerevisiae) and compare the results from the HILIC to those of the SEC separation. If the separation is successful on HILIC and the identification work with the standards was successful, then the potential identities of the ligands in the duplicate experiments could be explored. One of the other focuses of the lab was to eventually characterize the LMM metal complexes with other techniques (e.g., mass spectrometry) for identification. Since HILIC uses an organic/aqueous phase these techniques would be perfect to couple to a MS for species identification. The mobile phase could be matched with solvents preferable for MS sample introduction. With the recent modifications on the LC-ICP-MS system it would easily capable of running HILIC columns in concert with other separation techniques. Also, the ICP-MS was recently modified with an additional gas-line to allow for organic matrix analysis.

## 4.5. References


1 C. Hershko, G. Graham, G. W. Bates and E. a Rachmilewitz, Non-specific serum iron in thalassaemia: an abnormal serum iron fraction of potential toxicity., *Br. J. Haematol.*, 1978, **40**, 255–263.

2 C. Berg, S. Wilker, J. Roider and A. Klettner, Isolation of porcine monocyte population: A simple and efficient method, *Vet. Res. Commun.*, 2013, **37**, 239–241.

3 H. Kitani, M. Yoshioka, T. Takenouchi, M. Sato and N. Yamanaka, Characterization of the liver-macrophages isolated from a mixed primary culture of neonatal swine hepatocytes, *Results Immunol.*, 2014, **4**, 1–7.

4 E. A. Hod, G. M. Brittenham, G. B. Billote, R. O. Francis, Y. Z. Ginzburg, J. E. Hendrickson, J. Jhang, J. Schwartz, S. Sharma, S. Sheth, A. N. Sireci, H. L. Stephens, B. A. Stotler, B. S. Wojczyk, J. C. Zimring and S. L. Spitalnik, Transfusion of human volunteers with older, stored red blood cells produces extravascular hemolysis and circulating non-transferrin-bound iron, *Blood*, 2011, **118**, 6675–6682.

5 E. A. Hod, N. Zhang, S. A. Sokol, B. S. Wojczyk, R. O. Francis, D. Ansaldi, K. P. Francis, P. Della-Latta, S. Whittier, S. Sheth, J. E. Hendrickson, J. C. Zimring, G. M. Brittenham and S. L. Spitalnik, Transfusion of red blood cells after prolonged storage produces harmful effects that are mediated by iron and inflammation, *Blood*, 2010, **115**, 4284–4292.

6 C. J. Mitchell, A. Shawki, T. Ganz, E. Nemeth and B. Mackenzie, Functional properties of human ferroportin, a cellular iron exporter reactive also with cobalt and zinc, *Am. J. Physiol. - Cell Physiol.*, 2014, **306**, 450–459.

7 D. M. Smith, M. Newhouse, B. Naziruddin and L. Kresie, Blood groups and transfusions in pigs, *Xenotransplantation*, 2006, **13**, 186–194.

8 D. L. Zhang, J. Wu, B. N. Shah, K. C. Greutélaers, M. C. Ghosh, H. Ollivierre, X. Z. Su, P. E. Thuma, G. Bedu-Addo, F. P. Mockenhaupt, V. R. Gordeuk and T. A. Rouault, Erythrocytic ferroportin reduces intracellular iron accumulation, hemolysis, and malaria risk, *Science*, 2018, **359**, 1520–1523.

9 P. Flis, L. Ouerdane, L. Grillet, C. Curie, S. Mari and R. Lobinski, Inventory of metal complexes circulating in plant fluids: a reliable method based on HPLC coupled with dual elemental and high-resolution molecular mass spectrometric detection, *New Phytol.*, 2016, **211**, 1129–1141.

# 5. CONCLUSIONS

## 5.1. Summary

The overarching goals of these studies were to: a) speciate and determine the chemical identity of the NTBI pool, and b) understand how NTBI is formed and cleared from the body. In my first paper, we focused on speciating the LMM iron pool present in blood plasma from various mammals. Then, we tried to assign and identify the detected species by comparing it to ferric citrate, the proposed NTBI identity. This work laid the foundation for the next study, which focused on using a model system that allowed us to test the hypothesis of how NTBI can be generated and absorbed by the body. We assumed that this model system would give us the long sought after NTBI that is present under iron overload conditions.

## 5.2. First Publication

In the first publication, we first focused on the technique that we would use to speciate and detect the NTBI pool, to later probe its identity. We used LC-ICP-MS with size exclusion chromatography for the speciation. In LMM FTS from samples of humans, horses, pigs, and mice, we detected LMM iron species ranging between 2500-400 Da. Species at masses approximately 400 and 500 Da were observed more consistently than other species. The concentrations of the detected species were very low, on the order of approximately 100-10 nM. Samples from HC humans showed no chromatographic difference from a sample taken from a healthy human. These species

were also labile, as determined by stability studies comparing fresh versus frozen plasma and after incubation in a refrigerator for a number of days.

We probed the identity of the detected species by comparing their elution profile to that of ferric citrate standards. This comparison led us to the most important conclusion of the study, that ferric citrate is not the predominant species in the LMM iron pool. Comparison of ferric citrate solutions (at iron and citrate concentrations comparable to non-pathogenic conditions) and LMM FTS did not show identical elution profiles, even when the mobile phase pH was adjusted to three different conditions (i.e., pH 4.5, 6.5, 8.5). The ferric citrate standards appeared to be absorbed onto the column under more basic (pH 8.5) conditions when compared to the more acidic conditions (pH 6.5 and 4.5). Absorption of ferric citrate species onto the column also suggests that LMM FTS iron species may also be absorbed onto the column. LMM iron complexes between 400-500 Da were observed to coexist with Apo-Tf when the protein was incubated in LMM FTS samples. The species detected in this study may come from either a nutrient source or from erythrocyte recycling.

### 5.3. Second Publication

In the second publication, we utilized a model system that allowed us to detect and trace isotopically labeled iron from nutrient iron absorption. This system would allow for the analysis of generated LMM iron species originating from nutrient iron, and the liver's ability to absorb these species. We also assumed that some portion of the LMM iron pool would be composed of NTBI generated from nutrient iron trafficking, which would allow us to speciate and chromatographically characterize this pool.

However, our expectations were not met, yet we learned much about iron trafficking in this experiment.

In this study, we learned that nutrient iron is trafficked into the blood and quickly binds to apo-Tf without generating an observable LMM iron intermediate species. We proposed that trafficked nutrient iron is channeled into the blood by the proteins involved in iron trafficking (i.e., HP/CPN and FPN). This potential channeling effect would prevent the formation of any iron species that may be damaging to the body. However, we must concede that there is also a possibility that the sought after NTBI species were being absorbed by the columns used for chromatography.

The observed LMM iron pool was composed of 2-4 iron species. These LMM iron species that were not enriched, indicating that they did not originate from nutrient sources, but rather from some endogenous source. Presumably, the source of this iron comes from internal stores of iron, which could possibly be generated from erythrocyte recycling. Additionally, these LMM iron species were coexistent with apo-Tf. These detectable LMM iron species did not correlate with transferrin saturation. Their levels remained relatively stable and low in intensity, as transferrin saturation increased.

The liver appeared to have an effect on the LMM iron pool by absorbing higher molecular weight species (500-1500 Da) and releasing species in the mass region of 400 Da. There was also an observable difference in the detected Tf peaks, comparing the blood pre and post liver samples. We attributed these differences to the liver altering the isoforms of Tf as it is passed through. Additionally, we proposed that the liver rapidly absorbed the infused ferric gluconate in the blood after the infusion was terminated.

# APPENDIX A CHARACTERIZATION OF IRON DISTRIBUTION IN ORGANS AND BLOOD IN HFE$_{(-/-)}$ MICE AS A FUNCTION OF AGE AND DIETARY IRON SUPPLEMENTATION

## A.1. Contributions

The work done on this project was done in part also by Waseem Vali, a graduate student in the Lindahl lab, and Salvador Fernandez, an undergraduate in the Lindahl lab. They performed the animal sacrifices, organ harvests, and blood draws. I processed all organ samples for elemental analysis and processed all blood samples for LC-ICP-MS analysis. All individuals involved in the project performed animal care. Mr. Vali made the supplemented mouse chow.

## A.2. Project Summary:

Mice at 2 and 5 months of age showed elevated hepatic and splenic iron as the concentration of iron supplementation increased. The liver appears to be loading with iron first and then the spleen. All other organs did not exhibit elevated iron loading. The brain showed no change in iron concentration at any food group, unlike the other organs which showed a moderate increase. The LMM iron pool in the blood contained species with apparent masses ca. 3400, 1100, 600, and 400 Da. There was no elevation in signal intensity of these species as a function of age or iron supplementation. A possible cause for not observing elevated LMM iron in the blood may be because the mice are not fully saturated in transferrin or the liver, the later would absorb NTBI prevent it from reaching the heart where the blood is drawn. We also cannot exclude the possibility that the NTBI is being adsorbed to the column.

Though these experiments show interesting results, there are still unanswered questions. This was a work in progress project that I was part of and the results herein represent my contribution to this project. More is needed in this project to understand what is occurring within the animal. For instance, measurements on the status of transferrin bound iron, analysis of NTBI levels using the traditional NTBI assays, and sampling older mice exhibiting cardiac hypertrophy.

**A.3. Methods:**

**A.3.1. Animals and Husbandry:**

All procedures involving mice were approved by the Animal Use Committee at Texas A&M University (AUP IACUC 2018-0204). $HFE_{(-/-)}$ mice (B6.129S6-Hfe/J) were purchased from Jackson Laboratory and housed at the Laboratory Animal Resources and Research facility (LARR) at Texas A&M University. Mice were fed a standard chow and bred. Once weaned, pups were separated into four experimental groups and placed in iron-free disposable plastic cages with synthetic bedding and plastic water bottles. Two mice from each group were sacrificed 1 and 4 months after weaning (at 2 and 5 months old).

The experimental groups were given distilled, deionized, and redistilled water, and an iron-deficient diet (Envigo TD.80396.PWD) supplemented with either 0, 50, 500, 5000 mg of iron per Kg chow. The chow was mixed with ferrous sulfate heptahydrate powder and a 10-fold molar excess of ascorbic acid. Approximately 45 mL of high-purity water was added per Kg of chow, and the moistened mixture was manually pelleted using a 10 cm length of 2.5 mm OD diameter PVC piping and a 20 cm glass dowel approximately the diameter of the piping ID. Pellets were placed in a rectangular glass pan, and dried in

an oven at 80 °C for 6 -7 hr until the pellets were solid. Mice were given food and water *ad libitum*.

Mice were anesthetized by injecting them IP with a solution containing 4 mg ketamine and 0.5 mg xylazine per 20 g body weight. Euthanasia was by cardiac puncture exsanguination. Withdrawn blood was immediately injected into 3 mL lithium heparin vacutainer tubes (BD vacutainer) and stored at 4 °C for 2 hr or less. Samples were then centrifuged at 2,000 x g for 10-15 min at 4 °C. The resulting plasma was collected and imported into a refrigerated anaerobic glove box (4-8 °C, 1-10 ppm $O_2$) where the top plasma fraction was transferred into an Eppendorf tube. Tubes were sealed, removed from the box, and frozen immediately at -80 °C.

Carcasses were brought into the glove box and perfused with Ringer's solution similar to that described.[1] The pump tubing was attached to a needle that was inserted into the left ventricle of the heart. The heart also had an incision made in the right ventricle so the infused solution could drain after passing through the circulatory system. The solution was left to run until the circulated solution was clear. The heart, liver, spleen, kidney, and brain were dissected and placed in pre-weighed 15 mL plastic tubes with screw top caps (VWR). Organ masses were obtained by re-weighing the tubes and assuming a density of 1.06 gm/mL. Organ digestion was performed as described below.

**A.3.2. Plasma Processing:**

Plasma was diluted 1:1 with 20 mM Tris pH 7.4 and frozen in liquid $N_2$. Prior to thawing the frozen plasma, 10 kDa centrifugation filtration units (Amicon centricon, regenerated cellulose) were prepared by passing 2-3 mL of HPW through the membranes.

The filtration units were placed inside a SW 32.1 Ti rotor vessel and centrifuged in a Beckman Ultracentrifuge according to the manufacture's recommendations. Any remaining water was removed from the top and bottom portion of the vessel. Frozen plasma was thawed and placed inside a centrifugation vessel while inside a glove box. The vessel was sealed, removed from the box, and centrifuged in a similar manner to the HPW. Each sample was centrifugated until approximately 70% of the initial material had passed through the membrane. The flow-through-solution (FTS) volume was aliquoted into an Eppendorf tube for from the centricon.

**A.3.3. LC-ICP-MS Analysis:**

Samples were analyzed on a LC system located inside an anaerobic (1-10 ppm $O_2$) and chilled (4 -8°C) glovebox (LabMaster, Mbraun), as described.[2] The LC system was recently modified with a bio-inert multisampler (Agilent 1260 Infinity II, G5669A) installed with a 2 mL extended loop. Prior to the addition of the multisampler, 300 µL of samples were injected into a PEEK loop and injected onto the column. After the addition of the multisampler, instead of using a sample loop 170 µL of sample was aliquoted into a plastic multisampler vessel (Thermo Scientific) and placed inside of the multisampler. Less sample was used after the multisampler to help conserve sample volume for other analysis. The multisampler was programmed to inject 150 µL of sample a Superdex Peptide 10/300 GL column (Ge Healthcare, 17517601) operating at a flow rate of 0.6 mL* $min^{-1}$ with a mobile phase composition of 20 mM ammonium acetate pH 6.5. The LC system used a 100 mM stock of ammonium acetate pH 6.5 that was mixed in-line

using the LC pump with HPW to reach the desired final concentration. Both the HPW and stock mobile phase had been degassed using a Schlenk-line system.

**A.3.4. Calibration Curve:**

The calibration curve used in these experiments were prepared as described in Appendix A, Part 2). Calibrations were run on the system prior to the addition of the multisampler, due to the 2 mL offset from the extended loop the detected species elution volume from the data was reduced by 2 mL before calculating the apparent molecular mass. Species elution volume from mice sacrificed after 1 month have their elution profile subtracted by -2.0 mL to determine their mass using the above calibration curve.

**A.3.5. Column Cleaning:**

The column was cleaned as described with modifications. The modifications are as follows: after the system upgrade the chelator cocktail concentration was increased 10-fold and 500 uL of this stock was injected onto the column. The cleaning cycle was run at the same flow rate and mobile phase composition as the desired sample analysis. The cleaning ran for a minimum of 3 column volumes (column bed volume) prior to the analysis of samples.

**A.3.6. Elemental Analysis:**

The acid digestion of the organs was performed using a protocol as described.[3] The mass of the harvested organs was calculated by subtracting the total of the tube + organ mass by the tube mass. Concentrated trace metal grade nitric acid (Fisher) was added at a concentration of 0.1 g organ/ mL acid to the tubes. The acid was added directly to the 15 mL tube the organs were placed in, the tubes were sealed by capping

the tubes and wrapping it in electrical tape to make as tight of a seal as possible. The vessels were then inserted into a pre-heated over set to 70-80 °C and left to acid-digest for 12-16 hours. After digesting the vessels were left on the bench to cool down before placing in a 4 °C refrigerator for a minimum of 3 hours. The digested material was pipetted into an Eppendorf tube and then centrifuged on a tabletop centrifuge for 10,000xg for 15 minutes to pellet any undigested components. The supernatant of the centrifuged digest was then pipetted in triplicate. The replicates were made by pipetting 110 μL of digest into fresh 15 mL falcon tubes in triplicate to which 4.89 mL of HPW was added to each tube affording a final acid concentration of 2% (v/v) concentrated nitric acid (Fisher). Any remaining digest was stored in the refrigerator for later use if required. Instrumental analysis of these samples were performed as previously described.[2] The concentration of iron in the organs was estimated by converting the mass of the organs into volume, assuming a density of 1.06 g/mL.

**A.3.7. Data Analysis:**

All figures were generated using IgorPro (8.0). Data collected from mice sacrificed at 1 month were analyzed on the system before the multisampler was installed. Data collected from mice sacrificed at 5 months were analyzed on the system with the multisampler. Data from 2 month old mice have their elution profile modified by +2.0 mL to make data interpretation and analysis easier.

## A.4. Results:

### A.4.1. Distribution of iron in organs:

We fed $HFE_{(-/-)}$ mice an iron-deficient diet supplemented with 0, 50, 500, and 5000 mg of iron per Kg chow. The endogenous iron concentration in the iron-deficient chow was ca. 5 mg/Kg, and that value will be quoted (rather than 0) for the iron concentration in supplemented chow. Two mice from each of the four groups were sacrificed after 1 and 4 months on the diet (age 2 and 5 months), and blood-plasma and certain organs (brain, liver, heart, spleen, and kidneys) were analyzed. We anticipated that the concentration of non-transferrin bound iron (NTBI) in the plasma would increase with increasing iron in the diet, as would the concentration of iron in the organs, particularly the liver and spleen. We also anticipated that as the mice aged, the liver would become saturated with iron causing other organs to become iron-loaded. The results from this experiment are presented in Figure A-1.

Mice at 2 and 5 months of age all exhibited elevated concentration of iron in both the spleen and liver as the iron supplementation in the diet increased (Figure A-1 panels A and B). Older mice had higher concentrations of iron overall in the liver and spleen (Table A-1, 5 months old). As the concentration of iron in the diet increased so too did the iron content in the kidney and heart (Table A-1). However, the increase for the heart and kidney were only observed after iron was added to the diet, afterwards the increase in iron was invariant across supplementation (Table A-1). There appeared to be no change in the iron concentration within the brain at all, when comparing between food groups and age (Figure A-1 and Table A-1). The iron content in the heart and kidneys

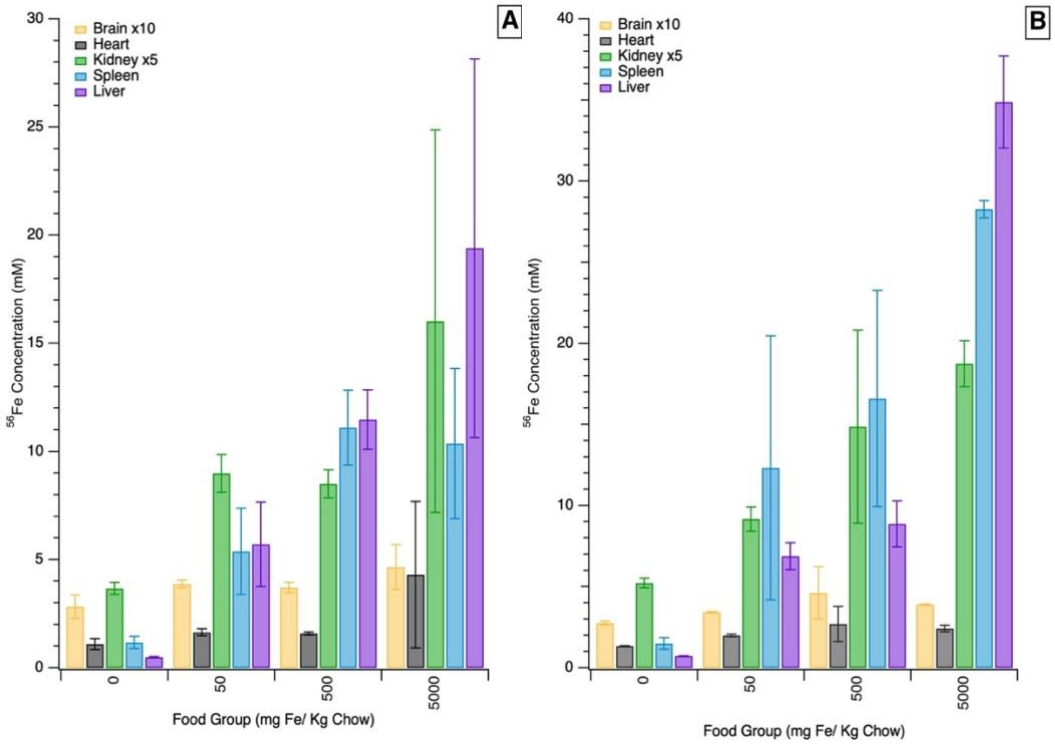


**Figure A-1. Average concentration of iron in mouse organs.**
Concentration of iron in the brain, heart, kidney, spleen and liver was averaged from the two mice sacrificed from each group. Standard deviations were calculated between the replicates for each food group. Bottom axis represents the food group. Two mice were sacrificed per food group. Food groups consisted of 0, 50, 500, and 5000 mg Fe per Kg of chow. Panels represent the age of mice, they are labeled as follows: A, 2 month of age; B, 5 months of age. The brain concentration was multiplied by 10 and the kidney by 5 to bring them in scale.

Iron Concentration In Organs (mM)

| | Food Groups (mg Fe / Kg Chow) | | | |
|---|---|---|---|---|
| | 0 | 50 | 500 | 5000 |
| Organ\|Age | Range | Range | Range | Range |
| L\|2 | 0.47-0.52 | 4.3-7.1 | 11-13 | 13-26 |
| L\|5 | 0.73-0.73 | 6.3-7.5 | 7.9-9.9 | 33-37 |
| S\|2 | 0.97-1.4 | 4.0-6.8 | 9.9-12 | 8.0-13 |
| S\|5 | 1.2-1.7 | 6.7-18 | 12-21 | 28-29 |
| H\|2 | 0.93-1.3 | 1.5-1.8 | 1.5-1.6 | 1.9-6.7* |
| H\|5 | 1.3-1.4 | 1.9-2.0 | 1.9-3.7 | 2.3-2.6 |
| K\|2 | 0.70-0.77 | 1.7-1.9 | 1.6-1.8 | 2.0-4.5 |
| K\|5 | 1.0-1.1 | 1.7-1.9 | 2.1-3.8 | 3.5-4.0 |
| B\|2 | 0.24-0.32 | 0.37-0.40 | 0.35-0.39 | 0.39-0.54 |
| B\|5 | 0.27-0.28 | 0.34-0.35 | 0.35-0.58 | 0.39-0.39 |

**Table A-1. Iron Concentration in Organs**

Range of concentrations from harvested organs across all food groups. The range displayed are for either of the mouse replicates per food group that have been ordered from lowest to highest concentration. Organ and age labels are as follows: L, liver; S, spleen; H, heart; B, brain.; 2, 2 month old at sacrifice; 5, 5 months old at sacrifice. * indicates a possible outlier due to incomplete perfusion. These values were used to calculate the average and standard deviation in Figure 1.

may not have become overloaded because the organs which act as iron buffers (i.e., the liver) were not fully saturated and still absorbing all of the NTBI species. We cannot determine at this time if the observed increase in iron concentration in the liver and spleen represent complete saturation or if this extent of loading is significant due to the low replicate number and lack of non-mutant controls.

**A.4.2. LMM analysis of plasma FTS:**

The blood from the mice was also collected and processed into an LMM FTS that was analyzed by SEC-ICP-MS in an attempt to speciate the LMM pool of iron in the blood that should contain NTBI. We anticipated that as the concentration of supplemented iron increased in the diet and/or as the mice aged, so too would the LMM pool of iron in the blood. The results of this experiment are presented in Figure A-2.

The LC traces of plasma FTS from 2 month old animals exhibited a dominant peak at ca. 600 Da (Figure A-2 panel A). One sample exhibited an additional peak at 1100 Da and two samples exhibited an additional peak at 3400 Da. The 600 Da peak tailed on the low-mass side and a 400 Da species could be present. There was no trend in the intensity of any of these peaks with the level of iron supplementation.

The LC traces from 5 month old animals were similar to those from the 2 month old animals, but also with important differences. The dominant peak in all four traces was at 1100 Da, with minor peaks at 600 Da and 400 Da (Figure A-2 panel B). The 3400 Da peak was absent from all traces and the 400 Da peak was resolved from the 600 Da peak. Most importantly, the intensity of these 1100, 600, and 400 Da peaks was virtually

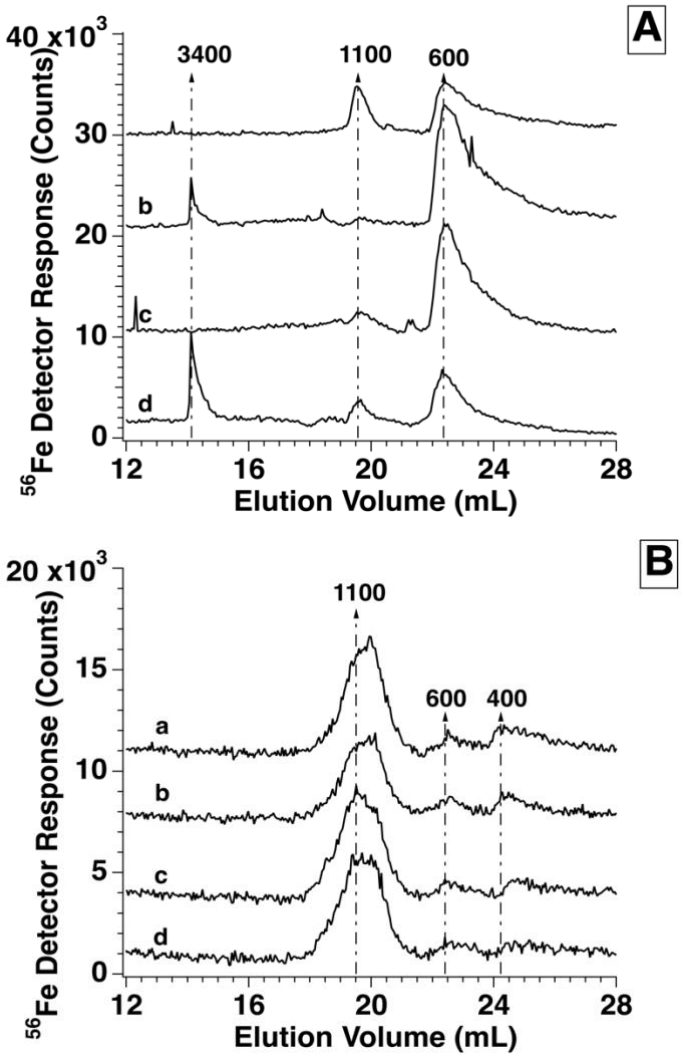


**Figure A-2. Speciation of Low Molecular Mass Plasma FTS**
Plasma was diluted 1:1 with 20 mM Tris pH 7.4 buffer and filtered through a 10 kDa device to generate FTS which was separated on a size-exclusion column. Panels represent mice of different ages and are as follows: A, 2 month old; B, 5 months old. Trace labels represent the different concentrations of supplemented iron in the food groups and are as follows: a, 0; b, 50; c, 500; d, 5000 mg Fe/ Kg chow. Traces from panel B were multiplied by a factor of two to allow for comparison of traces to panel A. Panel A used 300 µL of material, panel B used 150 µL of material. Panel A traces elution volume were modified by adding 2.0 mL to all data points for comparison to panel B.

identical in all four traces – there was no trend with the level of iron supplementation in the diet.

**A.5. Discussion:**

Hemochromatosis mice, lacking the HFE gene, accumulate iron within their bodies in both the organs and blood.[4,5] We wanted to detect the iron species in the blood that accumulates, as this should be NTBI, and then show that NTBI levels increase with increasing levels of iron in the diet. NTBI is known to accumulate in the liver and other organs, and we wanted to confirm this as well.

We study this distribution as the body aged and we speciated the LMM pool of iron in the blood. We expected that initially the liver would begin to load with iron at a faster rate than other organs, due to the liver's role in storing iron and involvement in the mononuclear phagocyte system.[6,7] Then as the body became saturated with iron, we expected the other organs to load. Due to the route of circulatory system and from clinical manifestations in HH patients, we expected that the heart would then begin to load next, of the organs we harvested.[8] The results we have collected so far begin to tell a story about the distribution of iron in the organs as a function of age and iron supplementation.

The liver and spleen were the first organs observed to be highly loaded with iron, followed by the spleen (Figure 1 and Table 1). We expected the liver to be elevated in iron as it filters the blood coming from the spleen and digestive tract; both are locations where iron can be exported.[9] Both the spleen and digestive track empty into the portal vein which leads into the liver. The next organ in this pathway is the heart. As for the

spleen, individuals with hemochromatosis don't always have elevated hemoglobin levels, though they can sometimes have splenomegaly, an enlarged spleen.[8] We also cannot discount the possibility that the perfusion performed on the mice was not exhaustive and that some RBC remained in these organs. We did not see the other organs begin to saturate with iron as we anticipated. This may be because the body's iron storage sites had not yet become full. Possibly once these systems become saturated then other organs (i.e., kidney and heart) will acquire iron to a larger extent than currently observed and cause the distinctive manifestations seen in HH individuals.

Mice with a similar genetic condition have been observed to have elevated NTBI levels compared to controls after only 11 weeks of age; NTBI was assayed using a chelator-colorimetric based assay.[10] We anticipated that the mice we studied would share a similar phenotype and that after 4 months post-weaning (5 months old, 20 wks) we would see elevated NTBI levels within the LMM iron pool via the LC. Surprisingly, we did not see such elevation across age or iron supplementation groups. Moreover, species that were observed were similar to those previously characterized in healthy animals.[2]

We expected to observe NTBI in these animals based on this previous research. A possible explanation as to why we did not observe an increase in the LMM iron pool where as others have might be due to the assay used to detect NTBI. The results gained by the previous group could be an artifact of the assay used which used NTA as a chelator. It has already been shown that the high concentrations of chelators used in the traditional NTBI assay can give false positives.[11] This might suggest that NTBI is not generated this early in the lifespan possibly because transferrin is not adequately

saturated or the liver is not fully saturated. Both systems would prevent the localization of NTBI to the heart. More experiments are required to determine the extent of transferrin saturation in the mice as they age and in the different supplementation groups. Future experiments are needed where older mice examined, to allow for adequate saturation of the liver and transferrin.

If the liver was not fully saturated at 5 months, it could continue to absorb NTBI. In this case, we would not observe NTBI in blood drawn downstream from the liver (i.e., the heart). The liver can absorb NTBI analogs relatively quickly.[12] Blood drawn from the heart might not contain NTBI if the liver is able to process NTBI, and only until the liver is essentially non-functional in NTBI absorption would NTBI be expected to be detectable in blood drawn from the heart. Hemochromatosis if left untreated can cause cardiomyopathy, the enlargement of the heart, proposed to be due to damaged caused by ROS from iron.[4,8] In this same strain of mice that we used, it has been demonstrated that after 12 months of age, these mice exhibited cardiomyopathy whereas mice aged at 5 months did not.[4] We may be required to use mice that are twice as old as we have currently used to observe some form of cardiomyopathy and cardiac iron loading before we will see an increase in the LMM pool of iron in the blood when drawn from the heart.

A less exciting hypothesis is that the chromatography technique we are utilizing may be unable to separate the NTBI. We may only be observing the stable species present in blood samples, and the separation technique may not be able to resolve the less stable species. We may need to probe the LMM iron pool using a different chromatographic technique to observe these less stable species. One such technique is

HILIC which has been used to speciate ferric citrate in plant fluids.[13] We may also want to examine the concentration of NTBI by using traditional assays to correlate our results with the field.[14]

In conclusion, the liver and spleen of the mice are elevated in iron concentration as the age and supplementation increases, though this increase does not correlate with observed LMM iron species in the blood. Either the species have not yet formed, as the conditions within the body are not adequate for generating NTBI (i.e., high transferrin saturation, liver saturation, etc.), or less stable species are lost during the analysis due to degradation and/or absorption onto the column. The species that we are observing may be the stable species, and the species we are most interested in are the less stable species which have adsorbed onto the column.

**A.6. References:**


1 G. P. Holmes-Hampton, M. Chakrabarti, A. L. Cockrell, S. P. McCormick, L. C. Abbott, L. S. Lindahl and P. A. Lindahl, Changing iron content of the mouse brain during development, *Metallomics*, 2012, **4**, 761–770.

2 N. Dziuba, J. Hardy and P. A. Lindahl, Low-molecular-mass iron in healthy blood plasma is not predominately ferric citrate, *Metallomics*, 2018, **10**, 802–817.

3 S. B. Niazi, D. Littlejohn and D. J. Halls, Rapid partial digestion of biological tissues with nitric acid for the determination of trace elements by atomic spectrometry, *Analyst*, 1993, **118**, 821–825.

4 A. Sukumaran, J. Chang, M. Han, S. Mintri, B. A. Khaw and J. Kim, Iron overload exacerbates age-Associated cardiac hypertrophy in a mouse model of hemochromatosis, *Sci. Rep.*, 2017, **7**, 1–10.

5 J. E. Levy, L. K. Montross, D. E. Cohen, M. D. Fleming and N. C. Andrews, The C282Y mutation causing hereditary hemochromatosis does not produce a null allele, *Blood*, 1999, **94**, 9–11.

6 K. P. Batts, Iron overload syndromes and the liver., *Mod. Pathol.*, 2007, **20**, S31-39.

7 W. Kong, X. Duan, Z. Shi and Y. Chang, Iron metabolism in the mononuclear phagocyte system, *Prog. Nat. Sci.*, 2008, **18**, 1197–1202.

8 B. K. Crownover and C. J. Covey, Hereditary hemochromatosis., *Am. Fam. Physician*, 2013, **87**, 183–90.

9 M. U. Muckenthaler, S. Rivella, M. W. Hentze and B. Galy, A Red Carpet for Iron Metabolism, *Cell*, 2017, **168**, 344–361.

10 A. C. G. Chua, J. K. Olynyk, P. J. Leedman and D. Trinder, Nontransferrin-bound iron uptake by hepatocytes is increased in the Hfe knockout mouse model of hereditary hemochromatosis, *Blood*, 2004, **104**, 1519–1525.

11 A. M. Kolb, N. P. M. Smit, R. Lentz-Ljuboje, S. Osanto and J. van Pelt, Non-transferrin bound iron measurement is influenced by chelator concentration, *Anal. Biochem.*, 2009, **385**, 13–19.

12 P. Brissot, T. L. Wright, W. L. Ma and R. A. Weisiger, Efficient clearance of non-transferrin-bound iron by rat liver. Implications for hepatic iron loading in iron overload states, *J. Clin. Invest.*, 1985, **76**, 1463–1470.

13 P. Flis, L. Ouerdane, L. Grillet, C. Curie, S. Mari and R. Lobinski, Inventory of metal complexes circulating in plant fluids: a reliable method based on HPLC coupled with dual elemental and high-resolution molecular mass spectrometric detection, *New Phytol.*, 2016, **211**, 1129–1141.

14 L. de Swart, J. C. M. Hendriks, L. N. van der Vorm, Z. I. Cabantchik, P. J. Evans, E. A. Hod, G. M. Brittenham, Y. Furman, B. Wojczyk, M. C. H. Janssen, J. B. Porter, V. E. J. M. Mattijssen, B. J. Biemond, M. A. Mackenzie, R. Origa, R. Galanello, R. C. Hider and D. W. Swinkels, Second international round robin for the quantification of serum non-transferrin-bound iron and labile plasma iron in patients with iron-overload disorders, *Haematologica*, 2016, **101**, 38–45.

# APPENDIX B LMM SPECIES EXPORTED BY THE MITOCHONDRIA

## B.1. Appendix B Details

This appendix details my work characterizing the iron and sulfur species exported from mitochondria; there are two sections. The first section is work done with Pandey et al., 2018 on the sulfur species '$S_{int}$' that is exported from mitochondria and is used in tRNA thiolation. I performed the liquid chromatography and peak fitting experiments; all other experiments were performed by the other authors. The second section is work done with Rachel Shepherd, another graduate student in the Lindahl lab, on characterizing the iron and sulfur species exported from intact mitochondria during various treatments to stimulate the mitochondria. Ms. Shepherd grew the cultures, isolated the mitochondria, and generated the samples. I prepared the samples for chromatographic analysis and performed LC-ICP-MS on these samples.

## B.2. Part 1:

## MITOCHONDRIA EXPORT SULFUR SPECIES REQUIRED FOR CYTOSOLIC TRNA THIOLATION‡

‡ Reproduced and adapted by permission from "Mitochondria Export Sulfur Species Required for Cytosolic tRNA Thiolation" by Alok Pandey, Jayashree Pain, Nathaniel Dziuba, Ashutosh K. Pandey, Andrew Dancis, Paul A. Lindahl, Debkumar Pain, 2018. *Cell Chemical Biology*, 25, 738-748, Copyright 2018 by Elsevier.

### B.2.1. Introduction

Correct and efficient protein translation is essential to cell survival, and a variety of post-transcriptional modifications of tRNAs are vital for their folding, stability, and decoding functions.[1] In the cytosol of eukaryotes, the wobble uridine (U34) of three tRNAs specific for lysine (tRNALysUUU), glutamate (tRNAGluUUC), and glutamine (tRNAGlnUUG) contain a methoxycarbonylmethyl (mcm5) functional group and a thio-modification (s2) at positions 5 and 2, respectively.[2] The thiolation of these cytosolic tRNAs promotes their binding to the ribosomal A site[3], prevents frameshifting[4], ensures accurate translation at an optimal rate[5], and senses cellular sulfur availability[6]. In yeast, impaired s2U34 modification leads to pleiotropic phenotypes including genome instability.[7] In humans, impaired thiolation of cytosolic tRNAs has been linked to familial dysautonomia.[8] Additional thio-modifications have been identified in mitochondrial tRNAs, such as 5-carboxymethylaminomethyl-2-thiouridine (cmnm5s2U34) in yeast and 5-taurinomethyl-2-thiouridine (τm5s2U34) in mammals.[2] Non-thiolated mitochondrial tRNAs in humans are associated with myoclonic epilepsy with ragged-red fibers.[9] Thus, thiolation of tRNAs is critical to maintaining overall cellular homeostasis. Here we focus on cytosolic tRNA thiolation in yeast, particularly the contribution of mitochondria to this process.

The amino acid cysteine is the source of sulfur for tRNA thiolation, and cysteine desulfurase is the only enzyme capable of abstracting sulfur from cysteine. It generates an enzyme-bound persulfide from cysteine and donates the activated sulfur to designated recipients.[10,11] In yeast, the Nfs1 cysteine desulfurase is present primarily in

mitochondria.[12] Trace amounts are probably also present in the nucleus and cytosol, as shown by sensitive genetic methods.[13] In vivo depletion of the mitochondrial form of Nfs1 leads to deficiencies of both mitochondrial and cytosolic tRNA thio-modifications.[10,14] The implication is that mitochondrial Nfs1 may generate some species, perhaps a sulfur intermediate, which is utilized directly or indirectly for cytosolic tRNA thiolation. However, none of the steps regarding the hypothesized sulfur intermediate, such as its generation, export, or utilization, has been demonstrated. Progress has been hampered because available assays mostly rely on measuring steady-state levels of thiolated tRNAs in vivo[14–16], making it difficult to identify the steps involved in mitochondrial formation of sulfur intermediates and export to the cytosol.

The idea that mitochondria might export some sulfur species originated from studies of iron-sulfur (Fe-S) cluster biogenesis.[17] Fe-S clusters are essential cofactors of proteins involved in vital processes including respiration, DNA repair, protein translation, and iron sensing. As with tRNA modifications, the biogenesis of Fe-S clusters in eukaryotes is also compartmentalized.[17] Fe-S cluster assembly is mediated by a multi-subunit machinery inside mitochondria, termed the ISC (iron-sulfur cluster), and outside of mitochondria in the cytosol, termed the CIA (cytosolic iron-sulfur protein assembly). Importantly, mitochondrial Nfs1 is required for mitochondrial as well as cytosolic Fe-S cluster synthesis[18], implying that a substrate or signal derived from Nfs1 activity is exported from mitochondria and utilized in the cytosol, similar to the proposed mechanism of tRNA thiolation. The species exported from mitochondria is unknown but likely involves sulfur in view of its dependence on the Nfs1 cysteine

desulfurase.[17] The best candidate for the exporter is Atm1, an ABC transporter situated in the mitochondrial inner membrane and oriented with its substrate-binding site and ATP-binding site facing the matrix.[19] The phenotype of Atm1-depleted cells is characterized by a deficiency of cytosolic Fe-S proteins.[17] The crystal structure of yeast Atm1[20] has been solved but its exported substrate remains elusive. Candidate substrates such as small thiol compounds were evaluated for their ability to stimulate the Atm1 ATPase activity or to be transported into Atm1-containing vesicles.[21–23] However, none qualifies as a truly exported and functional sulfur-containing molecule.[17] Interestingly, the sulfur export hypothesis has recently been extended to cytosolic tRNA thiolation[2], although no supporting evidence thus far exists. Here we have developed a strategy to track mitochondria-generated sulfur intermediates required for cytosolic tRNA thiolation. The experimental approach involves detecting de novo cytosolic tRNA thiolation using mitochondria and cytosol isolated from yeast cells, and using [$^{35}$S]cysteine as the sulfur source.

### B.2.2. Methods

#### B.2.2.1. Mitochondria and cytosol mixing assays

Assays were composed of isolated mitochondria which were then added to a cytosol solution. Ferrous ascorbate and [$^{35}$S]cysteine were added to different sample mixtures that were allowed to incubate at 30 °C for various times. Control assays were performed with mitochondria or cytosol alone. The resulting solutions were centrifuged giving a pellet (mitochondria) and a supernatant (cytosol). These fractions were further processed. The mitochondrial fractions were treated by rupturing the mitochondria then

centrifuging the sample to yield a supernatant solution that was used for gel analysis. The cytosolic fraction was treated by precipitating the fraction and then centrifuging to yield a supernatant. The supernatant solutions from the mitochondria and cytosolic processing were then run on native polyacrylamide gel electrophoresis. Sometimes the cytosolic supernatant was analyzed by SDS-PAGE.

**B.2.2.2. Isolation of unlabeled materials exported from mitochondria for SEC-ICP-MS chromatography**

Briefly, reactions were performed in six batches. Each batch contained intact WT mitochondria (5 mg of proteins) in a final volume of 0.5 ml HS buffer containing 40 mM KOAc, 10 mM $Mg(OAc)_2$, 2 mM ATPγS and 10 μM unlabeled cysteine. Samples were incubated at 30 °C for 30 min to allow generation of unlabeled Sint and to have it "trapped" within mitochondria. The reaction mixtures were diluted with ice-cold HS buffer and centrifuged at 15,000 x gfor 5 min at 4°C. The mitochondrial pellets thus obtained were washed twice with HS buffer to remove any residual ATPγS and unlabeled cysteine. Mitochondria were then resuspended in 100 μl of HS buffer containing 4 mM ATP and incubated at 30 °C for 30 min to allow the export process. Samples were centrifuged at 15,000 x g for 10 min at 4°C. The supernatant fractions containing exported Sint were pooled from six identical reaction mixtures (total volume ~0.6 ml) and extracted with an equal volume of water-saturated chloroform. After centrifugation at 15,000 x g for 2 min at 4 °C, the organic layer containing Sint was dried down in SpeedVac. The dried material was dissolved with 200 μl of 20 mM HEPES/KOH, pH 7.5 and stored at -80 °C until further use.

The nfs1-14 and Atm1-depleted (Atm1↓) mitochondria were similarly processed to obtain corresponding exported materials. Likewise, exported material from WT mitochondria with no preloaded cysteine served as a negative control. As another control, the export reaction with WT mitochondria (preloaded with unlabeled cysteine) was performed in the presence of ATPγS (2 mM) rather than ATP. All of these exported materials were tested in a competition assay for their ability to inhibit 35Sint-mediated radiolabeling of cytosolic tRNAs (see Figure S2, bottom panel), and further characterized by SEC-ICP-MS chromatography as described below.

**B.2.2.3. Immunoblotting**

Proteins were separated on an SDS gel and then transferred to nitrocellulose. The blot was stained with amido black. The blot was cut in half at the 55 kDa region. The top half was probed with rabbit anti-ATM1 antibodies and the bottom half with rabbit anti-Tom40 antibodies. The blots were treated with horseradish peroxidase-conjugated to donkey anti-rabbit antibody. The protein signals were detected using chemiluminescence.

**B.2.2.4. Chromatography and elemental spectroscopy**

Instrumentation and parameters: SEC-ICP-MS chromatography was performed on an Agilent 1260 Bio-inert HPLC quaternary pump system that was installed in an anaerobic and refrigerated glovebox (MBRAUN LabMaster, NH, USA). The glovebox was maintained with a nitrogen atmosphere at <1 ppm $O_2$ (Teledyne Analytical Instruments, CA, USA) and at 6 °C. The HPLC system was equipped with a bio-inert multivalve injector and a 200 µl PEEK injection loop. All column tubing and fittings

were made of PEEK. Two Superdex Peptide 10/300 GL columns (GE Healthcare Life Science, PA, USA) were connected in series via a male-to-male fitting. Ammonium bicarbonate (20 mM, pH 8.5), degassed via a Schlenk line, was used as the mobile phase and run at a flow rate of 0.350 mL $min^{-1}$. The eluent from the column was fed into the Diode Array and then into a splitter. A major portion (70%) of the eluent flowed to the fraction collector and the remaining 30% was exported from the glovebox and into an Agilent 7700x ICP-MS in an on-line configuration. This allowed for simultaneous separation, fraction collection, and elemental detection. Elements detected included $^{31}P$, $^{34}S$, $^{48}Ti$, $^{55}Mn$, $^{56/57}Fe$, $^{59}Co$, $^{60}Ni$, $^{63/65}Cu$, $^{66/68}Zn$, and $^{95}Mo$. The ICP-MS was fitted with a micromist nebulizer, Scott-type spray chamber, and nickel sampling/skimmer cones. ICP-MS operational parameters are as follows: RF Power 1550 W; Ar flow rate, 15 l $min^{-1}$; collision cell He flow rate, 4.1 mL $min^{-1}$; carrier gas flow rate, 1.05 L $min^{-1}$; dilution mode, OFF; spray chamber temperature, 2 °C; analysis time, 9600 sec.

All analytical solutions used high purity water, made from distilled, triple filtered, and deionized water. The sample loop was prepared by passing 3 loop-volumes of a 10% nitric acid solution and incubating for a minimum of 2 h prior to analysis, after which the loop was rinsed with 3 loop-volumes of high purity water. Samples were stored at -80 °C and thawed inside the glove box for analysis. The columns were regenerated after each day of use by running 10 column volumes of a chelator cocktail composed of 10 mM ascorbic acid and 10 μM each of EDTA, EGTA, 2,2'-bipyridine, 1,10 phenanthroline, and bathocuproinedisulfonic acid.

Species molecular mass and peak fitting: Molecular masses were determined by fitting peak elution volumes to a calibration curve, in which standards of known molecular masses were passed through the SEC-ICP-MS system. The calibration curve was generated by plotting the log of the molecular mass vs the elution volume divided by the void volume of the standards. The elution volume of blue dextran was used to determine the void volume. The standards used included: AMP, ADP, ATP, cyanocobalamin, insulin, and cytochrome c.

**B.2.2.5. Quantification and data analysis**

For the SEC-ICP-MS chromatography, the chromatogram peak fitting was performed with the Fityk software.[24] The Levenberg-Marquardt method was used and Gaussian line shapes were assumed. The minimum number of peaks required to fit the entire data set were used.

**B.2.3. Results**

**B.2.3.1. Radiolabeling of an endogenous species in the cytosol occurs only in the presence of mitochondria**

Radiolabel tracing of [$^{35}$S] from [$^{35}$S]cysteine treated mitochondria in the presence of cytosolic components show the export of a sulfur species that is incorporated into the cytosolic component of the mixture. The export of the sulfur species is dependent on the presence of both cytosol and mitochondria in the reaction mixture. The absence of cytosol in the reaction mixture had no detectable sulfur species indicating the sulfur species was not a simple export product of mitochondria.

### B.2.3.2. The radiolabeled endogenous species in the cytosol are tRNAs

The detected sulfur species exported from the mitochondria in the presence of cytosol is thiolated tRNA. Incubation of cytosol and mitochondria treated with [$^{35}$S]cysteine in the presence of tRNALys (a substrate for tRNA thiolation) showed an increase the exported sulfur species. Nuclease treatment showed no sulfur species when cytosol and mitochondria were mixed and treated with [$^{35}$S]cysteine in the presence or absence of tRNALys. Removing a component of the thiol tRNA modification machinery present in the cytosol showed reduced intensity of the sulfur species in Δurm1 (ubiquitin-related modifier, Urm1) isolated cytosol and mitochondria mixtures.

### B.2.3.3. Effects of impaired mitochondrial Fe-S cluster assembly on cytosolic tRNA thiolation

Cysteine desulfurase and Isu1/2, but not Ssq1 are required for generating sulfur species involved cytosolic tRNA modification. When either mitochondria with a mutant cysteine desulfurase (nfs1-14), exhibiting Fe-S cluster deficiencies, or with depleted Isu1/2 were mixed with WT cytosol and treated with [$^{35}$S]cysteine, there was reduced thiolated tRNA products and no labeled aconitase compared to WT mitochondria. Mitochondria ssq1 mutants mixed with WT cytosol showed no labeled tRNA products, but it did show labeled aconitase.

### B.2.3.4. Effects of disrupted cytosolic Fe-S cluster assembly on cytosolic tRNA thiolation

Reductase Dre2 is required for cytosolic tRNA thiolation and possibly other downstream cytosolic iron sulfur cluster assembly components. WT mitochondria and

dre2 depleted cytosol were mixed and treated with [$^{35}$S]cysteine showed little cytosolic tRNA thiolation even in the presence of tRNALys.

### B.2.3.5. Detection of active sulfur species accumulated within mitochondria

Mitochondria generate the sulfur intermediate species ($S_{int}$) in the matrix and is exported into the cytosol for tRNA thiolation. Pretreatment of WT mitochondria with [$^{35}$S]cysteine mixed with WT cytosol showed increased tRNA thiolation as the mitochondria concentration increased. Thiolated tRNA product was detected in matrix samples and not in the membrane fractions mitochondrial samples mixed with cytosol and treated with [$^{35}$S]cysteine. tRNA thiolation was detected in only mitochondrial matrix FTS and not the retentate after passing through a 3kDa membrane. Indicating that Sint is less than or equal to 3 kDa in size. The matrix from mitochondria derived from nfs1-14 mutant cells failed to generate $S_{int}$. The thiolation assay could be used as a competition assay if unlabeled Sint, isolated from mitochondria treated with unlabeled cysteine, is added to the cytosol fraction of the thiolation assay.

### B.2.3.6. Detection of $S_{int}$ exported from intact mitochondria in active form

Sint is exported out of the mitochondria by Atm1 in an ATP dependent manner. Mitochondria pretreated with [$^{35}$S] cysteine showed reduced tRNA thiolation in the thiolation assay. $S_{int}$ is generated in the mitochondria and then exported after export $S_{int}$ is used by the cytosol machinery to thiolate tRNA without further need of the mitochondria. This was determined using an assay where $S_{int}$ is generated in the mitochondria and then exported in a manner where it can be isolated separately from the

mitochondria without lysis. The isolated $S_{int}$ can then be added to cytosol solutions similar to the thiolation assay to detect generation of thiolated tRNA.

$S_{int}$ was generated in mitochondria using [$^{35}$S]cysteine, its export was stopped using ATPγS. The mitochondria were washed and then incubated in ATP to stimulate the export of $S_{int}$. If ATP is not used during this step there is no export of $S_{int}$. The resulting supernatant was incubated in cytosol and nucleotides but no cysteine resulting in the presence of thiolated tRNA. Unlabeled $S_{int}$ could compete with labeled $S_{int}$. The generated unlabeled $S_{int}$, could be isolated for use in characterization.

**B.2.3.7. Characterization of $S_{int}$**

Unlabeled materials exported from various mitochondria under different conditions were analyzed for competing for activity with $^{35}S_{int}$, and in parallel by size-exclusion chromatography combined with inductively coupled plasma mass spectrometry (SEC-ICP-MS) (Figure B-1).[25] The material exported from WT mitochondria (preloaded with unlabeled cysteine) exhibited competing activity and this sample contained six sulfur-containing species with approximate molecular masses of 1,500, 1,100, 1,000, 900, 800, and 700 Da (Figure B-1, trace a). These species are referred to as $S_{1500}$, $S_{1100}$, $S_{1000}$, $S_{900}$, $S_{800}$, and $S_{700}$, respectively. Some of these species may represent degradation or oxidatively damaged products. Uncertainties in these masses are significant (±25%), so the numbers should be viewed mainly as a means of distinguishing one species from another. $S_{1500}$ was present in all traces, including a trace of the HEPES/KOH buffer alone (Figure B-1, trace h), so it likely originated from HEPES, which contains a sulfur molecule. However, the mass of HEPES (238 Da) is

significantly less than 1,500 Da, suggesting that it formed a multimeric species, as has been reported by Saraiva et al. (2010).[26] A peak corresponding to the authentic mass of HEPES (238 Da) was not detected, likely due to unusual migration effects of very low molecular mass sulfur species down the liquid chromatography column.[25]

As a control, no sulfur species besides $S_{1500}$ was detected in the material exported from nfs1-14 mutant mitochondria (preloaded with unlabeled cysteine) or from WT mitochondria with no preloaded cysteine (Figure B-1, traces b and c, respectively), consistent with lack of competing activity of these samples. Likewise, when WT mitochondria were preloaded with unlabeled cysteine but the export process was blocked with ATPγS, no sulfur species other than $S_{1500}$ was detected (Figure B-1, trace d), nor was there any competing activity. The material exported from Atm1-depleted mitochondria (preloaded with unlabeled cysteine) did not exhibit any detectable competing activity. It completely lacked 1,000-, 900-, 800-, and 700-Da species and contained a small amount of S1100 in addition to the buffer peak (Figure B-1, trace e). We speculate that $S_{1100}$ might have been exported by a different ABC transporter in the mitochondrial inner membrane such as Mdl1.[27] In fact, $S_{1100}$ was detected in exported material from WT mitochondria only when ATP, and not ATPγS, was included during the export process (Figure B-1, compare traces a and d). In

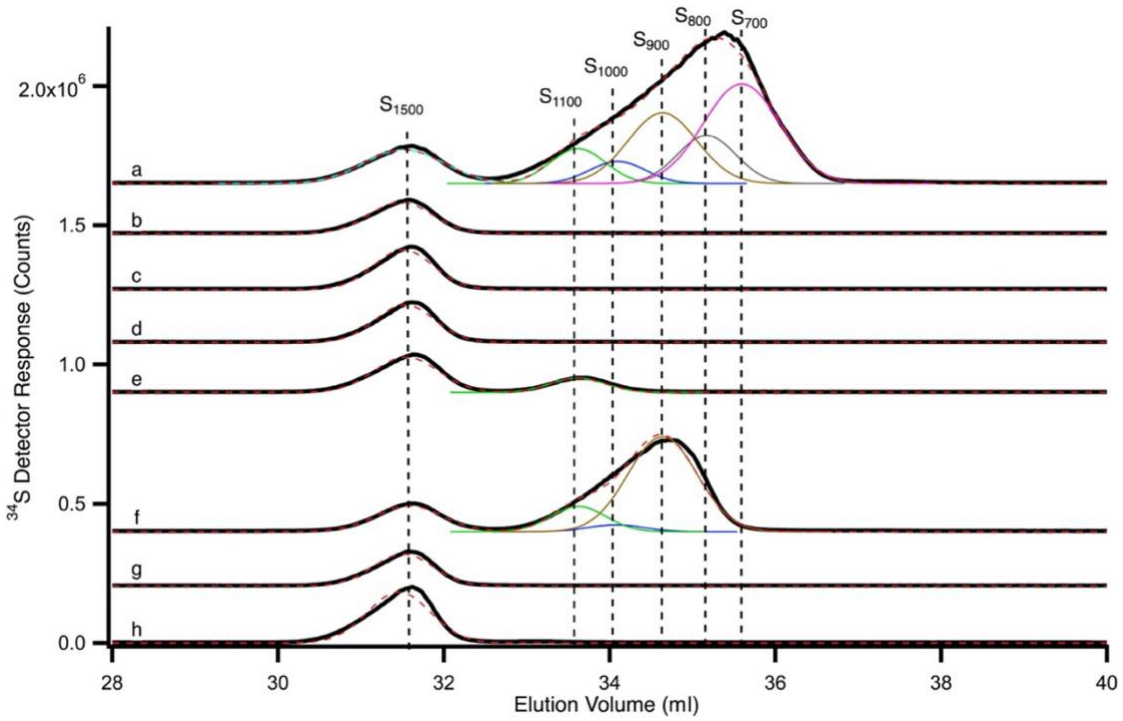


**Figure B-1:SEC-ICP-MS Chromatogram of Sulfur Species.**
Solid black lines are data and dashed red lines are composite fits. Simulations of individual peaks are color coded as follows: $S_{1100}$, green; $S_{1000}$, blue; $S_{900}$, brown; $S_{800}$, gray; $S_{700}$, pink. Trace a: Exported material from WT mitochondria (cysteine-preloaded); trace b: exported material from nfs1-14 mitochondria (cysteine-preloaded); trace c: exported material from WT mitochondria with no cysteine preloading; trace d: exported material from WT mitochondria (cysteine-preloaded) in which ATPγS rather than ATP was used during the export process; trace e: exported material from Atm1↓ mitochondria (cysteine-preloaded); trace f: material isolated from WT mitochondrial matrix after preloading with cysteine; trace g: material isolated from WT mitochondrial matrix with no cysteine preloading; trace h: sample buffer only (20 mM HEPES/KOH, pH 7.5). Reprinted with permission.[28]

mitochondria-cytosol mixing assays using [$^{35}$S]cysteine, cytosolic tRNA thiolation occurred poorly but a small signal was still detectable with both Atm1-depleted and nfs1-14 mitochondria because of high sensitivity. However, no relevant unlabeled sulfur species able to compete with $^{35}$Sint was detected in the materials exported from these mitochondria (Figures B-1). This could be due to loss of limited material during the multi-step isolation procedure. Regardless, all of the species exported from WT mitochondria as described above were consistently detected in another set of chromatograms from a separate experiment (Figure B-2), even though an additional species ($S_{600}$) was present (Figure B-2, trace a versus Figure B-1, trace a). Unlabeled and active material isolated from WT mitochondrial matrix with a molecular mass of <3 kDa also contained similar sulfur species, although the subspecies composition appeared slightly altered (Figure B-1, trace f; Figure B-2, trace f). The sulfur species that accumulated in the matrix might differ slightly from the exported forms. Alternatively, these subtle differences could be due to sample preparation: exported material from intact mitochondria versus fractionation of mitochondrial lysate/matrix. The relative intensities of the peaks associated with the various sulfur species are presented in Table B-2.

**B.2.4. Discussion**

Thio-modification of the wobble uridines of a subset of cytosolic tRNAs is vital for their roles in protein synthesis. Here we demonstrate that mitochondria play a direct and essential role in cytosolic tRNA thiolation. Specifically, mitochondria generate low molecular mass sulfur-containing intermediate species (Sint) and export them to the

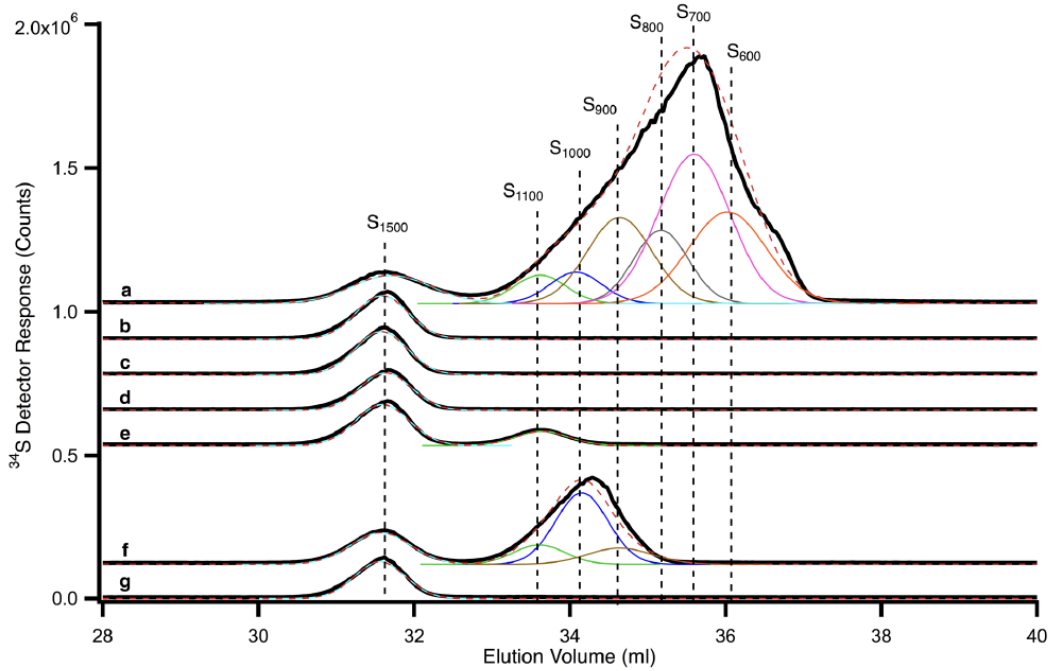


**Figure B-2:SEC-ICP-MS Chromatogram of Sulfur Species, Related to Table B-1.** Color-coding is the same as in Figure B-1. Specifically, solid black lines are data, and dashed red lines are composite fits. Simulations of individual peaks are color-coded as follows: $S_{1100}$, green; $S_{1000}$, blue; $S_{900}$, brown; $S_{800}$, grey; $S_{700}$, pink. Additional simulation for $S_{600}$ is indicated by orange color. Samples are: a) exported material from WT mitochondria (cysteine-preloaded), b) exported material from nfs1-14 mitochondria (cysteine-preloaded), c) exported material from WT mitochondria with no cysteine preloading, d) exported material from WT mitochondria (cysteine-preloaded) in which ATPgS rather than ATP was used during the export process, e) exported material from Atm1-depleted (Atm1⁻) mitochondria (cysteine-preloaded), f) material isolated from WT mitochondrial matrix after preloading with cysteine, and g) material isolated from WT mitochondrial matrix with no cysteine preloading. Reprinted with permission.[28]

cytosol. We detected the exported Sint species in an active form that was utilized by the cytosol to thiolate tRNAs. In prior work, other laboratories defined various mitochondrial and cytosolic proteins involved in thiolation of cytosolic tRNAs.[10,14–16] They measured steady-state levels of thiolated tRNAs in vivo but did not assess the individual contributions of mitochondria and cytosol to cytosolic tRNA thiolation and how they are functionally connected. We resolved these issues here by developing assays for de novo cytosolic tRNA thiolation, using metabolically active mitochondria and cytosol isolated from yeast cells. In these assays, [$^{35}$S]cysteine was used as the source of sulfur to simultaneously monitor radiolabeling of aconitase(Fe-S cluster assembly) in mitochondria and radiolabeling of tRNAs (s2U thiolation) in cytosol.

In yeast, Nfs1 cysteine desulfurase is found primarily in mitochondria[12] with a small amount located in the cytosol.[13] An experiment was performed in which mitochondrial Nfs1 was depleted while maintaining expression of cytosolic Nfs1.[14] This mitochondrial Nfs1-depleted strain lacked cytosolic tRNA thiolation, and based on these results it was concluded that mitochondrial Nfs1 is essential for cytosolic tRNA thiolation.[14] However, depletion of mitochondrial Nfs1 (cytosolic Nfs1 present) also leads to deficiency in cytosolic Fe-S cluster assembly[18]. Furthermore, in vivo depletion of some CIA components is associated with greatly reduced levels of thiolated tRNAs in the cytosol.[14] Therefore, the in vivo studies could not rule out the possibility that depletion of mitochondrial Nfs1 might indirectly block cytosolic

**Table B-1:Analysis of SEC-ICP-MS Chromatographic Traces.**

The most intense peak ($S_{700}$ of Figure B-2, trace *a*) was assigned a value of 100.

Reprinted with permission.[28]

| Trace | $S_{1500}$ | $S_{1100}$ | $S_{1000}$ | $S_{900}$ | $S_{800}$ | $S_{700}$ | $S_{600}$ |
|---|---|---|---|---|---|---|---|
| Center position (mL) | 31.5 | 33.6 | 34.1 | 34.6 | 35.2 | 35.6 | 36.0 |
| Linewidth (mL) | 0.9 ± 0.1 | 0.78 | 0.79 | 0.98 | 0.83 | 1.1 | 1.2 |
| | | | | | | | |
| Relative Intensities | | | | | | | |
| Figure B-1, trace a | 24 | 17 | 11 | 44 | 25 | 69 | 0 |
| Replicate | 24 | 16 | 9 | 45 | 10 | 83 | 0 |
| Replicate | 23 | 17 | 10 | 44 | 20 | 70 | 0 |
| Figure B-2, trace a | 21 | 14 | 16 | 51 | 37 | 100 | 66 |
| Exported from WT mito (Cys preloaded) (Av) | 23 ± 1 | 16 ± 1 | 12 ± 3 | 46 ± 3 | 23 ± 11 | 80 ± 14 | 16 ± 33 |
| | | | | | | | |
| Figure B-1, trace b | 17 | 0 | 0 | 0 | 0 | 0 | 0 |
| Replicate | 19 | 0 | 0 | 0 | 0 | 0 | 0 |
| Figure B-2, trace b | 21 | 0 | 0 | 0 | 0 | 0 | 0 |
| Exported from *nfs1-14* mito (Cys preloaded)(Av) | 19 ± 2 | | | | | | |
| | | | | | | | |
| Figure B-1, trace c | 21 | 0 | 0 | 0 | 0 | 0 | 0 |
| Figure B-2, trace c | 21 | 0 | 0 | 0 | 0 | 0 | 0 |
| Exported from WT mito with no Cys preloading (Av) | 21 | | | | | | |
| | | | | | | | |
| Figure B-1, trace d | 20 | 0 | 0 | 0 | 0 | 0 | 0 |
| Replicate | 17 | 0 | 0 | 0 | 0 | 0 | 0 |
| Figure B-2, trace d | 17 | 0 | 0 | 0 | 0 | 0 | 0 |
| Exported from WT mito (Cys preloaded) in the presence of ATP$\gamma$S (Av) | 18 ± 2 | | | | | | |
| | | | | | | | |
| Figure B-1, trace e | 24 | 9 | 0 | 0 | 0 | 0 | 0 |
| Replicate | 20 | 7 | 0 | 0 | 0 | 0 | 0 |
| Figure B-2, trace e | 20 | 7 | 0 | 0 | 0 | 0 | 0 |
| Exported from Atm1↓ mito (Cys preloaded) (Av) | 21 ± 2 | | | | | | |
| | | | | | | | |
| Figure B-1, trace f | 19 | 13 | 11 | 44 | 25 | 0 | 0 |
| Replicate | 16 | 13 | 4 | 59 | 0 | 0 | 0 |
| Figure B-2, trace f | 17 | 10 | 35 | 10 | 0 | 0 | 0 |
| Isolated from WT mito matrix (Cys preloaded) (Av) | 17 ± 2 | | | | | | |
| | | | | | | | |
| Figure B-1, trace g | 17 | 0 | 0 | 0 | 0 | 0 | 0 |
| Figure B-2, trace g | 17 | 0 | 0 | 0 | 0 | 0 | 0 |
| Isolated from WT mito matrix with no Cys preloading (Av) | 17 | | | | | | |
| | | | | | | | |
| Figure B-1, trace h Buffer control | 29 | 0 | 0 | 0 | 0 | 0 | 0 |

tRNA thiolation via inhibitory effects on cytosolic Fe-S cluster assembly. This is an important issue because the [4Fe-4S] cluster-containing Elp3[29] and the [3Fe-4S] cluster-containing Ncs6[30] are involved in mcm5s2U34 modification of cytosolic tRNAs.[2] In the absence of cytosolic Fe-S cluster assembly, these proteins are unlikely to be functional. Data presented here settle the issue and conclusively show that mitochondrial Nfs1 is directly required for cytosolic tRNA thiolation independent of its effects on cytosolic Fe-S cluster assembly. For example, no radiolabeled tRNA was detected when isolated WT cytosol alone was incubated with [$^{35}$S]cysteine. Thus, cytosolic Fe-S proteins, together with any trace amounts of cytosolic Nfs1, were unable to thiolate tRNAs. Upon addition of WT mitochondria, cytosol acquired thiolation activity because Nfs1 in mitochondria generated the critical sulfur species required for cytosolic tRNA thiolation. This conclusion was further substantiated by the observation that nfs1-14 mutant mitochondria with compromised cysteine desulfurase activity failed to efficiently promote cytosolic tRNA thiolation.

In mitochondria, Nfs1 binds its substrate cysteine through the cofactor pyridoxal phosphate. The cysteine sulfur is removed and used to form a covalent persulfide on an active-site cysteine (Nfs1-S-SH).[11] The persulfide sulfur is then transferred to the scaffold Isu1/2, where it combines with iron. The ISC intermediates thus formed are donated to apoproteins (e.g., apoaconitase), a process that requires chaperones.[17] Our data show that Isu1-depleted mitochondria (Isu2 absent) failed to support Fe-S cluster biogenesis within the organelle or tRNA thiolation in the cytosol. Thus, in addition to mitochondrial Nfs1, mitochondrial Isu1/2 are also required for generating sulfur

intermediates (Sint) necessary for thio-modification of cytosolic tRNAs. The ssq1mutant mitochondria did not support Fe-S cluster biogenesis of aconitase but surprisingly were able to efficiently promote cytosolic tRNA thiolation to WT levels. Thus, unlike Nfs1 and Isu1/2, Ssq1 is not involved in generating Sint. These results argue for a hitherto unidentified branch point in the sulfur delivery pathway at the Isu1/2 site for intra-organellar use in mitochondria or export to the cytosol.

The sulfur species generated within mitochondria involving Nfs1 and Isu1/2 must be exported to the cytosol for tRNA thiolation. The Atm1 ATPase in the mitochondrial inner membrane has been hypothesized to export a sulfur-containing molecule that is utilized for both tRNA thiolation and Fe-S cluster assembly in the cytosol.[2,17] However, none of the candidate Atm1 substrates thus far reported is supported by convincing biochemical data.[17] The Sint species that we detected here were exported from intact WT mitochondria in an ATP-dependent manner. The molecular masses of exported Sint ranged from 700 to 1,100 Da (Figure B-1). Mitochondria lacking Atm1 failed to efficiently support cytosolic tRNA thiolation because they were unable to export active Sint species. Importantly, once exported by WT mitochondria, Sint species were able to promote cytosolic tRNA thiolation by themselves, with no further dependence on mitochondria. Thus, the primary contribution of mitochondria in this process is to generate and export Sint species to cytosol.

Importantly, the cytosolic use of the exported species depended on Dre2, an essential component of the CIA machinery. Dre2 may participate in utilization of exported Sint either directly or indirectly via effects on Fe-S cluster-containing CIA

components such as Nbp35 and/or other proteins such as Elp3 and Ncs6.[2,29,30] Although the principal function of the cytosol in tRNA thiolation is to utilize exported Sint, it may also enhance Sint export from mitochondria. In the absence of cytosol some of the Sint species were exported in an ATP-dependent manner, but a significant portion of Sint still remained trapped within mitochondria in active form. It is therefore reasonable to speculate that cytosol is required for efficient Sint export, mimicking the in vivo situation. Cytosolic proteins or small molecules might "grab" exiting Sint, making the export process unidirectional and more efficient under physiological conditions within cells. How mitochondria sense the cytosolic need for exported sulfur species remains to be determined.

Most of the S. cerevisiae proteins involved in cytosolic tRNA thiolation or Fe-S cluster assembly are conserved and have human orthologs.[2,31,32] As in yeast, human NFS1 is also thought to be present in mitochondria with a small amount in cytosol/nucleus.[33] Furthermore, yeast Nfs1/human NFS1 forms an active enzyme complex with accessory proteins Isd11/ISD11 and Acp1/ACP.[34,35] More importantly, depletion of the mitochondrial Nfs1/NFS1 leads to Fe-S cluster deficiency in yeast or HeLa cells, and the plasmid-borne expression of the respective proteins without their mitochondrial targeting sequence cannot rescue the defect.[18,36] Thus, the underlying mechanism for cytosolic tRNA thiolation in humans appears to be very similar to that in yeast, involving mitochondrial NFS1. That similarity can now be tested using mitochondria and cytosol isolated from human cells.

**B.2.5. References:**


1 B. El Yacoubi, M. Bailly and V. de Crécy-Lagard, Biosynthesis and Function of Posttranscriptional Modifications of Transfer RNAs, *Annu. Rev. Genet.*, 2012, **46**, 69–95.

2 Y. Nakai, M. Nakai and T. Yano, Sulfur Modifications of the Wobble U34 in tRNAs and their Intracellular Localization in Eukaryotic Cells, *Biomolecules*, 2017, **7**, 17.

3 V. A. N. Rezgui, K. Tyagi, N. Ranjan, A. L. Konevega, J. Mittelstaet, M. V. Rodnina, M. Peter and P. G. A. Pedrioli, TRNA tKUUU, tQUUG, and tEUUC wobble position modifications fine-tune protein translation by promoting ribosome A-site binding, *Proc. Natl. Acad. Sci. U. S. A.*, , DOI:10.1073/pnas.1300781110.

4 J. Urbonavicius, Improvement of reading frame maintenance is a common function for several tRNA modifications, *EMBO J.*, 2001, **20**, 4863–4873.

5 D. D. Nedialkova and S. A. Leidel, Optimization of Codon Translation Rates via tRNA Modifications Maintains Proteome Integrity, *Cell*, 2015, **161**, 1606–1618.

6 S. Laxman, B. M. Sutter, X. Wu, S. Kumar, X. Guo, D. C. Trudgian, H. Mirzaei and B. P. Tu, Sulfur Amino Acids Regulate Translational Capacity and Metabolic Homeostasis through Modulation of tRNA Thiolation, *Cell*, 2013, **154**, 416–429.

7 M. Dewez, F. Bauer, M. Dieu, M. Raes, J. Vandenhaute and D. Hermand, The conserved Wobble uridine tRNA thiolase Ctu1-Ctu2 is required to maintain genome integrity, *Proc. Natl. Acad. Sci.*, 2008, **105**, 5459–5464.

8 T. Karlsborn, H. Tükenmez, C. Chen and A. S. Byström, Familial dysautonomia (FD) patients have reduced levels of the modified wobble nucleoside mcm5s2U in tRNA, *Biochem. Biophys. Res. Commun.*, 2014, **454**, 441–445.

9 T. Yasukawa, Wobble modification defect in tRNA disturbs codon-anticodon interaction in a mitochondrial disease, *EMBO J.*, 2001, **20**, 4794–4802.

10 Y. Nakai, N. Umeda, T. Suzuki, M. Nakai, H. Hayashi, K. Watanabe and H. Kagamiyama, Yeast Nfs1p Is Involved in Thio-modification of Both Mitochondrial and Cytoplasmic tRNAs, *J. Biol. Chem.*, 2004, **279**, 12363–12368.

11 A. Pandey, H. Yoon, E. R. Lyver, A. Dancis and D. Pain, Identification of a Nfs1p-bound persulfide intermediate in Fe–S cluster synthesis by intact mitochondria, *Mitochondrion*, 2012, **12**, 539–549.

12 J. Li, M. Kogan, S. A. B. Knight, D. Pain and A. Dancis, Yeast Mitochondrial Protein, Nfs1p, Coordinately Regulates Iron-Sulfur Cluster Proteins, Cellular Iron Uptake, and Iron Distribution, *J. Biol. Chem.*, 1999, **274**, 33025–33034.

13 A. Naamati, N. Regev-Rudzki, S. Galperin, R. Lill and O. Pines, Dual Targeting of Nfs1 and Discovery of Its Novel Processing Enzyme, Icp55, *J. Biol. Chem.*, 2009, **284**, 30200–30208.

14 Y. Nakai, M. Nakai, R. Lill, T. Suzuki and H. Hayashi, Thio Modification of Yeast Cytosolic tRNA Is an Iron-Sulfur Protein-Dependent Pathway, *Mol. Cell. Biol.*, 2007, **27**, 2841–2847.

15 S. Leidel, P. G. A. Pedrioli, T. Bucher, R. Brost, M. Costanzo, A. Schmidt, R. Aebersold, C. Boone, K. Hofmann and M. Peter, Ubiquitin-related modifier Urm1

acts as a sulphur carrier in thiolation of eukaryotic transfer RNA, *Nature*, 2009, **458**, 228–232.

16 A. Noma, Y. Sakaguchi and T. Suzuki, Mechanistic characterization of the sulfur-relay system for eukaryotic 2-thiouridine biogenesis at tRNA wobble positions, *Nucleic Acids Res.*, 2009, **37**, 1335–1352.

17 R. Lill, R. Dutkiewicz, S. A. Freibert, T. Heidenreich, J. Mascarenhas, D. J. Netz, V. D. Paul, A. J. Pierik, N. Richter, M. Stümpfig, V. Srinivasan, O. Stehling and U. Mühlenhoff, The role of mitochondria and the CIA machinery in the maturation of cytosolic and nuclear iron–sulfur proteins, *Eur. J. Cell Biol.*, 2015, **94**, 280–291.

18 G. Kispal, P. Csere, C. Prohl and R. Lill, The mitochondrial proteins Atm1p and Nfs1p are essential for biogenesis of cytosolic Fe / S proteins, 1999, **18**, 3981–3989.

19 J. Leighton and G. Schatz, An ABC transporter in the mitochondrial inner membrane is required for normal growth of yeast., *EMBO J.*, 1995, **14**, 188–195.

20 V. Srinivasan, A. J. Pierik and R. Lill, Crystal Structures of Nucleotide-Free and Glutathione-Bound Mitochondrial ABC Transporter Atm1, *Science (80-. ).*, 2014, **343**, 1137–1140.

21 G. Kuhnke, K. Neumann, U. Mühlenhoff and R. Lill, Stimulation of the ATPase activity of the yeast mitochondrial ABC transporter Atm1p by thiol compounds, *Mol. Membr. Biol.*, 2006, **23**, 173–184.

22 J. Li and J. A. Cowan, Glutathione-coordinated [2Fe–2S] cluster: a viable

physiological substrate for mitochondrial ABCB7 transport, *Chem. Commun.*, 2015, **51**, 2253–2255.

23 T. A. Schaedler, J. D. Thornton, I. Kruse, M. Schwarzländer, A. J. Meyer, H. W. van Veen and J. Balk, A Conserved Mitochondrial ATP-binding Cassette Transporter Exports Glutathione Polysulfide for Cytosolic Metal Cofactor Assembly, *J. Biol. Chem.*, 2014, **289**, 23264–23274.

24 M. Wojdyr, Fityk : a general-purpose peak fitting program, *J. Appl. Crystallogr.*, 2010, **43**, 1126–1128.

25 S. P. McCormick, M. J. Moore and P. A. Lindahl, Detection of Labile Low-Molecular-Mass Transition Metal Complexes in Mitochondria, *Biochemistry*, 2015, **54**, 3442–3453.

26 M. A. Saraiva, C. M. Borges and M. H. Florêncio, Behaviour of 4-(−2-Hydroxyethyl)-1-Piperazineethanesulphonic Acid under Electrospray Ionisation Mass Spectrometry Conditions, *Eur. J. Mass Spectrom.*, 2010, **16**, 199–213.

27 L. Young, Role of the ABC Transporter Mdl1 in Peptide Export from Mitochondria, *Science (80-. ).*, 2001, **291**, 2135–2138.

28 A. Pandey, J. Pain, N. Dziuba, A. K. Pandey, A. Dancis, P. A. Lindahl and D. Pain, Mitochondria Export Sulfur Species Required for Cytosolic tRNA Thiolation, *Cell Chem. Biol.*, 2018, **25**, 738-748.e3.

29 C. Paraskevopoulou, S. A. Fairhurst, D. J. Lowe, P. Brick and S. Onesti, The Elongator subunit Elp3 contains a Fe4S4 cluster and binds S-adenosylmethionine, *Mol. Microbiol.*, 2006, **59**, 795–806.

30 Y. Liu, D. J. Vinyard, M. E. Reesbeck, T. Suzuki, K. Manakongtreecheep, P. L. Holland, G. W. Brudvig and D. Söll, A [3Fe-4S] cluster is required for tRNA thiolation in archaea and eukaryotes, *Proc. Natl. Acad. Sci.*, 2016, **113**, 12703–12708.

31 S. Leimkühler, M. Bühning and L. Beilschmidt, Shared Sulfur Mobilization Routes for tRNA Thiolation and Molybdenum Cofactor Biosynthesis in Prokaryotes and Eukaryotes, *Biomolecules*, 2017, **7**, 5.

32 D. J. A. Netz, J. Mascarenhas, O. Stehling, A. J. Pierik and R. Lill, Maturation of cytosolic and nuclear iron–sulfur proteins, *Trends Cell Biol.*, 2014, **24**, 303–312.

33 T. Land and T. A. Rouault, Targeting of a Human Iron–Sulfur Cluster Assembly Enzyme, nifs, to Different Subcellular Compartments Is Regulated through Alternative AUG Utilization, *Mol. Cell*, 1998, **2**, 807–815.

34 S. A. Cory, J. G. Van Vranken, E. J. Brignole, S. Patra, D. R. Winge, C. L. Drennan, J. Rutter and D. P. Barondeau, Structure of human Fe-S assembly subcomplex reveals unexpected cysteine desulfurase architecture and acyl-ACP-ISD11 interactions., *Proc. Natl. Acad. Sci. U. S. A.*, 2017, **114**, E5325–E5334.

35 J. G. Van Vranken, M.-Y. Jeong, P. Wei, Y.-C. Chen, S. P. Gygi, D. R. Winge and J. Rutter, The mitochondrial acyl carrier protein (ACP) coordinates mitochondrial fatty acid synthesis with iron sulfur cluster biogenesis, *Elife*, , DOI:10.7554/eLife.17828.

36 A. Biederbick, O. Stehling, R. Rosser, B. Niggemeyer, Y. Nakai, H.-P. Elsasser and R. Lill, Role of Human Mitochondrial Nfs1 in Cytosolic Iron-Sulfur Protein

Biogenesis and Iron Regulation, *Mol. Cell. Biol.*, 2006, **26**, 5675–5687.

**B.3. Part 2:**

LMM IRON AND SULFUR SPECIES EXPORTED FROM BY MITOCHONDRIA

**B.3.1. Project Introduction:**

This project was inspired by work done in the Debkumar Pain Lab[1] The work in Part 1 showed the existence of an exported sulfur containing species from the mitochondria that was used in tRNA modification which was named Sint. We performed the liquid chromatography to speciate Sint from aqueous resuspensions of organic extracts. During these experiments the iron traces were void of iron species. We wondered whether organic extraction of the mitochondrial suspensions could cause species degradation. We also considered that analyzing aqueous samples that had undergone no organic extraction would provide the means to speciate both the sulfur and iron species exported from the mitochondria. Ms. Shepherd and I collaborated on experiments aimed at speciating the iron and sulfur species from aqueous samples of mitochondrial suspensions after the mitochondria had been treated in different buffers to stimulate the mitochondria for species export. I performed the LC and sample preparation for analysis and Rachel Shepherd made the samples, we both analyzed the results.

We anticipated that analyzing aqueous samples of supernatants from mitochondrial suspensions would allow us to speciate the notorious X-S species that is thought to be exported from the mitochondria as well as other exported iron or sulfur

species.[2] Recent evidence from the same researchers from Pandey, et al., 2018 had shown that there was an Fe-S intermediate species that was used for ISC assembly in the cytosol. We set our sights on speciating iron and sulfur species from the mitochondria with the hope of being able to observe X-S/Fe-S. The work presented here represents an ongoing project. The experiments listed in this portion of the dissertation represent the attempts we made to detect iron and sulfur species exported from mitochondria.

### B.3.2. Materials and Methods

#### B.3.2.1. Growth of Cells:

Respiring W303 cells were grown in complete synthetic media (CSM, Sunrise Science) supplemented with 3% glycerol before autoclaving. Media was additionally supplemented with sterile-filtered 1% ethanol, 1μM copper sulfate, and $Fe^{III}$ citrate of variable concentrations (10 - 40 μM) after autoclaving but before inoculation. Cells were harvested in mid-exponential phase from a 24 L bioreactor at an $OD_{600}$ between 1.5 - 2. Whole cell pellets of batches K and N were frozen in 15% glycerol and thawed before the isolation.

#### B.3.2.2. Mitochondria Isolation:

Mitochondria were isolated according to previous protocols with slight modifications.[3,4] After pelleting cells from a bioreactor in a Sorvall Evolution centrifuge with an SLC-6000 rotor at 5000xg for 5 min, all subsequent steps were performed inside a refrigerated anaerobic glove box (Mbraun) at 4-10°C and $O_2$ ~5 ppm. Briefly, the whole cell pellet was resuspended with 10 mM Dithiothreitol (DTT) in 100 mM Tris buffer pH 9.4 and repelleted. The cell pellet was resuspended with sorbitol phosphate

buffer (composed of 1.2 M sorbitol, 20 mM $KH_2PO_4$, and 1 mM EDTA), pelleted, and then resuspended in sorbitol phosphate buffer with an additional 2.5 mg of zymolyase (Amsbio) per g whole cell. Cell walls were digested until the $OD_{600}$, when diluted 1:100 with water, was less than 30% of the original value. The resulting spheroplasts were pelleted, resuspended in sorbitol HEPES buffer (20 mM HEPES 0.6 M Sorbitol buffer pH 7.4), and then homogenized in a two-step process. The first step used 25 strokes and the second step used 10 strokes, with a 5 min 2000xg centrifugation step between the two steps to repellet any unbroken spheroplasts and collect the ruptured spheroplasts and organelles in the supernatant. After batch J, instead of using Sorbitol-HEPES buffer, 20 mM Tris-0.6 M Sorbitol buffer pH 7.4 (defined as Buffer B) was used. Post-homogenization spheroplasts were first centrifuged at 2000xg for 5 min to remove most cell debris. The supernatant was collected, and then centrifuged at 4000xg to remove the rest of the cell debris. Crude mitochondria were pelleted via centrifugation at 12000xg. The pellet was resuspended in tris-sorbitol (or sorbitol-HEPES) buffer to a volume of approximately 50 mL, and then centrifuged again at 4000xg. The supernatant was collected and centrifuged at 12000xg. The pellet, containing crude mitochondria, was resuspended to either 2 mL of 5 mg/mL protein concentration or to 1mL of 10 mg/mL protein concentration. The suspension was laid on top of a 20 mM Tris 32% sucrose (10 mL) which was layered over a 20 mM tris-60% sucrose (10mL) solution before being centrifuged at 150,000xg for 1 hr with no break applied to the centrifuge during centrifugation. Mitochondria were collected at the 32%-60% sucrose interface and were diluted 3-fold with Buffer B to ~ 150 mL before pelleting via centrifugation at 12,000xg

for 10 min. The pelleted mitochondria were resuspended in approximately 10 mL of buffer B and then divided into aliquots for use in other experiments. The concentration of protein in this suspension of isolated intact mitochondria was determined using the BCA colorimetric method, using Bovine Serum Albumin as a standard (kit from Thermo Scientific). The mitochondrial suspension was diluted 50-fold with water to burst the mitochondria before adding the BCA solution.

**B.3.3. LC-ICP-MS:**

**B.3.3.1. Sample Preparation:**

Samples were filtered through a 0.2 micron filter (4 mm regenerated cellulose Titan3 filter tip, Thermo Scientific). Filtered samples were either stored in Eppendorf tubes before injection or pipetted into 400 µL plastic vials (9 mm plastic screw threaded vials, Thermo Scientific) for analysis with the multisampler. Samples were not analyzed the same day, but were frozen in liquid $N_2$ and stored in a -80 °C freezer. Frozen samples were thawed and immediately prepared for injection onto the LC-ICP-MS system on the day of analysis. Soluble mitochondrial extracts or samples containing cytosol were filtered using a 10 kDa ultracentrifugation filter system (Amicon centricon, regenerated cellulose) using a Beckman ultracentrifuge with a SW32.1 Ti rotor with air tight centrifugation bottles. Amicon filters were prepared by passing 3 mL of high purity water through them; any remaining water was removed before applying samples. Samples were diluted in 20 mM tris pH 7.4 buffer as required if available sample volume was insufficient for the complete analysis.

**B.3.3.2. Sample Analysis:**

Samples were analyzed using an anaerobic (1 - 10 ppm $O_2$) and chilled (4 - 8°C) chromatography system coupled to an inductively coupled plasma mass spectrometer, as described.[5] Samples (200 µL) were injected onto a Superdex Peptide 10/300 GL column (Ge Healthcare, 17517601) at a flow rate of 0.6 mL·min$^{-1}$ with a mobile phase composed of 20 mM ammonium acetate pH 6.5. A 100 mM stock of the mobile phase buffer was diluted with high purity water (defined as distilled, filtered (> 18 MΩ), and re-distilled) in real-time using the HPLCs pump. Both water and stock mobile phase were degassed using a Schlenk-line system prior to use.

After the batch K was performed, the LC-ICP system was modified to include a bio-inert multisampler (Agilent 1260 Infinity II, G5669A) with the 2 mL extended loop installed. The extended loop caused the elution volume profiles between of all traces after batch K to be greater by 2 mL.

**B.3.3.3. Calibration Curves:**

The chromatography calibration curve and standards were prepared as described.[5] Standards were prepared in 20 mM MOPS pH 7.4 buffer, and included: riboflavin (376 Da, ran 0.45-micron filtrate from a 1mM solution); ADP (427 Da, 200 µM); human insulin (Alfa Aesar, 5808 Da, 90 µM) instead of bovine insulin was used. Cytochrome C and Ni-BPS were not run. The best-fit linear regression equation generated and used was: logarithm (Da) = $-0.673(V_e/V_o)+4.6238$, with $R_2$ of 0.9053, the Vo was 7.4898 mL. The calibration curve was generated before the addition of the multisampler. Peak elution volume from data after the addition of the multisampler was reduced by 2 mL before calculating the apparent molecular mass. The adjusted elution

volume was used in plotting so that traces could be compared to those collected prior to installing the multisampler.

**B.3.3.4. Column Cleaning:**

Prior to installing the multisampler, the column was cleaned as described using a chelator buffer mobile phase.[5] After installation, the concentration of that mobile phase chelators was increased in concentration 10 fold and 500 μL of this solution was injected onto the column. The column was run with the analysis mobile phase and flow rate for 3 column volumes (column bed volume) before samples were analyzed. Samples injected after this cleaning method did not show spurious peaks in subsequent runs.

**B.3.3.5. Data Analysis:**

Figures were generated using IgorPro (version 6.0 or 8.0). Data from samples analyzed prior to the multisampler addition had their x-axis increased by 2.00 mL for direct comparison to later traces. Data that has been modified in this way is indicated in the figure legends.

**Table B-2**. **Buffer Table**

The buffer labels, abbreviations, and composition used in the experiments.

| Buffer | Abbreviation | Additional Components |
|---|---|---|
| Control Buffer | B | 0.6 M Sorbitol, 20 mM Tris pH 7.4 |
| Activation Buffer | BA | + 10 mM $Mg(OAc)_2$, 40 mM K(OAc), 4 mM ATP, 1 mM GTP, 2 mM NADH, 1 mM NADPH |
| Activation + cysteine | BAC | + 10 μM cytsteine |
| Activation + cysteine + iron | BACF | + 10 μM $Fe_{II}$ ascorbate |
| Activation + cysteine + iron + glutathione | BACFG | + 2 mM GSH |

**B.3.4. Batch J Reactions:**

All buffer solutions in Batch J contained 1 mM TCEP (tris(2-carboxyethyl)phosphine) and used HEPES buffer instead of Tris, in addition to the other constituents listed in Table B-2. Buffers using TCEP are demarcated with a prime (‘) symbol following the B abbreviation. A suspension of 30 mg fresh mitochondria in sorbitol-HEPES buffer (Buffer B’) was pelleted into an epitube by spinning them in a

micro-centrifuge at 12,000xg for 10 min at 4 °C in an anaerobic glove box (oxygen ~5 ppm). Pelleted mitochondria were resuspended to a concentration of 15 mg/mL using 2.0 mL of Buffer B' (Table B-2). The suspension was heated to 30 °C in an Al block. Five hundred µL aliquots were removed 5, 30, 60, and 90 min after heating commenced. Each of the four aliquots was centrifuged, and the resulting supernatant fractions were analyzed by LC. The resulting pellets from the 5, 30, and 60 min samples were resuspended in 500 µL of Buffer B' and incubated at 30 °C until the 90 min sample was completed. This generated mitochondrial pellets that had all been incubated for 90 min, in preparation for the second step. To begin the second step of the experiment, the mitochondrial suspensions were combined, repelleted, and resuspended in 2 mL of buffer B'A. The suspension was again heated to 30 °C and four supernatant fractions were collected and analyzed by LC.

Mitochondria were incubated in the control buffer for various times as a control; no iron-containing species were expected to be exported. Unexpectedly, chromatograms of all supernatants taken in the first step exhibited two major iron-containing species, with apparent masses of ca. 1100 and 800 Da (Figure B-3, left side). A shoulder was also evident at ca. 600 Da. As the time of incubation increased, the peak at 1100 Da increased relative to that at 800 Da. An attractive interpretation is that mitochondria exported these two iron species, with the 1100 Da species exported more slowly (over the course of 90 min) than the 800 Da species (constant at all times). Accordingly, the concentration of the 800 Da species in the supernatant would be controlled by an equilibrium that is established within 5 min. We considered that buffer B' may be contaminated with these

two iron species, but traces of buffer B alone was nearly devoid of iron signals (Figure B-3, trace e). We cannot exclude the possibility that the detected iron desorbed from the exterior surface of the mitochondria rather than being exported from the mitochondrial interior.

In a second step, the same mitochondria were treated with buffer B' plus components that should have activated/energized the mitochondria (buffer B'A). We expected that incubation in this "activation" buffer would cause iron-containing species to be exported from mitochondria. However, the same species observed after incubation in buffer B' were observed at all times measured after incubation in buffer B'A (Figure B-3, right side). Interestingly, the intensities of these peaks increased with time of exposure to buffer B'A. During this step, the intensity of the species at 1100 Da increased relative to that at 800 Da – similar to that observed in the first step. An

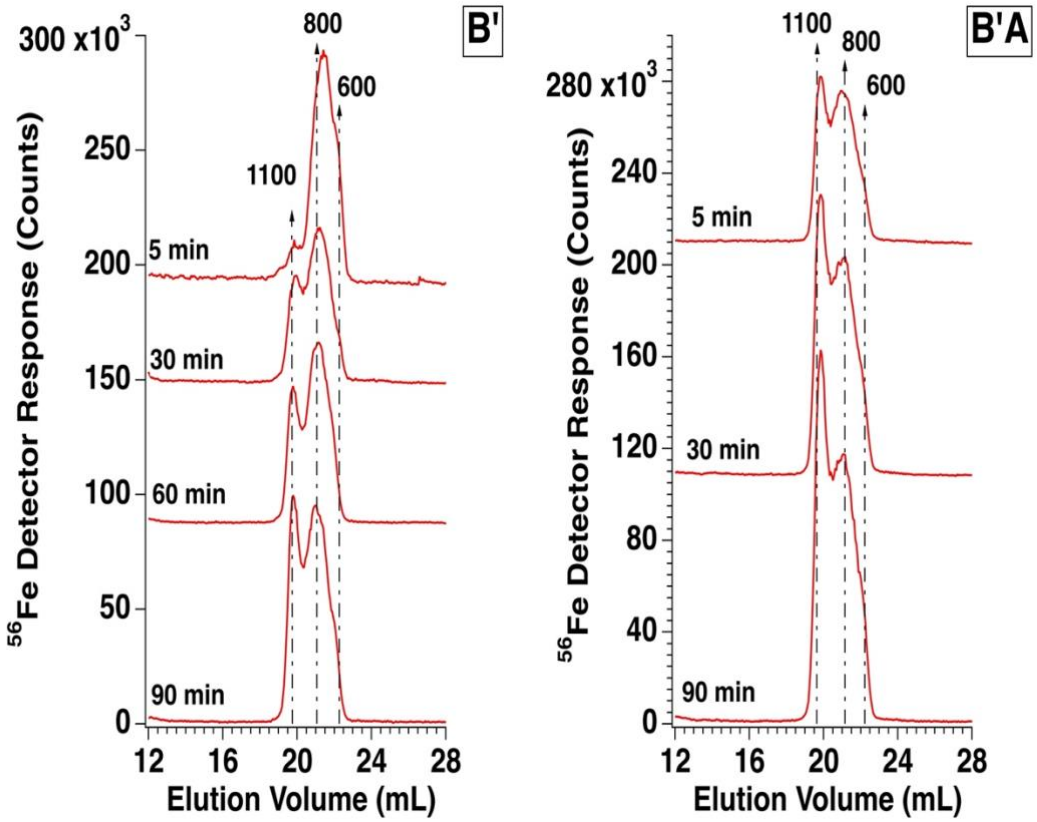


**Figure B-3: Iron chromatograms of supernatants from Batch J mitochondria treatments.**
Mitochondria were incubated in different treatments and samples were pulled from the same suspension over time. Panel labels represent the different buffer solutions. Traces indicate time of incubation. Mass assignments are in Da. All treatment solutions contained TCEP. Elution volume was offset by +2 mL for all traces.

attractive interpretation is that both species continued to be exported from activated mitochondria (either internal or surface-bound) but at an increased rate. However, this effect, if real, is small. Parenthetically, the corresponding sulfur chromatograms were dominated by a single sulfur species due to the HEPES buffer. This prompted us to replace HEPES with Tris in subsequent experiments.

**B.3.5. Batch K Reactions:**

Mitochondria were isolated from WT cells grown on CSM respiring media and 10 μM $^{56}Fe$ citrate. In a glove box with $O_2$ at ~5 ppm, a suspension of isolated mitochondria in buffer B was distributed into four plastic 1.5 mL Eppendorf vials and spun down. Mitochondria (5 mg per vial) and 1 mM TCEP were resuspended separately in buffers B, BA, BAC, and BACF. Suspensions were incubated for 15 min at 30 °C, and then spun by centrifugation at 12,000xg for 10 min. Supernatants were collected and used immediately for LC-ICP-MS analysis. Pelleted mitochondria from each sample were then resuspended in the same buffer as had been used for the first 15 min incubation, and suspensions were incubated for second 15 min (30 min total) as above, then centrifuged. Supernatants were again collected and analyzed by LC; these were the 30-min samples. This process was repeated to prepare the 45 and 60 min samples. The 30, 45, and 60 min samples were frozen and thawed immediately before being run on the LC-ICP-MS system.

We anticipated that mitochondria treated with Buffer B would not export any iron-containing species and that export would commence in buffers BA, BAC and/or BACF. In contrast to this expectation, the supernatants obtained after incubation in

Buffer B exhibited two major iron species with apparent masses ca. 1100 Da and 800 Da, as well as a 600 Da shoulder (Figure B-4B). This was similar to the Batch J results even though the experiment K was different. In Batch J a common reaction vessel was sampled at different times whereas in Batch K the entire supernatant was removed every 15 min and replaced with fresh buffer of the same type. However, in contrast to Batch J, the intensity of these features *declined* with length of incubation. If the species were exported at a constant rate throughout the experiment, the intensity of the corresponding peak would increase in Batch J type experiments but remain constant in Batch K type experiments. If the species ceased to be exported during the experiment, the intensity of the peak would remain constant in Batch J type experiments but would decrease in Batch K type experiments. This latter situation appears to hold for the two experiments; the species is exported quickly and immediately, and then the rate of export declines or export ceases. However time points from 30 min and on in batch K had undergone a freeze-thaw cycle which may have caused species degradation (see below).

The mitochondria treated with buffer BA (Figure B-4BA) exhibited LC traces with the same two components but with ca. 4-fold higher intensities, suggesting stimulation of export due to activation. In contrast to the results of the Batch J experiments, the iron-associated peak at 1100 Da *declined* with time (whereas that at 800 Da remained fairly constant). This again implies that the species at 1100 Da is exported quickly and that the rate of export declined during the experiment – probably because the supply of that species (either on the interior or exterior of the mitochondria) becomes exhausted during the experiment.

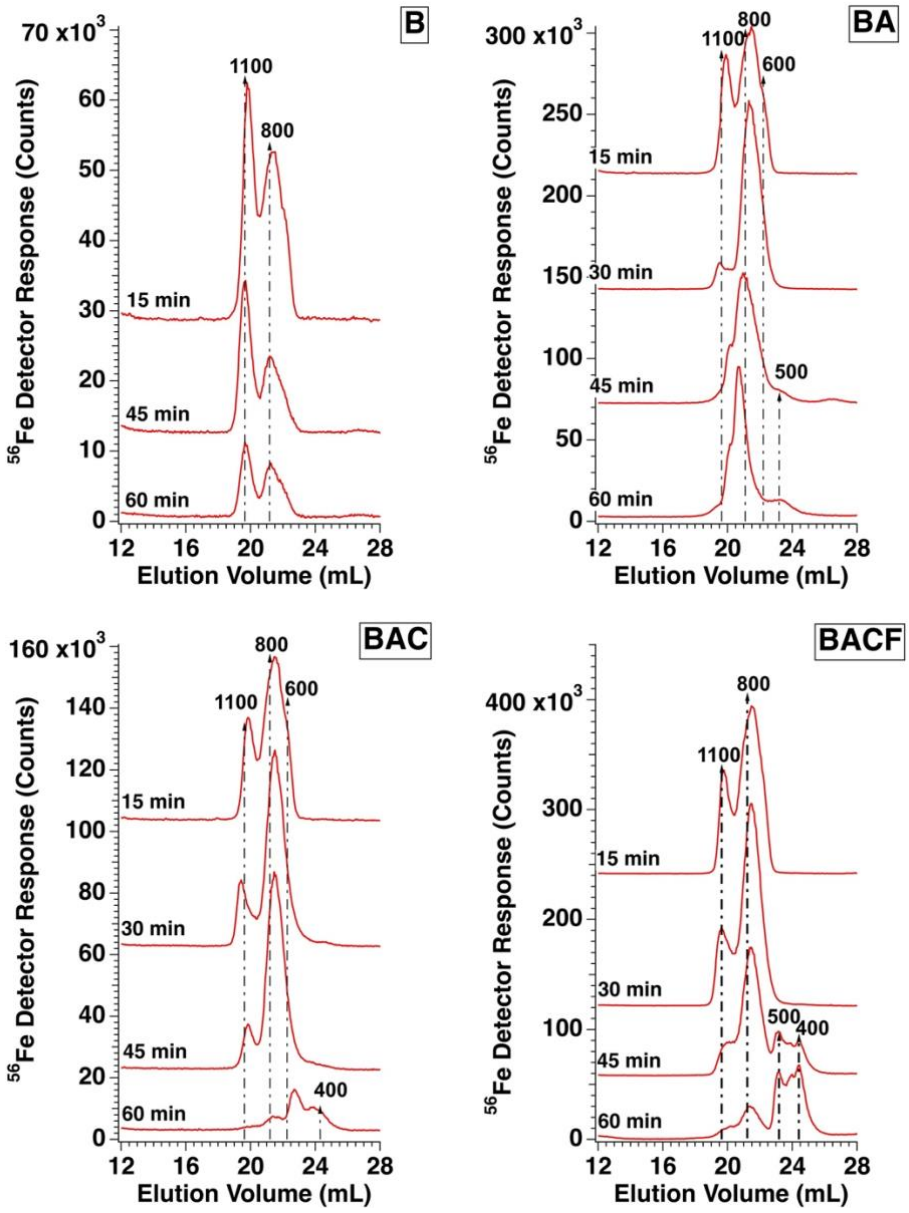


**Figure B-4: Iron chromatograms of supernatants from Batch K mitochondria treatments.**

Mitochondria were incubated in different treatment solutions for 15 minutes, pelleted and run in the same solution a number of times. Panel labels represent the different buffer, when iron was added in the buffer it was as $^{56}Fe^{II}$ ascorbate . Trace labels represent total treatment times of the mitochondria. All 15 min traces were run fresh, all other treatment times were frozen, thawed and then immediately run for LC-ICP-MS analysis. Mass assignments are in Da. All treatment solutions contained TCEP. Elution volume was offset by +2 mL for all traces.

The same two iron peaks were observed in LC traces of the supernatants obtained from mitochondria treated with BAC (Figure B-4BAC) – suggesting that adding cysteine does not further stimulate the release of iron species.

In the LC traces of supernatant obtained from mitochondria incubated in buffer BACF, the intensities of the two iron-containing components increased 2-fold (Figure B-4BACF). As with the other experiments in the batch K study, the intensities declined slowly with time of incubation. Maximum export was at ca. 30 min. One caveat was that the BACF buffer contained 10 μM $Fe^{II}$, and this iron may have given rise to the detected high-intensity peaks. However, in this case, all four time-points examined should have shown the same peaks and same intensities. This was not the case; the intensities of the iron components at 1100 and 800 Da were much lower at 45 and 60 min than they were at 15 min and 30 min (Figure B-4BACF, traces at 45-60 min vs 15-30 min, respectively). As with the Batch K experiment, iron contamination from the buffers may have contributed to the detected species, particularly the 1100 Da species (see below).

The corresponding sulfur peaks for the Batch K experiments were low-intensity but they migrated with an apparent mass similar to those of iron (ca. 900 Da; Figure B-5 BA-BACF). No sulfur peaks were present in supernatant fractions from mitochondrial samples incubated in Buffer B (Figure B-5B). Sulfur peaks were evident in traces from the samples incubated in Buffers BA and BAC, but their intensities were minor relative to those in traces of samples incubated with Buffer BACF (Figure B-5, panel BA-BAC vs BACF, respectively). However, the intensities of the sulfur peak for buffers BA, BAC, and BACF in traces from all four time points (15, 30, 45, and 60 min) were

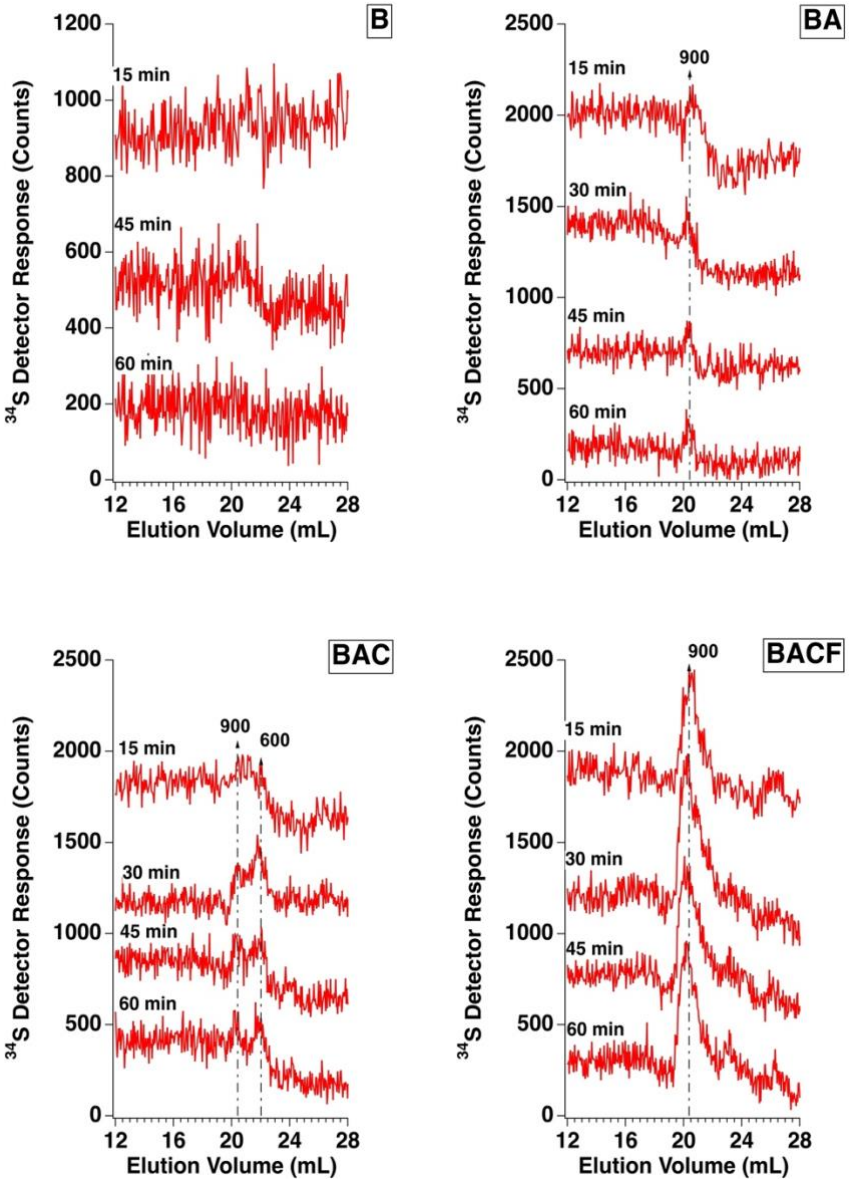


**Figure B-5: Sulfur chromatograms of supernatants from Batch K mitochondria treatments.**
Mitochondria were incubated in different treatment solutions for 15 minutes, pelleted and run in the same solution a number of times. Panel labels represent the different buffer solutions, when iron was added in the buffer it was as $^{56}Fe^{II}$ ascorbate. Trace labels represent total treatment times of the mitochondria. All 15 min traces were run fresh, all other treatment times were frozen, thawed and then immediately run for LC-ICP-MS analysis. Mass assignment as in Da. All treatment solutions all contained TCEP. Elution volume was offset by +2 mL for all traces.

invariant, and their elution profiles were nearly identical to the buffer controls (see below). The most likely interpretation is that the mitochondria are *not* exporting a sulfur species and we are observing very weak buffer-associated features in the supernatants. We cannot exclude the possibility that the 900 Da sulfur species is being exported from mitochondria, but it seems overly coincidental that this peak is also present in buffer (albeit at lower intensity). Also, the low signal/noise ratios associated with these peaks limits our ability to interpret and analyze the data.

We also used Batch K mitochondria to examine whether freezing supernatant fractions in liquid $N_2$ and then thawing them for analysis affected the LC peaks. Activated supernatants from mitochondria (10 mg·mL$^{-1}$) that had been incubated at 30°C for 30 min were split in two; half was run fresh by LC while the other half was frozen and then rethawed at a later time and run in the same way. The LC traces from both samples exhibited the same two iron-containing peaks (at 1100 Da and 800 Da) with a 600 Da shoulder (Figure B-5, panels A and B). However, the intensities of the peaks in the trace from the fresh sample were substantially higher, especially for the 800 Da species, than those from the trace of the frozen sample. Also, the intensity of the sulfur peak (in the same mass region) was much stronger in the trace from the fresh sample. We conclude that fresh samples are preferred relative to frozen ones in their ability to export iron and/or sulfur species.

We also used Batch K to evaluate the effect of $O_2$ on the detected iron-containing species. Pelleted mitochondria were resuspended in 500 μL of BAC buffer and exposed to various quantities of $O_2$ (~5 ppm, 2000 ppm, 20,000 ppm, and 200,000 ppm). After

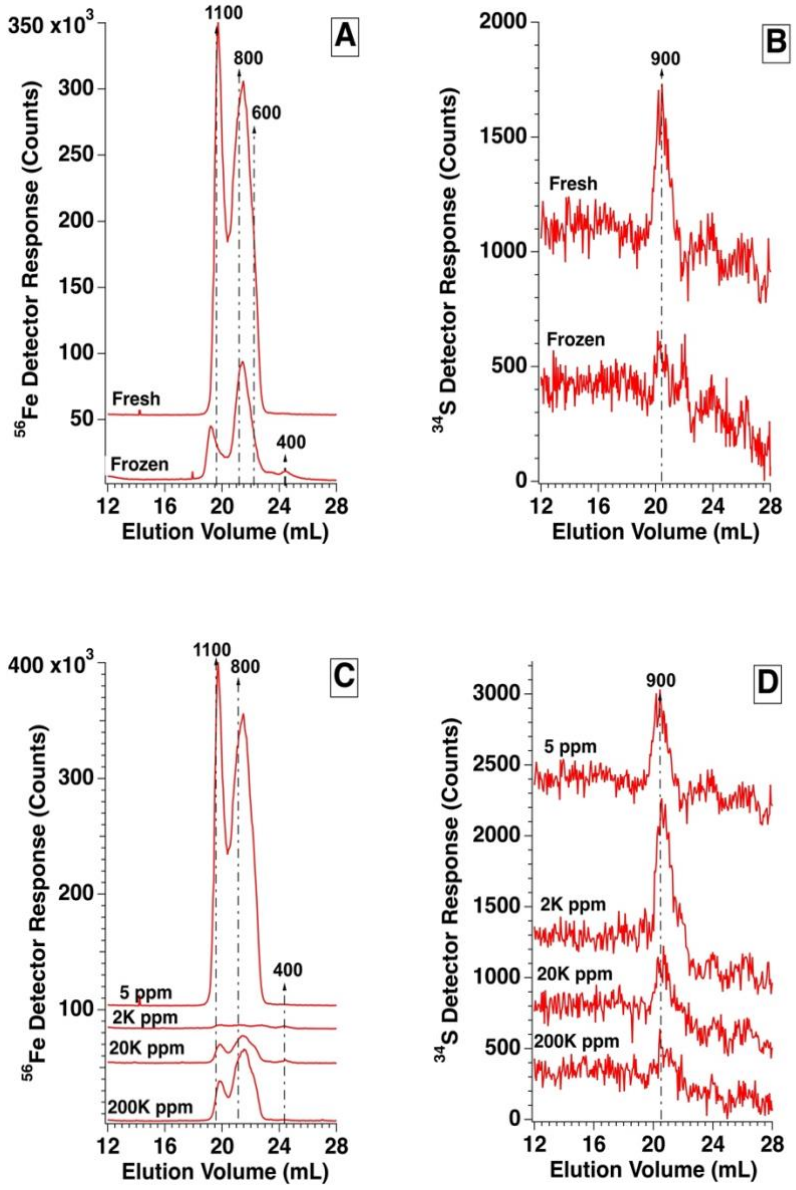


**Figure B-6. Iron and sulfur chromatograms of fresh, frozen, and oxygen treated supernatants from Batch K mitochondria.**
Mitochondria were incubated general activating solution for 30 min. Panels A + B are fresh versus frozen experiment, traces are labeled respectively. Panels C + D are the oxygen treatment experiment. Trace labels for panels C + D represent oxygen concentration mitochondria were exposed to. All treatment solutions contained TCEP. Elution volume was offset by +2 mL for every traces labeld as Fresh and 5 ppm. Traces labeled as Fresh and 5 ppm are duplicates.

centrifugation supernatants were analyzed by LC-ICP-MS. The effect of exposing samples to $O_2$ are also shown in Figure B-6, panels C and D. The two iron-containing peaks were present in all samples, but the intensities followed an oxygen-dependent trend. The most intense traces, by a factor of about 5, were of samples exposed only to glovebox atmosphere, so we decided to continue to perform these experiments under anaerobic conditions. The corresponding sulfur traces were also variable, but the anaerobic sample was relatively intense, and so this condition was again favored for future studies.

**B.3.6. Batch M Reactions:**

Batch M experiments were performed in the same way as Batch K, albeit with a few modifications. For Batch K experiments, cells were grown on $^{57}Fe$ instead of $^{56}Fe$, and buffers did not contain TCEP. In a glove box with oxygen ~5 ppm, a suspension of mitochondria in buffer B was placed into 5 plastic 1.5 mL Eppendorf vials, which were spun by centrifugation as above. The mitochondrial pellets (5 mg each) were resuspended in 500 μL of buffers B, BA, BAC, BACF, and BACFG (for BACF and BACFG, 10 μM $^{57}Fe^{III}$ citrate with 10 fold molar excess of ascorbic acid was used). Each suspension was incubated in an Al block for 15 min at 30 C. The suspension was then centrifuged (12000xg, 10 min) and the supernatant was collected for LC analysis. The mitochondrial pellet was resuspended in 500 μL of the same buffer as was used in the previous step and the process was repeated for the 30, 45, and 60 min samples. All supernatants were analyzed by LC.

We expected the results to be similar to those of Batch K. However, in the Batch M experiment, cells were grown in $^{57}Fe$ so that we could be certain that any species observed in the $^{57}Fe$ chromatograms had arisen from the mitochondria, not the buffer (see buffer experiment below). Buffer BACFG was included because GSH has been hypothesized to coordinate and stabilize nonproteinaceous iron-sulfur clusters and to increase export of iron species from mitochondria[5]. All Batch M samples were run without freezing.

LC traces of supernatants from buffer B and BA at a total incubation time of 15 and 30 min exhibited similar peaks (Figure B-7, B and BA) relative to the Batch K study, with a dominant peak at 1100 Da. The 800 Da peak intensity was weaker than in the Batch K traces and was only present in the buffer B trace of Batch M (for Batch K, this peak was present throughout). For the 15 min samples, the intensity of the 1100 Da peak was similar for buffers B, BA, and BAC but it was 10-fold higher for buffers BACF and BACFG (Figure B-7, B – BACFG, 15 min traces). A similar iron-dependent increase in the intensity of the 1100 Da peak was observed in the Batch K study.

The intensity of the 1100 Da peak declined with time of incubation in all buffers. A similar trend was observed in the Batch K experiment. This suggests a rapid export of the 1100 Da species during the first 15 min, followed by a decline in the rate of export. Since iron was present in buffers BACF and BACFG, we were suspicious that the enhanced intensity of the 1100 Da peak in these samples was due to the iron in the buffer. However, in this case, the same peak and same intensity ought to be observed for all time points – which was not the case. For incubation times beyond 30 min, LC traces

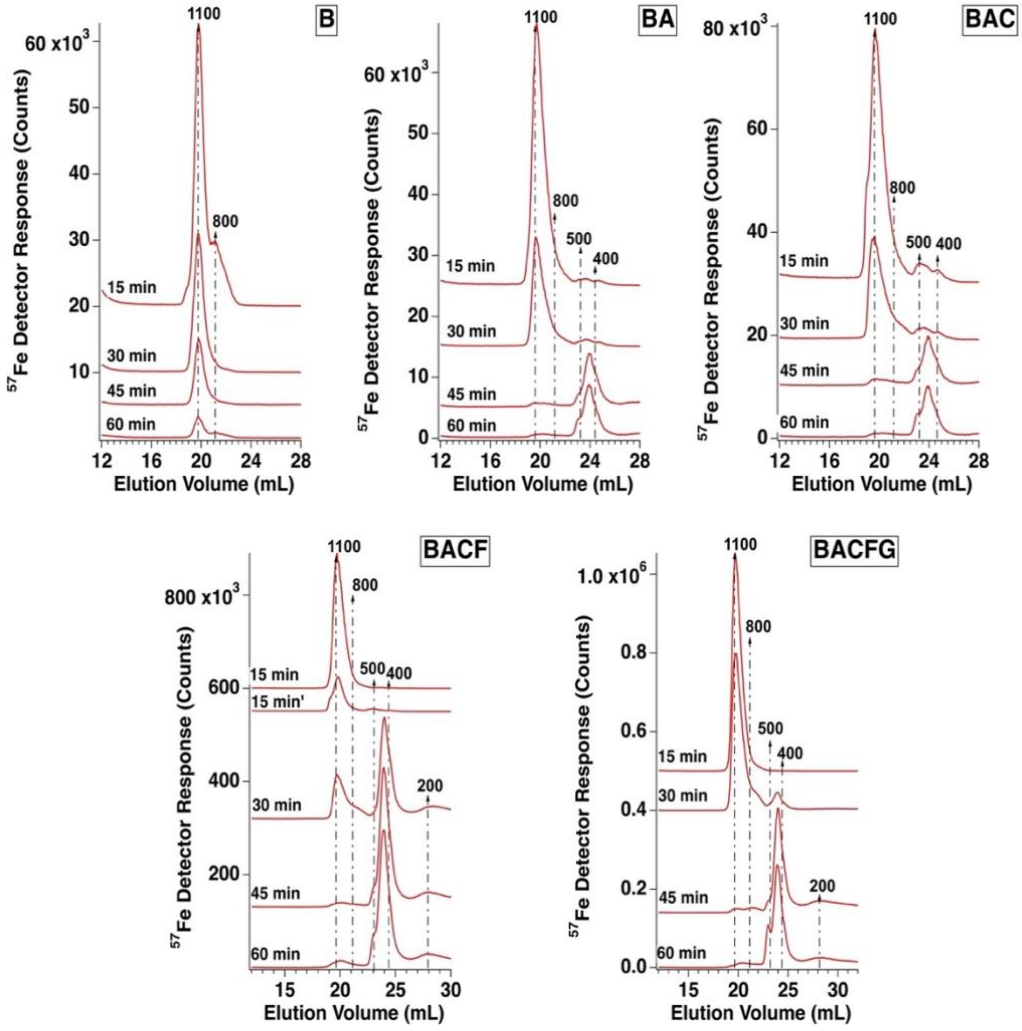


**Figure B-7: Iron chromatograms of supernatants from Batch M mitochondria treatments.**

Mitochondria were grown in $^{57}Fe^{III}$citrate. Mitochondria were incubated in different treatment solutions for 15 minutes, pelleted and run in the same solution a number of times. Panel labels represent the different buffer solutions, when iron was added it was as $^{57}Fe^{II}$ ascorbate. Trace labels represent total treatment times of the mitochondria treatments; Panel BACF 15 min' trace represents a control sample where TCEP is added in the buffer. Mass assignment as in Da.

of BA, BAC, BACF, and BACFG samples show the disappearance of the major 1100 Da species.

Also evident from the traces were the emergence of 1 – 2 species with apparent masses ca. 500 - 400 Da (Figure B-7 BA-BACFG, traces 45 and 60 min ). The peak intensities of these lower-mass species increased gradually over the 60 min experiment. The trend was similar for samples incubated in BACF and BACFG (Figure B-7, BACF and BACFG, trace c and d), though the intensities of these lower-mass peaks were higher. Traces of samples treated with buffer B did not exhibit these lower-mass species (Figure B-7B, traces c and d). These species may have been slowly exported from the mitochondria.

The intensity of the 1100 Da peak was somewhat greater in traces of samples that had been treated with GSH than in those that had not, especially for the 30 min point (Figure B-7BACFG, 30 min trace). GSH may stimulate mitochondrial iron export but the effect, if real, is not major. The changing intensity of the 1100 Da peak suggests that these peaks arise from mitochondria rather than iron-GSH complexes (since iron and GSH were present in every timepoint) (Figure B-7BACFG).

A sample using BCAF with TCEP was run as a control to allow for comparison of samples run in previous batches. The addition of TCEP reduced both iron (Figure B-7BACF, 15 min' trace) and sulfur (Figure B-8BACF, 15 min trace) peak intensities as compared to equivalent samples that did not use TCEP (Figure B-7 and 7-8 B-BACF, 15 min trace) The peaks that were observed were at the same elution time as the samples

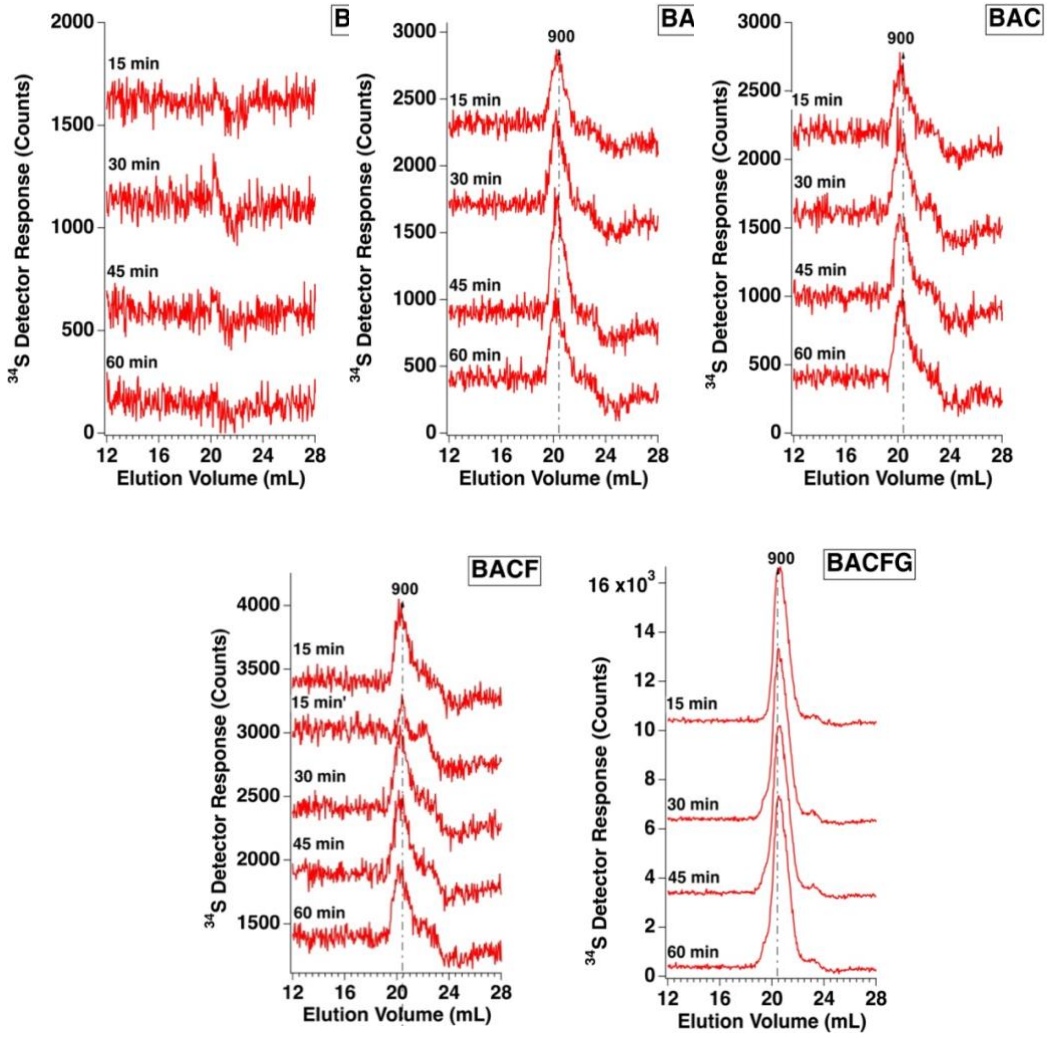


**Figure B-8. Sulfur chromatograms of supernatants from Batch M mitochondria treatments.**

Mitochondria were grown in $^{57}Fe^{III}$citrate. Mitochondria were incubated in different treatment solutions for 15 minutes, pelleted and run in the same solution a number of times. Panel labels represent the different buffer solutions, when iron was added it was as $^{57}Fe^{II}$ ascorbate. Trace labels represent total treatment times of the mitochondria treatments; Panel BACF 15 min' trace represents a control sample where TCEP is added in the buffer. Mass assignment as in Da.

without TCEP. TCEP may somehow reduce the export of iron species or cause their degradation in solution by reduction.

The sulfur peaks of the GSH containing samples were obscured by the presence of what is probably oxidized glutathione (GSSG) (Figure B-8BACFG). The sulfur traces for sample in buffer B contained no sulfur peaks (Figure B-8B), whereas all other buffer treatments contained similar sulfur species with apparent mass ca. 900 Da (Figure B-8BA-BACF). These sulfur peaks are consistent across all time points and do not appear to be stimulated by the addition of cysteine (Figure B-8BAC). The elution profile of exported species appears to be very similar to those of the buffers (see below), but with slightly lower intensities.

**B.3.7. Batch N Reactions:**

Mitochondria were isolated as described above from respiring cells grown with 10 μM $^{57}Fe^{III}$ citrate. The organelles were pelleted and then resuspended in buffers B, BA, BAC, BACF, and BACFG (with $^{57}Fe^{III}$ citrate with 10-fold molar excess of ascorbic acid for BACF and BACFG) to a final protein concentration of 9 mg·mL$^{-1}$. Suspensions were incubated for 15 min at 30 C, then spun by centrifugation at 12000xg for 10 min. The supernatants were collected for LC analysis. This was the first step of a three-step experiment; our objective for this step was to activate and "load" $^{57}$Fe-enriched mitochondria with $^{57}Fe^{II}$, along with performing the requisite controls.

For the second step, the pellets were resuspended in the same buffers (with $^{56}Fe^{II}$ ascorbate made with ferrous ammonium sulfate and a tenfold molar excess of ascorbic acid) plus cytosol obtained from cells unenriched in $^{57}$Fe, the final volume was the same

as the first step. The final protein concentration of the cytosol was 2 mg/mL. The cytosol was generously provided by Dr. Trang Nguyen. Thus, any $^{57}$Fe iron detected should have originated from the mitochondria. Suspensions were incubated in these solutions for 15 min and then centrifuged as above. Supernatants were collected and filtered through separate 10 kDa-cutoff Amicon centrifugation filtration units following the manufactures instructions; both flow-through solution (FTS) and retentate were collected separately for LC analysis. If samples were not run the same day they were frozen and stored at -80 °C.

For the third step of the experiment, the $^{57}$Fe-enriched mitochondrial pellets were collected, washed twice with 20 mM ammonium bicarbonate pH 8.5, and then resuspended with 1 mL of the same buffer but containing Triton-x100 (2% w/v). The suspension was vortexed for 15 min and any insoluble portions were pelleted via centrifugation at 12000xg for 15 min, and then discarded. Supernatants were passed through 10 kDa cutoff membranes and FTSs were collected for LC analysis. The objective of this step was to examine the low-molecular-mass content of mitochondria after the treatments from the first two steps.

LC traces of the supernatant fractions obtained from the first step of the experiment (Figure B-9A) exhibited the 1100 Da and 800 Da species, as had been observed in previous experiments. A minor shoulder at 600 Da was also present (Figure B-9A). The intensities of the 1100 and 800 Da peaks were highly variable. For the samples incubated in buffers B, BA, and BAC, the intensities were essentially invariant (Figure B-9A, traces B-BAC). This invariance within the first 15 min was similar to that

of Batch M (Figure B-7B-BAC,15 min trace). For the sample incubated in buffer BACF and BACFG, the intensities were 20-30 fold higher (Figure B-9A, traces B-BAC vs BACF and BACFG).

We have considered that the increased intensity in $^{57}Fe$ in these two samples may be due to the iron in the buffer being absorbed by the mitochondria. The sample treated with GSH was invariant compared to the equivalent sample without GSH (Figure B-9A, traces BACF and BACFG). This was different in comparison to Batch M where addition of GSH showed a dominant peak that was two-fold higher than in the similar buffer not containing GSH (Figure B-7 BACF vs BACFG, 15 min trace). There is no apparent trend with addition of GSH.

For the second step of the experiment, cytosol was added as a new constituent to all of the buffers. In these samples, the 800 Da species was more intense and broader than the 1100 Da species (Figure B-9B). Though overall the species were less intense than in the first step. The intensities of the 1100 Da and 800 Da species were more intense in samples with iron in the buffer than in samples without iron (Figure B-9B, traces BACF and BACFG vs B, BA, and BAC, respectively). Again, this may be due to iron being absorbed and utilized by the mitochondria and possibly stimulated for species generation/export from the buffer. The overall signal intensities of the samples not treated with iron in step 2 were invariant (Figure B-9B, traces B-BAC). It is unlikely that any of the detected $^{57}Fe$ species originated from the cytosol because the cytosol was $^{56}Fe$ enriched. No effect of GSH was evident.

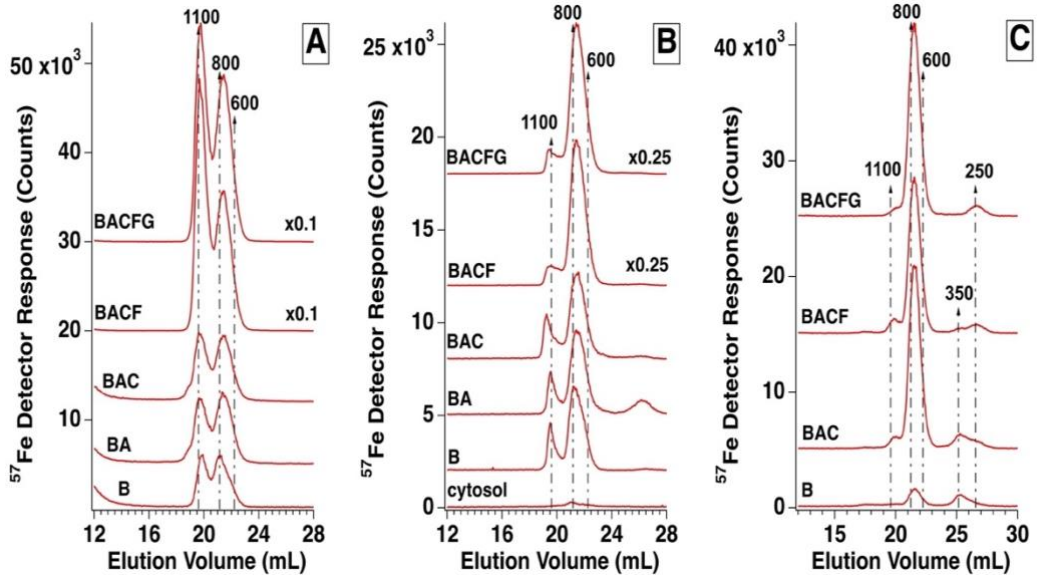


**Figure B-9. Iron chromatograms of supernatants and soluble mitochondrial extracts after treatment with cytosol from Batch N mitochondria equilibrium experiments.**

Mitochondria were grown in $^{57}Fe^{III}$citrate. Mitochondria were incubated in different treatment solutions for 15 minutes, pelleted and run in the same solution but with the addition of cytosol. Cytosol was grown in $^{56}Fe$. Panel labels represent different experiments and are as follows: A, pre-cytosol treatment; B, addition of cytosol in treatment solutions; C, LMM FTS of soluble mitochondrial extracts of mitochondria from Panel B. Trace labels represent the different buffer solutions used for treatment, when iron was added to the buffer it was in the form of $^{57}Fe^{II}$ ascorbate. Panel B, cytosol trace is a control to determine the contribution of cytosol to the chromatograms. Mass assignment as in Da. Select traces were multiplied to keep on scale with other traces. Panel A, B trace had undergone 1 freeze-thaw cycle before analysis.

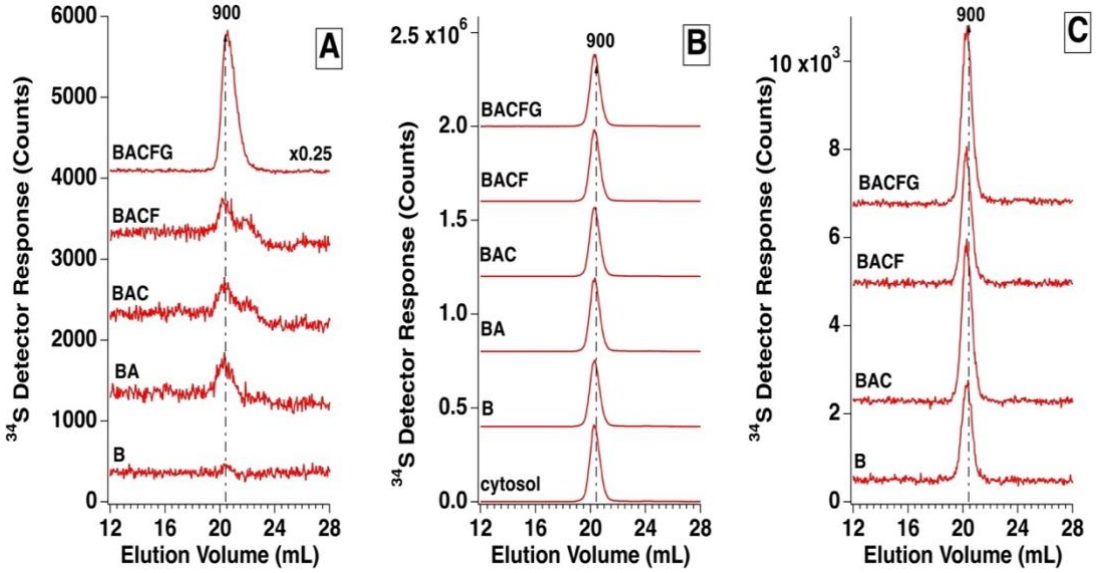


**Figure B-10. Sulfur chromatograms of supernatants from Batch N mitochondria treatments.**

Mitochondria were grown in $^{57}Fe^{III}$citrate. Mitochondria were incubated in different treatment solutions for 15 minutes, pelleted and run in the same solution but with the addition of cytosol. Cytosol was grown in $^{56}$Fe. Panel labels represent different experiments and are as follows: A, pre-cytosol treatment; B, addition of cytosol in treatment solutions; C, LMM FTS of soluble mitochondrial extracts of mitochondria from Panel B. Trace labels represent the different buffer solutions used for treatment, when iron was added to the buffer it was in the form of $^{57}Fe^{II}$ ascorbate. Panel B, cytosol trace is a control to determine the contribution of cytosol to the chromatograms. Mass assignment as in Da. Panel A, BACFG trace was multiplied by 0.25 to keep in scale with other traces. Panel A, B trace had undergone 1 freeze-thaw cycle before analysis.

LC traces of the FTS of the mitochondrial extracts were dominated by an 800 Da peak with a minor 1100 Da peak (Figure B-9C). The mitochondrial FTS also exhibited a peak with apparent mass ca. 350 Da (Figure B-9C, traces B, BAC, and BACF). Traces originating from mitochondria that had been incubated in buffer B exhibited peaks at 800 Da and 250 Da, but their intensities were less. (Figure B-9C, trace B vs BAC-BACFG, respectively).

The sulfur peaks observed had an apparent mass ca. 900 Da in all experiments involving Batch N (Figure B-10). The LC traces from the GSH-containing sample of Step 1 exhibited an intense peak at 900 Da, which comigrates with GSSG (Figure B-10A, trace BACFG). In the second step, the sulfur peaks from the LC traces from cytosol addition appear to originate from the cytosol (Figure B-10B, trace cytosol vs B-BACFG, respectively) which is known to contain high concentrations of GSH/GSSG. All sulfur peaks found in the mitochondrial FTS traces are near-identical. They are either due to leftover endogenous sulfur species from the cytosol or from a singular sulfur species in mitochondria (Figure B-10C).

**B.3.8. Buffer Controls:**

Buffers B, BA, BAC, BACF, and BACFG, all without TCEP, were run down the LC-ICP-MS system as controls (Figure B-11). Traces of all buffers except the Buffer B contained $^{56}$Fe species with apparent masses ca. 1100-800 Da and 600-400 Da (Figure B-11A). Samples with added $^{56}$Fe in the buffer (BACF/BACFG) had substantially larger peaks including with a predominant left shoulder at 1100 Da (Figure B-11A, traces BAC$^{56}$f and BAC$^{56}$FG). For $^{57}$Fe detection, buffer B contained peaks with apparent

masses ca. 1700 Da and 1100 Da, though at a weaker signal intensity (Figure B-11B, trace B). The weak intensity would contribute a marginal amount to sample species. LC traces of Buffer BA and BAC contained a weak broad species spanning an apparent mass range ca, 600-400 Da (Figure B-11B, traces BA and BAC), which would contribute a marginal amount to sample species. All buffers that contained additional iron (i.e. BACF and BACFG) had detectable $^{57}$Fe species, similar to the detected $^{56}$Fe species in controls (Figure B-11B, traces BAC$^{56}$F, BAC$^{57}$F, BAC$^{56}$FG, BAC$^{57}$FG). The iron species in the buffers do not contain any resolvable 800 Da species that has been observed in mitochondrial supernatant samples across all batches. There is some overlap with the 1100 Da species and the smaller 600-400 Da species detected in buffer controls and mitochondrial samples. When mitochondria were treated with buffer B, we expected that the detected iron species in mitochondria supernatants originated from the mitochondria and not the buffer in experiments J, K, M and N. However, we cannot exclude the possibility that this iron originates from the outside of the mitochondria as a form of iron that was adsorbed to its membrane.

For sulfur species, all buffers except B contained sulfur peaks present at ca. 900 Da and 600 Da (Figure B-11C, traces BA-BAC$^{57}$FG), and the elution profile was similar to other sulfur species detected in Batches K, M, and N. The addition of glutathione exhibited a strong 900 Da species which as observed in experimental samples (Figure B-11C, traces BAC$^{56}$FG and BAC$^{57}$FG. The intensities of the buffer signals appeared to be weaker compared to experimental samples, however the change in signal intensity was modest and may not represent species originating from the mitochondria.

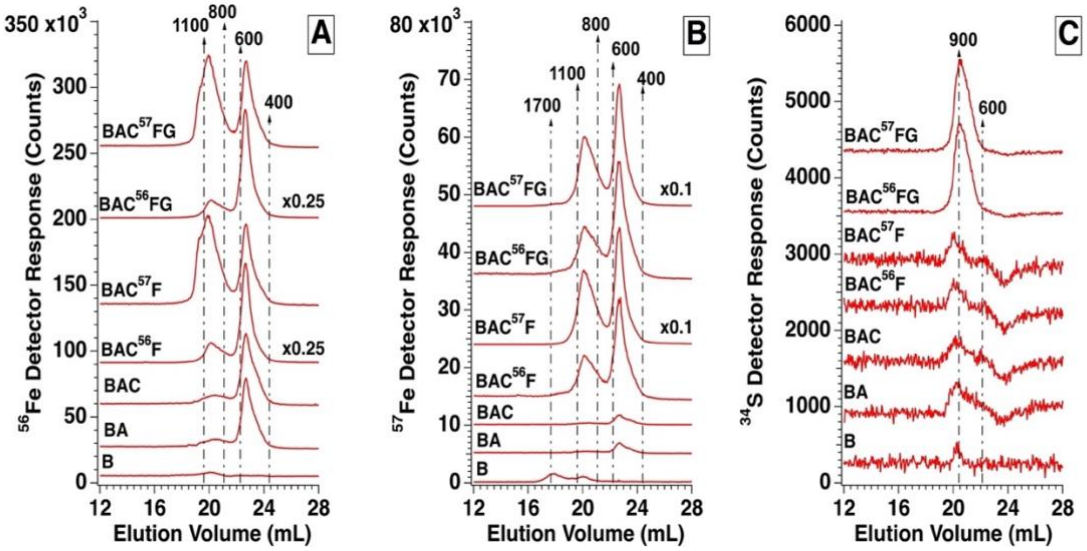


**Figure B-11: Iron and sulfur chromatograms of the treatment solutions used in batches M and N**.

Panel labels represent different elements and isotopes detector responses for buffer solutions, they are as follows: A, $^{56}$Fe, B, $^{57}$Fe, C, $^{34}$S. Trace labels represent the different buffer solutions used for treatment, when iron was added it was either in for form $^{56}$Fe$^{II}$ ascorbate or with $^{57}$Fe$^{II}$ ascorbate. Samples containing either are indicated with superscript 56 or 57. Select traces were multiplied by a scaling factor to keep in scale with other traces. TCEP was not present in any treatment solution.

To determine the location of the detected iron, each component of the activation solution was prepared separately at the same concentration as in the activation solution, and with 10 molar equivalents ascorbate and bathophenanthrolinedisulfonic acid (BPS). Solutions of GTP, NADH, NADPH, tris-sorbitol, and cysteine were all negative for iron (yielding an absorbance of < 0.001 at 535 nm). A 4 mM ATP solution contained 1 uM iron, corresponding to an absorbance of 0.022. After batch M, a new vial of ATP was purchased, and a 4 mM solution of it contained an undetectable amount of iron when analyzed via BPS.

Besides using iron-free buffers, we will also develop more extreme methods of cleaning the column. Our current hypothesis is that a small amount of iron is absorbed onto the column, despite our efforts to keep the column iron-free, and that passage of buffers (other than buffer B) through the column is sufficient to desorb some of the iron, leading to the background signals that we observed.

**B.3.9. Discussion:**

Arguably the most daunting question in the field of eukaryotic iron trafficking is whether an iron and/or sulfur species is exported from the mitochondria via ATM1 (a mitochondrial inner membrane transport protein) to the cytosol where it is used in the assembly of iron sulfur clusters (by the CIA). This idea was first proposed two decades ago by Roland Lill and coworkers.[6] Since then, abundant, albeit indirect, evidence for this hypothesis has been published and virtually all groups in the cell-biology-of-iron community operate under the assumption that it is correct. However, prior to Pandy et al., 2019, no such species has been directly detected much less identified. The overall

objective of the studies just described was to detect and characterize such species for the first time, thereby providing the most stringent test of this lynchpin hypothesis.

We devised a number of experiments to probe this export process. Overall, in most conditions and experiments we observed predominate species with apparent masses at 1100 Da and/or 800 Da, and sometimes observed minor species ranging between 600 Da – 400 Da. Caution must be taken when attributing these detected species to export products of the mitochondria. No iron species were detected in buffer B, suggesting that at a minimum the species observed from treatment of buffer B originate from the mitochondria. When buffer controls were run for all other buffers they exhibited species ranging from 1100 – 800 Da and 600-400 Da. We suspect that the 800 Da species may originate from the mitochondria as the buffer controls did not contain a resolvable 800 Da species. Based on experimental results we cannot yet firmly conclude that the detected species from the supernatant of mitochondrial suspensions originate from the mitochondria as an export product. There is still a possibility that the detected species originate from the mitochondrial surface; perhaps some membrane bound iron that had adsorbed to the mitochondria dissociates into solution.

We first wanted a condition where we could either halt or prevent the export of these species and then find conditions where we could biochemically stimulate Fe/S species export. Incubating mitochondria with buffer B alone was not expected to stimulate iron export. However, we still observed iron species from the supernatant of mitochondria suspensions. The predominate species observed had apparent masses at 1100 Da and/or 800 Da. We then hypothesized that if iron species were exported from

the mitochondrial matrix region, then treatment of the mitochondria with activating components which stimulate ISC assembly in mitochondria, should stimulate export of these species. We observed that addition of nucleotides (buffer BA) did increase the intensity of the 1100 Da and/or 800 Da species, but the effect was cysteine-independent, and only observed in a few experiments. We cannot conclude that the stimulation of mitochondria with nucleotides was able to increase species generation, these possible trends require further replicates. We were able to observe with a single replicate, that the detected species are sensitive to freeze-thaw effects and O2; signals were more intense using fresh material maintained under anaerobic conditions.

The species with masses at 1100 Da and 800 Da appear to be exported rather quickly. In most experiments the export of these species reached a maximum after 15 - 30 min. Additionally, species ranging from 600 - 400 Da appeared to be released at a slower rate due to their presence at later timepoints. This timeframe may be an effect of the mitochondria becoming depleted of these iron species or the mitochondria are becoming damaged due to the stress of the experiment. There appeared to be a variable export rate between the 1100 Da and 800 Da species. Species appeared to be exported faster when mitochondria are stimulated with nucleotides, when compared to buffers with no nucleotides. Though this effect was not observed in every batch/experiment and requires further studies are required to establish an explanation to this phenomenon. A lead we have in this regard is the use of reducing agent in the buffers. Sample that showed a variable export rate (batch J and K) contained TCEP and whereas the batch that did not have this variable rate was without TCEP(batch M). Though a control was

run in batch M with the addition of TCEP to the buffer, the results were counterintuitive to TCEP having a beneficial effect.

We also anticipated that stimulation of the mitochondria with buffers containing iron (buffer BACF) or GSH (buffer BACFG) would give rise to larger intensity species. Due to recent research on an Fe-S mitochondrial exported species where iron was used to stimulate export and from evidence suggesting that GSH is involved in or is a ligand of the X-S species.[7–9] The effect of increased species intensity was observed in all experiments where iron was added to the buffer (buffers BACF and BACFG). We speculate that the species observed under these conditions arise from the mitochondria due to their absorption of the iron in the buffer and subsequent utilization of this new iron pool and not from the buffers partly because these species are not observed in every time point of the experiments. However we cannot confirm that these species are truly exported products from the mitochondria and not from iron originating from the mitochondria membrane which may have become saturated due to the buffer. In the buffer BACFG, which contained GSH, there was no apparent trend due to GSH. More replicates utilizing this condition are required before to ascertain if a trend is truly not present.

We were hopeful that using aqueous samples would allow us to observe sulfur species, such as $S_{int}$, like we previously had observed in the organic extracts. In cases where buffer B was used, there was no detectable sulfur species. Though in all other cases where any other buffer was used which did not contain GSH (buffer BA, BAC, BACF) we observed a 900 Da species. However, this species observed was similar in

elution profile to buffer controls and sometimes larger in intensity. We cannot conclude that the mitochondria export a sulfur species under these conditions, and if this species is indeed coming from the mitochondria the effect is weak. In all cases where buffer BACFG or cytosol was added, there was a strong signal attributed to GSSG which came from either the added GSH or the cytosol. This feature was present in cytosol and BACFG solution controls, indicating it is not a mitochondrial product, but present in the reaction solutions.

Curiously enough we did not see results similar to Pandey et.al., 2018, in these experiments. The concentration of the species that were exported may be very small, which was why the researchers pooled 6 reactions together for organic extraction. Additionally, their methodology utilized a two-step process: 1) the sulfur species were allowed to build up in the mitochondria; and 2) the same species were exported out of the mitochondria. The supernatants from these solutions were then pooled together and concentrated. Additional experiments in aqueous solutions using a higher protein concentration of mitochondria and possibly mimicking their two-step process may yield similar results in the future.

This work provides some evidence that low-molecular-mass iron species may be exported from the mitochondria. However, further work is required to determine if the species we observe are actual export products and to determine other means to stimulate the mitochondria for iron as well as sulfur export. More stringent controls, buffer composition contamination checks, and more intensive chromatography column cleaning may be required. More replicates for these experiments are also needed to determine if

trends are present for species rate of occurrence. Other avenues of experimentation are required that could help in stimulating export. One such route is through the use of cytosol similar to Pandey, et.al., 2019, where they showed that cytosol was able to stimulate export of Fe-S from the mitochondria. Although we have performed such an experiment in Batch N, additional studies might be required to observe a stimulatory effect of cytosol.

**B.3.10. References:**


1 A. Pandey, J. Pain, N. Dziuba, A. K. Pandey, A. Dancis, P. A. Lindahl and D. Pain, Mitochondria Export Sulfur Species Required for Cytosolic tRNA Thiolation, *Cell Chem. Biol.*, 2018, **25**, 738-748.e3.

2 M. Cardenas, R. Afroditi and C. Kostas, Iron – sulfur clusters : from metals through mitochondria biogenesis to disease, *JBIC J. Biol. Inorg. Chem.*, 2018, **23**, 509–520.

3 W. Xiao, *Yeast Protocols*, Humana Press, New Jersey, 2nd edn., 2005, vol. 313.

4 M. J. Moore, J. D. Wofford, A. Dancis and P. A. Lindahl, Recovery of mrs3Δmrs4Δ Saccharomyces cerevisiae Cells under Iron-Sufficient Conditions and the Role of Fe 580, *Biochemistry*, 2018, **57**, 672–683.

5 N. Dziuba, J. Hardy and P. A. Lindahl, Low-molecular-mass iron in healthy blood plasma is not predominately ferric citrate, *Metallomics*, 2018, **10**, 802–817.

6 G. Kispal, P. Csere, C. Prohl and R. Lill, The mitochondrial proteins Atm1p and Nfs1p are essential for biogenesis of cytosolic Fe / S proteins, 1999, **18**, 3981–3989.

7 C. Kumar, A. Igbaria, B. D'Autreaux, A. G. Planson, C. Junot, E. Godat, A. K. Bachhawat, A. Delaunay-Moisan and M. B. Toledano, Glutathione revisited: A vital function in iron metabolism and ancillary role in thiol-redox control, *EMBO J.*, 2011, **30**, 2044–2056.

8 J. Li and J. A. Cowan, Glutathione-coordinated [2Fe–2S] cluster: a viable physiological substrate for mitochondrial ABCB7 transport, *Chem. Commun.*, 2015, **51**, 2253–2255.

9 A. K. Pandey, J. Pain, A. Dancis and D. Pain, Mitochondria export iron–sulfur and sulfur intermediates to the cytoplasm for iron–sulfur cluster assembly and tRNA thiolation in yeast, *J. Biol. Chem.*, 2019, **294**, 9489–9502.

### B.4. Final Remarks of Appendix B:

In our collaboration with Dr. Pain in characterizing the $S_{int}$ species we were able to speciate Sint and determined it had a mass range between 1100 – 700 Da. The experiments performed in this collaboration were the foundation which we used to explore the export of iron and sulfur species from the mitochondria. We attempted to analyze aqueous supernatants from activated mitochondria suspensions rather than use aqueous resuspensions of organic phase extracts of these supernatants. We believed that the organic extraction caused the degradation of iron species or that these species were lost during the extraction process, which ever occurred no iron was detected in the resuspended organic extracts. There also exists the possibility that maybe endogenous sulfur species were also degraded and were then detected by LC.

We determined that the incubation of mitochondria in solution generates two predominate and observable iron species via LC, these species masses are 1100 and 800 Da, and species that appear to be released at a much slower rate with masses ranging from 600 – 400 Da. Observed species appear to be maximally detected after 15 or 30 min under our experimental conditions. No sulfur species were determined to have originated from the mitochondria, but more probably from the buffers. Though it is unknown if these iron species are exported from the mitochondria or are from iron bound to its membrane. These works represent my efforts in the ongoing project that is aimed at characterizing iron and sulfur species exported by the mitochondria. My work with Rachel Shepherd was in exploring a new avenue to characterize exported LMM iron and sulfur species from mitochondria.

# APPENDIX C COA6 IS STRUCTURALLY TUNED TO FUNCTION AS A THIOL-DISULFIDE OXIDOREDUCTASE IN COPPER DELIVERY TO MITOCHONDRIAL CYTOCHROME C OXIDASE§

## C.1. Contributions:

My contribution to this project was in analyzing purified protein samples of COA6 and mitochondrial extracts via LC-ICP-MS. My work is represented in the source within the following figures: Part of Figure 5 and all Figure S4. All other work was performed by the respective authors, especially Shivatheja Soma and Dr. Vishal Gohil from Texas A&M University.

## C.2. Summary:

In eukaryotes, cellular respiration is driven by mitochondrial cytochrome *c* oxidase (CcO), an enzyme complex that requires copper cofactors for its catalytic activity. The insertion of copper into its catalytically active subunits, including COX2, is a surprisingly complex process that requires metallochaperones and redox proteins including SCO1, SCO2 and COA6, a recently discovered protein whose molecular function is unknown. To uncover the molecular mechanism by which COA6 and SCO

§ *Reproduced and adapted by permission from "COA6 is structurally tuned to function as a thiol-disulfide oxidoreductase in copper delivery to mitochondrial cytochrome *c* oxidase" by Shivatheja Soma, Marcos N. Morgada, Mandar T. Naik, Aren Boulet, Anna A. Roesler, Nathaniel Dziuba, Alok Ghosh, Qinhong You, Paul A. Lindahl, James B. Ames, Scot C. Leary, Alejandro J. Vila, Vishal M. Gohil, 2019**.** *Cell Reports*, 29, P4114-4126.E5, Copyright 2019 by Elsevier. Publication is forthcoming. https://doi.org/10.1016/j.celrep.2019.11.054

proteins mediate copper delivery to COX2, we solved the solution structure of COA6, which revealed a coiled-coil-helix-coiled-coil-helix domain typical of redox-active proteins found in the mitochondrial inter-membrane space. Accordingly, we demonstrated that COA6 can reduce copper-coordinating disulfides of its client proteins, SCO1 and COX2, allowing for copper binding. Finally, our determination of the interaction surfaces and reduction potentials of COA6 and its client proteins provides a mechanism of how metallochaperone and disulfide reductase activities are coordinated to deliver copper to CcO.

**C.3. Method:**

**C.3.1. LC-ICP-MS**

The LC-ICP-MS used for analysis is described in Dziuba, et al., 2018.[1] Samples were analyzed either with two Superdex Peptide 10/300 GL (GE Healthcare) columns connected in series or with a Bio SEC-3 (Agilent Technologies) column. Samples were passed through either a Titan regenerated cellulose 0.2 μm filter (Thermo scientific) or a 0.2 μm cellulose acetate filter (VWR). The dual peptide columns used a mobile phase of 20 mM Tris (pH 7.4) and 10 mM NaCl at a flow rate of 0.350 mL/min for a total of 160 min per run and a loop volume of 300 μL. The Bio SEC-3 column used a mobile phase of 20 mM Tris (pH 7.4) and 150 mM NaCl at a flow rate of 0.4 mL/min for a total of 10 min per run and a loop of 20 μL. The diode array was set for detection and data collection at 280 nm. Molecular mass standards were cyanocobalamin (1.3 kDa) from Fisher BioReagents and cytochrome c (12 kDa), carbonic anhydrase (30 kDa), albumin (66 kDa) and apoferritin (443 kDa) all from Sigma.

**C.4. Results:**

The Gohil group had previously observed that purified COA6 did not contain copper, where as other researchers had reported that human COA6 could bind copper *in vitro*.[2] We suspected that copper could coordinate to COA6 because it is rich in cysteine residues. Due to these issues, it was speculated that COA6 does not bind copper as a physiological function. To probe this issue recombinant COA6 was purified from E. *coli* and reconstituted in the presence and absence of copper and reduced glutathione. These solutions were analyzed via SEC, with both UV-VIS (280 nm) and ICP-MS ($^{63}$Cu) detection occurring. A peak was observed in a chromatogram (UV 280) trace, which was proposed to be a COA6 dimer (Figure C-1). A chromatogram ($^{63}$Cu) trace of a solution without copper and glutathione had no observable copper peak (Figure C-1A). When the solution contained reduced glutathione and copper, a copper peak coeluted with the proposed COA6 dimer peak along with an additional high molecular weight peak which was speculated to arise from a protein-copper aggregate (Figure C-1B). This indicates that recombinant COA6 can coordinate copper when reconstituted in the presence of copper and glutathione, but not endogenous copper present in E. *coli*.

These experiments were performed *in vitro* and may not accurately represent the proteins *in vivo* function. To probe the *in vivo* protein, mitochondrial lysate extracts from S. *cerevisiae* were analyzed by SEC to determine if COA6 binds to copper *in vivo*. Two strains were used, including wild type, and *coa6Δ*. Mitochondrial extracts were injected onto a SEC column where the eluent was fraction-collected. These fractions were then probed for COA6 by Western blot. The copper chromatograms from the WT

mitochondria extracts showed 4 predominate species with apparent masses ca. 30, 20, and 10 kDa, (a larger species was detected that eluted in the column void volume) (Figure C-2A). The corresponding *coa6Δ* mitochondria extracts showed the same three copper species which were invariant when compared to the WT traces, indicating that COA6 *in vivo* does not bind to copper (Figure C-2B). Western blot for coa6 detected the absence of COA6 in *coa6Δ* mitochondria, though fractions containing COA6 in WT mitochondria did not elute with any of the copper species (Figure C-2C and D). If COA6 did bind copper, we would have observed a copper peak corresponding to the fractions where COA6 was detected in WT mitochondria. This peak would then have been absent in the *coa6Δ* mitochondria. Both chromatograms were invariant suggesting that COA6 is not a copper binding protein within yeast.

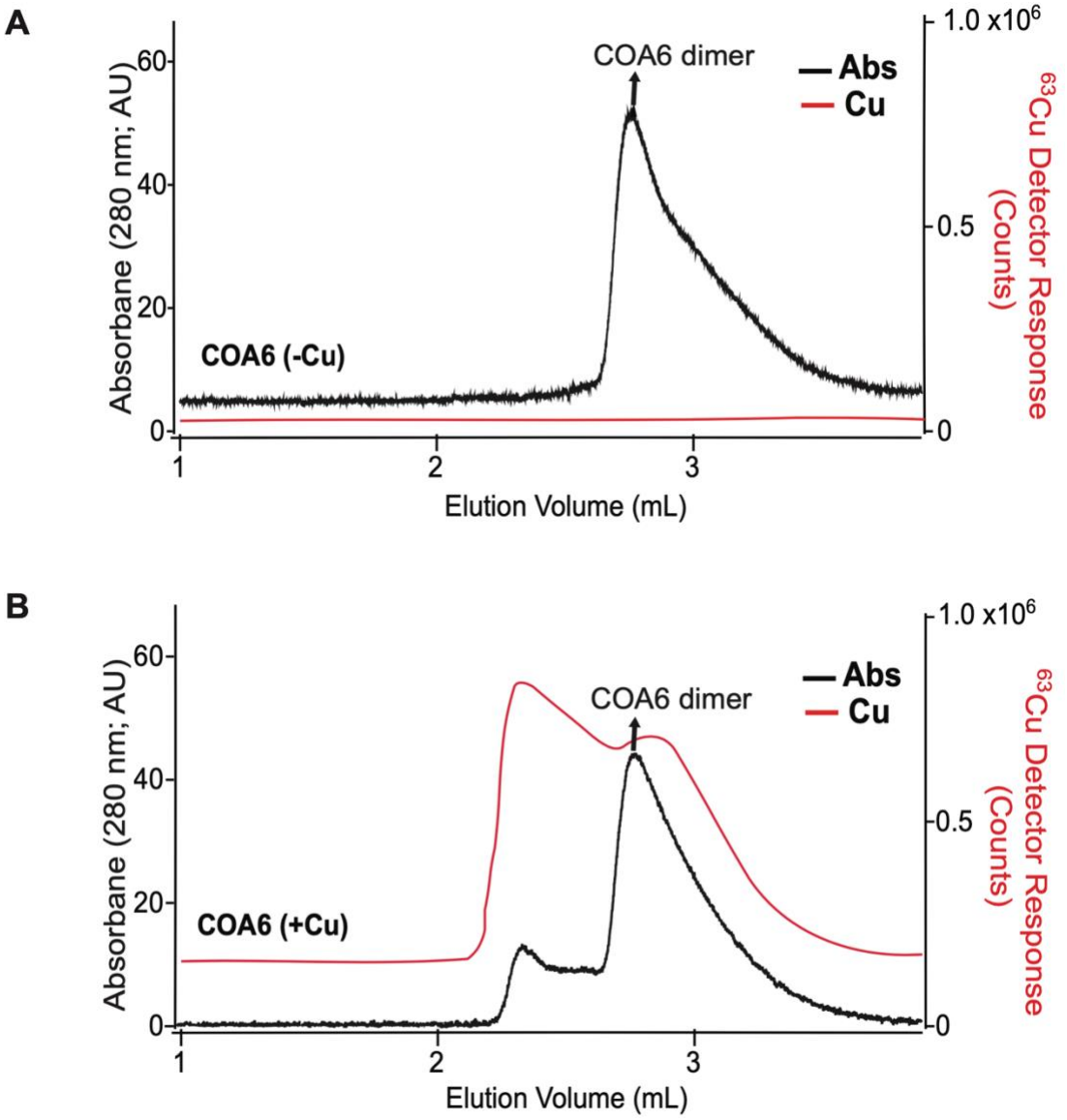


**Figure C-1. Recombinant COA6 only binds copper when reconstituted with metal ion and reductant.**

Black traces are absorbance at 280 nm and red traces are copper detection response. Panel labels are as follows: A) $^{63}Cu$ and protein traces of recombinant COA6 analyzed by LC-ICP-MS; B) $^{63}Cu$ and protein traces of recombinant COA6 reconstitute with $CuSO_4$ and reduced glutathione. Adapted with permission.[3]

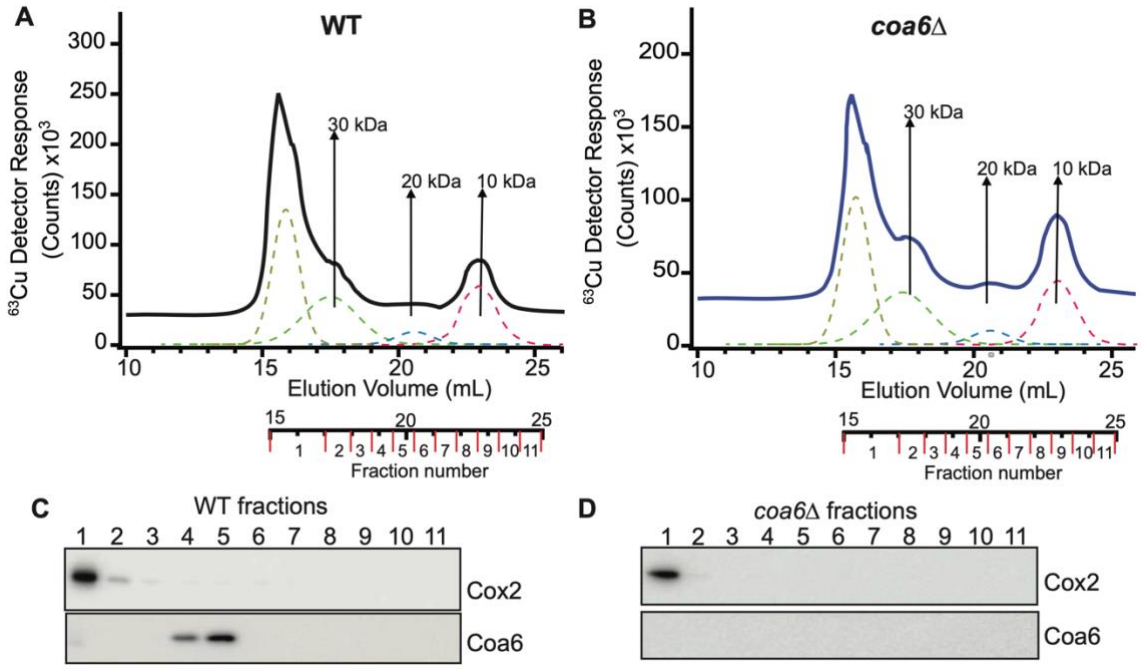


**Figure C-2. Copper chromatograms of isolated WT and *coa6Δ* mitochondria from S. *cerevisiae*.**[3]

(A&B) Copper traces from online LC-ICP-MS of solubilized mitochondrial extracts from WT (A) or *coa6Δ* cells (B). The dotted lines indicate simulated curves generated by peak fitting. (C&D) SDS-PAGE/Western blot depicting Cox2 and Coa6 protein levels in the different LC-ICP-MS fractions of WT (C) and *coa6Δ* (D) soluble mitochondrial extracts. Adapted with permission.[3]

**C.5. Reference:**


1 N. Dziuba, J. Hardy and P. A. Lindahl, Low-molecular-mass iron in healthy blood plasma is not predominately ferric citrate, *Metallomics*, 2018, 10, 802-817.

2 D. A. Stroud, M. J. Maher, C. Lindau, F. Vögtle, A. E. Frazier, E. Surgenor, H. Mountford, A. P. Singh, M. Bonas, S. Oeljeklaus, B. Warscheid, C. Meisinger, D. R. Thorburn and M. T. Ryan, COA6 is a mitochondrial complex IV assembly factor critical for biogenesis of mtDNA-encoded COX2, 2015, **24**, 5404–5415.

3 S. Soma, M. N. Morgada, A. Boulet, A. A. Roesler, N. Dziuba, A. Gosh, Q. Yu, P. A. Lindahl, J. B. Ames, S. C. Leary, A. J. Vila, V. M. Gohil, COA6 is Structurally Tuned to Function as a Thiol-Disulfide Oxidoreductase in Copper Delivery to Mitochondrial Cytochrome c Oxidase, *Cell Reports*, 2019, **29**, P4114-4126.E5.

# APPENDIX D PROTOCOL FOR LIQUID CHROMATOGRAPHY (LC) OR LIQUID CHROMATOGRAPHY-INDUCTIVELY COUPLED PLASMA MASS SPECTROMETRY (LC-ICP-MS)

## D.1. About the Instruments – LC and ICP-MS systems:

### D.1.1. System configuration:

#### D.1.1.1. Liquid Chromatography System

We use a high performance liquid chromatography system manufactured by Agilent Technologies. The system is from the Bio-Inert line up of the HPLC suite. The system is equipped with a quaternary pump, diode array detector, and fraction collection modules. It has recently been upgraded to also include a multisampler, two valve drivers, and three manual valve switches. This entire system is installed inside of a chilled and anaerobic glovebox with a argon environment. The glovebox is maintained at approximately 8°C and between 1-10 ppm of $O_2$.

The system is now controlled with the updated Opel Lab CDS software suite from Agilent. The computer driving the software for these modules is connected to the internet. This allows for remote access of the LC modules through native Windows remote access software or third party software (e.g., AnyDesk, TeamViewer).

The addition of the multisampler has allowed for the connection of seven different columns, four of which can be accessed at any point remotely. The remaining three columns requires manually switching the flow path of the system using the manual input and output switches (Figure D-1). In addition to the current LC configuration, it

can also be coupled to an inductively coupled plasma mass spectrophotometer (ICP-MS) located adjacent to the glovebox. The ICP-MS is utilized as the detector.

#### D.1.1.2. Inductively Coupled Plasma Mass Spectrometer System

The ICP-MS system is an Agilent 7700X system using a concentric quartz nebulizer, Scott type spray chamber, and a reaction cell using helium as the reaction gas. The ICP-MS is coupled to the LC system via a piece of PEEK tubing coming out of the glovebox. There is a direct flow of the column eluent from the column going into the ICP-MS which is driven by the quaternary pump. The system has also been equipped with an optional gas line to allow for analysis of solutions containing organic solvents. This gas line is used with a 80% ultra-high purity Ar (99.999% purity) and 20% $O_2$ gas cylinder.

The ICP-MS software – Masshunter – has a chromatographic license allowing for time resolved data to be collected and analyzed. Additionally the system can be configured to have an Agilent LC system be used as the sample introduction method. This configuration gives Masshunter direct access to the LC quaternary pump and multisampler.

#### D.1.1.3. LC-ICP-MS

Both the LC and ICP-MS are connected to a local network. This allows Masshunter to communicate and control the LC modules. The initiation of a run is performed through a communication cable that connects the LC and ICP-MS system together. This communication cable is what transmits the start command to begin an analysis. The provided LC-ICP-MS coupling allows for Masshunter to collect any

elemental spectroscopic data on predetermined isotopes. In this configuration the diode array of the LC system is not utilized.

To perform 2-dimensional analysis using both the diode array and the ICP-MS the LC system software – Open Lab CDS – must be configured to have all modules except the pump and multisampler be accessible to the software. This allows a user to implement a run for data collection in the Open Lab CDS software and the Masshunter software. This also allows the Open Lab software to control the columns being used and the diode array settings. Masshunter will control the pump and sample injection via the multisampler.

### D.1.2. Chromatographic separation and elemental detection

#### D.1.2.1. Size-exclusion chromatography: Primary separation technique

Size-exclusion chromatography (SEC) allows for the separation of molecules/compounds based on their hydrodynamic volume or size.[1] This volume has a direct correlation to a molecules/compounds mass. Typically, the larger a species being separated is, the larger its mass. The columns function as a molecular sieve. The column stationary phase/resin is a porous material. The holes present can be a variety of different sizes depending on the purpose of the column, these sizes dictate the mass range the column can separate. If compounds pass through many of these pores, then the compound will be retained on the column longer than compounds that pass through fewer pores.[1] In other words, smaller molecular weight (smaller hydrodynamic volume) compounds will pass through many pores whereas larger molecular weight (larger hydrodynamic volume) compounds will pass through fewer. The smaller compounds

will elute from the column at a larger elution volume and the larger compounds will elute at a smaller elution volume.

**D.1.2.2. Void volume:**

An important characteristic of chromatography columns is their void volume. This is the volume of the column that is composed of mobile phase.[1] This property can be determined for SEC columns by injecting a very large molecular weight compound – well above the limit of the column – onto the column and determining its elution volume. This property of the column is used when generating a calibration curve.

**D.1.2.3. SEC calibration curve:**

Compounds with known masses can be run on a column to generate a calibration curve to correlate the elution volume of an unknown species with an apparent molecular weight. The calibration plot is generated by plotting a standard's elution volume/the column's void volume by the log of the standard's molecular weight.

**D.1.2.4. Elemental spectroscopy and ICP-MS: basic principles**

The basic process for sample analysis for an ICP-MS includes the following: sample introduction, aerosol formation, desolvation, vaporization, atomization, ionization, and detection.[2] ICP-MS operates by ionizing and detecting atoms in a +1 charge state using an argon based plasma as the source of ionization. This plasma can reach temperatures of 10K and has enough energy to perform first level ionization of atoms to create singly charged species.[2]

The basics of a liquid sample introduction are as follows.[2] A liquid sample is introduced into the instruments nebulizer via a peristaltic pump which generates a fine

aerosol inside of a spray chamber. This aerosol is sampled by the spray chamber to create a uniformly sized distribution of water droplets that enter the instrument's flow path towards the torch and plasma. During this transit into the plasma the sample aerosol droplets are subsequently desolvated, vaporized, atomized, and finally ionized as it exists the plasma. The ions then travel through the interface of the instrument where the ion path is adjusted via ion lenses before it travels into the quadrupole for mass selection. These ions are isolated based on its mass/charge for a desired isotope. The isolated atoms are then sent to an ion detector for detection.

The MS of the instrument is a single quadrupole and cannot differentiate between doubly charged species or polyatomic species, giving the potential for false positives for certain isotopes. To alleviate this issue we utilize the reaction cell that is placed in front of the quadrupole. The reaction cell uses helium gas to perform kinetic energy discrimination.[2] The helium interacts with the larger species (i.e., the polyatomic and doubly charged species) more than with the smaller species. The interaction with helium pushes the ions outside of the ion path, preventing them from reaching the detector. Polyatomic species like $^{56}$ArO or $^{57}$ArOH are of concern for us as they can obscure the naturally abundant $^{56}$Fe or enriched $^{57}$Fe present in a sample.

### D.1.3. System benefits

#### D.1.3.1. Bio-Inert:

This distinction means that the flow path of the system has no or minimal metal components This allows us to maintain minimal metal leeching into our buffers during analysis for the best chromatographic analysis of metal complexes.

#### D.1.3.2. Chilled and anaerobic environment:

The anaerobic environment of the chromatography system prevents the oxidation of any ferrous iron present in samples or thiols like glutathione. The oxidation of the coordinated metals or the ligands of a native metal complexes would destroy these complexes. The effect of oxidation could cause a mixture of native metal complexes and nascent metal complex that would be observed. Distinguishing which species are native and which are nascent would be difficult. There is also the possibility of the oxidized metals precipitating out of solution and damaging the column.

The low temperature of the glovebox also slows any kinetic phenomenon, either decomposition of metal complexes or formation of new metal complexes. This allows us to view the native metal complexes present inside of our samples without worrying about artifacts.

#### D.1.3.3. Remote access

Remote access of the LC system gives users the ability to view the results and progress of a run in real-time from anywhere with an internet connection. The system can be accessed at any time during the day to check on the progress of sample analysis. Additionally, a sample can be rerun if required during a multi-sample analysis. This prevents the need to rerun a sample days or weeks when time becomes available or having to be in the same room as the instrument.

#### D.1.3.4. Multisampler and valve drivers

Previously samples had to be manually injected one at a time and an individual needed to be physically present to begin the equilibration of the columns. This was a

very time consuming process as our analysis times are approximately 2 hours and 30 minutes for our most used separation technique. Not taking into account the time to equilibrate the system, an individual could stay in the lab injecting sample till the early morning while only achieving a moderate number of injection during this time (2-5 injections). Automation of the sample injection and equilibrium process allows multiple samples to be processed throughout the course of the day. The automation does not require the presence of an individual to monitor the instrument. This greatly increases the number of samples that can be injected and frees up the individuals time to perform other work(e.g., sample processing).

The valve drivers also give the option to perform different analysis throughout the day. Typically only one separation technique (e.g., low molecular pass analysis, high molecular mass analysis, ion exchange) can be performed a day due to time constraints with cleaning and equilibrating the column. The multisampler and valve drivers allows for multiple samples to be analyzed with different separation techniques. For instance, during the night a column could be cleaned and equilibrated allowing for sample analysis until the midafternoon. Then the column could be switched, cleaned, and equilibrated and samples could be analyzed overnight. This process would only require an individual to be present in the morning or the day prior to load samples into the multisampler.

**D.1.3.5. Optional Gas Line: Organic Solvent Analysis**

With the addition of the optional gas line, the ICP-MS can be used to analyze samples containing organic solvents. The system needs to be configured in the organic

solvent mode to allow for proper plasma ignition. This setting can be found in the settings option in Masshunter for the instrument. The system can be tuned similar to aqueous mode, though the tuning should be done manually. The user must make a record of the optimal tune parameters after the instrument has been thoroughly cleaned, this will be the baseline tuning parameters. The baseline parameters will be the basis for determining if the instrument is tuning properly in organic mode. The system must use the optional gas line which is made of 80% ultra-high purity argon and 20% oxygen. The oxygen is present to prevent the buildup of carbon debris on the cones, which can potentially clog the cones. This mode must be utilized if running organic solvents, either on the Superdex increase/peptide columns or on the HILIC column.

**D.2. Prior to Analysis – LC Standalone:**

**D.2.1. Load the well plate**

(a) Load your sample

*(i) Load your sample into a well plate for use with the LC multisampler*

(b) Load the cleaning cocktail solution

*(i) Load a vial of cleaning cocktail solution in the same well plate as your sample*

*(ii) Minimum recommended volume: 0.550 mL; per injection*

**D.3. LC Standalone:**

**D.3.1. Log into the computer**

(a) Log in

*(i) Credentials are located on the desktop tower on a sticker*

1) Note: if credentials on sticker do not work, seek out a senior lab member to verify credentials. If computer cannot be accessed then talk with the IT department for assistance.

**D.3.2. Launch the software:**

(a) Open the software “Control Panel”

*(i) On the computer desktop select the shortcut Control Panel*

(b) Launch software for LC standalone configuration

*(i) In control panel select the instrument LC01*

1) Select **Launch**

2) Note: Launch Offline should be used for data processing when the system is being used, such as during yours or a colleague’s analysis

(c) Software loading time

*(i) Opening Lab CDS may take time to fully load*

1) Note: Wait 5 min before taking any other actions such as force closing the application

*(d)* Ready the modules when they are loaded

*(i) See D.9. Troubleshooting LC errors for more details on readying the modules*

**D.3.3. Load a method:**

(a) Set the software in Method and Run Control

*(i) On the right hand option bar in Open Lab select **Method and Run Control***

*(ii) Note: This window allows you to control the instrument and view the analysis in real time*

(b) Select desired method

*(i) In Open Lab select your desired method or default method*

1) Go to Method -> Load Method

a) Search through the file directory

2) Note: If using a default method be sure to resave the method under a new filename and place it into your sub-directory

**D.3.4. Making and running a sequence for multiple samples:**

(a) Open the Sample Entry tab

*(i) Select the tab Sample Entry in the main window of Open Lab*

1) Note: This tab opens the option to make sequences using a nicely made GUI

2) This panel is divided into 4 different panels

a) Multisampler plate location (top left)

b) Selected plate well positions (top middle)

c) Sample type (top right)

d) Sequence list (bottom)

(b) Select the sample plate

*(i) In the multisampler plate location:*

1) Select the plate with your loaded samples

(c) Sample Type: Select where your sample is loaded and its sample type

*(i) Right click where your sample is located in the well/plate*

*(ii) Select: **Append Samples** -> "Sample Type"*

1) For sample type select if it is a sampler, blank, calibration, or control sampler

a) Note: Most people will only be using samples so select sample

(d) Fill in sample information in the sequence list:

*(i) In the sequence list a new line should have been generated containing the container location and sample location*

1) Fill in the information for Sample Name and Sample Info

2) Insert the desired method to be used for the sampler

a) Select the column for the method name

b) Click on the box to the left of the dropdown arrow in the Method Name box and search the directory for your method

(e) Set the directory your sequence will save to:

*(i) In the sequence list panel tool bar select the gear cog icon on the far right*

1) A new window will open up

2) Select the sub directory that the sequence will be store post-run

(f) Save your sequence:

*(i) In the Sample Entry panel tool bar select save*

1) Save your sequence and give it a name

(g) Appending more samples:

*(i) Follow the above steps from step 'c'*

*(ii) Remember to save your sequence when finished*

(h) Adding to queue

*(i) When all samples have been inserted and the sequence has been saved select **Add to queue** in the Sample Entry box*

1) Two popups will appear

a) Save the sequence

*i) Give the sequence a name and click **OK***

b) Append sequence to Run Queue

*i) Append to the Run Queue by clicking **OK***

2) Make appropriate choices for either pop-up

(i) Sample sequence location

*(i) The sample sequence will be located in the Run Queue Tab located to the left of the Sample Entry tab*

**D.3.5. Running one sample:**

(a) Opening Queue Method In the Open Lab:

*(i) In the main toolbar select:*

1) RunControl -> Queue Method

(b) Queue Method Window:

*(i) Select the method for your sample*

1) Select **Browse** and search through the directory for your method

2) When finished select the method and select **Okay** in the directory window

*(ii) Select the subdirectory*

1) Give a folder name where your data will be stored in

*(iii) Note: You can make a subdirectory for the analysis performed on the date of analysis or by experiment, this is a user choice. Lab norms are to make a folder based on the experiment date (date you injected the sample into the LC system) as it is easier to search for a date then various experiment folders*

*(iv) Injection volume (ul)*

1) Add the volume you plan to inject onto the column

2) Give a numerical value with no units

*(v) Sample amount*

1) Same as injection volume

*(vi) Sample name*

1) Give your sample a name

*(vii) Sample Comment*

1) Describe your sample in a useful manner that can be deciphered in 1-3 years

(c) Appending sample to sample queue:

*(i) Add the back of queue*

1) Note: Select if appending a run to a current run queue

*(ii) Add the front of queue*

1) Note: Select if no other sample or sequence is running

**D.4. Prior to Analysis- LC-ICP-MS:**

**D.4.1. Prepare tune solution**

(a) Tune solution protocol:

*(i) Prepare a tune solution according to the manufactures recommendations*

*(ii) Stock tune solution purchased from Agilent Technologies*

**D.4.2. Peristaltic tubing check**

(a) Tube check

*(i) Check the integrity of any tube: sample introduction, drain tube, internal standard*

*(ii) Inspect tube for any divots or flat regions, if present then replace tube*

*(iii) Inspect tube for elasticity at region that attached to peristaltic pump, if rigid then replace*

*(iv) If any tubing is damaged, (i.e., no elasticity or flat) replace*

(b) Install tubing

*(i) Install any new tubing if required, peristaltic positions are assigned from left to right when facing the front of the ICP-MS*

*(ii) Peristaltic position 1 = sample introduction tube*

*(iii) Peristaltic position 2 = internal standard tube*

*(iv) Peristaltic position 3 = drain tube*

*(v) Properly install any new tubing and prepare for instrument warm-up*

### D.4.3. Instrument warm up

(a) Warm up time

*(i) Allow the instrument to warm up with plasma lit (e.g., 10-15 minutes)*

(b) Sample introduction during warm up

*(i) Take up 2% (v/v) concentrated nitric acid in high purity water while warming up*

## D.5. LC-ICP-MS

### D.5.1. Log into the computer

(a) Log in

*(i) Credentials are located on the desktop tower on a sticker*

1) Note: if credentials on sticker do not work, seek out a senior lab member to verify credentials. If computer cannot be accessed then talk with the IT department for assistance.

### D.5.2. Masshunter

(a) Open Masshunter

*(i) Open ICP-MS Masshunter from the shortcut located on the desktop*

1) Note: Make sure to open Masshunter first and tune the ICP-MS before loading Openlab. After you are done tuning the instrument then you can change the ICP-MS sample configuration for Agilent 1200 LC instead of Peripump. When you have the new sample introduction system configured then you can

clear the errors from the pump and multisampler. For more details see: Example Workflow

(b) Configure and tune the instrument

*(i) Go to Settings*

1) Select **System** from the top toolbar

a) Select the arrow pointing to the Hardware button in the right panel

*i) A new window will appear*

b) In the left panel select Sample Introduction

*i) In the right panel under Properties*

a. Select Peripump for Sample introduction

*ii) Above select the check box to use the autosampler*

a. Note: This will configure the autosampler for the ICP-MS to be able to move to the tune solution

2) Make a performance report and tune the instrument

*(ii) Performance Report*

1) After the system has warmed up select the plasma icon located next to the hardware iron on the top of the Masshunter window

2) Select **Autosampler** from within the Plasma window and move the autosampler to the correct vial position

a) Allow the system to uptake the tune solution for 2 min before proceeding

*i) Note: Make sure the tubing for the instrument is connected, if it is not connected correctly you will receive an error during the performance report of low counts for*

*expected isotopes. Fix by either adjusting the sample introduction, drainage tubing, aspiring for longer, and/or move the autosampler probe to the correct vial*

b) **Select**: Torch Axis, Plasma Correction, Standard Lens Tune, Resolution/Axis, Performance Report, Full Spectrum

*i) Make sure the box has a check mark next to these names*

c) Select **Add to Queue** and wait for the performance report to finish

3) Note: Running a performance report IS NOT TUNING

*(iii) Tune by batch or use Global Tune*

1) Note: View help files in software for more information on instrument tuning

2) After the performance report has finished select the **Tune** iron in the main window of Masshunter to perform a Global Tune or select the **Batch** icon in the main window of Masshunter to Tune by Batch

a) Note: all steps are similar for either tuning methodology

3) Global Tune:

a) Select autosampler and move the sampling probe to the tune solution vial and allow the system to uptake the solution for 2 min

b) Import any Tune files you desire

*i) The HE mode should be set as the default*

c) Select Start Auto Tune and let the system perform the autotuned

d) When the autotuned is completed a tune report will be generated

e) Save this tune report to the Desktop folder called Tune Reports

i) *In the event a tune report is not generated go to the **Report** icon in the main window of Masshunter and select **Generate Tune Repo**rt, make sure that Generate a Tune Report is selected then rerun the autotuned*

f) After tuning select the Global Tune icon in the Tune window

i) *Note: This sets the parameters in the HE tune file as the default for any batch that will be run containing the HE tune tile*

ii) *Note: make sure the tune file in the Tune window matches the tune file in the batch*

4) Batch Tune:

a) Follow steps 3.A-C under Global Tune

*(iv) When finished tuning reconfigure the instrument back for LC-ICP-MS*

1) Under the Masshunter heading, follow from D.5.2. Masshunter at step (b), b)

a) Select Agilent 1200 LC as the sample introduction instead of peripump

*(v) Ready the LC modules when they are loaded*

*1)* See D.9. Troubleshooting LC errors for more details

(c) Loading a batch file:

*(i) Open a default batch file that corresponds to the method loaded in OpenLab CDS by clicking **Batch** -> **Open Batch folder** in the Masshunter toolbar*

*(ii) Match the analysis time in the ICP-MS batch folder to the OpenLab CDS method*

1) Select the Batch icon in the large iron toolbar (contains hardware, plasma,…)

a) Note: The software panes will change, on top will be instrument status and below will be the batch pane

2) In the batch pane select **Acq Method tab**

3) In the sub-tab select **Acq Parameters tab**

4) There will be a table with elements detected, the integration time, at the bottom of the table will be acquisition time, fill in the acquisition time accordingly

*(iii) Save the batch under a new file name*

1) Example: [Batch Name] [Date]

a) Batch name with the date of the analysis appended to the end

(d) Modifying a batch file for analysis:

*(i) Load the Batch information panel:*

1) Select the Batch Icon on the top toolbar of Masshunter

a) Above should be Instrument Status pane

*(ii) Editing batch LC settings*

1) In the batch information panel select the **Acq Method tab** then select **Agilent 1200 LC tab**

2) Note: There will be three new tabs that appear

a) Quaternary Pump

b) Wellplate Sampler

*i) Modify default settings for multisampler*

c) Wellplate Sampler Injection Programming Panel

*i) Don't mess with this unless you really need it*

*ii) If you are running normal viscosity (like water) aqueous samples you don't need it*

*iii) When to use the injector programing panel:*

a. Note: If your solution is easy to pipette then it's a "normal" viscosity, if not, then…

b. Utilizing the analytical sampling head for automatic dilutions/mixing

c. When you have an incredibly sticky/viscous analyte that then requires a special needle washing sequence

d. You'll need this after you figure out that your samples contaminate the entire system no way to know prior unless you know your sample is viscous and hard to pipette…

(e) Edit LC parameters

*(i) Modifying the pump settings:*

1) Go to the Quaternary Pump tab

2) Change the pump speed and mobile phase composition accordingly

*(ii) Modifying the multisampler*

1) Go to the first Wellplate Sampler tab:

2) Change the sample volume to the desired amount

3) Make sure to have

a) Draw speed at 100 uL/min

b) Ejection speed at 500 uL/min

c) Wait time post draw at 10 seconds

d) Check the box for the needle head vial bottom detection

e) Under the advanced settings tab keep the washing to 15 seconds in the flush port

*(iii) Finalized LC settings:*

1) Select Send to LC

a) Note: This will send the batch parameters for the pump and multisampler to the LC system

*(iv) Save the modified batch:*

1) Go to Batch -> Save Batch

(f) Sample list edit/modify:

*(i) Select the sample list tab from the batch panel*

1) Add the samples to run here

2) Match the samples according to the sequence or list of queued samples in OpenLab CDS

*(ii) Insert the following information, match as best as possible to OpenLab CDS sample list*

1) Sample type

a) Decide on the sample type

b) Note: Select sample unless you are running something specific

2) Sample Name

a) Give your sample a name

3) Comment

a) Describe your sample in a meaningful way that will still be useful 1-3 years in the future

i) *Note: In case you need to know exactly what you ran don't just put down 'yeast batch, test run'. This level of detail is useless, instead use 'yeast batch G [date harvested], experiment on xyz'. Use a description which will serve you 1-3 years in the future when you are trying to publish a paper*

4) File Name

a) Can make the same as sample name for simplicity

5) Vial# example:

a) P1-X

i) *P1 is tray 1*

ii) *X = A1 or B1 or …*

iii) *If vial is in location B5 the vial# = P1-B8*

b) Note: Vial numbering is based off the labeling system the LC system has while in Masshunter, it is not the same as in OpenLab CDS

i) *To view labeling system select the Agilent 1200 LC tab under the instrument status panel and select the icon of the hotel draws in the multisampler module*

*(iii) When finished inserting the information select **Validate Method** in the Batch panel then **Save Batch***

*(iv) When the batch has been verified select **Add to Queue** when you are ready to initiate analysis*

1) Note: Be sure your samples and LC methods/queues are setup appropriately prior to adding the batch to the queue

### D.5.3. Open the Open Lab CDS software

(a) Open the software “Control Panel”

*(i) On the computer desktop select the shortcut Control Panel*

(b) Select LC instrument configuration for ICP-MS

*(i) In control panel select the instrument LC_ICP_MS01*

1) Select Launch

2) Launch Offline should be used for data processing when the system is being used, such as during yours or a colleagues analysis

3) While the software initiates loading, a pop-up will occur asking to confirm the instrument configuration

a) Select Okay

(c) Open Lab CDS launch time

*(i) The software may take time to fully load*

1) Note: Wait 5 min before taking any other actions such as force closing the application

(d) Ready the modules when

*(i) When the software has loaded ready the modules*

*(ii) See D.9. Troubleshooting LC errors for more details*

### D.5.3.2. Load a Method in OpenLab CDS:

(a) In Open Lab select your desired method or default method

*(i) Go to Method -> Load Method*

1) Search through the file directory

*(ii) If using a default method be sure to resave the method under a new filename and place it into your sub-directory*

*(iii) *** Methods for LC-ICP-MS and LC-Standalone are NOT the same****

1) LC methods have the start command triggered via the "HiALPS" selection, this is a start command coming from the multisampler
2) LC-ICP-MS methods have a start command triggered via a "Manual" selection
   a) The manual start occurs from the start command coming from the pump/multisampler that is controlled via Masshunter
3) Methods for each instrument selection are located in different root folders be careful when selecting a method

**D.5.4. Making a sequence: Skip to D.5.5 if running only 1 sample**

(a) Opening Method and Run Control

*(i) On the left hand bar in OpenLab select **Method and Run Control***

(b) Opening sequence table

*(i) In the main toolbar of OpenLab CDS select*

1) Sequence -> Sequence Table
2) This bring up the sequence table which can be modified

*(ii) Note: A single sample line should be present which is blank*

(c) Fill in the sequence line:

*(i) Sample Location*

1) Insert the value “1” to the sample location field
2) Note: The multisampler is NOT configured in this instrument configuration
3) Note: A value of “1”:
   a) This tells the instrument that it will not be a blank run and will come from location 1
      *i) Location 1 is an arbitrary location that has no meaning in the current instrument configuration*
      *ii) Likewise you could use location 108275639 if you wanted, granted that there is not a maximum location limit programmed into the software*
   b) If 0 then the system registers the sample type as a blank and the system will automatically initiate a start command even if the injection profile is set to “Manual”

*(ii) Sample Name*

1) Give your sample a name

*(iii) Select the Method from the dropdown list/directory*

1) Search through the directory window that appears and select your desired method
2) Then click **Okay** to accept the method and close the window

*(iv) Injection Source*

1) Use “As Method”

*(v) Injection volume*

1) Note: Can put in a value, but the system will take the injection volume from the method used

*(vi) Sample Information*

1) Scroll to the right to find this column
2) Describe your sample in a meaningful way that will still be useful 1-3 years in the future
   a) Note: In case you need to know exactly what you ran don't just put down 'yeast batch, test run'. This level of detail is useless, instead use 'yeast batch G [date harvested], experiment on xyz'. Use a description which will serve you 1-3 years in the future when you are trying to publish a paper.

(d) Adding additional sample lines in the sequence table:

*(i) Additional samples that are using the same/similar parameters (method)*

1) Highlight the template sample line by clicking the left most column of the line
   a) In the sequence table main tool bars select the third from the left button **Append Line**
2) A new window will appear
3) Under the new sequence lines heading select the number of times you wish to append or insert the selected lines
4) Click "OK" when finished
   a) New lines should appear

5) Highlight the previously made line and select the button fill-down button from the sequence table toolbar

a) Note: This will just copy the settings of the highlighted sequence line into the newly made lines

6) Adjust the sample name and comment for each line added

7) When finished making the sequence table select **apply** and **okay**

(e) Saving the sequence table:

*(i) Save the sequence table by selecting from the OpenLab CDS main toolbar:*

1) Sequence -> Save Sequence Template As

(f) Running the sequence table

*(i) Run the sequence table by selecting from the OpenLab CDS main toolbar:*

1) Sequence -> Sequence Table -> Run

**D.5.5. Running one sample:**

(a) In the Open Lab main toolbar select:

*(i) RunControl -> Queue Method*

(b) Queue Method Window:

*(i) Select the method for your sample*

1) Select **Browse** and search through the directory for your method

2) When finished select the method and select **Okay** in the directory window

*(ii) Select the subdirectory*

1) Give a folder name where your data will be stored in

2) Note: You can make a subdirectory for the analysis performed on the date of analysis or by experiment, this is a user choice. Lab norms are to make a folder based on the experiment date (date you injected the sample into the LC system) as it is easier to search for a date then various experiment folders.

*(iii) Add sample location*

1) Click on the drop-down box and a small window will appear of the multisampler hotel draw and plate
2) Select the sample location in the plate
3) Injection volume (ul)
   a) Add the volume you plan to inject onto the column
   b) Give a numerical value with no units
4) Sample amount
   a) Same as injection volume
5) Sample name
   a) Give your sample a name
6) Sample Comment
   a) Describe your sample in a useful manner that can be deciphered in 1-3 years when you will be publishing your results

(c) Appending sample to sample queue:

*(i) Add the back of queue*

1) Note: Select if appending a run to a current run queue

*(ii) Add the front of queue*

1) Note: Select if no other sample or sequence is running

**D.6. Turning off the instruments**

(a) This section will discuss how to turn off the system remotely at the end of the analysis for the day and while in person

**D.6.2. Open Lab CDS:**

(a) Note: Protocol to turn off instrument whether in LC standalone or LC-ICP-MS the protocol to turn off the instrument will not change

(b) Manual: Turn off of pump and diode array

*(i) In the Instrument panel select the off icon in the module widow of the pump and diode array*

*(ii) Selecting the off button will set the flow rate of the pump to 0 mL/min and turn off the bulb of the diode array*

(c) Automatic: append to a run a stop command

*(i) Select RunControl, then select Queue Command*

*(ii) In the new window select from the drop down list **Turn off Pump** and select **Add to Back of Queue***

*(iii) Repeat step ii from above but select **Turn off Lamp***

*(iv) When the queue is finished the pump and lamp will be turned off automatically*

**D.6.3. Masshunter**

(a) Manual: Turn off plasma

*(i) Select the drop down button from the **Plasma** icon in the main window of Masshunter*

*(ii) Select Turn off Plasma*

*(iii) The plasma has been turned off*

*(iv) Note: if the system is configured in LC-ICP-MS mode the LC system will automatically go into error mode and shut down all modules, this is normal*

(b) Automatic: At the end of queue

*(i) Select the Queue icon in the main window of Masshunter*

*(ii) Select Plasma Off **at End** in the Queue window*

*(iii) The plasma will shut down at the end of the analysis whether it is offline (quantitative elemental analysis) or if the system is in the LC-ICP-MS configuration*

*(iv) Note: if the system is configured in LC-ICP-MS mode the LC system will automatically go into error mode and shut down all modules, this is normal*

**D.7. Appending sequences/batches**

**D.7.1. A sample/batch may be appended at the end of another analysis**

*(a) This can be performed while the instruments are running and the appropriate software is in use*

(b) OpenLab CDS

*(i) Open the "Offline" version of the software to make your sequence/adjust your methods while another analysis is running*

*(ii) When your sequence and/or method(s) are completed you can queue them in the "online" software*

(c) Masshunter

*(i) You can open the "Demo" version of the software*

1) To open "Demo" version hit the Windows Start button and navigate to the "I" folders, open the ICP-MS… folder and scroll through the list and select ICP-MS Masshunter Demo

*(ii) Adjust any batches in the demo version, then open to "live" version of the software and add your adjusted batch to the queue*

## D.8. Sample-preparation

### D.8.1. Filter all samples for any LC analysis

(a) Filters

*(i) 0.45 or 0.2 um filter*

*(ii) Molecular weight filtration is acceptable with either a stir-celled concentrator or centricon based system*

1) Note: Only the FILTRATE can be used, not the retentate

2) Note: Filter the retentate prior to injection

(b) Use either the 54 vial plate or 27 Eppendorf plate

*(i) Eppendorf plate is also compatible with fraction collector*

(c) When using the Eppendorf plate:

*(i) Use only 1.5 mL tubes*

1) Uses a preprogrammed depth for sample draw so if you use a 2mL tube you might not get the last bit of sample

(d) When using the 54 vial plate:

*(i) 2mL amber glass vials*

1) Use 2mL vials with rubber septum screw cap
2) Vials can technically hold up to 2 mL but fill to a maximum of 1.5 mL
   a) Can't pick up last ~200uL in vial
3) Using 200-500uL use plastic inserts
   a) Place insert into 2mL vial and screw on septum cap

*(ii) 300uL or 700 uL plastic vials*

1) Vials use a rubber/silicone septum screw cap
2) 300 uL vials can be used for sample injections of 250 uL or less
3) 700 uL vials can be sued for sample injections of 650 uL or less

*(iii) When loading the plate into the white tray make sure the plate is orientated correctly*

1) The white tray has a marking on it to tell you the orientation to insert the plate by aligning the A1 well to a specific corner

**D.9. Troubleshooting LC errors**

**D.9.1. Switching between LC standalone and LC-ICP-MS**

(a) Switching configurations

*(i) When switching between LC standalone and LC-ICP-MS the LC modules may error out*

*(ii) You are switching communication by swapping to the different instrument configurations*

(b) Clear the LC module errors

*(i) See D.9. Troubleshooting LC errors*

*(ii) Note: The modules can only communicate with one software at a time*

**D.9.2. LC-errors:**

(a) Multisampler

*(i) Never reaches the ready state, make sure:*

1) The door of the module is correctly installed

2) Both well plates must be installed

a) Note: this include a well plate and the plate tray

**D.9.3. Fixing Instrument Errors:**

(a) Logbook

*(i) View logbook for details on why modules errored out*

*(ii) This can give an individual information on which module errored out and a potential error code to troubleshoot the issues*

(b) Open Logbook:

*(i) View -> logbook -> current logbook*

*(ii) A new window will appear in the methods and control panel*

(c) Typical errors:

*(i) Water sensor*

*(ii) Connection Issues*

(d) Fixing typical errors:

*(i) Note: See D.9. Troubleshooting LC errors for how to clear errors*

*(ii) Water sensor detected a leak*

1) Find the module that detected the leak

a) Logbook records actions per module model number

2) Clean up the leak and find out what caused the leak

a) Check ferrules, tube connections,…

b) Perform basic troubleshooting strategies to determine leak location and possible solutions

*(iii) Connection issues*

1) There is no communication between the software and the instruments

2) Check the router if instruments are connected or if the router is powered on

3) Ping the LC via command prompt

a) LC IP: 192.168.254.11

*i) IP for ICP-MS is 192.168.254.12*

*ii) Local is 192.168.254.10*

4) If there is no communication, make sure the BootTable is active

a) BootTable is located under the “ICP-MS Masshunter…” folder in the windows start pane

b) MAC addresses are located on the desktop along with default IP addresses for LC and ICP-MS

5) If you don’t get communication after step 3 and/or you don’t know what command prompt is then call Agilent Technologies and explain the situation to the Support Center

*(iv) Clearing Errors:*

1) Hit the power button in the module within OpenLab CDS or Masshunter to clear the error

2) If the cause of the error hasn’t been solved the module will never reach a ready state and will sit at a “waiting” state or error out again

**D.9.4. Instrument modules are not ready – Clearing Errors**

(a) Readying the modules

*(i) Select the power on button in the module pane within OpenLab CDS (Online) or within Masshunter when the sample introduction is set to Agilent 1200 LC*

*(ii) Note: This is how to clear module errors*

**D.9.5. Error cannot be diagnosed**

(a) Call Agilent Technical Support

*(i) If troubleshooting fails and/or if the troubleshooting help given in module manual fails to solve the problem call the tech support*

## D.10. ICP-MS errors

### D.10.1. Instrument Errors:

(a) ICP-MS recent errors list:

*(i) Under **Instrument Status**, located in any window of Masshunter, select the **ICP-MS** tab*

1) This is a drop-down error list that details the error that occurred and the time it occurred.

*(ii) Errors shown in this list have a corresponding error code which can be searched for a more detailed description of the error*

1) Use the search function located in the Help icon in the main window of Masshunter

2) Type in the error code to find a list of potential errors

a) Not all potential errors can be troubleshooted by an individual (e.g., RF generator failure, faulty power supply, faulty network card) and will require an onsite engineer to assistance

*(iii) Use the more detailed error description from the search function of the manual to aid in troubleshooting by using basic troubleshooting strategies*

1) Search Google for "methodology of basic troubleshooting strategies", this will provide basic steps on how to trouble shoot. Examples may be from other fields like computer science or engineering though the general concepts (e.g, find the problem, determine probable cause) will remain the same.

(b) Analysis Errors:

*(i) Errors occurred during an analysis that do not shutdown the instrument can be found under the Queue Icon in the main window of Masshunter*

*(ii) In the Queue window is a list of all batches running or waiting to be run, there is a corresponding error message column in this window which will have information in it if the run fails*

1) Note: if the run is successful no information will be present in the error message column

(c) Failed troubleshooting:

*(i) If troubleshooting attempts have failed call the Technical Support department at Agilent Technologies for more assistance*

*(ii) If you are new to the instrument then ask the tech support to assist over the phone first. Explain to them that you are new and are willing to work over the phone and would greatly appreciate if they could help. This is a great learning opportunity to gain valuable knowledge from trained professionals. Treat these interactions with the tech support and onsite engineers like mini-seminars and you will quickly gain insight in how to take care of and understand the function of this complex instrument.*

1) Note: Onsite engineers absolutely love when someone is around to ask questions about the instrument. This helps them educate the users so that they do not have to come out as often to service the instrument. These individuals

will not be bothered if you ask them questions or ask if you can observe or assist them during the servicing process.

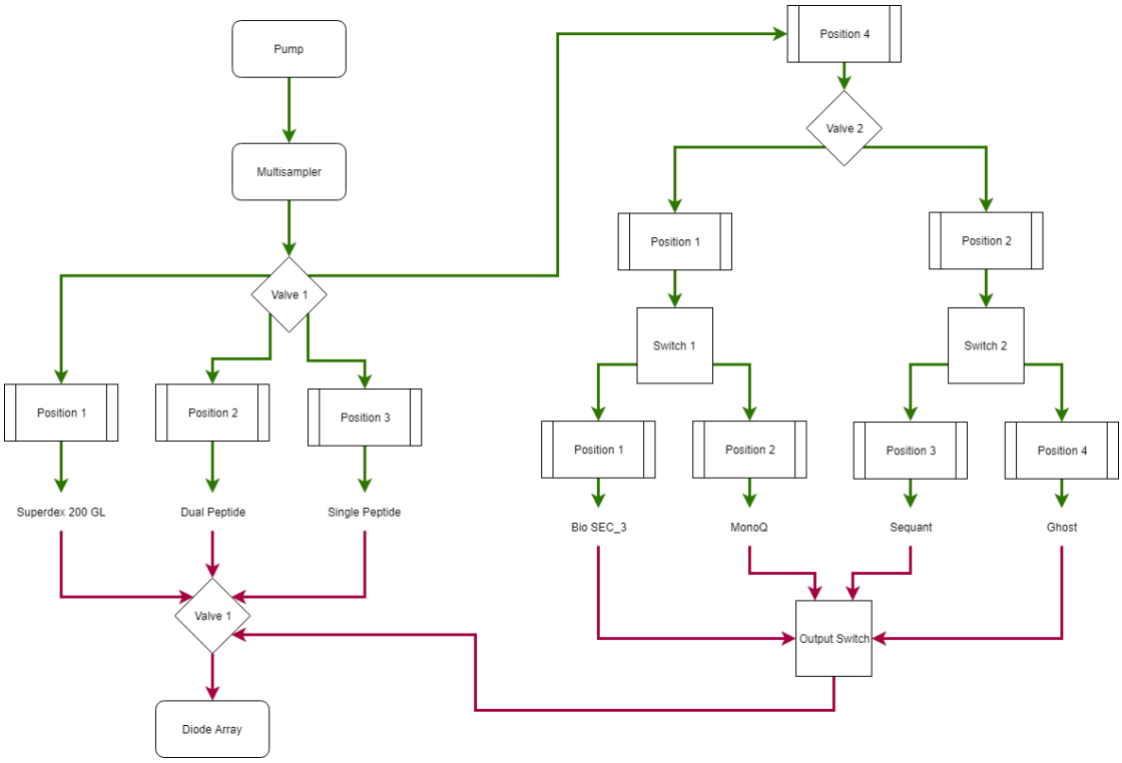


**Figure D-1: Plumbing flow chart for new configuration of LC system after multisampler and valve driver upgrade.**
Green lines indicate flow path leading to columns and red lines indicate flow path leaving columns. Valve 1/2 reference the automatic valve drivers and their corresponding positions; Valve 1 has 4 positions and Valve 2 has 2 positions. The Switches are manual switches which only have two different positions. Output Switch is a manual switch with four different positions, these positions are not shown in the flow chart. Dual and single peptide columns are shorthand for either GE Healthcare Superdex Increase 30 or Superdex Peptide columns. Bio SEC_3 column is short hand for the Agilent Bio-SEC3 column. Ghost is in reference to a “ghost” column which is a piece of PEEK tubing connected to the flow path of the system in the absence of a typical column.

## D.11. References


1 S. C. Moldoveanu and V. David, *Essentials in Modern HPLC Separations*, Elsevier, Waltham, 2013.

2 R. Thomas, *Practical Guide to ICP-MS*, CRC Press, Boca Raton, 3rd edn., 2013.